Evaluating the Role of Bone Marrow Microenvironment in the Pathogenesis of Therapy-related Myeloid Neoplasms

Monika Maria Kutyna
Student ID: a1738920

Myelodysplastic Syndromes Research Group

South Australian Health & Medical Institute (SAHMRI)
&
Adelaide Medical School
Faculty of Health Science
University of Adelaide





A thesis submitted to the University of Adelaide
For the degree of Doctor of Philosophy
October 2022

DECLARATION ..... **ix**

ACKNOWLEDGEMENTS ..... **x**

ABBREVIATIONS ..... **xiii**

HONOURS ..... **xxv**

PUBLICATIONS ..... **xxv**

ABSTRACT ..... **xxix**

CHAPTER 1: INTRODUCTION **1**

1.1. NORMAL HAEMATOPOIESIS **2**

1.2. INTRODUCTION TO MYELOID MALIGNANCIES **3**

1.2.1. Myelodysplastic Syndromes 4

1.2.2. Acute Myeloid Leukaemia 5

1.3. THERAPY-RELATED MYELOID NEOPLASMS OVERVIEW **6**

1.4. ROLE OF HAEMATOPOIETIC STEM CELLS IN TMN PATHOGENESIS **9**

1.4.1. Inherited Predisposition 9

1.4.2. Acquired Risk Factors 12

1.4.2.1. Patient-related factors 12

1.4.2.2. Acquired genetic predisposition to tMN 13

1.4.2.3. Treatment-related factors 14

1.5. ROLE OF BM MICROENVIRONMENT IN TMN PATHOGENESIS **16**

1.5.1. Normal BM Architecture 16

1.5.1.1. Non-cellular components 16

1.5.1.2. Cellular components 16

1.5.2. Genetic Alterations in BM Microenvironment Contributing to Development of Myeloid Malignancies 18

1.5.3. Cytotoxic Therapy-induced BM Microenvironment Dysregulation 19

1.6. HYPOTHESIS **21**

1.7. PROJECT AIMS **21**

CHAPTER 2: MATERIALS AND METHODS **22**

2.1. GENERAL TECHNIQUES **23**

2.1.1. Commonly Used Reagents and Suppliers 23

2.1.2. Common Buffers and Solutions 27

2.1.3. Isolation of Bone Marrow Mononuclear Cells (BMNC) 28

2.1.4. Cell Counts and Viability 29

2.1.5. Cryopreservation of Cells 29

2.1.6. Thawing of Cryopreserved Cells 29

2.1.7. Isolation of $CD34^+$ Cells 30

2.1.7.1. Magnetic Assisted Cell Sorting (MACS) 30

2.1.7.2. Sorting $CD34^+$ population 31

2.1.8. Flow Cytometry to Check $CD34^+$ Purity 32

2.2. CELL CULTURE TECHNIQUES **34**

2.2.1. Culture Media, Buffers, Solutions and Stains 34

2.2.2. Cell Culture Settings 37

2.2.3. Isolation and Expansion of BMSC 38

2.2.4. Surface Antigen Expression Assessment 38

2.3. FUNCTIONAL ANALYSIS **40**

2.3.1. Colony Forming Unit-Fibroblast (CFU-F) 40

2.3.2. Assessment of Population Doublings 40

2.3.3. Cytoskeleton Assay 40

2.3.4. Long Term Culture-Initiating Cells (LTC-IC) 41

2.3.5. Apoptosis Assay 42

2.3.6. Cellular Senescence Assay 43
2.3.7. Alkaline Comet Assay 43
2.3.8. Reactive Oxygen Species (ROS) Level 43
2.3.9. DNA Damage Repair Potential Following Irradiation 44
2.3.10. DNA Damage Induction by *in vitro* Exposure to Doxorubicin 45
2.3.11. Assessment of Osteogenic Differentiation Potential 45
2.3.11.1. Staining with Alizarin Red 45
2.3.11.2. Mineral quantification 45
2.3.12. Assessment of Adipogenic Differentiation Potential 47
2.3.12.1. Adipocytes visualisation with Oil Red O staining 47
2.3.12.2. Quantification of Nile Red labelled adipocytes 48
2.3.13. Assessment of Chondrogenic Differentiation Potential 48
2.3.14. Real-Time ATP Rate Assay 49
2.3.14.1. Normalization of Real-Time ATP Rate assay 49
2.3.14.2. Effect of glycolysis inhibitor on ATP production 50
2.3.15. Immunobead-based Multiplex Assay for Measurements of Cytokines/Chemokines 50
2.3.15.1. BMSC-conditioned media collection 52
2.3.16. Senolytics 52
2.4. RNA TECHNIQUES 53
2.4.1. Preparation of Total Cellular RNA 53
2.4.2. Quantification and Purity Analysis of RNA 53
2.4.3. Synthesis of Complementary DNA (cDNA) 54
2.4.4. Real-time Polymerase Chain Reaction (RT-PCR) 55
2.4.5. Whole Transcriptome Analysis 57
2.4.5.1. Identification of senescence gene expression based on β-Galactosidase levels 58

2.4.5.2. Pathway analysis....58
2.4.5.3. Gene Set Enrichment Analysis....58
2.5. PROTEIN ANALYSIS....60
2.5.1. Protein Lysates Preparation....60
2.5.2. Westerns Blot Analysis....61
2.6. STATISTICAL ANALYSIS....63
CHAPTER 3: DEFECTIVE GROWTH KINETICS OF TMN STROMAL CELLS....64
3.1. INTRODUCTION....65
3.1.1. Morphology and Immunophenotype of MN-BMSC....67
3.1.2. Proliferative Capacity of MN-BMSC....68
3.2. RESULTS....70
3.2.1. Patients and Control Samples....70
3.2.2. No Differences in Immunophenotype Profile Between tMN and Control BMSC....75
3.3.3. tMN Stromal Cells Display Abnormal Morphology....79
3.3.4. Defective Growth Kinetics of tMN BMSC....80
3.3. DISCUSSION....84
CHAPTER 4: DISTINCT SENESCENT PHENOTYPE OF TMN BMSC....86
4.1. INTRODUCTION....87
4.1.1. DNA Damage....87
4.1.2. Cellular Senescence....89
4.1.2.1. Main features of senescent cells....91
4.2. RESULTS....100
4.2.1. No Difference in Apoptosis Rate Between tMN, Healthy and Other MN BMSC....100
4.2.2. Increased Levels of β-Galactosidase of BMSC from Patients with tMN....101

4.2.3. tMN Senescence Can Occur Within a Short Latency After Cytotoxic Exposure 102
4.2.4. Distinct Senescent Transcriptome in tMN Stromal Cells Compared to Healthy and Other, Typical MN Stromal Cells 102
4.2.5. Higher Levels of SASP Cytokines in Conditioned Media of tMN Stromal Cells Compared to Healthy Stromal Cells..... 105
4.2.6. Defective DNA Damage Repair Potential of tMN Compared to Healthy and Other, Typical MN Stromal Cells 107
4.2.7. tMN Stromal Cells Demonstrate a Glycolytic Metabolic State 117
4.3. DISCUSSION..... 123
CHAPTER 5: FUNCTIONAL DEFECTS OF TMN BMSC..... 128
5.1. INTRODUCTION 129
5.1.1. Osteogenic, Adipogenic and Chondrogenic Differentiation of MN-BMSC..... 130
5.1.2. Haematopoietic Support by MN-BMSC 136
5.2. RESULTS..... 141
5.2.1. BMSC from tMN Patients Show Reduced Adipogenic Differentiation 141
5.2.2. BMSC from tMN Patients Secrete Adipogenesis Associated-Inhibitory Cytokines 145
5.2.3. Treatment with OXPHOS Inhibitor robustly Inhibited Adipogenic Differentiation in Healthy BMSC 147
5.2.4. Inhibition of Glycolysis does not Restore Defective Adipogenesis in tMN BMSC..... 148
5.2.5. BMSC from tMN Patients Exhibit Increased Osteogenic Differentiation Potential..... 150
5.2.6. Normal Chondrogenic Differentiation Potential of tMN BMSC 152
5.2.7. Diminished Haematopoietic Stem Cell Supporting Capacity of tMN BMSC 153
5.3. DISCUSSION..... 158
CHAPTER 6: SENOLYTIC THERAPIES CAN RESTORE DEFECTIVE ADIPOGENIC AND OSTEOGENIC DIFFERENTIATION OF TMN BMSC 162

6.1. INTRODUCTION 163

6.1.1. Inhibition of SASP using Senomorphic Agents 163

6.1.2. Selective Elimination of Senescent Cells using Senolytic Agents 165

6.2. RESULTS 168

6.2.1. Effect of Dose Titration of Senolytic Agents on Morphology and Viability in Healthy BMSC 168

6.2.2. Reduced Senescence Burden in tMN BMSC after Treatment with Senolytic Agents 172

6.2.3. *In vitro* Culture with Senolytic Agents Restores tMN BMSC Adipogenic Differentiation Capacity 173

6.2.4. *In vitro* Culture with Senolytic Agents Reduced Aberrantly Excessive Osteogenic Differentiation Capacity in tMN BMSC 174

6.3. DISCUSSION 175

CHAPTER 7: LONG-TERM IRREVERSIBLE DAMAGE TO BM MICROENVIRONMENT IS INDUCED BY CT 178

7.1. INTRODUCTION 179

7.2. RESULTS 185

7.2.1. Cytotoxic Therapy Affects Proliferative Capacity of BMSC 185

7.2.2. Irreversible Long-term Cytotoxic Therapy- induced Senescence in BMSC 187

7.2.3. Defective Adipogenic and Osteogenic Potential of BMSC Occurring after CT 188

7.3. DISCUSSION 190

CHAPTER 8: DISCUSSION AND FUTURE DIRECTIONS 192

8.1. GENERAL DISCUSSION 193

8.2. FUTURE DIRECTIONS 198

8.2.1. To Provide Direct Evidence for Role of Senescence in Cytotoxic Therapy- induced BMSC Dysfunction by Eliminating Senescent Cells 199
8.2.2. To Explore the Connection Between Metabolism and BMSC Function 200
8.2.2.1. Manipulation of Metabolic Enzymes Selected from RNA-seq Analysis 200
8.2.2.2. Assessing Lipid Metabolism 200
8.2.3. To Determine whether Specific Type of Cancer and Cytotoxicity Result in Specific BMSC Phenotypes 201
8.2.4. To Assess the Impact of Pathogenic Germline Mutations on tMN BMSC 201
8.2.5. To Evaluate BM Niche Forming Capacity in NSG Mice by Developing a Humanised Ossicle Model of tMN BMSC and Healthy Controls 202
8.2.6. To Correlate BM Microenvironment and Engraftment Kinetics and Outcome in Allogeneic Transplantation 202
CHAPTER 9: REFERENCES 204

DECLARATION

I certify that this work contains no material which has been accepted for the award of any other degree or diploma in my name, in any university or other tertiary institution and, to the best of my knowledge and belief, contains no material previously published or written by another person, except where due reference has been made in the text. In addition, I certify that no part of this work will, in the future, be used in a submission in my name, for any other degree or diploma in any university or other tertiary institution without the prior approval of the University of Adelaide and where applicable, any partner institution responsible for the joint award of this degree. I acknowledge that copyright of published works contained within this thesis resides with the copyright holder(s) of those works. I also give permission for the digital version of my thesis to be made available on the web, via the University's digital research repository, the Library Search and also through web search engines, unless permission has been granted by the University to restrict access for a period of time.

I acknowledge the support I have received for my research through the provision of an Australian Government Research Training Program Scholarship.

Signed

Monika Kutyna

Date: 11/10/2022

ACKNOWLEDGEMENTS

The work described in this thesis was funded by the Faculty of Health Sciences Divisional Scholarship, University of Adelaide; Dawes Top-Up Scholarship, Royal Adelaide Hospital and Grant Funded Short-Term Scholarship, SAHMRI.

First, I would like to direct my extreme appreciation to both of my supervisors, Professor Stan Gronthos and A/Professor Devendra Hiwase. Thank you both for giving me the opportunity to do PhD with you. Without both of you I won't be able to start my scientific journey. I highly appreciate and recognised that. To Stan, thank you being very organised and timing very well my progression during PhD, which was also very crucial for the thesis to be edited and submitted in the timely manner. You always found time to provide your input on the chapters of my thesis within exceptional one to two days. To Devendra, thank you for believing in me and giving me a lot of freedom to design and drive my PhD research. I highly appreciate your thorough and valuable insight into the content of the manuscript and thesis. Despite your extremely busy clinical and other commitments schedule, you have been critical for the success of my publication and my PhD.

Huge thanks to all the patients and their families for generously providing samples for this study. Without you, this work would not have been possible.

The work detailed within this thesis would not have been possible without significant help from several people. Huge thanks to A/Professor Dan Thomas, I greatly appreciate his extraordinary guidance and valuable advice he provided during my PhD. Thanks to Dr Chung Kok for his help with RNA sequencing analysis with his extraordinary bioinformatic skills. To Professor

Sharad Kumar and Dr Yoon Lim for their assistance with westerns blots and expertise advice their provided for the manuscript.

My thanks are also to my “work family” both past and present, Agnes, Amilia, Chloe, Deepak, Jo, Julie, Kelly, Liz, Michaela, Michelle, Rakchha, Shazzy and Sue for their constant support, encouragement, excellent atmosphere they have created in the office and beyond and friendship through low and high of my PhD. I truly appreciate it!

I would like to also thank my close friends and their respective families, especially Adele, Agnieszka, Aneta, Ania, Asia, Bozena, Ella, Jess, Jowita, Kate, Katie, Natacha, and Magda for their constant support through laughs and cries over last few years either with glass of wine or without 😉. Special thank goes to Bron, my PhD “partner” and friend, thank you for all the chats about PhD experience and life in general, endless coffees and just for being there for me. You guys are the best!

My immense gratitude to my family back in Poland, my Mum Ewa, my auntie Malgosia, my cousin Agnieszka and my parents in law, Wiesia and Mieciu. They have supported me, believing in me, and helped me enormously, each of them in different way. I’ll never forget your support and kindness! DZIEKUJE!

Lastly but foremost, I would like to direct my biggest thank to my amazing husband Darek and my beautiful kids, Dominik and Mela. I greatly appreciate your patience, enormous dedication, help, friendship, and tremendous understanding during the period of this research. You have been main drive behind this research and my main mental strength! Without your constant support, and encouragement, this work would not have been possible! To my sweet, precious,

little Mela, your constant affection, millions cuddles and kisses, little love notes you left me, gave me enormous strength and motivation each day. To my thoughtful, gorgeous in wide range of this word son Dominik, your caring nature, friendship, kindness, endless cuddles, again were inspiring me each day. To my darling husband Darek, you did amazing job by keeping our family together through my long hours at work (both at institute and home), being everything, I and kids needed! Words cannot express how much this mean to me. Darek, Dominik and Mela, thank you for being there and seeing me through, “family business” for now and always. I love you very much! THIS IS FOR YOU!!!!

ABBREVIATIONS

17-AAG	17-allylamino-17-demethoxy-geldanamycin
17-DMAG	17-dimethylaminoethylamino- 17-demethoxygeldanamycin
2DG	2-deoxy-d-glucose
7AAD	aminoactinomycin D
ABC	ATP-binding cassette
ACD	acid citrate-dextrose
ADIPOQ	adiponectin
ADP	adenosine diphosphate
ACAN (AGC1)	aggrecan
ALL	acute lymphoblastic leukaemia
ALP	alkaline phosphatase
AML	acute myeloid leukaemia
AMP	adenosine monophosphate
AMPK	AMP-activated protein kinase
ANGPT1	angiopoietin 1
ANKRD26	ankyrin repeat domain-containing protein 26
aP2 (FABP4)	adipocyte protein 2 (fatty acid-binding protein 4)
AP-1	activator protein 1
APC	adenomatous polyposis coli
ARSB	arylsulfatase B
Allo-HSCT	allogeneic haematopoietic stem cells transplant
Auto-HSCT	autologous haematopoietic stem cells transplant
ASXL1	additional sex combs like-1

ATM	ataxia telangiectasia mutated
ATP	adenosine triphosphate
ATR	ataxia telangiectasia and RAD3
B-ALL	B-cell acute lymphoblastic leukaemia
BARD1	BRCA1-associated RING domain 1
bp	base pair
BCL	B-cell lymphoma
BCORL1	B-cell lymphoma 6 corepressor like 1
BFU-E	burst forming unit-erythroid
BM	bone marrow
BMNC	bone marrow mononuclear cells
BMP	bone morphogenetic protein
BMSC	bone marrow derived mesenchymal stromal cells
BNIP3	B-cell lymphoma-2 interacting protein 3
BRAF	proto-oncogene B-Raf and v-Raf murine sarcoma viral oncogene
BRCA1/2	breast cancer gene 1/2
BSA	bovine serum albumin
BSP	bone sialoprotein
C/CH	cytokines/chemokines
Ca	cancer
Ca2+	calcium
CAFC	cobblestone area-forming cells
CAR	CXCL12-abundant reticular cells
CBL	casitas B-lineage lymphoma
CCL	chemokine (C-C motif) ligand

CCR1	chemokine (C-C motif) receptor type 1
CD36	cluster of differentiation 36
CDK	cyclin dependent kinase
CDKN1A/2A/2B	cyclin dependent kinase inhibitor 1A (p21)/2A(p16)/2B(p15)
cDNA	complementary DNA
CEBP	CCAAT/enhancer binding protein
CFU-F	colony forming unit-fibroblastic cells
CFU-GM	colony forming unit-granulocyte/macrophage
CHK1/2	checkpoint 1/2
CHIP	clonal haematopoiesis of indeterminate potential
CLL	chronic lymphoblastic leukaemia
CM	conditioned media
CML	chronic myeloid leukaemia
CMT	combined modality treatment
COL1	collagen type 1, alpha 1
COL2A1	collagen type 2, alpha 1
COX-2	cyclooxygenase 2
CPD	cumulative population doublings
CRP	reactive C-protein
CT	cytotoxic therapy
CUX1	cut like homeobox 1
CXCL12 (SDF-1)	C-X-C motif chemokine 12 (stromal cell-derived factor 1)
CXCR4	C-X-C chemokine receptor type 4
DAPI	4′,6-diamidino-2-phenylindole
DCF	dichloro fluorescein

DDR	DNA damage response
DDX41	DEAD-box helicase 41
DEPC	diethyl pyrocarbonate
DICER1	Dicer 1, ribonuclease III
DLX5	distal-less homeobox 5
DMEM	Dulbecco's modified Eagle's medium
DMSO	dimethyl sulfoxide
DNA	deoxyribonucleic acid
DNA-SCARS	DNA segments with chromatin alterations reinforcing senescence
DNASE1	deoxyribonuclease I
DNMT3A	DNA methyltransferase 3 alpha
dNTP	deoxyribonucleotide triphosphate
dsDNA	double stranded DNA
DTT	dithiothreitol
Dx	diagnosis
ECAR	extracellular acidification rate
ECM	extracellular matrix
EDTA	ethylenediaminetetraacetic acid
EGF	epidermal growth factor
EGM	establishment growth media
EGR1	early growth response 1
ETV6	ETS variant transcription factor 6
EZH2	enhancer of zeste homolog 2
FA	Fanconi anaemia
FACS	fluorescence-activated cell sorting

FANCB/C/D2/J	FA complementation group B/C/D2/J
FCS	foetal calf serum
FDR	false discovery rate
FGF	fibroblast growth factor
FITC	fluorescein isothiocyanate
FLT3-ITD	fms related receptor tyrosine kinase 3- internal tandem duplication
FOS	Fos proto-oncogene
FOXO4	forkhead box protein O4
FOXO4-DRI	FOXO4-D-retro-inverso
G1	growth 1 phase
GAG	glycosaminoglycan
GAPDH	glyceraldehyde 3-phosphate dehydrogenase
GATA2/4	GATA binding protein 2/4
G-CSF	granulocyte-colony stimulating factor
gDNA	genomic DNA
GLB1	galactosidase beta 1
GM-CSF	granulocyte-macrophage colony-stimulating factor
GNAS	guanine nucleotide binding protein, alpha stimulating complex locus
GNB1	G protein subunit beta 1
GO	gene ontology
GRO	growth-related oncogene
GSEA	gene set enrichment analysis
Gy	Gray
H2AX	H2A histone family member X
γH2AX	phosphorylated form of H2AX

HBSS	Hanks buffered saline solution
HCl	hydrochloric acid
HDCT	high dose chemotherapy
HEPES	4-(2-hydroxyethyl)-1-piperazineethanesulfonic acid
HMGB1	high mobility group box 1
hr	hours
HSC	haematopoietic stem cells
HSCT	haematopoietic stem cells transplant
HSP90	heat shock protein 90
HSPC	haematopoietic stem and progenitor cells
HUVEC	human umbilical vein endothelial cells
ICAM	intercellular adhesion molecule
IDH1/2	isocitrate dehydrogenase (NADP (+)) 1/2
IFITM1	interferon-induced transmembrane protein 1
IFN	interferon
IGF	insulin like growth factor
IGFBP	insulin like growth factor binding protein
IL	interleukin
IMDM	Iscove's modified Dulbecco's medium
	nuclear factor of kappa light polypeptide gene enhancer in B-cells
IκBα	inhibitor, alpha
JAK2	Janus kinase 2
KEGG	Kyoto encyclopedia of genes and genomes
KH_2PO_4	potassium dihydrogen orthophosphate
KRAS/NRAS	Kirsten RAS/neuroblastoma RAS oncogene

L	litre
LDL	low density lipoprotein
LDLRAP1	low density lipoprotein receptor adaptor protein 1
LGRF4	leucine rich repeat containing G protein-coupled receptor 4
LH	low hypodiploid
LIF	leukemia inhibitory factor
LOXL	lysyl oxidase like 1
LPL	lipoprotein lipase
LTC-IC	long-term culture initiating cell
M	molar
mA	milliampere
MACS	magnetic assisted cell sorting
MAPK	mitogen-activated protein kinase
MCP	membrane cofactor protein
MDS	myelodysplastic syndromes
MDS-EB1/2	MDS with excess blasts 1/2
MDS-MLD	MDS with multilineage dysplasia
MDS-RS-MLD	MDS with ring sideroblasts with MLD
ME1	malic enzyme 1
MEF	mouse embryonic fibroblasts
MEK	MAPK/ERK kinase
MFI	mean fluorescence intensity
MGM	maintenance growth media
mg/ml/mm/mM	milligram/millilitre/millimetre/millimolar
MIB1	mind-bomb E3 ubiquitin protein ligase 1

MIP-1/3	macrophage inflammatory protein 1/3
MLL	mixed lineage leukaemia
MM	multiple myeloma
MMP	matrix metalloproteinase
MN	myeloid neoplasms
MOS	MOS-proto-oncogene, serine/threonine kinase
MPN	myeloproliferative neoplasms
mRNA	messenger RNA
MSC	mesenchymal stromal cells
MTMR4	myotubularin related protein 4
mTOR	mammalian target of rapamycin
n	number
NaCl	sodium chloride
NAD+	oxidised form of nicotinamide adenine dinucleotide (NAD)
NADH	reduced form of nicotinamide adenine dinucleotide (NAD) (H for hydrogen)
NADPH	reduced form of nicotinamide adenine dinucleotide phosphate (NADP) (H for hydrogen)
NES	normalised enrichment score
NF-κB	nuclear factor kappa B
ng/nM	nanogram/nanomolar
NHL	non-Hodgkin lymphoma
NOS	nitric oxide synthase
NP	neuropoietin
NPM1	nucleophosmin

NSG	NOD scid gamma
OCN	osteocalcin
OCR	oxygen consumption rate
OIS	oncogene-induced senescence
OPG	osteoprotegerin
OPN	osteopontin
OS	overall survival
OSM	oncostatin M
OSX	osterix
OXPHOS	oxidative phosphorylation
P	passage
p38MAPK	subfamily of MAPK
PAI	plasminogen activator inhibitor
pAML	primary acute myeloid leukaemia
PARG1	poly (ADP-ribose) glycohydrolase 1
PARP	poly ADP ribose polymerase
PBS	phosphate buffered saline
PCNA	proliferating cell nuclear antigen
PCR	polymerase chain reaction
PD	population doublings
PDGF	platelet derived growth factor
PE	phycoerythrin
PI3K-PKB/Akt	phosphoinositide 3 kinase- protein kinase B/Akt
PLT	platelets
pMDS	primary myelodysplastic syndromes

pMN	primary myeloid neoplasms
pMN+Ca	primary myeloid neoplasms + cancer
pmol	picomoles
PNPLA2	patatin-like phospholipase domain containing-2
PPARγ	peroxisome proliferator-activated receptor gamma
PS	phosphatidlyserine
PTGDS	prostaglandin-H2 D-isomerase
PTPN11	tyrosine-protein phosphatase non-receptor type 11
RAF	proto-oncogene c-RAF
RAR-γ	retinoic acid receptor gamma
RAS	rat sarcoma virus oncogene homolog
RB	retinoblastoma
RBC	red blood cells
RFC	replication factor C
RNA	ribonucleic acid
RO	reverse osmosis
ROS	reactive oxygen species
RPA	replication protein A
RT-PCR	real-time polymerase chain reaction
RUNX1/2	runt-related transcription factor1/ 2
SA	South Australia
SAHF	senescence associated heterochromatin foci
SAMD9	sterile alpha motif domain-containing protein 9
SAMD9-L	SAMD9-like
SASP	senescence associated secretory phenotype

SBDS	Shwachman-Bodian-Diamond syndrome
SCF	stem cell factor
SD	standard deviation
SDM	serum deprived media
SDS-PAGE	sodium dodecyl sulphate -polyacrylamide gel electrophoresis
SETBP1	SET binding protein 1
SF3B1	splicing factor 3b subunit 1
SIPA1	signal-induced proliferation-associated 1
SLC44A2	solute carrier family 44-member 2
SOX	SRY-box transcription factor
SRDSA1	steroid 5 alpha-reductase 1
SREBP1	sterol regulatory element-binding protein 1
SRSF2	serine and arginine rich splicing factor 2
STC2	stanniocalcin 2
STRO-1	stromal precursor antigen 1
tAML	therapy-related acute myeloid leukaemia
TBS-T	tris-buffered saline with Tween 20
TCA	tricarboxylic acid
TE	Tris-EDTA
TET2	Tet methylcytosine dioxygenase 2
TGFα/β1/β3	transforming growth factor alpha /beta 1/beta 3
TIS	therapy-induced senescence
tMDS	therapy-related myelodysplastic syndromes
tMN	therapy-related myeloid neoplasms
TNFRSF19	TNF receptor superfamily member 19

TNFα/β	tumour necrosis factor alpha/ beta
TP53	tumour protein p53
TPO	thrombopoietin
TRITC	tetramethylrhodamine
Trp53	mouse p53 tumour suppressor
Tween20	polyethylene glycol sorbitan monolaurate
TXNRD1	thioredoxin reductase 1
U2AF1	U2 small nuclear RNA auxiliary factor 1
UHRF2	ubiquitin like with PHD and ring finger domains 2
VCAM1	vascular cell adhesion molecule 1
VEGF	vascular endothelial growth factor
WCF	white cell fluid
WNT	Wingless-related integration site
WT1	Wilms tumour 1
ZRSR2	zinc finger CCCH-type, RNA binding motif and serine/arginine rich 2
αMEM	αModified Eagle's medium
µg/µl/µm/µM	microgram/ microliter/ micrometre/ micromolar

HONOURS

- Associated Investigator on successful 2021 Ideas Grant- Cancer Australia; Identifying synthetic lethal and microenvironmental targets to improve outcome of therapy-related myeloid neoplasms (APP#2013617)
- American Society of Hematology (ASH) Abstract Achievement Award (2021)
- Haematology Society of Australia and New Zealand Blood 2021 Meeting Grant (2021)
- Adelaide Medical School HDR Research Support Award (2021)
- American Society of Hematology (ASH) Abstract Achievement Award (2020)
- Adelaide Medical School HDR Research Support Award (2020)
- Adelaide Medical School Research Travel Awards (2019)
- Faculty of Health Sciences Divisional Scholarship (2017)
- RAH Research Dawes Top Up Scholarship (2017)

PUBLICATIONS

Scientific Manuscripts

1. **Kutyna MM**, Kok CH, Lim Y, Tran ENH, Campbell D, Paton S, Thompson-Peach C, Lim K, Cakouros D, Arthur A, Hughes T, Kumar S, Thomas D, Gronthos S, Hiwase DK. Senescence stress secretome is a hallmark of therapy-related myeloid neoplasm stromal tissue occurring soon after cytotoxic exposure. **Leukemia 2022**; doi: 10.1038/s41375-022-01686-y.
2. Singhal D, Hahn CN, Feurstein S, Wee LYA, Moma L, **Kutyna MM**, Chhetri R, Eshraghi L, Schreiber AW, Feng J, Wang PP, Babic M, Parker WT, Gao S, Moore S, Das S, Thomas D, Pattnaik S, Brown AL, D'Andrea RJ, Poplawski NK, Thomas D, Scott HS, Godley LA, Hiwase DK. Targeted gene panels identify a high frequency of

pathogenic germline variants in patients diagnosed with a hematological malignancy and at least one other independent cancer. **Leukemia 2021**; doi: 10.1038/s41375-021-01246-w.

3. Singhal D, Wee LYA, **Kutyna MM,** Chhetri R, Geoghegan J, Schreiber AW, Feng J, Wang PP, Babic M, Parker WT, Hiwase S, Edwards S, Moore S, Branford S, Kuzmanovic T, Singhal N, Gowda R, Brown AL, Arts P, To LB, Bardy PG, Lewis ID, D'Andrea RJ, Maciejewski JP, Scott HS, Hahn CN, Hiwase DK. The mutational burden of therapy-related myeloid neoplasms is similar to primary myelodysplastic syndrome but has a distinctive distribution. **Leukemia 2019**; doi: 10.1038/s41375-019-0479-8.

Conference Proceedings

1. **Kutyna MM**, Kok CH, Lim Y, Tran ENH, Campbell D, Paton S, Thompson-Peach C, Lim K, Cakouros D, Arthur A, Hughes T, Kumar S, Thomas D, Gronthos S, Hiwase DK. Senolytics can restore function of profoundly senescent tMN bone marrow stroma. **Haematology Society of Australia and New Zealand (Blood) Conference, Sydney, Australia, September 2022 (oral presentation).**
2. **Kutyna MM**, Kok CH, Campbell D, Paton S, Lim K, Cakouros D, Arthur A, Hughes T, Kumar S, Thomas D, Gronthos S, Hiwase DK. Therapy-related myeloid neoplasm has profoundly senescent stroma and adipogenic defect occurring soon after cytotoxics. **New Directions in Leukemia Research (NDLR) Conference, Brisbane, Australia, June 2022 (poster presentation).**
3. **Kutyna MM**, Kok CH, Paton S, Cakouros D, Arthur A, Hughes T, Thomas D, Campbell D, Gronthos S, Hiwase DK. Distinct Senescent Bone Marrow Microenvironment in Therapy-Related Myeloid Neoplasms. **ASH Annual Meeting, New Orleans, USA, December 2021 (poster presentation).**

4. **Kutyna MM**, Kok CH, Paton S, Cakouros D, Arthur A, Hughes T, Thomas D, Campbell D, Gronthos S, Hiwase DK. Bone Marrow Microenvironment in Therapy-Related Myeloid Neoplasms is distinct from other Myeloid Neoplasms, probably driven by prior Cytotoxic Therapy. **17th International Congress on Myelodysplastic Syndromes (MDS), Toronto, Canada, September 2021 (oral presentation).**
5. **Kutyna MM**, Kok CH, Paton S, Cakouros D, Arthur A, Hughes T, Thomas D, Campbell D, Gronthos S, Hiwase DK. Therapy-related myeloid neoplasm has a distinct bone marrow microenvironment, probably induced by prior cytotoxic therapy. **Blood Conference, Adelaide, Australia, September 2021 (oral presentation).**
6. **Kutyna MM**, Kok CH, Paton S, Cakouros D, Arthur A, Hughes T, Thomas D, Campbell D, Gronthos S, Hiwase DK Senescent bone marrow microenvironment in therapy-related myeloid neoplasms. **SAHMRI Research Showcase, Adelaide, Australia, October 2021 (poster presentation).**
7. **Kutyna MM**, Wee LYA, Paton S, Cakouros D, Arthur A, Chhetri R, Schreiber A, Hoow Kok C, Singhal D, Thomas D, Hughes T, Campbell D, Gronthos S, Hiwase DK. Therapy-related myeloid neoplasm has a distinct pro-inflammatory bone marrow microenvironment and delayed DNA damage repair. **ASH Annual Meeting, San Diego, USA, December 2020 (oral presentation)**.
8. **Kutyna MM**, Wee LYA, Paton S, Cakouros D, Arthur A, Chhetri R, Singhal D, Gronthos S, Hiwase DK. Aberrant bone marrow microenvironment in therapy-related myeloid neoplasms. **14th Annual Florey Postgraduate Research Conference, Adelaide, Australia, September 2020 (poster presentation).**
9. **Kutyna MM**, Wee LYA, Paton S, Cakouros D, Arthur A, Chhetri R, Singhal D, Gronthos S, Hiwase DK. Therapy-related myeloid neoplasm has a distinct pro-inflammatory bone marrow microenvironment and delayed DNA damage repair.

Annual Australian Society for Medical Research (ASMR) Meeting, Adelaide, Australia, June 2020 (poster presentation).

10. **Kutyna MM**, Wee LYA, Paton S, Cakouros D, Arthur A, Chhetri R, Singhal D, Gronthos S, Hiwase DK. Aberrant bone marrow microenvironment in therapy-related myeloid neoplasms. **Cancer in SA Translational Research Meeting 2020, Adelaide, Australia, March 2020 (oral presentation).**
11. **Kutyna MM**, Wee LYA, Paton S, Cakouros D, Arthur A, Chhetri R, Singhal D, Gronthos S, Hiwase DK. Aberrant Bone Marrow Microenvironment in Therapy Related Myeloid Neoplasm. **ASH Annual Meeting, Orlando, USA, December 2019 (poster presentation).**
12. **Kutyna MM**, Wee LYA, Paton S, Cakouros D, Arthur A, Chhetri R, Singhal D, Gronthos S, Hiwase DK. Aberrant Bone Marrow Microenvironment in Therapy Related Myeloid Neoplasm. **International Society for Experimental Hematology (ISEH)Meeting, Brisbane, Australia, August 2019 (poster presentation).**
13. **Kutyna MM**, Wee LYA, Paton S, Cakouros D, Arthur A, Chhetri R, Singhal D, Gronthos S, Hiwase DK. Aberrant Bone Marrow Microenvironment in Therapy Related Myeloid Neoplasm. **13th Annual Florey Postgraduate Research Conference, Adelaide, Australia, September 2019 (poster presentation).**
14. Singhal D, Hahn CN, Wee LYA, Kerr C, **Kutyna MM**, *et al.* & Hiwase DK. Genetic Predisposition to Therapy-Related Myeloid Neoplasm By Rare, Deleterious Germline Variants in DNA Repair Pathway and Myeloid Driver Genes. **ASH Annual Meeting, San Diego, USA, December 2018 (poster presentation).**

ABSTRACT

Therapy-related myeloid neoplasm (tMN), lethal blood cancer developing in long-term cancer survivors, is considered to be direct consequence of cytotoxic therapy-induced DNA damage in haematopoietic stem cells. Despite increased recognition that altered bone marrow stroma can also drive leukemogenesis, the functional biology of tMN bone marrow microenvironment remains unknown. Comprehensive multiomic (transcriptome, DNA damage response, cytokine secretome and functional profiling) characterisation of bone marrow stromal cells from tMN was performed and compared with (i) patients with myeloid neoplasm and a history of another cancer but *without* cytotoxic exposure, (ii) typical primary myeloid neoplasm and (iii) age-matched controls, to decipher bone marrow microenvironmental changes induced by cytotoxics from that age related and myeloid neoplasm induced changes.

tMN bone marrow mesenchymal stromal cells exhibited profound senescence with *CDKN1A* induction, high levels of β-Galactosidase, aberrant morphology, defective proliferation, differentiation and haematopoietic stem cell supportive capacity. Highly senescence phenotype is probably driven by defective DNA repair capacity. Strikingly, despite their dormant state, tMN stromal cells were metabolically highly active with a switch towards glycolysis and secreted multiple pro-inflammatory cytokines indicative of a senescent-secretory phenotype that inhibited adipogenesis. Critically, senolytics not only eliminated dormant cells, but also restored adipogenesis. Finally, sequential patient sampling showed senescence phenotypes are induced within months of cytotoxic exposure, well prior to the onset of secondary cancer.

This thesis provides novel insight into role of pro-inflammatory and senescent stromal milieu to tMN pathogenesis and provide a valuable resource for future strategies to delay/prevent the tMN.

Chapter 1: Introduction

1.1. NORMAL HAEMATOPOIESIS

Haematopoiesis is a life-long process involve self-renewal, commitment and differentiation of pluripotent haematopoietic stem cells (HSC) and progenitor cells to mature blood cells [1]. Haematopoiesis arises in adults mainly in the bone marrow (BM) (medullary), but it can also occur in the other tissues for example the thymus, spleen, and liver (extramedullary). Remarkably, the HSC from different sites have discrete features, indicating the diversity in the supporting microenvironment and in the intrinsic properties of HSC at each developmental phase (Figure 1.1). HSC comprise less than 0.01% of cells in the BM [1, 2] and enforced to constantly self-renew and differentiate to replace the short-lived progenitor and mature blood cells. There are several different types of mature cells, such as red blood cells (RBC), megakaryocytes, myeloid cells (monocytes/macrophage and neutrophil) and lymphocytes [3].

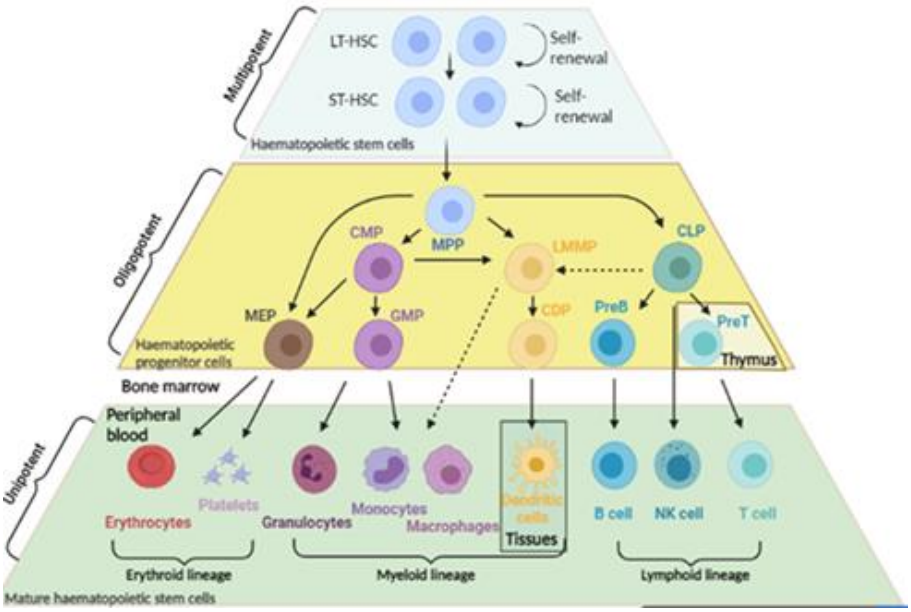


Figure 1.1. Model of human haematopoietic hierarchy consists of multipotent, oligopotent and unipotent cell types.

Abbreviations: LT-HSC, long-term haematopoietic stem cells; ST-HSC, short-term haematopoietic stem cells; MPP, multipotent progenitors; CMP, common myeloid progenitors; CLP, common lymphoid progenitors; LMMP, lymphoid-primed multipotent progenitor; MEP, megakaryocyte-erythroid progenitor; GMP, granulocyte-macrophage progenitor; CDP, common dendritic cell progenitor.

1.2. INTRODUCTION TO MYELOID MALIGNANCIES

Myeloid malignancies (myeloid neoplasms; MN) are a heterogeneous group of clonal disorders, outlined by enhanced proliferation, impaired self-renewal and /or differentiation defects of haematopoietic cells and myeloid progenitor cells. Myeloid neoplasms include myeloproliferative neoplasms (MPN), myelodysplastic syndromes (MDS) and acute myeloid leukaemia (AML) (Figure 1.2).

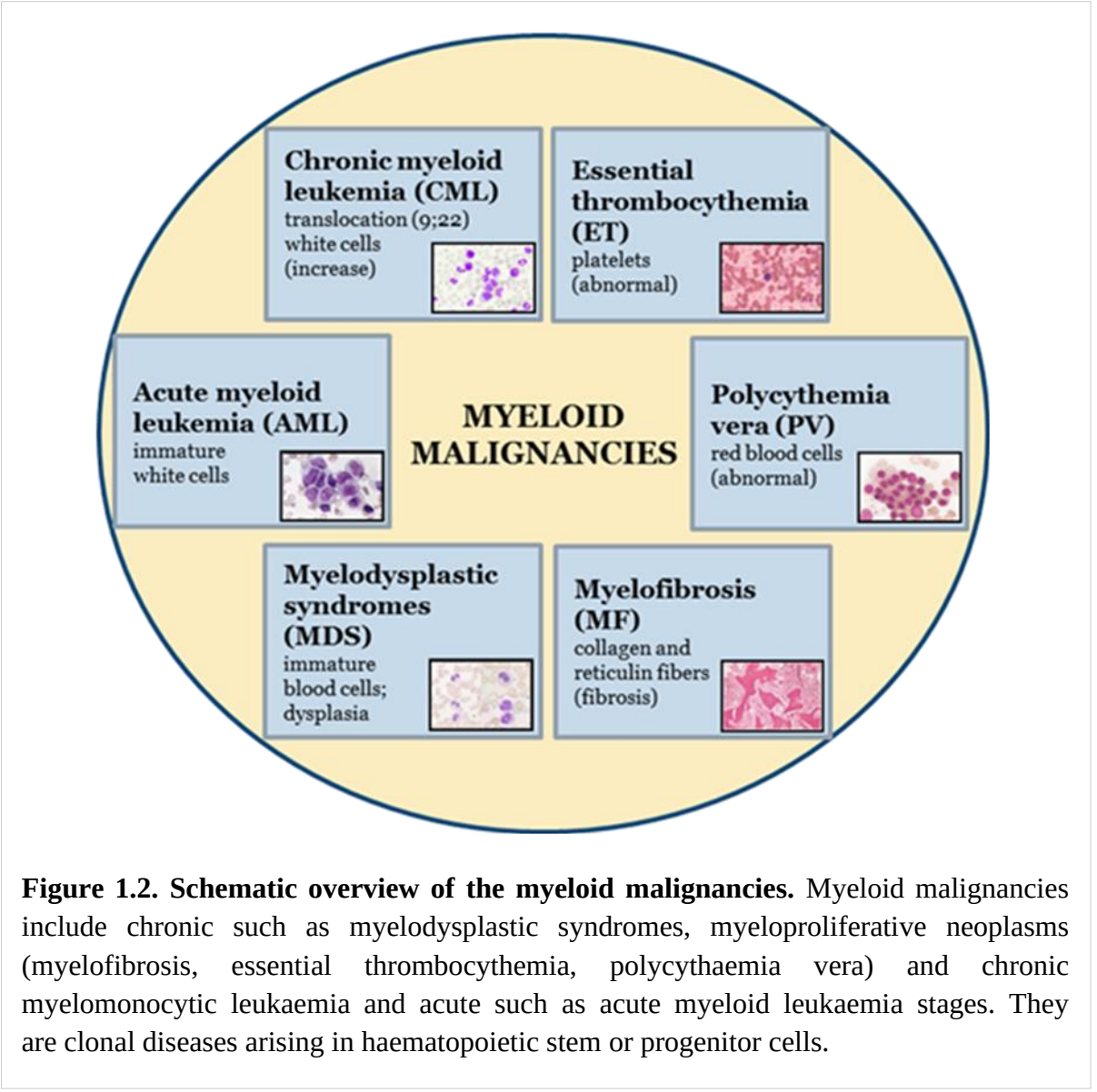


Figure 1.2. Schematic overview of the myeloid malignancies. Myeloid malignancies include chronic such as myelodysplastic syndromes, myeloproliferative neoplasms (myelofibrosis, essential thrombocythemia, polycythaemia vera) and chronic myelomonocytic leukaemia and acute such as acute myeloid leukaemia stages. They are clonal diseases arising in haematopoietic stem or progenitor cells.

1.2.1. Myelodysplastic Syndromes

MDS are amongst the most common haematologic cancers in patients over 70 years of age with median overall survival (OS) 12-15 months in higher risk MDS cases [4, 5]. The annual rate of MDS ranges from 2–12 cases per 100,000 people, however surges to 50 cases per 100,000 among persons aged 70 or older [6]. Importantly, Azacitidine, the only approved therapy for higher risk MDS cases, prolongs median survival by 9 months only (15 months in conventional care versus 24 months in patients treated with Azacitidine) and only 17% of treated patients achieve complete response [7]. However, while allogeneic haematopoietic stem cell transplantation (allo-HSCT) is a possibly curative therapy, ~10-15% patients are eligible for this treatment. The current therapeutic options in lower risk patients (Low and Intermediate-1 risk) rely largely on symptomatic management of cytopaenia, mainly RBC and/or platelets (PLT) transfusions [8]. The limited therapeutic choices in MDS stems from a poor understanding of molecular processes underlining the disease. MDS are a heterogeneous group of clonal HSC diseases characterised by peripheral cytopaenia, dysplasia, ineffective haematopoiesis, and a high propensity to transform into AML [9]. They display marked heterogeneity in degree of cytopaenia, morphology and clinical course leading to difficulties in accurate diagnosis and choice of optimal therapeutic regime, and uncertainties in reliable prognosis for the patient. In the majority of MDS cases, the BM is hypercellular or normocellular, however the BM is hypocellular in 10-20% of MDS cases [10-12] (defined as BM cellularity < 30% in patients ≤ 60 years or < 20% in > 60 years) [13, 14].

1.2.2. Acute Myeloid Leukaemia

AML is one of the most frequent myeloid neoplasm in adults with an incidence of ~ 3.7 cases per 100,00 people causing up to 180,00 deaths per annum world-wide [15, 16]. The median age of patients at diagnosis is 70 years who typically present with pancytopaenia, which is a key cause of morbidity and mortality in these patients. There is also a decrease of normal HSC of myeloid and lymphoid lineages in the BM. Additionally, BM is governed by a leukemic blast population; immature myeloid cells due to persistent and deregulated proliferation and survival in addition to a block in differentiation [15-17]. Chemotherapy and allo-HSCT are the most effective treatments presently available, where 80% of patients undergo complete remission, however approximately 75% relapse within 2 years of remission [16, 18-20].

1.3. THERAPY-RELATED MYELOID NEOPLASMS OVERVIEW

Therapy-related myeloid neoplasm (tMN) is a lethal haematological malignancy diagnosed following exposure to cytotoxic therapy such as chemotherapy and radiotherapy (CT) for primary cancers or autoimmune diseases, according to the 2016 World Health Organisation classification [21] (Figure 1.3). Those primary cancers could be haematological such as multiple myeloma (MM) or non-Hodgkin lymphoma (NHL) or solid cancers such as breast or prostate [22]. It accounts for 10-20% of patients with MDS and AML [23]. Around 70% of tMN present as therapy-related MDS (tMDS) while 30% as therapy-related AML (tAML) [22] (Table 1.1). tMN patients tend to be younger than primary MDS (pMDS) and primary AML (pAML). tMN is characterised by cytogenetic abnormalities including complex karyotype, chromosome 5 and 7 deletion and almost 1/3rd patients harbor *TP53* mutations [22, 24].



Figure 1.3. Schematic overview of tMN patient disease development journey. tMN is a haematological malignancy following exposure to cytotoxic therapies for other, unrelated cancers.

Table 1.1. Comparison of primary- and therapy-related myeloid neoplasms

	pMN	tMN	
	(pMDS and pAML)	tMDS	tAML
Median age (years)	70-75	64	
Percentage of all MDS and AML cases	80-90%	10-20%	
Frequency according to all tMN cases	NA	70%	30%
Prior exposure to DNA damaging cytotoxic therapies	No	Yes	
Interval between exposure to cytotoxic therapies and tMN diagnosis	NA	5-7 years	2-3 years
Bone marrow cytogenetic abnormalities	50% normal karyotype Common abnormal karyotypes: del(20q), -Y, del(5q), +8	-7/del(7q), -5/del(5q) Complex karyotype	t(11q23.3), t(21q22.1) Complex karyotype

Abbreviations: pMN, primary myeloid neoplasms; pMDS, primary myelodysplastic syndromes; pAML, primary acute myeloid leukaemia; tMN, therapy-related myeloid neoplasms; tMDS, therapy-related myelodysplastic syndromes; tAML, therapy-related acute myeloid leukaemia; NA, non-applicable.

Adapted from McNerney *et al.* [22]

Though tMN is rare, it occurs with high frequency in some cancers. For example, the risk of tMN ranges from 0.2-1.1% in patients with breast cancer to 6-24.3% in patients who had autologous haematopoietic stem cell transplantation (auto-HSCT) for non-Hodgkin lymphoma [25, 26]. With an ageing population and increasing long-term survival of cancer patients, the incidence of tMN is rising (Figure 1.4A). According to the Australian Institute of Health and Welfare, an additional 150,000 new cases of cancer were estimated to be diagnosed in 2020 and almost 1.1 million people (4.6% of the Australian population) are estimated to be alive after their cancer diagnosis [27].

Survival of tMN patients is dismal with median survival <12 months [28, 29] (Figure 1.4B) and no effective therapeutic options. Although allo-HSCT is a potential cure, it is offered to only < 10% of tMN patients and is associated with high transplant-related complications and mortality. Hence, there is an urgent and unmet need to understand the pathogenesis of tMN with the aim to prevent and develop novel therapies to improve outcome.

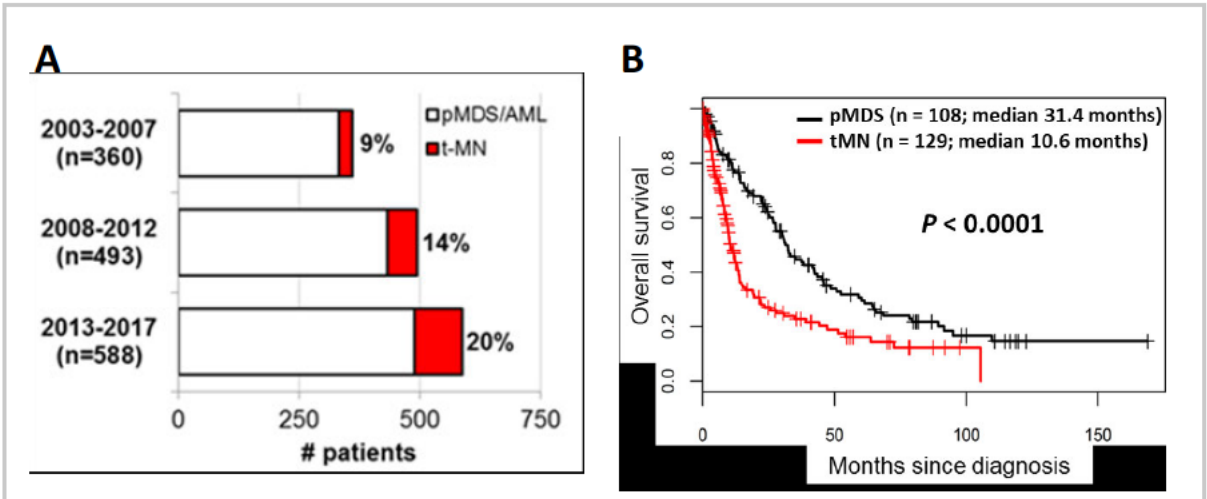


Figure 1.4. tMN epidemiology. (A) Increase incidence of tMN in South Australia based on data from SA-MDS Registry; (B) the overall survival of tMN patients is poorer compared to primary MDS (pMDS).

1.4. ROLE OF HAEMATOPOIETIC STEM CELLS IN tMN PATHOGENESIS

There are numerous pathways that may lead to tMN. It has been implied that cytotoxic agents are not the sole cause of tMN. Several risk factors either inherited or acquired may influence whether a patient develops tMN (Figure 1.5).

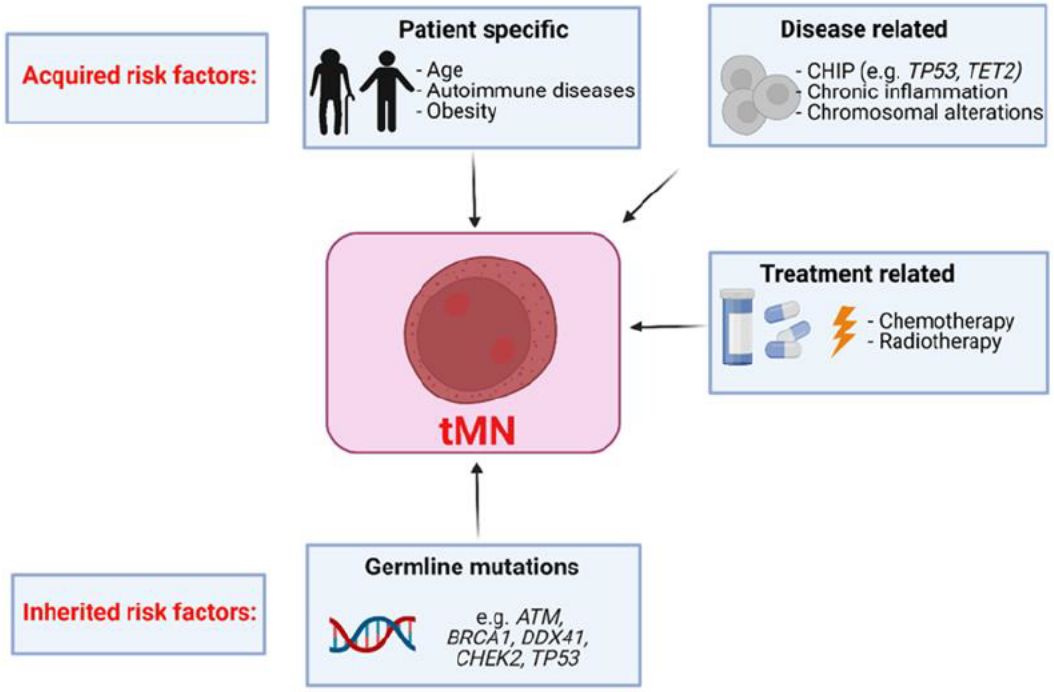


Figure 1.5. Various risk factors for the development of tMN either acquired or inherited.

Abbreviations: CHIP, Clonal Haematopoiesis of Indeterminate Potential.

1.4.1. Inherited Predisposition

Study of the German AML Group demonstrated that 3% of AML patients developed after prior cancer had never been exposed to CT. Their latency time was similar to tAML which was 5 years [30], indicating that some tMN might be cause by an inherited factor. Direct and indirect evidence suggests inherited predisposition to tMN. Many studies show an increased

malignancy risk in families of cancer patients and tMN is not an exception. For example, breast cancer patients with family history of breast/ovarian cancers have an increased secondary leukaemia risk compared to patients without family history and general population [31]. Further, genes in several different pathways including master transcription factors significant in lineage development are affected by germline variants such as runt-related transcription factor (*RUNX1),* CCAAT/enhancer binding protein alpha *(CEBPα), DDX41, GATA2, ANKRD26, ETV6 or SAMD9/SAMD9-L* [32-34] and, more recently, in DNA repair genes have been reported in myeloid neoplasms [35-38] (Figure 1.6) .

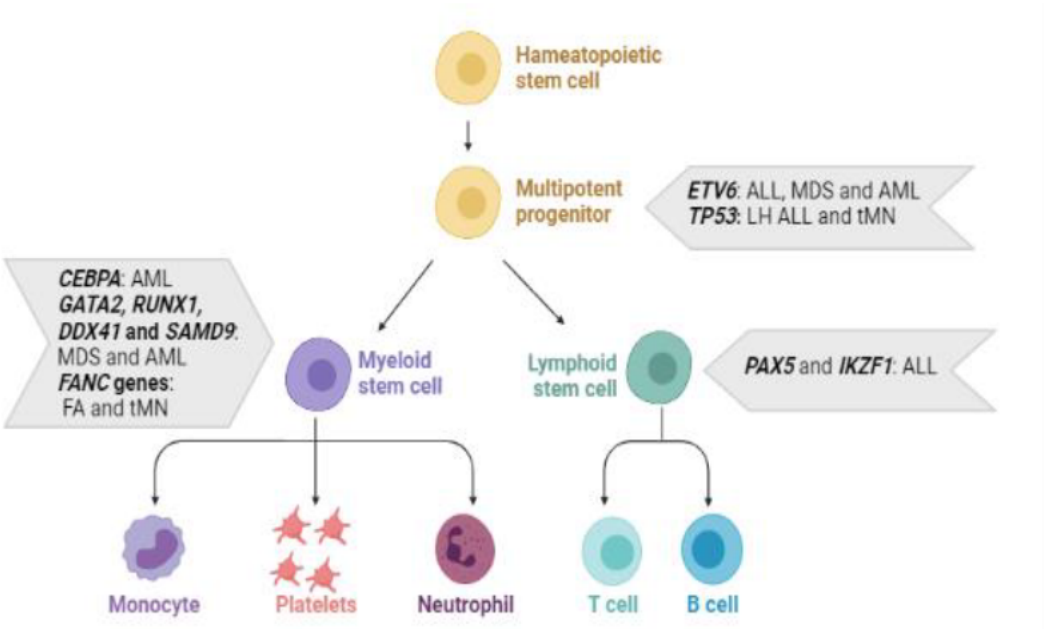


Figure 1.6. Relationship between germline variants and blood lineage development. Schematic overview shows the main blood lineages which are dysregulated in patients with germline variants. Germline mutations in *ETV6* and *TP53* can results in development of haematopoietic neoplasms (ALL, MDS, AML or tMN) in both myeloid and lymphoid lineages, whereas other germline variants are more lineage dependent such as *CEBPA*, *GATA2*, *RUNX1*, *DDX41* and *FANC* genes in myeloid neoplasms and *PAX5* and *IKZF1* in lymphoid neoplasms.

Abbreviations: ALL, acute lymphoblastic leukaemia; MDS, myelodysplastic syndromes; AML, acute myeloid leukaemia; LH, Low hypodiploid, tMN, therapy-related myeloid neoplasm; FA, Fanconi Anaemia.

Adapted from Klco *et al.* [39]

Other inherited BM failure syndromes such as Fanconi Anaemia (FA), Diamond-Blackfan anaemia or Shwachman-Diamond syndrome can lead to the development of MN. FA pathway proteins are required to maintain genomic integrity in HSC by orchestrating a DNA damage response to repair lesions associated with endogenous and exogenous interstrand crosslinks. FA is a rare (1 in 100,000 births) chromosomal instability disorder caused by homozygous germline variants in one of the FA genes. Importantly, patients with FA have cellular hypersensitivity to DNA cross-linking agents, with 800-fold increased risk of developing MDS and AML [40, 41]. Although it does not lead to FA, heterozygous germline variants in FA pathway genes have been shown to be implicated in other malignancies. Notably, in *BRCA1* and *BRCA2* mutation carrier females, the risk of developing breast and ovarian cancer is 40-87% and 27-84% respectively [42, 43]. Similarly, the risk of prostate cancer is significantly higher in male carriers of *BRCA2* [44, 45]. It is estimated that between 16 to 21% of tMN patients have a germline cancer predisposing mutation [46-48]. Most frequently identified germline mutations in tMN patients are *FANC* genes, *BRCA1*, tumour protein p53 (*TP53), BARD1, BRCA2, CHEK2* and *DDX41* [49-55] (Figure 1.7).

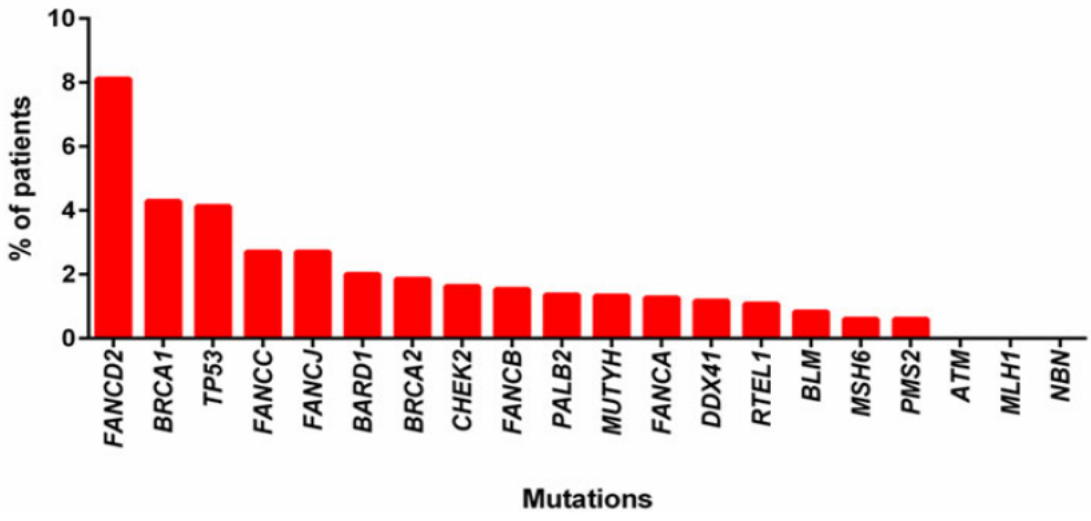


Figure 1.7. Germline mutations frequency in tMN patients.

Based on seven major studies [49-55]

1.4.2. Acquired Risk Factors

1.4.2.1. Patient-related factors

Patients diagnosed with tMN tend to be younger compared to primary MN (pMN), with median age of 64 years [56, 57] compared with 71 years in MDS [58] and 68 years in AML [59], however the disease can occur at any age, as young as 20 and as old as 97 years old [56, 60]. Although the incidence of tMN increases with age, 0.02/100,000 individuals of 20-39 years to 0.39/100,000 of 60-79 years of age [56], the impact of ageing is more complex and influenced by primary cancer histology and treatment. The risk of tMN is higher in MM and NHL patients > 55 years of age at the time of auto-HSCT, compared to younger patients [61, 62]. While the risk of tMN is higher in younger breast cancer patients treated with chemotherapy compared to patients older than 65 years of age [56-58].

Furthermore, some comorbidities such as autoimmune diseases are at a greater risk of developing myeloid neoplasms in patients, which is owed to both use of immunosuppressive agents and underlying immune dysregulation [63, 64]. In a large dataset of 40, 011 patients with autoimmune conditions, 86 patients subsequently developed MDS or AML more than 1 month after an autoimmune disease diagnosis and majority 66.3% (57/86) of these patients had cytotoxic or an immuno-modulating agent prior to diagnosis of MDS/AML. Rheumatoid arthritis (26.7%), psoriasis (20.9%), and systemic lupus erythematosus (14.0%) were the most common autoimmune conditions in AML/MDS patients, and median time of onset, from autoimmune disease diagnosis to myeloid neoplasm, was 8 (range 4-15) years [65]. Similarly obesity, has been related to increase of AML incidence after MM diagnosis [62], which could be due to obesity -associated chronic inflammation [66, 67]. Obesity has also been previously associated with unfavourable cytogenetics in tMN [68].

1.4.2.2. Acquired genetic predisposition to tMN

Approximately 10% of individuals ≥ 70 years of age, without haematological abnormalities, harbour somatic mutations in genes known to drive myeloid malignancies [69-72]. Clonal haematopoiesis at variant allele frequency > 2% in individuals without haematological malignancies is defined as clonal haematopoiesis of indeterminate potential (CHIP). Frequency of CH increases with ageing population and almost 20% individual > 90 years of age harbour CH [71, 72]. The majority of CHIP mutations are thought to occur in HSC [73, 74], can undergo clonal expansion over time [70, 75] and associated with increased risk of developing haematological malignancy, by almost 13-fold, cardiovascular event and all-cause mortality.

Frequency of CHIP in cancer patients is significantly higher than healthy individual > 70 years of age (20-30% versus 10%) [73, 76-79] and is associated with increased risk of progression to tMN following cytotoxic exposure [78-80], as CHIP is reported in 54-71% of tMN patients at the time of primary diagnosis, prior to receiving CT [73, 77-79]. Nearly 30% (120/401) of lymphoma patients harboured CHIP at the time of auto-HSCT and was associated with an increased risk of tMN five-years post auto-HSCT (7.4% versus 1.7%) [81]. Interestingly, AML-associated mutations were detected in 97% of tested AML patients up to 22 years before AML diagnosis [82]. Moreover, the risk of progression to tMN depends on the gene in which a mutation occurs [83, 84] and type of genotoxic stress. For example, *TP53* mutations exhibit fitness advantage and selectively expand during genotoxic stress induced by cytotoxic therapies [54] while DNMT3A clones expand during stress of self-renewal following stem cell transplant. Similarly, *PPM1D* mutations confer selective advantage and expands during genotoxic stress. Selective expansion these clones under genotoxic stress contribute to high frequency of *PPM1D* (~20%) and *TP53* (~35%) mutations in tMN [85].

1.4.2.3. Treatment-related factors

1.4.2.3.1 Direct impact of cytotoxics on HSC

Currently, AML, MDS and tMN are considered to be HSC-autonomous disorders, in which initiation and progression are mainly driven by HSC-intrinsic genetic events [29, 86-91]. Chemotherapy/radiotherapy may induce genome-wide DNA damage (loss of genetic material, genomic and chromosomal instability, mutation inducement), and eventually malignant transformation. These mutations give advantage to abnormal proliferation over normal haematopoiesis, causing stem cells exhaustion and accumulation of genomic instability, supporting leukaemic cells [92]. Somatic mutation frequency in tMN is highly variable ranging 42 to 94% [89-91, 93]. We reported that though frequency of somatic mutations is similar between tMN and pMN, mutation pattern is distinct [29] (Figure 1.8). Whole-genome and targeted-sequencing studies indicated that *TP53* is the most mutated gene in tMN patients [29, 54, 89, 90], occurring between 23 to 37% tMN patients. Other genes with mutational load above 5% include: *DNMT3A, ABC* family, *ASXL1*, *RUNX1*, *TET2*, *SRSF2*, *NRAS, NPM1*, *FLT3-ITD, KRAS* and *PTPN11*. There are some differences in mutation's frequency between tMDS and tAML, such as *RUNX1* and *ASXL1* are more mutated in tMDS compared to tAML. Until recently somatic mutations in HSC were thought to be induced by cytotoxic therapies. This was supported by genomic heterogeneity according to type of cytotoxic therapies such as association between topoisomerase II inhibitor exposure and *MLL* rearrangements [94], complex karyotypes and unbalanced loss of genetic material (related to chromosomes 5 and/or 7) with alkylating agents and radiation [95]. Secondly, high frequency of poor-risk cytogenetics, including complex karyotypes and abnormalities of chromosome 5 and/or 7 in tMN compared to pMN (70% versus 20%). However, recent studies provide paradigm shift by demonstrating *TP53 and PPM1D* mutations were detectable at the time of primary cancer

diagnosis prior to cytotoxic exposure and cytotoxic stress provide microenvironment conducive for clonal expansion and evolution [29, 54, 90, 95].

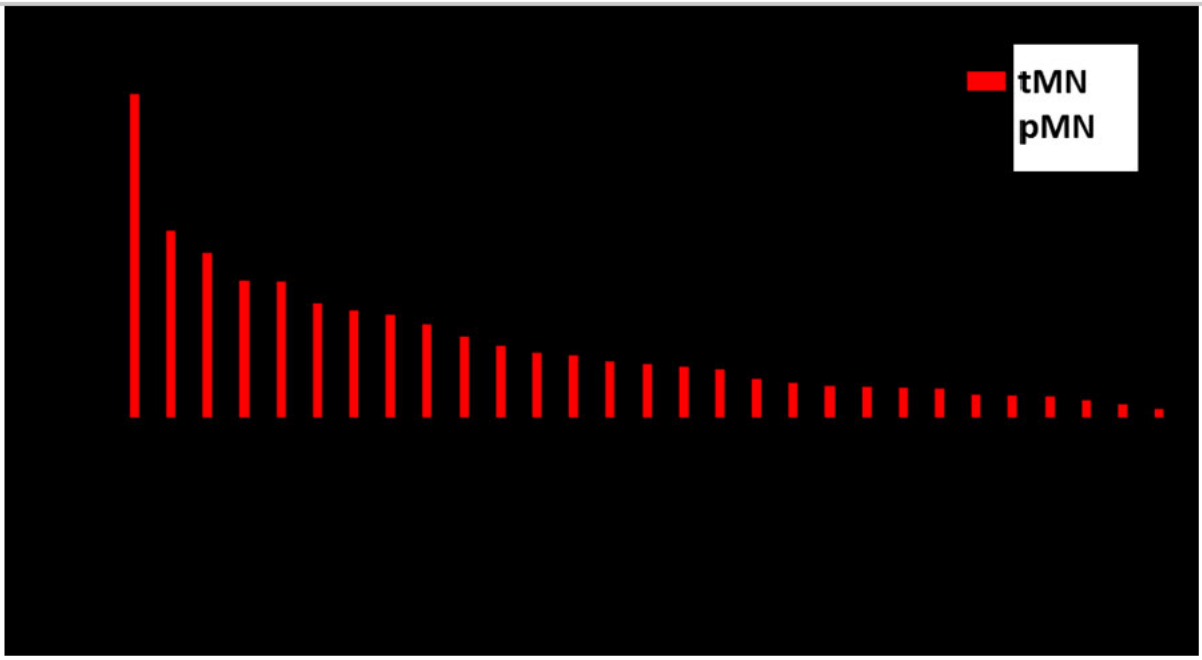


Figure 1.8. Recurrent somatic mutations in patients diagnosed with tMN as compared to primary MN. Each bar graph represents percentage of total number of particular somatic mutation to total number of patients tested across all studies. Comparison of the differences between tMN and pMN were performed using Fisher's exact test. All tests were two-sided. Asterisks display *P*-values $*P < 0.05$, $**P < 0.01$ and $****P < 0.001$.

Based on comprehensive literature review [29, 54, 55, 89-91, 93, 96-118].

1.5. ROLE OF BONE MARROW MICROENVIRONMENT IN tMN PATHOGENESIS

1.5.1. Normal BM Architecture

HSC maintenance and progenitor differentiation occur in greatly exclusive niches. The relations of haematopoietic stem and progenitor cells (HSPC) with stromal cells, growth factors, extracellular matrix (ECM) and other components of the BM microenvironment under physiologic and pathophysiologic conditions regulate haematopoiesis [119-122].

1.5.1.1. Non-cellular components

BM microenvironment includes non-cellular components comprising of extracellular matrix proteins, represented by collagen, fibronectin, laminin, hyaluronic acid, and tenascin-C [123-127]. Extracellular matrix is an often-ignored part of the BM microenvironment; however, it provides not only a mechanical support but also acts as a reservoir of growth factors. ECM is a three-dimensional, composite and extremely dynamic non-cellular network comprised of (1) proteoglycans; (2) fibrous proteins e.g. collagens, fibronectins, elastins, tenascins, vitronectin, and laminins; (3) glycosaminoglycans e.g. hyaluronic acid, chondroitin sulfate, heparan sulfate, keratansulfate, dermatan sulfate, and heparin; and (4) matricellular proteins e.g. osteocalcin and periostin, which support the association between other ECM proteins and cellular receptors [123-129].

1.5.1.2. Cellular components

The BM microenvironment consists of cellular components which can be classified as cells having a haematopoietic origin (macrophages, osteoclasts and lymphocytes) and non-haematopoietic cells (mesenchymal stem and progenitor cells, osteoprogenitors, osteoblasts,

endothelial cells, smooth muscle cells, adipocytes) [130] which support haematopoiesis. Multiple stromal components of the BM microenvironment such as osteoblasts/osteoprogenitor cells, vascular endothelial cells, mesenchymal stem cells (MSC), monocytes, and macrophages support the haematopoietic stem cell niche [131-133], whereas adipocytes are thought to inhibit HSC [134]. MSC are one of the most important components of the BM microenvironment, that regulate functioning HSC niches through direct cellular interactions and by secretion of regulatory factors such as C-X-C motif chemokine 12/ stromal cell-derived factor 1 (CXCL12/ SDF-1), transforming growth factor beta (TGFβ), angiopoietin 1 (ANGPT1) and thrombopoietin (TPO), which regulates HSC retention, quiescence, and the ability to induce multilineage potential [135-139]. Alongside these soluble factors, bi-directional crosstalk among surrounding cells and HSC is also facilitated by cell-bound molecules such as adhesion molecules and Notch ligands [140-142].

1.5.1.2.1. Mesenchymal Stromal Cells

MSC were first recognised in the aspirates of guineapig and mouse marrow by their capability to form adherent colonies of colony forming unit-fibroblastic cells (CFU-F) [143, 144]. Further reports exhibited that these adherent fibroblastic cells were also present in the BM of other species including humans [145-147] . MSC are capable of giving rise to several types of stromal cells, including fat, smooth muscle, cartilage, bone and fibroblasts [148-150]. There is also evidence indicating that MSC can give rise to myoblasts and neural cells [146, 151]. Originally isolated from BM, MSC have also been isolated from a variety of other tissues like adipose tissue [152], tendons, blood [153], blood vessels, dental tissues [154, 155] and umbilical cord blood [156]. Several methods have been described for isolating MSC from BM, including the use of density gradient separation, direct BM plating [157], immune-magnetic bead selection and fluorescence activated cell sorting [158]. Selection of stromal precursor

antigen-1 $(STRO-1)^+$ and co-expressed non-haematopoietic markers such as CD106 or CD146, allows for the high enrichment of CFU-F fraction containing the purified MSC population [145].

1.5.2. Genetic Alterations in BM Microenvironment Contributing to Development of Myeloid Malignancies

Aberrant BM microenvironment such as inflammatory microenvironment [159] and BM fibrosis is well known in myeloid malignancies [160, 161] however, whether this is a cause or effect of malignant clone is currently debated. Malignant clones can shape the BM microenvironment conducive for its survival and proliferation [162], while aberrant BM microenvironment can lead to myeloid neoplasm [162-167]. The latter findings were based on murine models of myeloid neoplasms including reduced function of genes such as retinoic acid receptor gamma (*RAR-γ)*, retinoblastoma (*Rb)*, mind-bomb E3 ubiquitin protein ligase 1 (*Mib1)*, nuclear factor of kappa light polypeptide gene enhancer in B-cells inhibitor alpha (*IκBα)*, signal-induced proliferation-associated 1 (*Sipa1)*, Dicer 1, ribonuclease III (*Dicer1)* and concordant loss of the early growth response 1 (*Egr1)*, adenomatous polyposis coli (*Apc)*, and mouse p53 tumour suppressor gene (*Trp53)* in non-haematopoietic cells [162-167]. For instance, deletion of *Dicer1*, an RNAse III endonuclease essential for microRNA biogenesis, in mouse osteoprogenitors, disrupted haematopoiesis, leading to blood cytopaenia and granulocytic and megakaryocytic dysplasia, followed by development of AML with several genetic abnormalities [166]. In this murine model, *Dicer1* deletion resulted in impaired osteogenic differentiation, which led to downregulation of Shwachman-Bodian-Diamond syndrome (SBDS) gene expression. Similarly, other murine models show that mice deficient for *SBDS* expression in BM derived MSC (BMSC) [159, 168] but not HSC [168, 169] can develop MDS. These studies provide evidence that deregulation in BM microenvironment is

associated with the development of MDS. Furthermore, reduced gene expression levels of *Dicer1* and the SBDS have been described in MDS–derived BMSC, suggesting that impaired osteogenic differentiation of BMSC also contributes to the pathogenesis of MDS in humans [170-172]. In another mouse model, knock-out of *Mib1*, an E3 ubiquitin ligase essential for Notch ligand endocytosis, resulted in development of BM microenvironment induced myeloproliferative disease [173]. Mice with a non-functional β-catenin mutation in osteoblasts showed expansion of myeloid cells and development of AML [174]. In a mouse model of tMN, based on haploinsufficiency of two del(5q) genes, *Egr1* and *Apc*, together with *Trp53* knockdown, exposure of BM microenvironment to radiation and/or a chemotherapy accelerates myeloid disease development [167, 175, 176].

1.5.3. Cytotoxic Therapy-induced BM Microenvironment Dysregulation

It has been reported previously that CT not only induces genetic alterations in HSC [177, 178] but can also damage the stromal cell compartment [179-182] causing BM microenvironment to have a compromised HSC-supporting capacity. High dose chemotherapy prior to HSCT can cause short- and long-term damage to BMSC [179-181]. Similarly, in *vitro* [179, 183] and *in vivo* [181, 184] exposure to cytotoxic therapies compromise BMSC proliferative [179, 181, 183, 185, 186], differentiation [179, 183], DNA-damage repair potential [187], and induce senescence [188-190]. These defects can persist for varying periods [167, 181, 184, 187] following completion of therapies and drug exposure. However, these findings are not without conjecture. Some studies reported normal proliferative rates [184, 191], HSC-supporting potential [181, 185, 191] and differentiation capacity of BMSC following CT.

Importantly, cytotoxic therapy induced damage to bone marrow microenvironment can profoundly compromise its ability to support haematopoiesis [179, 184] by: (i) releasing

inflammatory cytokines such as IL-6, tumour necrosis factor alpha (TNFα), TGFβ and generating active oxygen; (ii) reduced secretion of cytokines crucial for supporting haematopoiesis such as stem cell factor (SCF), CXCL12, ANGPT1, vascular cell adhesion molecule 1 (VCAM1) and IL-7 [192, 193]; (iii) damaging sympathetic neurons which are essential for HSC recovery. Vincristine and cisplatin damaged bone marrow catecholaminergic thymidine hydroxylase (Th+) neurons and adversely affect haematopoietic recovery and survival after BM transplantation compared to mice treated with saline or non-neurotoxic drug [193].

Contradictory findings in the literature could be due to inter-patient variability, type of chemotherapy received, underlying malignancy and interval between chemotherapy exposure and sample collection for the assays. Furthermore, literature reporting CT-induced long-term damage to BM microenvironment is very limited and based on very small numbers of patient samples [187] and different experimental design/methods [185]. Additionally, none of these studies focused on patients developing tMN. Further insight into stromal-derived factors that contribute to tMN is critical for preventing or delaying disease onset and/or targeting interaction between HSC and BM microenvironment to improve outcomes for tMN. BM derived stromal cells from MN have been shown to secrete increased levels of IL-6, IL-1β and TNFα [194-196], whereas CXCL12 was found to be expressed at lower levels [197]. However, little is known about how the BMSC cytokine milieu changes after CT and whether this occurs prior to the onset of tMN.

1.6. HYPOTHESIS

Chemotherapy/radiotherapy exposure leads to long-term irreversible damage of BM microenvironment in tMN.

1.7. PROJECT AIMS

Aim 1: To characterise bone marrow microenvironment in tMN patients and compare with other, typical MN and age-matched healthy controls

Aim 2: To compare cytotoxic therapy- induced BMSC changes and myeloid neoplasms-induced BMSC changes

Chapter 2: Materials and Methods

2.1. GENERAL TECHNIQUES

2.1.1. Commonly Used Reagents and Suppliers

Table 2.1. Suppliers of commonly used reagents

Reagent	Catalogue No	Supplier
Acetic Acid	AA009-2.5L-P	Chem Supply
Acid citrate-dextrose (ACD)	AHB7898	Aurora Bioscience
Actrapid (Insulin), 100IU/ml	1676	RAH Pharmacy
Albumin Bovine Fraction V (BSA), 100g	A9418-100G	Sigma Aldrich
Alizarin Red S LR	AL080-100G	Chem Supply
Aminoactinomycin D (7AAD)	559925	BD Biosciences
Annexin V phycoerythrin (PE)	640908	Australian Biosearch
Anti-ATM	1873	Cell Signalling Technology
Anti-β-actin	A1978	Sigma Aldrich
Anti-p21	5567430	BD Bioscience
Anti-p53	sc-126	Santa Cruz Biotechnology
Anti–phospho-ATM	AF1655	R&D Systems
Anti-phospho-CHK2 (T68)	2661	Cell Signalling Technology
Anti-phospho-p53	9284	Cell Signalling Technology
BCA Protein Assay	23227	ThermoFisher Sceintific
Calcium chloride	CA01940500	Sacharlau
CD34 MicroBead Kit, human	130-046-702	Miltenyi Biotech Aust
Cellular Reactive Oxygen Species (ROS) Assay Kit (DCFDA/H2DCFDA)	ab113851	Abcam
Comet Assay Kit	ab238544	Abcam
Dasatinib		Bristol Myers Squibb
DBL Dexamethasone Sodium Phosphate	163199	RAH Pharmacy
D-glucose	G7528	Sigma Aldrich
Diethyl pyrocarbonate (DEPC) water	821739	MP Biomedicals
Dimethylformamide	12767	Cell signaling technology
Dimethyl sulfoxide (DMSO)	DA013-2.5L-P	Chem Supply
Distilled water Ultrapure	10977015	Life Technologies

DNASE1 amplification grade	18068015	Life Technologies
dNTP's mix (10mM solution)	FISBIODN-10M/01	Adelab
Doxorubicin	D1515	Sigma Aldrich
Dulbecco's modified Eagle's medium (DMEM)- high glucose	D6546-500ml	Sigma Aldrich
DMEM without phenol red	D1145-500ml	Sigma Aldrich
Ethanol Undenatured 100%	EA043-2.5L-P	Chem Supply
Ethanol Undenatured 80% v/v	EL156-20L-P	Chem Supply
Ethylenediaminetetraacetic acid (EDTA)	ED-500G	Sigma Aldrich
F(ab)2-Goat anti-Mouse IgG (H+L) Alexa Fluor 488 Cross-Adsorbed (secondary antibody)	LTSA-11017	Thermo Fisher
Foetal Calf Serum 500mL Batch: F21701 (FCS)	AU-FBS/PG	CellSera
Formaldehyde, 40% (w/v)	FL010-10L-P	Chem Supply
Formalin, 10% neutral buffered	AJA2518-5L	Thermo Fisher
Glycerol (Glycerine)	GA010-2.5L-P	Chem Supply
Goat anti-mouse IgG-fluorescein isothiocyanate (FITC) (secondary antibody)	SB 1030-02	Assay Matrix
Goat anti-mouse IgM-FITC (secondary antibody)	SB 1020-02	Assay Matrix
Goat anti-Rabbit IgG H&L (HRP)	ab205718	Abcam
Halt™ Protease and Phosphatase Inhibitor Cocktail, EDTA-free (100X)	78441	ThermoFisher Scientific
Hanks' buffered saline solution (HBSS)	H9394-500ml	Sigma Aldrich
HEPES Solution 1M, pH 7.0-7.6	H0887-100ml	Sigma Aldrich
High molecular weight DNA, 5mg	D4522	Sigma Aldrich
Human recombinant granulocyte-colony stimulating factor (G-CSF), 2µg	300-23-2	Lonza
Human recombinant IL-3, research grade, 10µg	130-093-908	Miltenyi Biotech Aust
Human recombinant IL-6, research grade, 10µg	130-095-365	Miltenyi Biotech Aust
Human recombinant SCF, research grade, 10µg	130-093-991	Miltenyi Biotech Aust
Hydrochloric Acid (HCl) 32%	HT020-500M	Chem Supply
Hydrocortisone 21-hemisuccinate sodium salt	H2270-100mg	Sigma Aldrich
IACS (OXPHOS inhibitor)	010759	Selleckchem
Indomethacin	I8280-5g	Sigma Aldrich

Iscove's Modified Dulbecco's Medium liquid (IMDM)	I3390-500ml	Sigma Aldrich
ITS Universal Culture Supplements (ITS+Premix)	BDAA354352	Bio-strategy
L-Ascorbic acid 2-phosphate	A8960-5G	Sigma Aldrich
L-Glutamine, 200mM	G7513-100ml	Sigma Aldrich
Lipoprotein, low density from human plasma (LDL), 5mg	L8292-1VL	Sigma Aldrich
Lymphoprep	0 7811	Stemcell Technologies
MethoCult H4230, 80ml	H04230	Stemcell Technologies
Milliplex Human Cyto MAG Premix 38plex Kit	MPHCYTMAG60KPX 38	Abacus
Mouse anti-human CD34-PE, 8G12 antibody	15006126	BD Biosciences
Mouse anti-human CD73 Pure AD2, 100µg	550256	BD Biosciences
Mouse anti-human CD90 Biotin 5E10, 100µg	555594	BD Biosciences
Mouse anti-human CD105 Pure 266, 100µg	555690	BD Biosciences
Mouse anti-human CD146 Pure P1H12, 100µg	550314	BD Biosciences
Mouse anti-phospho-Histone H2A.X (Ser139), clone JBW301 (γH2AX)	05-636	Merck
MyeloCult H5100, 500ml	H05150	Stemcell Technologies
Nile Red	N3013	Sigma Aldrich
Oil Red O	155984	MP Biomedicals
Oligo(dT)12-18 Primer	18418012	Thermo Fisher
Paraformaldehyde solution 4% in PBS	SANTSC-281692	Bio-strategy
Penicillin/Streptomycin	P4333-100ml	Sigma Aldrich
Pico Green DNA Kit	P11496	Life Technologies
Phosphate buffered saline (PBS)	D8537-500ml	Sigma Aldrich
Pointe Calcium Arsenazo, 500ml	C7529-500PT	PM Separation
Potassium dihydrogen orthophosphate (KH_2PO_4)	10203	BDH AnalaR
Propan-2-ol-AR (isoPropyl Alcohol)	PA013-2.5L-P	Chem Supply
Proteinase K	19131	QIAGEN
RT² SYBR Green ROX qPCR Mastermix	330523	Bio-Rad
Random Hexamers	RP-6	Geneworks
Recombinant Human TGFβ1, 10µg	100-21-10	Lonza
RLT buffer, 220ml	79216	Qiagen
RNeasy Plus Micro Kit	74034	Qiagen

R-Phycoerythrin (RPE)-conjugated mouse IgG1 negative control	X0928	Elitechgroup
QIAamp DNA Minikit	51306	Qiagen
QUANT-IT Picogreen dsDNA	LTSP11496	Thermo Fisher
Qubit RNA Assay Kit	Q32852	Invitrogen
Quercetin	Q4951	Sigma Aldrich
Safranin O, 0.1%	S888-25g	Sigma Aldrich
Seahorse XF ATP Real-Time rate Kit	103592-100	Agilent Technologies
Senescence β-Galactosidase Staining Kit	9860S	Australian Biosearch
Sodium azide	8591	Sigma Aldrich
Sodium chloride LR 2.5L	SL046-2.5kg	Chem Supply
Sodium hypochlorite 8-12.5%	ST044-5L	Chem Supply
Sodium pyruvate, 100mM	S8636-100ml	Sigma Aldrich
Streptavidin- FITC, 1ml (secondary antibody)	LTSSA1001	Thermo Fisher
SUPERSCRIPT IV 10,000 units Kit	18090050	Life Tech Supply Centre
Test Kit PE Mouse Anti-Human CD34	BD 348057	BD Biosciences
Tetramethylrhodamine (TRITC)-Phalloidin	P1951	Sigma Aldrich
Toluidine Blue O	198161-25g	Sigma Aldrich
Transferrin, human	T8158-100MG	Sigma Aldrich
TritonX-100	X100-1L	Sigma Aldrich
Trypan blue (0.4%)	T8154-100ml	Sigma Aldrich
TrypLE Express 500ml without phenol red	15006195	Life Technologies
Tween 20	P1379	Sigma Aldrich
αModified Eagle's medium (αMEM)	M4526-500ml	Sigma Aldrich
β-mercaptoethanol	21985-023	Life Technologies
2-deoxy-d-glucose (2DG) (glycolysis inhibitor)	D8375	Sigma Aldrich
4′,6-diamidino-2-phenylindole (DAPI)	D9542-10mg	Sigma Aldrich

2.1.2. Common Buffers and Solutions

Table 2.2. Common buffers and solutions

Name	Components
1x PBS	MilliQ water 10% PBS, Ca^{+}/Mg^{+} free
Binding buffer	HBSS 100mM Calcium chloride
Blocking solution for Fluorescence-activated cell sorting (FACS)	1xPBS 3%FCS 5mM EDTA
FACS wash buffer	1x PBS 2% FCS
Flow Cytometry Fixative (FACS FIX)	1xPBS 1% formalin 0.1M D-glucose 0.02% sodium azide
Freeze Mix	70% HBSS 20% FCS 10% DMSO
Hanks Balanced Salt Solution (HBSS)	Ca^{+} and Mg^{+} Free Add 1% HEPES prior to use
Magnetic-assisted cell sorting (MACS) buffer	1x PBS 1% BSA 5mM EDTA 0.01% sodium azide
Recovery media	IMDM 20% FCS
Sort buffer	FACS wash buffer 20% FCS

Thaw solution	HBSS 5% FCS 5% ACD The solution (without ACD) was stored at 4ºC. ACD was added and the solution pre-warm to 37ºC prior to use
dNTP Set (N = A, C, G, T)	25mM stock = 40µl of each dNTP Working stock: 5mM = 20µl of 25mM stock in 80µl DEPC water

Abbreviations: ACD, acid citrate-dextrose; BSA, bovine serum albumin; DEPC, diethyl pyrocarbonate; DMSO, dimethyl sulfoxide; EDTA, ethylenediaminetetraacetic acid; FCS, foetal calf serum; HBSS, Hanks' buffered saline solution; IMDM, Iscove's modified Dulbecco's medium.

2.1.3. Isolation of Bone Marrow Mononuclear Cells (BMNC)

Diagnostic BM samples from MN patients, and age-matched controls at the time of hip replacement were collected after informed consent. The study was approved by the Ethics Committees of participating institutions (Central Adelaide Local Health Network- HREC reference number: HREC/15/RAH/496, CALHN reference number: R20151123 and Calvary Health Care Adelaide- 19-CHREC-E004) and performed in accordance with the Declaration of Helsinki.

40ml of BM from patients with myeloid neoplasms and age-matched controls were collected in lithium heparin tubes. Up to 15ml of BM were transferred into a 50ml polypropylene conical tubes (Falcon tubes) and HBSS (Table 2.2) was added to a volume of 35ml. Using a syringe and cannula 15ml of Lymphoprep (Table 2.1) were underlain. Tubes were then centrifuged (Eppendorf 5810R centrifuge; Eppendorf South Pacific, Macquarie Park, Australia) at 400 x *g* for 30 minutes with no brake. The interface containing the MNC was then transferred using a

sterile transfer pipette to a fresh 15ml polypropylene conical tube (Falcon tubes), washed in 10ml HBSS twice followed by centrifugation at 580 x *g* for 10 minutes.

2.1.4. Cell Counts and Viability

To assess cell concentration only, cells were diluted in white cell fluid (WCF). Depending on the estimated cell number, a dilution factor between two and ten was used to count cells. Diluted solution was loaded into the haematocytometer (Neubauer Improved, Assistant, Germany) to count the total number of cells using light microscope (Olympus BX45) (Olympus, Tokyo, Japan). Viability of cells was assessed by diluting samples (1/2) with trypan blue dye (Table 2.1), as live cells exclude trypan blue efficiently, however dead cells cannot. 10µl of these suspensions was loaded to a haemocytometer counting chamber and cell concentration and viability calculated accordingly. To obtain an accurate cell number at least 100 cells were counted.

2.1.5. Cryopreservation of Cells

Cells were pelleted at the desired concentration, resuspended in 1ml of Freeze Mix (Table 2.2) per up to 1×10^7 cells per cryo-vail dropwise and immediately transferred to cryo-vials (Greiner Bio-One, Kremsmünster, Austria). Cells were cryopreserved using a 'Mr Frosty' freezing container (C1562 Freezing Container, Nalgene, USA) for at least 4 hours at -80ºC. Next samples were transferred to the vapour phase of liquid nitrogen (-196°C) and stored for up to 10 years.

2.1.6. Thawing of Cryopreserved Cells

Cells were removed from liquid nitrogen (-196ºC) and rapidly thawed in a 37ºC water bath (DKSH, Braeside, Australia). In a Biological Safety Cabinet Class II (Gelman Sciences, Ann

Arbor, USA), the cell suspension (in FCS 10% (v/v) of DMSO) was quickly transferred to a 14ml polypropylene tube containing approximately 11ml of thaw solution (Table 2.2) (warmed to 37^{o}C) and was added dropwise with constant mixing. This preparation was centrifuged at 580 x *g* for 7 minutes (Eppendorf 5810R centrifuge; Eppendorf South Pacific, Macquarie Park, Australia). The supernatant was aspirated, and the procedure repeated to remove all residual DMSO.

2.1.7. Isolation of CD34^{+} Cells

2.1.7.1. Magnetic Assisted Cell Sorting (MACS)

CD34^{+} progenitor cells were isolated by MACS (Miltenyi Biotech, Germany). MNC pellet was resuspended in a final volume of 300µl MACS buffer (Table 2.2) for up to 10^{8} cells. To prevent non-specific binding, 100µl FcR Blocking Reagent per 10^{8} total cells were added which was followed by 100µl CD34 Microbeads per 10^{8} total cells to label cells. Cells were incubated for 30 minutes at 4^{o}C with constant mixing (using the MACS mixer; Miltenyi Biotech, Germany). While cells were incubating, MACS columns and plungers (Miltenyi Biotech, Germany) were placed on ice to prevent bubbles in the columns during the CD34^{+} cell isolation process. After incubation, cells were washed with 2ml of ice-cold MACS buffer and centrifuge at 580 x *g* for 10 minutes (Eppendorf 5810R centrifuge; Eppendorf South Pacific, Macquarie Park, Australia) and supernatant was aspirated completely. During centrifugation, MACS columns were mounted on the magnetic cell separator and MACS Pre-Separation Filter (Miltenyi Biotech, Germany) was placed on the top of each MACS column. 500µl of MACS buffer was added to wet the column and new tube was placed underneath the column to collect the CD34 negative fraction of cells. Incubated and centrifuged cells were resuspended in 500µl of MACS buffer and added to the column and allowed to drip through. Flow-through containing unlabelled cells was collected and columns were flushed with MACS buffer twice with 500µl each time to

remove any non-specifically bound $CD34^-$ cells. Cells reactive to CD34 antibody (labelled cells) were bound to the magnetised matrix of the column, while the flow-through were unlabelled cells. Columns were removed from the magnetic cell separator and placed in the new 10ml tube. 500µl of MACS buffer was added in the column and magnetically labelled cells were flushed using the plunger. $CD34^+$ purity, cell count and cell viability of collected cells were checked by flow cytometry, WCF and trypan blue (described in 2.1.8 and 2.1.4 respectively) and used in long-term culture- initiating cell (LTC-IC) assays (described in 2.3.4).

2.1.7.2. Sorting $CD34^+$ population

Cells expressing CD34 were sorted using a BD FACS Fusion Cell Sorter (BD Biosciences). Briefly, appropriate number of cells for unstained control ($1x10^4$ cells), and CD34 antigen staining were transferred to sterile FACS tubes with addition of appropriate antibodies according to the Table 2.3 and stained cells for 30 minutes, protected from light at 4ºC. After incubation, cells were washed in 1ml cold sort buffer (Table 2.2) and resuspended in 100µl of sort buffer if < $5x10^6$ cells or 200µl if > $5x10^6$ cells. Collection tubes for collecting $CD34^+$ and $CD34^-$ cells were prepared by adding 1ml of sort buffer. After sorting, cells were centrifuged at 580 x *g* for 10 minutes (Eppendorf 5810R centrifuge; Eppendorf South Pacific, Macquarie Park, Australia) and resuspended in 2ml recovery media (Table 2.2) on 6-well plate for 2 hours after which cells were counted and used in LTC-IC assays (described in 2.3.4).

Table 2.3. Cells, antibodies, and media use for sorting

Tubes	Number of cells	Antibody (CD34-PE)	DAPI	Sort buffer
PRE-SORT				
1. Unstained control	$1x10^4$	-	1µl	100µl
2. CD34 stain		10µl/10^6 cells 5µl if < $1x10^6$	1µl	100µl
POST-SORT				
3. $CD34^+$		-	-	1ml
4. $CD34^-$		-	-	1ml

2.1.8. Flow Cytometry to Check $CD34^+$ Purity

Aliquots of 0.5-$2x10^5$ $CD34^+$ labelled and unlabelled cells (Table 2.4) were positioned in four 6ml FACS tubes and stain in 100µl of FACS wash buffer (Table 2.2) by adding antibodies as shown in Table 2.5. Mixed cells were incubated on ice for 30 minutes. At the end of the incubation, 1ml FACS wash buffer was added to each tube and tubes were centrifuged 580 x *g* for 10 minutes (Eppendorf 5810R centrifuge; Eppendorf South Pacific, Macquarie Park, Australia). Supernatant was discarded and additional 1ml of FACS wash buffer (Table 2.2) was added before centrifugation. After aspirating the supernatant, cells were resuspended in 250µl of FACS FIX reagent (Table 2.2), and flow cytometry was performed using BD FACS Canto II Flow Cytometer (BD Biosciences).

Table 2.4. Labelling cells for flow cytometry

Tube #	Number of cells	Type of cells	Antibody
1	$2x10^5$	MNC pre-sort or $CD34^-$ cells (unlabelled cells)	IgG1 PE- 5µl
2	$2x10^5$	MNC pre-sort (labelled)	CD34 PE-10µl
3	$2x10^5$	$CD34^+$ fraction	CD34 PE-10µl
4	$2x10^5$	$CD34^-$ fraction	CD34 PE-10µl

Abbreviations: MNC; mononuclear cells.

2.2. CELL CULTURE TECHNIQUES

2.2.1. Culture Media, Buffers, Solutions and Stains

Table 2.5. Culture media

Name	Content
Establishment Growth Media (EGM)	αMEM 20% FCS 100μM L-asorbate-2-phosphate 2mM L-glutamine 50U/ml penicillin 50μg/ml streptomycin 1mM sodium pyruvate
Maintenance Growth Media (MGM)	αMEM 10% FCS 100μM L-asorbate-2-phosphate 2mM L-glutamine 50U/ml penicillin 50μg/ml streptomycin 1mM sodium pyruvate
Osteogenic Inducing Media	αMEM 5% FCS 50U/ml, 5μg/ml penicillin, streptomycin 1mM sodium pyruvate 100μM L-ascorbate-2-phosphate 2mM L-glutamine 10mM HEPES 10^{-7}M dexamethasone phosphate 1.8mM inorganic phosphate KH_2PO_4
Adipogenic Inducing Media	αMEM 5% FCS 50U/ml, 5μg/ml penicillin, streptomycin

	1mM sodium pyruvate
	100µM L-ascorbate-2-phosphate
	2mM L-glutamine
	10mM HEPES
	0.5µM hydrocortisone
	60µM indomethacin
	10^{-7}M dexamethasone phosphate
Chondrogenic Inducing Media	DMEM-high glucose
	ITS + Premix
	100µM L-ascorbate-2-phosphate
	50U/ml,50µg/ml penicillin, streptomycin
	2mM L-glutamine
	10^{-5}M dexamethasone phosphate
	0.125% BSA
	10ng/ml TGFβ3

Abbreviations: αMEM, αModified Eagle's medium; BSA, bovine serum albumin; FCS, foetal calf serum; TGFβ3, transforming growth factor beta 3.

Table 2.6. Cell culture solutions

Name	Components
Calcium chloride (5mM)	Dilute 250mM calcium chloride in 0.6M HCl
0.6M HCl	Concentrated HCl (Check density and % HCl. m.w. = 36.46). If d = 1.18g/l and solution is 34% HCl, then molarity is 11M Dilute concentrated HCl in sterile MiliQ water
Dexamethasone sodium phosphate	Molarity of stock solution (4mg/ml; m.w. 516.4) is 7.746mM To prepare 10^{-5}M solution: 65µl Dexamethasone sodium phosphate 50ml αMEM
Dilute Proteinase K	Dilute stock (10mg/ml) to 100µg/ml in 1xPBS pH 7.4 Discard unused. Do not re-freeze as enzyme activity is reduced
1x TE buffer	Dilute stock TE buffer (20x) to 1x in RO water
Blocking buffer (use in γH2AX staining protocol)	1% BSA 5% normal goat serum 5% normal rabbit serum in 1xPBS
SDM	IMDM + 1% BSA 2mM L-glutamine 0.2mg/ml transferrin 1U/ml insulin 100µM β-mercaptoethanol 20µg/ml LDL

Abbreviations: αMEM, αModified Eagle's medium; BSA, bovine serum albumin; IMDM, Iscove's modified Dulbecco's medium; LDL, low-density lipoprotein; RO, reverse osmosis; SDM, serum deprived media; TE, Tris-EDTA.

Table 2.7. Cell culture stains

Name	Components
Alizarin Red S stain	2g Alizarin Red S 100ml RO water Mix the solution and adjust the pH to 4.1 - 4.3 using 0.5% ammonium hydroxide
Nile Red stain	2.5µl of 50µg/ml Nile Red for final 25ng/ml 2.5µl of 600µM DAPI for final 300nM 250µl 1xPBS 4.75ml Miliq water
Oil Red O stain	0.5g Oil Red O 100ml of isopropanol and further diluted 1.5:1 in RO water
Safranin O stain	0.05g Safranin O 50ml RO water
Toluidine Blue stain	30ml 40% formaldehyde 480ml 1xPBS 0.51g Toluidine Blue

Abbreviations: RO, reverse osmosis.

2.2.2. Cell Culture Settings

All cell culture procedures were performed in a Biological Safety Cabinet Class II (Gelman Sciences, Ann Arbor, USA). Cells cultures were kept in Sanyo CO_2 incubator (Sanyo Oceania, North Ryde, Australia), at 37°C, 5% CO_2 in a humidified environment. Eppendorf 5810R centrifuge (Eppendorf South Pacific, Macquarie Park, Australia) was used for centrifugation of cell pellets.

2.2.3. Isolation and Expansion of BMSC

BMSC were isolated and expanded from BMNC as previously described [145]. In brief, primary cultures were established by culturing $3x10^4$ MNC per cm^2 in EGM (Table 2.5) at 37ºC humidified atmosphere in the presence of 5% CO^2. Non-adherent haematopoietic cells were removed, and medium was replaced twice per week. Upon achieving 80%–90% confluent, cells were detached using TrypLE Express (Table 2.1), counted using haematocytometer (Neubauer Improved, Assistant, Germany), reseeded at a concentration of $1x10^4$ cells per cm^2, and further expanded in MGM (Table 2.5).

2.2.4. Surface Antigen Expression Assessment

To meet the criteria of the International Society for Cellular Therapy and to exclude haematopoietic contamination, BMSC at passage 3 were analysed by flow cytometry for the expression of CD34, CD45, CD73, CD90, CD105, B478 and CD146 (Table 2.1). BMSC were detached from flasks by TrypLE Express (Table 2.1) for 5 minutes at 37ºC. The cells suspension was then washed twice with MGM (Table 2.5) and strained through a 70-micron cell strainer (In vitro Technologies, Noble Park North, Australia) to ensure a single cell suspension. Next cells were centrifuged at 400 x *g* for 5 minutes and resuspended in 1.2ml blocking buffer (Table 2.2). Viability assessment and cell count was performed as described in Section 2.1.4. Cells were incubated with blocking buffer (Table 2.2) for 30 minutes on ice. Cells were split ($2x10^4$/tube) into 5ml polypropylene tubes (Corning, New York, USA), corresponding to primary antibodies being used specific to MSC associated markers, haematopoietic cells-associated markers, and isotype controls at 20µg/ml for 1 hour on ice. Cells were washed twice with 1ml cold wash buffer (Table 2.2) and incubated with secondary detection antibodies; FITC-conjugated antibody (Table 2.1) (1:50 dilution) for 30 minutes on ice, followed by two washes in 1ml cold wash buffer (Table 2.2) and fixed in 500µl of FACS

FIX (Table 2.2). Detailed list of primary and secondary antibodies used in the study is in Table 2.8. Samples were analysed with BD FACS Canto II Flow Cytometer (BD Biosciences, San Jose, CA, USA).

Table 2.8. List of antibodies

Primary antibody	Isotype	Secondary antibody
1B5	IgG1	IgG FITC
1D4.5	IgG2a	IgG FITC
CD105	IgG1	IgG FITC
CD90	IgG1	Streptavidin FITC
CD73	IgG1	IgG FITC
B478	IgG1	IgG FITC
CD34	IgG1	IgG FITC
CD45	IgG1	IgG FITC
CD146	IgG2a	IgG FITC

2.3. FUNCTIONAL ANALYSIS

2.3.1. Colony Forming Unit-Fibroblast (CFU-F)

CFU-F was assessed by culturing MNC at densities of $2x10^4$-$6x10^4$ cells per well of 24-well plate in triplicate in EGM (Table 2.5), over 14 days. After two weeks of incubation media was removed gently, plate washed three times with 1x phosphate buffered saline (PBS), and cells were fixed in 500µl of Toluidine Blue Stain (Table 2.7). After minimum 2 hours incubation on the reciprocating mixer (Ratek, Boronia, Australia) wells were rinsed gently with deionised water until the water ran clear. Stained wells were then counted using inverted microscope (Olympus CKX41) (Olympus, Tokyo, Japan) (Colony = 50 or more cells).

2.3.2. Assessment of Population Doublings

BMSC cultures were initiated at passage 0 and cells were reseeded at fixed density ($8x10^3$cells per cm^2) in 24-well plates until population expansion had ceased. Cell counts were performed at each passage. The formula logN/log2 was used to calculate the cell population doublings (PD) at each passage. N was the ratio of cells counted at the end of particular passage and the number of cells initially plated. Days for one PD at a given passage was based on the length of culture in days divided by the number of the respective cell PD. Cumulative PD (CPD) were regarded as total cell expansion, represented as the sum of population doubling values obtained at each passage.

2.3.3. Cytoskeleton Assay

BMSC cytoskeleton was assessed using TRITC- labelled Phalloidin (Table 2.1) and counterstaining nuclei with DAPI (Table 2.1). BMSC were washed with PBS and fixed in 4% paraformaldehyde (Table 2.1) for 30 minutes, then wash three times with PBS + 0.1% Tween

20 (Table 2.1), followed up by 2 hours incubation with TRITC- labelled Phalloidin, 1:2000 at room temperature. The nuclei were counterstained with DAPI and viewed under inverted fluorescence microscopy (Olympus IX81) (Olympus, Tokyo, Japan). Image analysis and quantification was performed using ImageJ Software (National Institutes of Health and the Laboratory for Optical and Computational Instrumentation (LOCI, University of Wisconsin, USA)).

2.3.4. Long Term Culture-Initiating Cells (LTC-IC)

To assess haematopoietic supporting capacity of BMSC, LTC-IC assays were performed. Briefly, feeder layer cells ($7.5x10^4$ stromal cells per well of 24-well plate) were cultured until at least 80% confluence was reached and then irradiated (30Gy) using X-ray irradiator (RS 2000 X-ray irradiator, Rad Source Technologies, Suwanee, GA, USA). Subsequently, purified $CD34^+$ HSC ($1x10^4$ $CD34^+$ per well) were re-suspended in 500µl LTC medium H5100 (Table 2.1) with freshly added Hydrocortisone (Table 2.1) (final concentration 10^{-6} M) and plated on pre-established stromal layers. Cultures were maintained for 5 weeks at 37ºC, 5% CO_2 using Sanyo incubator with weekly changes of half medium. Afterwards, cells from each well were harvested and were plated in methylcellulose medium H4230 (Table 2.1) with 5-growth factor mix (G-CSF, GM-CSF, SCF, IL-3, IL-6) for colony forming unit-granulocyte/macrophage (CFU-GM) assay (Table 2.1; Table 2.9) resuspended in serum deprived media (SDM) as shown in Table 2.6 and cultured for 14 days at 37ºC, 5% CO_2. After two weeks, colonies were scored based on their morphology under an inverted microscope (Olympus CKX41) (Olympus, Tokyo, Japan).

Table 2.9. 5-growth factor mix for colony forming unit-granulocyte/macrophage (CFU-GM) assay

Growth factor	Final conc. (ng/ml)	Stock conc. (µg/ml)	330µl per sample (8x stock) (µl)
G-CSF	20	10	5.3
GM-CSF	20	5	10.6
SCF	50	10	13.2
IL-3	20	10	5.3
IL-6	20	5	10.6
SDM	-	-	285

Abbreviations: conc., concentration; G-CSF, granulocyte-colony stimulating factor; GM-CSF, granulocyte-macrophage colony-stimulating factor; SDM, serum deprived media; SCF, stem cell factor.

2.3.5. Apoptosis Assay

The number of apoptotic cells at passage 3 was quantified using both the 7AAD and Annexin-V-PE Kit (Table 2.1) according to the manufacturer's instructions. 7AAD is a fluorescent DNA binding dye that intercalates in double-stranded DNA therefore cells with compromised membranes (non-viable) stain with 7AAD. Annexin V- a Ca^{2+}-dependent phospholipid-binding protein is commonly used to detect apoptotic cells due to its ability to bind to phosphatidlyserine (PS) when it is outside of the cell (extracellular side), for example during apoptosis. In healthy cells, PS are in the inner surface of the cell membrane and are therefore not reachable to Annexin V. Apoptotic cells were defined as Annexin-V-positive, 7AAD negative cells. The analyses were performed on an FACS Canto II flow cytometer (BD Biosciences, San Jose, CA, USA).

2.3.6. Cellular Senescence Assay

Cellular senescence of BMSC at third passage was evaluated by assessing expression of β-Galactosidase as β-Galactosidase is only present in senescent cells but not found in pre-senescent, quiescent, or immortal cells, according to the manufacturer's specifications (Table 2.1). Growth media was aspirated, and cells were rinsed once with 1xPBS, fixed with 1ml of 1x Fixative Solution and incubated for 15 minutes at room temperature. Next, 1ml of β-Galactosidase staining solution was added to each well and plates were incubated at 37ºC overnight in a dry-air incubator (no CO_2) (orbital mixer incubator) (Ratek, Boronia, Australia), as the presence of CO_2 can cause changes to the pH which may affect staining results. Once stained, number of β-Galactosidase positive cells (blue) was evaluated using Olympus IX81 inverted fluorescence microscope (Olympus, Tokyo, Japan) and normalised to DAPI (Table 2.1) stained nuclei per field of view in triplicate wells. Image analysis and quantification was performed using ImageJ Software (National Institutes of Health and the Laboratory for Optical and Computational Instrumentation (LOCI, University of Wisconsin, USA)).

2.3.7. Alkaline Comet Assay

Comet assay was performed under alkaline electrophoresis conditions at 20V/300mA for 30 minutes following the manufacturer's instructions (Table 2.1) at baseline and after 24 hours of 0.1µM and 1µM Doxorubicin (Table 2.1) treatment. Once stained, image analysis was performed using Olympus IX81 inverted fluorescence microscope (Olympus, Tokyo, Japan).

2.3.8. Reactive Oxygen Species (ROS) Level

ROS production was determined by measuring the formation of fluorescent dichloro fluorescein (DCF) at an Excitation 485 and Emission 535 nm on VictorTM X4, PerkinElmer

2030 Multilabel Reader using Cellular ROS Assay Kit (Table 2.1). The final value was obtained by calculating the ratio of fluorescence intensity at specific time point and DAPI stained nuclei.

2.3.9. DNA Damage Repair Potential Following Irradiation

DNA damage repair potential of BMSC following sublethal dose of radiotherapy was assessed by phosphorylation of H2A histone family member X (H2AX) known as γH2AX, a dsDNA break-associated histone. BMSC were seeded in 24-well plates ($1x10^4$ per well) and cultured under normal conditions until 80—90% confluency was reached before exposing them to 20Gy irradiation using X-ray irradiator (RS 2000 X-ray irradiator, Rad Source Technologies, Suwanee, GA, USA). DNA damage response was assessed in non-irradiated and 1, 3, 5 and 8 hours post irradiation. Briefly, cells were washed in PBS and permeabilized in 0.25% TritonX-100 (Table 2.1) in PBS for 30 minutes, followed by two PBS washes and incubation in blocking buffer (Table 2.6) for one hour. Followed by two-hour staining against γH2AX using the mouse anti-phospho-Histone H2A.X (Ser139), clone JBW301, antibody (Table 2.1), 1:1000 according to the manufacturer's protocol. Goat anti-mouse Alexa 488 (Table 2.1), 1:2000 was used as secondary antibody for which incubation time was 1 hour. Number of γH2AX foci was evaluated using Olympus IX81 inverted fluorescence microscope (Olympus, Tokyo, Japan) and normalised to DAPI stained nuclei per four fields of view in triplicate wells once cells were stained against γH2AX. Image analysis and quantification was performed using ImageJ Software (National Institutes of Health and the Laboratory for Optical and Computational Instrumentation (LOCI, University of Wisconsin, USA)).

2.3.10. DNA Damage Induction by *in vitro* Exposure to Doxorubicin

Healthy and tMN BMSC were seeded in 24-well plates ($1x10^4$ per well) and cultured under normal conditions until 80—90% confluency was reached before *in vitro* administration of 0.1µM and 1µM of Doxorubicin (Table 2.1) for 4, 12 and 24 hours. Following drug exposure, cells were washed and stained with γH2AX as per section 2.2.5.

2.3.11. Assessment of Osteogenic Differentiation Potential

2.3.11.1. Staining with Alizarin Red

In vitro expanded BMSC at passage three were seeded at $8x10^3$ cells/cm^2 in 96 well plates and cultured in osteogenic media (Table 2.5) for up to 28 days with media changes twice weekly. At 28 days wells with cells were washed five times in 1x PBS and fixed with 10% Formalin (Table 2.1) for 1 hour at room temperature. Alizarin Red staining (Table 2.7) was used to visualise mineralized bone matrix in reverse osmosis (RO) water overnight at 4ºC before photographing using Olympus IX81 inverted fluorescence microscope (Olympus, Tokyo, Japan).

2.3.11.2. Mineral quantification

2.3.11.2.1. Colorimetric calcium assay

For quantification of mineral deposits, cells were seeded at $8x10^3$ cells/cm^2 in 96 well plates and cultured in osteogenic media (Table 2.5) for 28 days with media changes twice weekly. Next, wells were washed three times in 1 x PBS and the mineralized matrix was dissolved in 100µl of 0.6M HCl (Table 2.6) overnight at 4ºC. Acid solubilised mineral was then transferred to 96-well plates and calcium levels were quantitated using the Calcium Arsenazo (Table 2.1). Briefly, 4µl of each supernatant was moved to a single well of a fresh 96-well plate. A calcium

chloride (Table 2.1; Table 2.6) standard curve was also established in triplicate (Table 2.10). Arsenazo solution was added to each well at 200µl per well. The absorbance was read at 650nm on a microplate reader (iMark™ Microplate Absorbance Reader, BIO-RAD).

Table 2.10. Calcium chloride standards preparation

Final concentration (mM)	Stock volume (µl)	Diluent volume (µl) (RO water)
2.5	100	-
2	80	20
1.5	60	40
1	40	60
0.75	30	70
0.5	20	80
0.25	10	90
0	-	100

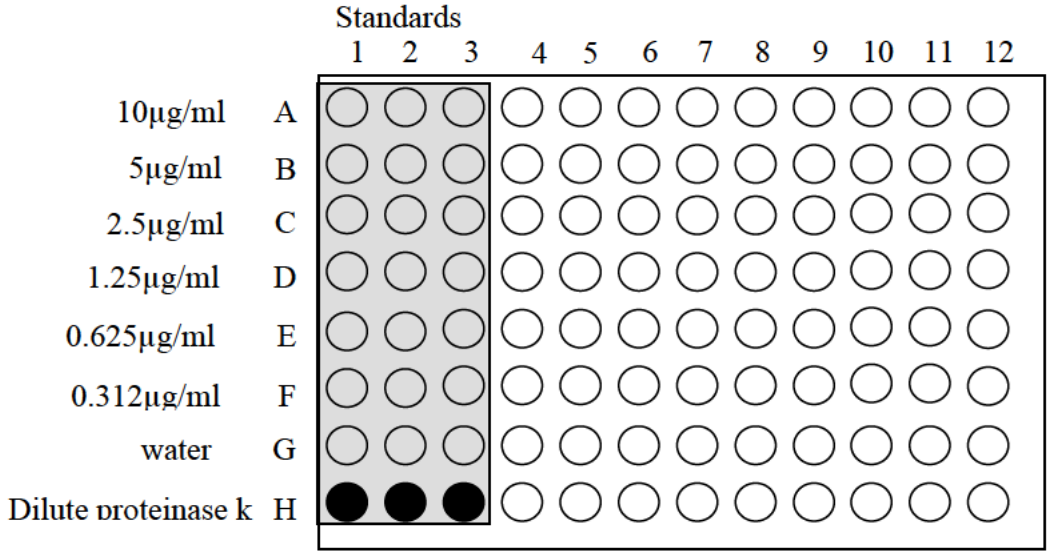
Abbreviations: RO, reverse osmosis

2.3.11.2.2. Fluorometric DNA quantification assay

Fluorometric DNA quantification assay was performed using the original plate following solubilisation of mineral with acid. The wells were washed with 1x PBS and digestion with 100µl Proteinase K (Table 2.1; Table 2.6) for 1 hour at 55°C was performed, followed by overnight incubation at 4ºC. The cells were then pipetted thoroughly to ensure homogenous cell mixture and 50µl volumes were transferred to a white 96- well plate. DNA content per well was then quantified using the Pico Green (Table 2.1) assay. 50µl of DNA standards were added to appropriate wells and 50µl of sample digests to appropriate wells (Table 2.11). Pico Green stock was diluted 1:300 into 1x TE buffer (Table 2.6). Diluted Pico Green (150µl) was

added to all wells with slight agitation to mix and protected from light with aluminium foil. The plate was then read on the VictorTM X4, PerkinElmer 2030 Multilabel Reader, under fluorescence settings (Absorbance 485/535).

Table 2.11. High molecular weight DNA standards



2.3.12. Assessment of Adipogenic Differentiation Potential

Adipogenic assays were performed as previously described [198-200]. BMSC were seeded at $8x10^3$cell/cm^2 in 6- well plates and cultured for 28 days in the presence of adipogenic media (Table 2.5) with media changes twice a week. At 28 days, the wells were washed three times with 1x PBS and cells fixed in 10% phosphate buffered formalin (Table 2.1) for 15 minutes at room temperature.

2.3.12.1. Adipocytes visualisation with Oil Red O staining

Formation of lipid-laden fat cells was assessed by Oil Red O staining (Table 2.1; Table 2.7) for at least 2 hours at room temperature, following three-time rinse with water before being

visualised using an Olympus IX81 inverted fluorescence microscope (Olympus, Tokyo, Japan).

2.3.12.2. Quantification of Nile Red labelled adipocytes

For quantitative assessment, fixed cells were labelled with Nile Red stain (Table 2.1; Table 2.7) and DAPI for 15 minutes in room temperature in dark. Labelled lipids droplets were visualised using an Olympus IX81 inverted fluorescence microscope (Olympus, Tokyo, Japan). Image analysis and quantification was performed using ImageJ Software (National Institutes of Health and the Laboratory for Optical and Computational Instrumentation (LOCI, University of Wisconsin, USA)).

2.3.13. Assessment of Chondrogenic Differentiation Potential

Analysing glycosaminoglycan (GAG) expression is a common method for identifying chondrogenic cells *in vitro*. To induce chondrogenesis, BMSC were seeded at $2x10^3$ and/or $4x10^3$ /cm^2 in 96-well plate and cultured for 7 days in chondrogenic induction media (Table 2.5) with one media change on 3 or 4 day. On day 7 cells were fixed 4% Paraformaldehyde (Table 2.1) at room temperature for 15 minutes. As cell numbers needed be quantified to normalize the expressed GAG, DAPI stain was introduced for 15 minutes. The fluorescence of each well was measured at Ex355nm/Em460nm using a microplate reader (Omega Fluostar) (BMG Labtech, Mornington, Australia) and background values from empty wells were subtracted. For Safranin O staining (Table 2.1; Table 2.7), cells were rinsed with 1% Acetic Acid for 1 minute and then stained with 0.1% Safranin O at room temperature for 5 minutes on reciprocating mixer (Ratek, Boronia, Australia), followed by four PBS washes for 5 minutes each with gentle shaking. To liberate Safranin O stain, 75% ethanol (Table 2.1) was placed into the wells with gentle shake for 5 minutes at room temperature. The fluorescence of the

ethanol-extracted Safranin O was measured at Ex544nm/Em590nm. Lastly, the fluorescence ratio of Safranin O/DAPI was calculated as normalised stained GAG values.

2.3.14. Real-Time ATP Rate Assay

The rate of ATP production from glycolytic and mitochondrial (oxidative phosphorylation, OXPHOS) system was measured and quantified using the Agilent Seahorse XF ATP Real-Time rate assay (Table 2.1). Briefly, tMN and Healthy BMSC were seeded into the Seahorse XF96 Cell Culture Microplates (Agilent Technologies, Santa Clara, USA) at the cell density of 10^4 cells/well and cultured until confluence. Prior to the start of the assay, a sensor cartridge was hydrated in Seahorse XF Calibrant following the manufacturer's instruction. Immediately before the experiment, growth media was replaced with Seahorse XF DMEM Medium, containing 10 mM glucose, 2 mM L-glutamine and 1mM sodium pyruvate. After calibration of the Seahorse XF96 Analyzer (Agilent Technologies, Santa Clara, USA), the sensor cartridge was removed from the instrument and Seahorse XF96 Cell Culture Microplate was inserted. A baseline and over time measurements of the oxygen consumption rate (OCR) and the extracellular acidification rate (ECAR) was taken, and then an inhibitory analysis was performed using injections of mitochondrial inhibitors Oligomycin at 1µM, and Rotenone+ Antimycin A at 1µM.

2.3.14.1. Normalization of Real-Time ATP Rate assay

For the normalization of the Seahorse data, we used a PicoGreen dsNDNA quantification kit (Table 2.1) (described also in section 2.3.11.2.2). Results were exported by using the Seahorse Wave 2.4 XF-96 software and the data obtained were expressed relative to the total DNA per well and expressed in pmol/min/µg DNA.

2.3.14.2. Effect of glycolysis inhibitor on ATP production

The effect of glycolysis inhibitor on ATP production was also evaluated by culturing tMN and Healthy BMSC with 1mM or 2mM of 2-deoxy-d-glucose (2DG) (Table 2.1) for 72 hours. Different concentrations of this drug were tested first to assess its effect on BMSC viability without toxicity to cells.

2.3.15. Immunobead-based Multiplex Assay for the Measurements of Cytokines/Chemokines (C/CH)

C/CH levels from BMSC-conditional media was assessed using Merck 38-plex HCYTOMAG-60K MILLIPLEX MAP Human Cytokines/Chemokines magnetic bead panel (Table 2.1; Table 2.12) and MagPix 4.2 instrument (Luminex, Austin, TX, USA) using Luminex xMAP technology according to the manufacturer's protocol. Briefly, patient BMSC conditional media (described in section 2.3.15.1) was mixed with beads (part of the kit) and incubated overnight at 4ºC with shaking, followed by two washes in wash buffer (part of the kit) using handheld magnet (EMD Millipore, Burlington, USA). Then incubated for 1 hour with 25µl detection antibody (part of the kit), followed by incubation with 25µl streptavidin-phycoerythin (part of the kit) for further 30 minutes, and washed twice in assay buffer (part of the kit) at room temperature. The observed concentrations of duplicate samples were averaged and mapped to a fitted curve derived from a serial dilution series of known C/CH standards.

Table 2.12. List of cytokines/chemokines tested and assay sensitivities (minimum detectable concentrations, pg/ml)

Cytokine	Min DC (pg/ml)
EGF	2.8
FGF2	7.6
Eotaxin	4.0
TGFα	0.8
G-CSF	1.8
Flt-3L	5.4
GM-CSF	7.5
Fractalkine	22.7
IFNα2	2.9
IFNγ	0.8
GRO	9.9
IL-10	1.1
MCP-3	3.8
IL-12P40	7.4
MDC	3.6
IL-12P70	0.6
IL-13	1.3
IL-15	1.2
sCD40L	5.1
IL-17	0.7
IL-1RA	8.3
IL-1α	9.4
IL-9	1.2
IL-1β	0.8
IL-2	1.0
IL-3	0.7
IL-4	4.5
IL-5	0.5
IL-6	0.9
IL-7	1.4
IL-8	0.4
IP-10	8.6
MCP-1	1.9
MIP-1α	2.9
MIP-1β	3.0
TNFα	0.7
TNFβ	1.5
VEGF	26.3

2.3.15.1. BMSC-conditioned media collection

BMSC-conditioned media was collected after culture of confluent BMSC at passage 3 in serum free αMEM media for 24 hours.

2.3.16. Senolytics

To assess the *in vitro* effect of senolytic therapy on tMN BMSC differentiation capacity, Dasatinib and Quercetin (Table 2.1) alone or in combination were added two times a week for 21 days to adipogenic and osteogenic induction media (Table 2.5) using the same methods as described in section 2.3.11 and 2.3.12.

2.4. RNA TECHNIQUES

2.4.1. Preparation of Total Cellular RNA

Total cellular RNA was extracted from 1-5x10^5 cells using the RNeasy Plus Micro Kit (Table 2.1). First, harvested cells were disrupted by adding Buffer RLT Plus (Table 2.1) and homogenised by passing the lysate at least 5 times through a blunt 20-gauge needle fitted to an RNase-free syringe. The homogenised lysates were transferred to a gDNA Eliminator spin column (part of the kit) to remove genomic DNA. Following centrifugation at ≥8000 x *g* (Eppendorf Centrifuge 5424R; Eppendorf, Hamburg, Germany), for 1 minute, flow through was saved and 350µl of 70% ethanol (Table 2.1) was added before transferring the sample to a RNeasy MinElute spin column (part of the kit) and centrifuging for 15secundes at ≥8000 x *g*. The spin column was then transferred to a clean collection tube (part of the kit) and washed twice with 700µl and 500µl of wash buffers (Buffer RW1 and buffer RPE respectively; part of the kit) via centrifugation at ≥8000 x *g* for 1 minute each wash. The spin column was transferred to a clean collection tube and 500µl of 80% ethanol (Table 2.1) was added and centrifuged for 2 minutes at ≥8000 x *g*. The spin column was transferred to a clean collection tube and dried by centrifugation at full speed (13000 x *g*) for 5 minutes. The spin column was transferred to another clean collection tube, 14µl RNase-free water (part of the kit) added to the enter of the spin column membrane and centrifuged for 1 minute at full speed (13000 x *g*) to elute the RNA.

2.4.2. Quantification and Purity Analysis of RNA

The concentration of RNA was determined by measuring the fluorescence on Qubit 2.0 Fluorometer (Invitrogen, Waltham, USA) using Qubit RNA Assay Kit (Table 2.1).

2.4.3. Synthesis of Complementary DNA (cDNA)

Total RNA (100ng) was reverse transcribed into single-stranded cDNA using Superscript IV (Table 2.1) according to manufacturer's instructions. Briefly,100ng of RNA, 1µl of 500ng oligo(dT) (Table 2.1), 1µl 10mM dNTP mix (Table 2.2) and DEPC water (Table 2.1) to total volume of 11µl was added to each 0.2ml strip tube (LabGear, South Melbourne, Australia). The mixture was heated to 65°C for 5 minutes and chilled briefly at 4°C (Eppendorf Mastercycler; Eppendorf, Hamburg, Germany) in order to denature the RNA. The first strand synthesis reagent mix was prepared as described below in Table 2.13.

Table 2.13. First strand synthesis reagent mix

Reagent/concentration	Volume (per sample)
5x First-Strand Buffer	4µl
0.1 M DTT	1µl
RNaseOUT Recombinant RNase Inhibitor	1µl
Superscript IV	1µl

7µl of the reagent mix was then added to each 0.2ml strip tube followed by gentle mix and position in Eppendorf Mastercycler. Incubation requirements are as follows in Table 2.14.

Table 2.14. Mastercycler parameters

Mastercycler parameters
Pre-heat lid to 105°C
50°C for 45 min
70°C for 15 min
4°C ∞

The cDNA samples were used directly for PCR or frozen at –20°C.

2.4.4. Real-time Polymerase Chain Reaction (RT-PCR)

RT-PCR reactions were performed in a CFX Conncet Real-Time PCR Detection Sytem (Bio-Rad, Hercules, USA) according to the parameters outlined in Table 2.15.

Table 2.15. RT- PCR cycling parameters

PCR cycling parameters
50°C - 2 min
95°C- 15 min
Cycling 95°C- 15 sec
60°C- 30 sec 45-52 cycles
72°C- 10 sec
72°C- 3 minutes
Melt cycle stepwise increase in temperature from 65°C to 95°C with an increment of 0.5°C

Primers (see Table 2.16) were designated using PrimerBank, followed by dilution in DEPC water to a working stock of 100ng/µl.

Table 2.16. Real-time PCR primers used in this study

Primer Name	Sequence 5' to 3'
Genes of interest	
Adipsin forward	GACACCATCGACCACGAC
Adipsin reverse	CCACGTCGCAGAGAGTTC
β-actin froward	GATCATTGCTCCTCCTGAGC
β-actin reverse	GTCATAGTCCGCCTAGAAGCAT
CDKN1A forward	TGTCCGTCAGAACCCATGC
CDKN1A reverse	AAAGTCGAAGTTCCATCGCTC
CXCL12 forward	ATTCTCAACACTCCAAACTGTGC
CXCL12 reverse	ACTTTAGCTTCGGGTCAATGC
FGF2 forward	AGTGTGTGCTAACCGTTACCT
FGF2 reverse	ACTGCCCAGTTCGTTTCAGTG
FOS forward	GGGGCAAGGTGGAACAGTTAT
FOS reverse	CCGCTTGGAGTGTATCAGTCA
IFITM1 forward	CCAAGGTCCACCGTGATTAAC
IFITM1 reverse	ACCAGTTCAAGAAGAGGGTGTT
Osteopontin forward	GCAGACCTGACATCCAGTACC
Osteopontin reverse	GATGGCCTTGTATGCACCATTC
PPARγ forward	CTCCTATTGACCCAGAAAGC
PPARγ reverse	TCAAAGGAGTGGGAGTGGTC
RUNX2 forward	GTGGACGAGGCAAGAGTTTCA
RUNX2 reverse	CATCAAGCTTCTGTCTGTGCC
STC2 forward	ACAGGTTCGGCTGCATAAGC
STC2 reverse	GAGGTCCACGTAGGGTTCG
UHRF2 forward	ATTGAGGACGTGTCTCGCAAA
UHRF2 reverse	GGTCTGGGCGAACTAGCAG

PCR master mix was prepared as per Table 2.17 for each primer set to be tested.

All RT-PCR reactions were performed in triplicate with changes in gene expression made relative to the housekeeping gene GAPDH or β-actin, using the 2-ΔCT method.

Table 2.17. Preparation of PCR master mix

Reagent	Volume (per sample)
SYBR Green	7.5µl
Forward Primer (100ng/µl)	0.75µl
Reverse Primer (100ng/µl)	0.75µl
DEPC water	4.75µl

2.4.5. Whole Transcriptome Analysis

Whole transcriptome analysis was performed on BMSC isolated from tMN (n = 3) and compared with age-matched healthy controls (n = 3), pMN (n = 3), and pMN+Ca (n = 3). Transcriptome sequencing libraries were prepared with Illuimina TruSeq Total RNA protocol (Illumina, San Diego, USA) for 150bp paired-end sequencing on a NextSeq500 instrument.

Adapters were trimmed off raw sequencing read pairs using cutadapt (v2.10) and aligned to version b37 of the human genome with STAR (v2.7.2c), using in-house scripts that made use of 10bp UMIs in order to remove PCR duplicate fragments (umitools v1.0.0, sambamba v0.8.0, bedtools v2.27.1). Counts of fragments under gene models were carried out through STAR quantmode GeneCounts, mapping statistics were quantified using Picard (v2.16.0) and samtools (v1.9). Gene expression was analysed via the BioConductor R (v4.0.3) package

edgeR (3.30.3). Genes were filtered out as 'unexpressed' if expression was not greater than 1 count per million for all samples in at least one of the four groups of samples. Finally, gene expression was normalised using the trimmed mean of medians method. Only genes with adjusted *P*-value (based on false discovery rate, FDR) less than 0.127, nominal $P < 0.05$, were considered as statistically significant.

Heatmaps were generated using the pheatmap R package.

2.4.5.1. Identification of senescence gene expression based on β-Galactosidase levels

Gene expression was analysed similar to the Transcriptome sequencing section above (2.4.5). Briefly, the differential gene expression was analysed based on the β-Galactosidase value (described in section 2.3.6) via the BioConductor R (v4.0.3) package edgeR (3.30.3). Only genes with FDR $P < 0.05$ derived from edgeR analysis were considered as statistically significant. The Pearson product-moment correlation coefficient was calculated for each gene against the β-Galactosidase to measure the strength of a linear association.

2.4.5.2. Pathway analysis

Functional enrichment analysis was performed using EnrichR software 28. Those gene ontology (GO) terms or Kyoto Encyclopedia of Genes and Genomes (KEGG) and Reactome pathways showing FDR < 0.1, nominal $P < 0.05$ were considered significant.

2.4.5.3. Gene Set Enrichment Analysis

Gene set enrichment analysis (GSEA) was performed using Broad Institute GSEA software version 4.0 and Molecular Signature Database (MSigDB) version 7.2. MSigDB is a collection of annotated gene sets for use with the GSEA software. Briefly, the pre-ranked gene list that

ranked by edgeR was used to perform GSEA. The pre-ranked gene list was used to perform gene-set enrichment analysis against MSigDB hallmark gene sets (H), curated gene sets (C2), and gene ontology gene sets (C5). The default setting was used when performing the GSEA analysis. Only gene sets with FDR < 0.1 will be considered as statistically significant enriched in the gene list.

2.5. PROTEIN ANALYSIS

Response to *in vitro* DNA damaging radiotherapy was assessed in tMN and age matched Healthy BMSC by assessing phosphorylation of early responders such as ataxia telangiectasia mutated (ATM) and checkpoint 2 (CHK2), and effector proteins (p53 and p21) of DNA damage repair. Phosphorylated and total ATM, CHK2, p53 and p21 were assessed at 0.5, 1, 3, 5, 8 and 24 hours following 20 Gy irradiation in Healthy and tMN BMSC and compared with baseline (non-irradiated cells).

2.5.1. Protein Lysates Preparation

The cells were harvested and lysed in 150µl RIPA buffer (Table 2.18). The lysate tubes were incubated at 4°C with gentle rocking for 20 minutes. Lysed cells were cleared by centrifugation at 400 x g (4°C) (Eppendorf South Pacific, Macquarie Park, Australia) for 10 minutes.

Table 2.18. RIPA buffer

Reagent	Amount
Tris-HCl	25mM, pH 7.4
NaCl	150mM
NP-40	1%
Sodium deoxycholate	1%
SDS	0.1%
Halt™ Protease and Phosphatase Inhibitor Cocktail, EDTA-free (100X)	1X

Abbreviations: NP-40, nonyl-phenoxylpolyethoxylethanol; SDS, sodium dodecyl sulphate.

Protein concentration was quantitated with BCA Protein Assay (Table 2.1) and stored in aliquots at −80 °C until used.

2.5.2. Westerns Blot Analysis

Beta-actin was used as the protein loading control. The following primary antibodies were used: Anti–phospho-ATM, anti-phospho-p53, anti-phospho-CHK2 (T68), anti-ATM, anti–p53, anti-p21 and anti-β-actin (Table 2.1). Thirty micrograms of protein samples were denatured and electrophoresed on Mini or Midi TGX- Stain-free precast gels (Bio-Rad, Hercules, USA) at 110V for 60-80 minutes in sodium dodecyl sulphate (SDS)- polyacrylamide gel electrophoresis (PAGE) running buffer (Table 2.19). Proteins were then transferred onto PVDF membrane (Bio-Rad) using a Trans-Blot Turbo (Bio-Rad) according to the manufacturer's instructions. Membranes were then incubated in blocking buffer (Table 2.19) for 1 hour at room temperature, followed by incubation with primary antibody for 1 hour at room temperature or overnight at 4°C. Membranes were washed in tris-buffered saline with Tween 20 (TBS-T) (Table 2.20) for 4 x 15 minutes, followed by incubation with horseradish peroxidase (HRP), alkaline phosphatase (AP) or Cy5-conjugated secondary antibodies for 1 hour at room temperature. Following membrane washing in TBS-T for 4 x 10 minutes, Enhanced Chemi-Luminescence (ECL) reagent (Pierce Chemical Co., Rockford, USA) or Enhanced Chemifluorescence (ECF) reagent (Cytiva, Marlborough, USA) were used for immunoblot development. Fuji LAS4000 System (GE Healthcare) or Typhoon FLA 9000 (Cytiva) were used for detecting luminescence or fluorescence signals.

Table 2.19. SDS-PAGE running buffer

Reagent	Amount
BSA	5%
TBS-T:	
- **Tris**	20mM
- **NaCl**	150nM (pH 7.4)
- **Tween-20**	0.05%

Abbreviations: SDS, sodium dodecyl sulphate.

Table 2.20. Blocking solution

Reagent	Amount
Tris	250mM
Glycine	192mM
SDS	0.06%

Abbreviations: BSA, bovine serum albumin; TBS-T, tris-buffered saline with Tween 20.

2.6. STATISTICAL ANALYSIS

Data analysis was carried out using R statistical software (https://www.r-project.org) or Microsoft GrapPad Prism 8 (GraphPad Software, LA Jolla, CA, http://www.graphpad.com/), which was used for the generation of graphs and statistical significance. Statistical analysis was performed using Mann-Whitney, Two-way Anova or Student's t-test (unpaired and 2-sided) for between groups comparison. Normality test was performed using GraphPad prism 8 software. $P < 0.05$ was considered statistically significant. Details regarding statistical methods for transcriptome sequencing, quantitative real-time PCR, and cytokines/chemokines heatmap are explained in respective sections.

Chapter 3: Defective Growth Kinetics of tMN Stromal Cells

3.1. INTRODUCTION

Currently, genetic and epigenetic alterations in HSC are thought to drive myeloid malignancies, including pMN [88] and tMN [201]. Although, BM microenvironment factors play a critical role in the fate and maturation of normal haematopoiesis [202], the role of the BM microenvironment in pathogenesis of MN remains largely unknown. Emerging literature suggests that BMSC from pMN exhibit abnormal morphology [197, 203] and slow growth kinetics [170, 204, 205], while tri-lineage differentiation potential [172, 206-208] and haematopoietic supportive capacity of BMSC [170, 196] from pMN is highly variable (Table 3.1).

Historically, tMN was considered a direct consequence of DNA damage induced in normal HSC by DNA damaging cytotoxics [177, 178]. However, more recent findings suggest that CT can cause damage not only to HSC but also damage to components within the BM microenvironment [179-182, 209]. The present thesis assessed BM-microenvironmental changes in tMN and compared with carefully annotated controls.

Table 3.1. Overview of published data on BMSC characteristics in primary MDS, primary AML and tMN patients

	pMDS	pAML	tMN
Immunophenotype	No different than healthy controls [170, 206, 210-213] (some altered CD90 and CD105 [197, 214])	No different than healthy controls [208, 212, 213, 215, 216] (some altered CD73 [217])	No different than healthy controls [203]
Cell morphology	Aberrant [170, 172, 197, 204, 205, 212, 218]	Aberrant [208, 212, 215, 216]	Not reported
Cell growth	Aberrant [170, 172, 197, 204-206, 210, 211, 213, 218]	Aberrant [208, 213, 216, 219, 220]	Aberrant [203]
Multipotency	Defective (?) [170, 172, 197, 204, 206, 207, 210]	Defective (?) [208, 215, 216, 221, 222]	Defective (?) [223]
Haematopoietic support	Impaired (?) [170, 196, 197, 204, 205]	Impaired (?) [208, 217, 220]	Not reported

Aberrant cell morphology- larger and/or disorganised

Aberrant cell growth- decreased proliferative rates, reduced clonogenic ability and/or increased population doubling time

Defective multipotency- reduced or increased

Impaired haematopoietic support- not able to support normal haematopoiesis

Abbreviations: pMDS, primary myelodysplastic syndromes; pAML, primary acute myeloid leukaemia; tMN, therapy related myeloid neoplasms.

3.1.1. Morphology and Immunophenotype of MN-BMSC

Whilst several groups have reported altered characteristics of BMSC derived from MN-BM, it is not without conjecture. With regards to morphology, several studies reported that MN-derived BMSC are larger and more disorganised compared to the healthy controls [170, 197, 203, 205, 208, 212, 215, 216, 224]. However, some other investigators observed no change in the morphology of MN-derived BMSC compared to healthy controls [196, 210, 211, 221, 225-227]. Similarly, majority of the studies reported a normal immunophenotype for pMN-derived BMSC [170, 194, 196, 208, 210-212, 215, 216, 220, 227]. MN-BMSC express well recognised BMSC associated markers such as CD73, CD90, CD29, CD44 and CD105, and are negative for haematopoietic markers such as CD34, CD45 and CD14. However, CD90 and CD105 positive BMSC were significantly lower in MDS BM compared to healthy controls [214, 224] and correlated with increased angiogenic potential of BM cells. Interestingly, expression of CD90 and CD105 also varies in MDS-risk groups with lower expression in BMSC derived from higher risk MDS compared to lower risk MDS, which inversely correlates with BM angiogenesis [197]. These findings indicate that abnormal release of anti-angiogenic cytokines by BMSC is associated with a downregulation of CD105 and CD90 expression [197]. In one study, AML derived BMSC at passage 4 expressed lower CD73 levels compared with healthy-BMSC, despite similar expression levels of CD105 and CD90 [217]. Other markers expressed in BM derived clonogenic stromal cells have been proposed, such as CD106 [145], CD146 [216, 228, 229], STRO-1 [145, 230-232], CD63 [233], CD271[234, 235], STRO-3 [236] but have not been widely used in analysis of MN-derived BMSC. STRO-1 has been used to prospectively immunoselected BMSC to high purity and is regarded as a marker of early mesenchymal/stromal precursor cells, because it has been strongly linked to MSC clonogenic potential, capacity for haematopoietic support with the capability to generate adherent cell layers containing multiple cell types such as osteoblasts, chondrocytes and adipocytes [237,

238]. The STRO-1 antigen is expressed on the surface of approximately 10-20% of adult human BM but it is also expressed on the surface of other human BM cells such as glycophorin-A^+ nucleated red cells and a small subset of $CD19^+$ B-cells. However, it is not expressed in HSC [230]. Another early MSC marker, CD146, is co-expressed with STRO-1 positive BMSC with the capacity to generate mineralised tissues with haematopoietic supportive capacity *in vitro* and *in vivo* [239]. Alkaline phosphatase (ALP) is an osteoblast associated marker [240] as well as a selection marker of clonogenic BMSC [236].

Very limited literature reporting normal immunophenotype of BMSC isolated from tMN [203].

3.1.2. Proliferative Capacity of MN-BMSC

Regardless of inconsistent data on morphology, the majority of studies demonstrate impaired growth characteristics in pMN-derived BMSC [170, 197, 203-206, 210-212, 216, 220, 224, 241-243]. BMSC derived from pMN display decreased proliferative rates, reduced clonogenic ability, increased population doubling time and have a shorter lifespan *in vitro* compared to BMSC derived from healthy controls. Interestingly, proliferative capacity also varies according to disease risk group and cytogenetic abnormalities. BMSC from lower risk MDS [170, 197, 204, 242, 244] have reduced proliferation potential compared to higher risk MDS [242], but this is not without conjecture [197, 242]. To date, only one study has assessed the proliferation potential of tMN BMSC, which found a reduced CFU-F potential in BMSC derived from tMN compared to healthy control [203].

Various signalling pathways regulate BMSC proliferation including phosphoinositide 3 kinase-protein kinase B/Akt (PI3K-PKB/Akt), bone morphogenic protein (BMP), mitogen-activated protein kinase (MAPK), Hedgehog, fibroblast growth factor (FGF), mammalian target of

rapamycin (mTOR), TGFβ, Notch, and Wingless-related integration site (Wnt) [203, 245-251]. Previous studies have found the platelet-derived growth factor (PDGF) and epidermal growth factor (EGF) are the main mitogens for BMSC growth under serum deprived conditions [231]. Interestingly, downregulation of canonical Wnt signalling pathway [203, 204], and upregulation of canonical Wnt inhibitors[204] were detected in MN-derived BMSC. Gene expression profiling of HSC has revealed a deregulation of the Wnt signalling pathway in MDS, AML and tMN with del5(q) [203, 252, 253]. Concurrently, activation of β-catenin, the nuclear mediator of Wnt signalling, was observed in niche osteoblasts and the following increase in Notch signalling in HSC in 38% of MDS/AML patients studied [174]. Thus, deregulation in Wnt signalling may explain the impaired proliferative potential of MN-derived BMSC, as well as may affect their differentiation [254].

Another common signalling pathway potentially contributing to BMSC dysfunction is PI3K-PKB/Akt, associated with cancer development, progression, and drug resistance. Interestingly, out of 84 PI3K-PKB/Akt-related genes analysed by the Human PI3K-PKB/Akt Signaling PCR array, only 4 were differentially expressed, in pMDS, pAML and tMN BMSC. However, validation studies showed a significant decrease in mRNA expression only in pMDS-derived BMSC; whereas no differences were observed in AML and tMN patients compared to healthy controls, suggesting that role of BM microenvironment factors could be different within these groups [203].

In summary, published reports by several groups have detect altered pMN BMSC, however little is known about tMN BMSC. Therefore, the first aim of this thesis was to characterise BMSC derived from tMN patients and compare with other, typical MN and healthy controls.

3.2. RESULTS

3.2.1. Patients and Control Samples

Our preliminary observations of a striking defect in the proliferative capacity of BMSC from tMN (n = 20) compared to MDS/AML (n = 26), as well as to healthy controls (n = 13) (Figure 3.1) led to further examination of the phenotypic, functional, and mechanistic analysis of tMN BMSC and control samples. This observation led to the further comprehensive research detailed in this thesis.

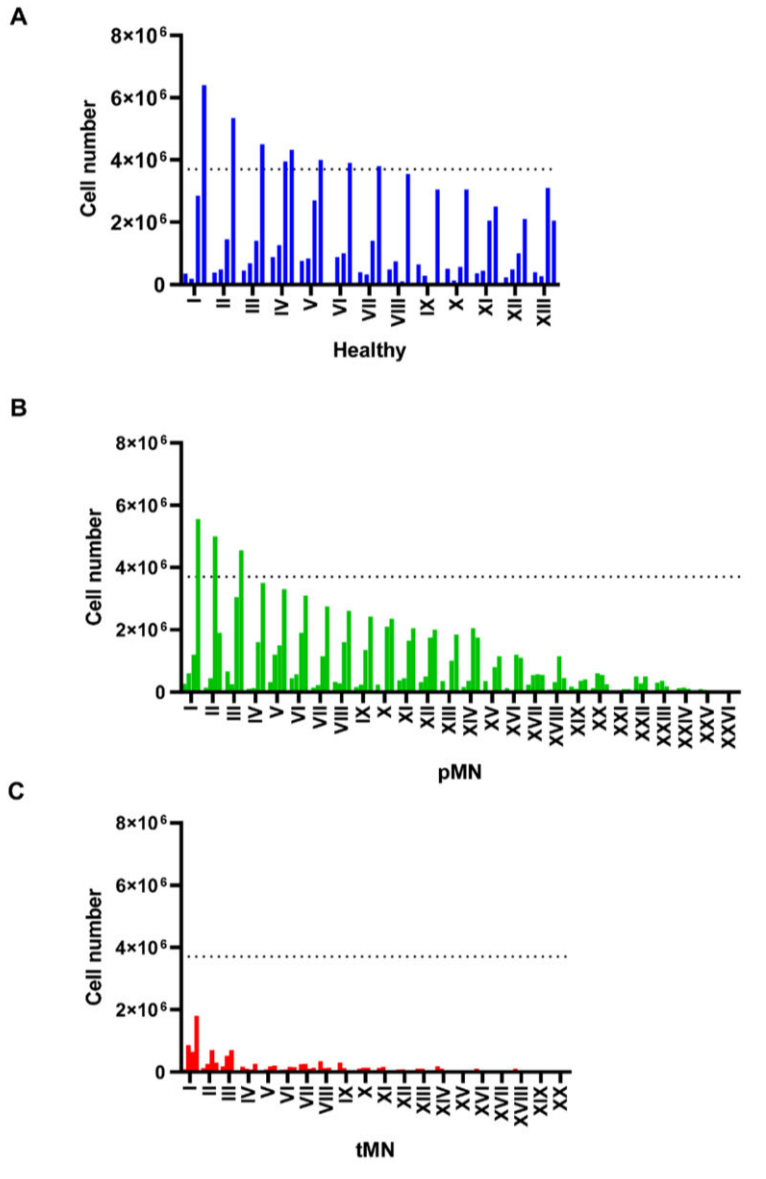


Figure 3.1. Proliferative capacity of a pilot study cohort. Proliferation potential of (A) Healthy (n = 13), (B) pMN (n = 26) and (C) tMN (n = 20). Each bar represents number of cells at the end of each passage. Samples were expanded up to passage 4 (samples without bars did not grow).

Majority of myeloid neoplasm patients are older, and ageing can affect bone marrow microenvironment. Similarly, myeloid neoplasm can induce changes in bone marrow conducive for expansion of malignant clone. In order to decipher the effects induced by CT rather than age and myeloid neoplasm, multi-omic profiling was performed (Figure 3.2) in

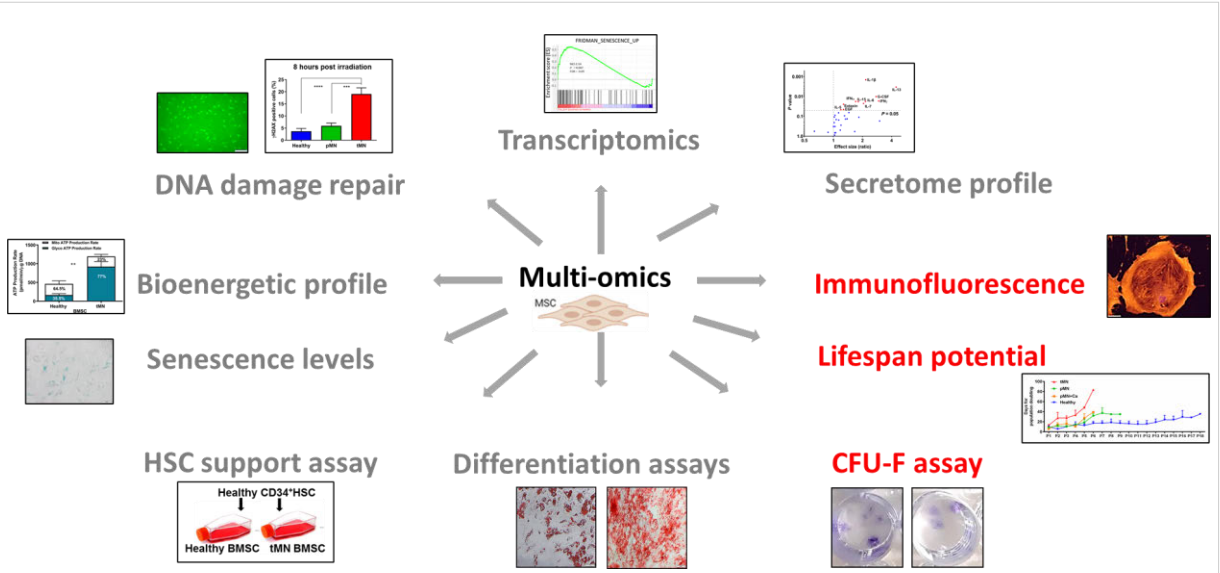


Figure 3.2. Schematic overview of multi-omic profiling of BMSC used in the study. Assays highlighted in red are described in current chapter, while the other ones will be detailed in the following chapters.

BMSC isolated from four carefully selected cohorts (Figure 3.3): (i) tMN, in which a MN occurred in a cancer survivor following CT (n = 18); (ii) MN developing in unrelated cancer survivors with *no prior CT* (a diagnosis of primary MN and another cancer; pMN+Ca) (n = 10). For example, this group included MDS/AML occurring in patients managed with surgical resection of prostate cancer but no CT; (iii) primary MN without preceding cancer and/or CT (pMN) (n = 7); (iv) age-matched healthy controls (Healthy) (n = 17) at the time of hip replacement without preceding cancer, CT or osteoarthritis. Of note, the critical difference between tMN and pMN+Ca is prior to CT in tMN but not in pMN+Ca.

Healthy	Primary MN (pMN)	Primary MN+ cancer (pMN+Ca)	Therapy- related MN (tMN)
Median 69 years	Median 70 years	Median 75 years	Median 74 years
Normal blood counts	Abnormal blood counts	Abnormal blood counts	Abnormal blood counts
No dysplastic BM	Dysplastic BM	Dysplastic BM	Dysplastic BM
No prior CT/RT	**No** prior CT	**No** prior CT	Had prior CT
No cancer	**No** previous cancer	Developed MN after primary cancer	Developed MN after primary cancer

Figure 3.3. Crucial differences between four cohorts used in the study.

Abbreviations: MN, myeloid neoplasms; MDS, myelodysplastic syndromes; AML, acute myeloid leukaemia; BM, bone marrow; CT, cytotoxic therapy.

Demographic and disease parameters of each cohort are detailed in Table 3.2. CT details used for treating primary cancer in tMN patients are listed in Table 3.3. Out of 18 tMN patients, 78% had documented previous chemotherapy with or without radiotherapy, whereas 22% received only radiotherapy. There was no significant difference in median age of Healthy (69 years, range 43-92) and MN patients (73 years, range 58-87).

Table 3.2. Demographics and clinical characteristics of pMN, pMN+Ca and tMN patients

Variable	pMDS/pAML (pMN) (n = 7)	pMN+Ca (n = 10)	tMN (n = 18)
Median age at first malignancy	NA	68 (48-82)	66 (46-81)
Median age at myeloid malignancy	70 (64-86)	75 (64-87)	74 (58-85)
Median latency from first malignancy to myeloid	NA	3 (0-19)	5 (1-19)
Median latency from last dose of first malignancy treatment to myeloid malignancy	NA	NA	3 (0.3-18)
Gender (Male/Female)	7/3	7/3	9/9
Myeloid malignancy diagnosis:			
MDS-MLD/MDS-RS-MLD	1 (14%)	4 (40%)	8 (44%)
MDS-EB-1/EB-2	3 (43%)	3 (30%)	5 (28%)
MDS/MPN overlap	2 (29%)	2 (20%)	2 (11%)
AML	1 (14%)	1 (10%)	3 (17%)
Primary malignancy diagnosis:			
Non-Hodgkin Lymphoma	NA	1 (10%)	4 (22%)
Multiple Myeloma	NA	1 (10%)	4 (22%)
Breast Cancer	NA	0	3 (17%)
Prostate Cancer	NA	2 (20%)	2 (11%)
Rectum Cancer	NA	1 (10%)	1 (6%)
Autoimmune Disease- Psoriasis	NA	0	2 (11%)
Other malignancies	NA	5 (50%)	2 (11%)
Treatment type of first malignancy:			
Chemotherapy only	NA	NA	7 (39%)
Radiotherapy only	NA	NA	4 (22%)
CMT	NA	NA	7 (39%)
Karyotype:			
Normal	6 (86%)	5 (50%)	7 (39%)
Complex (≥3 abnormalities)	1 (14%)	1 (10%)	3 (17%)
Other abnormalities	0	3 (30%)	8 (44%)
Not performed	0	1 (10%)	0

Abbreviations: pMDS, primary myelodysplastic syndromes; pAML, primary acute myeloid leukaemia; pMN, primary myeloid neoplasms; pMN+Ca, primary myeloid neoplasms + Cancer; tMN, therapy related myeloid neoplasms; 1°, primary; NA, no applicable; MDS-MLD, MDS with multilineage dysplasia; MDS-RS-MLD, MDS with ring sideroblasts with MLD; MDS-EB-1, MDS with excess blasts-1; MDS-EB-2, MDS with excess blasts-2; myelodysplastic/ myeloproliferative neoplasms overlap syndrome (MDS/MPN overlap) include chronic myelomonocytic leukaemia and atypical chronic leukaemia. Other malignancies include sarcoma, melanoma, cancers of lung/ovary/ neochroid/ bowel/colon/ throat); CMT, combined modality treatment (chemotherapy plus radiotherapy).

Table 3.3. Treatment details for primary diseases in tMN patients

ID	Primary disease	Previous therapy
tMN-1	NHL	Combination chemotherapy including cyclophosphamide, vincristine, prednisolone, and local radiotherapy
tMN-2	MM	Melphalan and prednisolone and local radiotherapy
tMN-3	Sarcoma	Ifosfamide and Doxorubicin, local radiotherapy, resection surgery
tMN-4	MM	Vincristine, doxorubicin and dexamethasone, local radiotherapy, auto-HSCT and lenalidomide maintenance
tMN-5	Rectum Ca and SLE	Immunomodulatory therapies including azathioprine, mycophenolate, cyclosporine for SLE. Chemoradiotherapy and surgical resection for cancer
tMN-6	MM	Combination chemotherapy of dexamethasone, thalidomide, cisplatin, doxorubicin, cyclophosphamide, and etoposide followed by auto-HSCT and thalidomide maintenance
tMN-7	Breast Ca	Combination chemotherapy including adriamycin, cyclophosphamide, methotrexate, fluorouracil, local radiotherapy, and left mastectomy followed by hormonal therapy tamoxifen
tMN-8	Prostate Ca	Local radiotherapy
tMN-9	Psoriasis	Weekly methotrexate for 6-7 years
tMN-10	NHL	Combination chemotherapy including cyclophosphamide, vincristine, doxorubicin, prednisolone (R-CHOP). Repeated cycles of rituximab, dexamethasone, cytarabine, cisplatin (R-DHAP) followed by auto-HSCT
tMN-11	Throat Ca	Local radiotherapy
tMN-12	NHL	Combination chemotherapy including cyclophosphamide, vincristine, doxorubicin, prednisolone (R-CHOP) and high dose methotrexate. Gemcitabine based chemotherapy for relapse
tMN-13	Psoriasis	Weekly methotrexate for four years
tMN-14	NHL	Combination chemotherapy including cyclophosphamide, vincristine, doxorubicin, prednisolone (R-CHOP) and intrathecal methotrexate
tMN-15	MM	Combination chemotherapy including cyclophosphamide, vincristine, prednisolone, and local radiotherapy
tMN-16	Breast Ca	Surgical resection and local radiotherapy
tMN-17	Prostate Ca	Surgical resection and local radiotherapy
tMN-18	Breast Ca	Combination chemotherapy, local radiotherapy, and left breast mastectomy

Abbreviations: auto-HSCT, autologous haematopoietic stem cell transplant; tMN, therapy related myeloid neoplasms; NHL, non-Hodgkins's lymphoma; MM. multiple myeloma; Ca, cancer; SLE, systemic lupus erythematosus.

3.2.2. No Differences in Immunophenotype Profile Between tMN and Control BMSC

BMSC used in our study satisfied the minimal essential criteria of the International Society for Cellular Therapy such as plastic adherence, multi-differentiation and immunophenotype characteristics *in vitro* [255]. BMSC were positive for known BMSC associated markers (CD73, CD90, CD105, ALK-Phos (ALP) and CD146) (Figure 3.4, Figure 3.5) and negative for the haematopoietic markers such as haematopoietic stem/progenitor cell marker CD34, and the leukocyte marker CD45 (Figure 3.4, Figure 3.6).

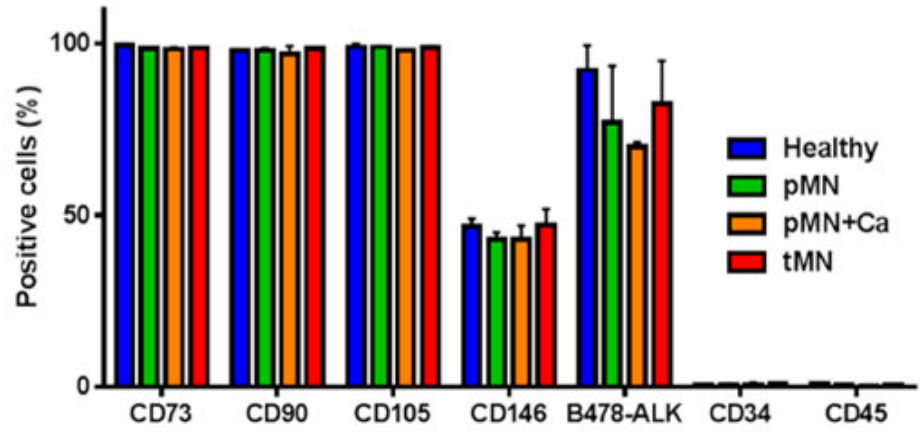


Figure 3.4. Phenotype of tMN and control cohorts BMSC (Healthy n = 17; pMN n = 7; pMN+Ca n = 10; tMN n = 18). Expression of positive and negative CD markers of culture expanded at passage 3 (P3) BMSC analysed by flow cytometry. Bars indicate mean and all error bars indicate SD.

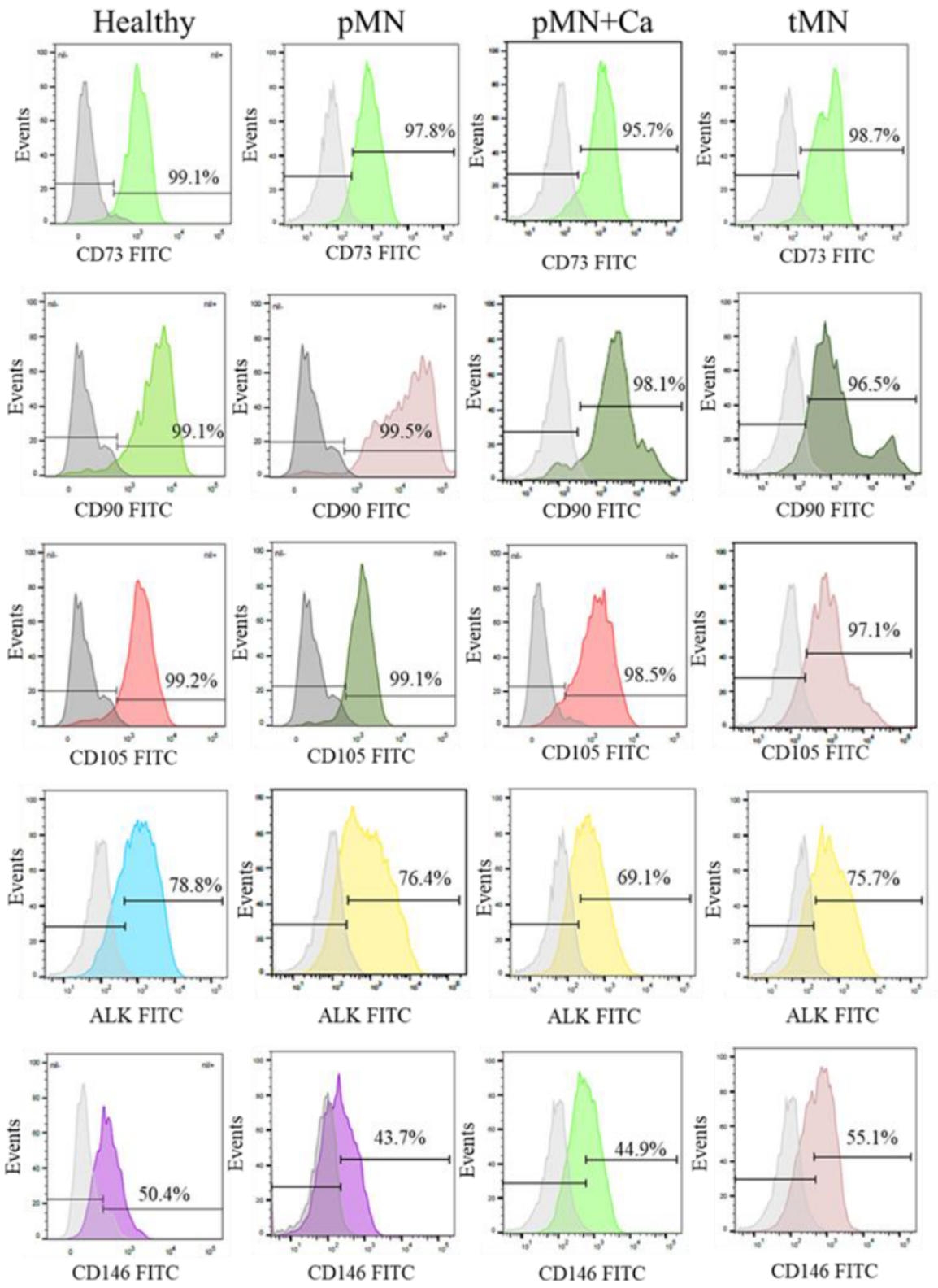


Figure 3.5. Cell surface expression of known MSC markers, CD73, CD90, CD105, ALK Phos (ALP) and CD146. Representative histograms of MFI are shown. Grey colour peak represents the respective isotype control and colour peak represents respective cohort derived BMSC.

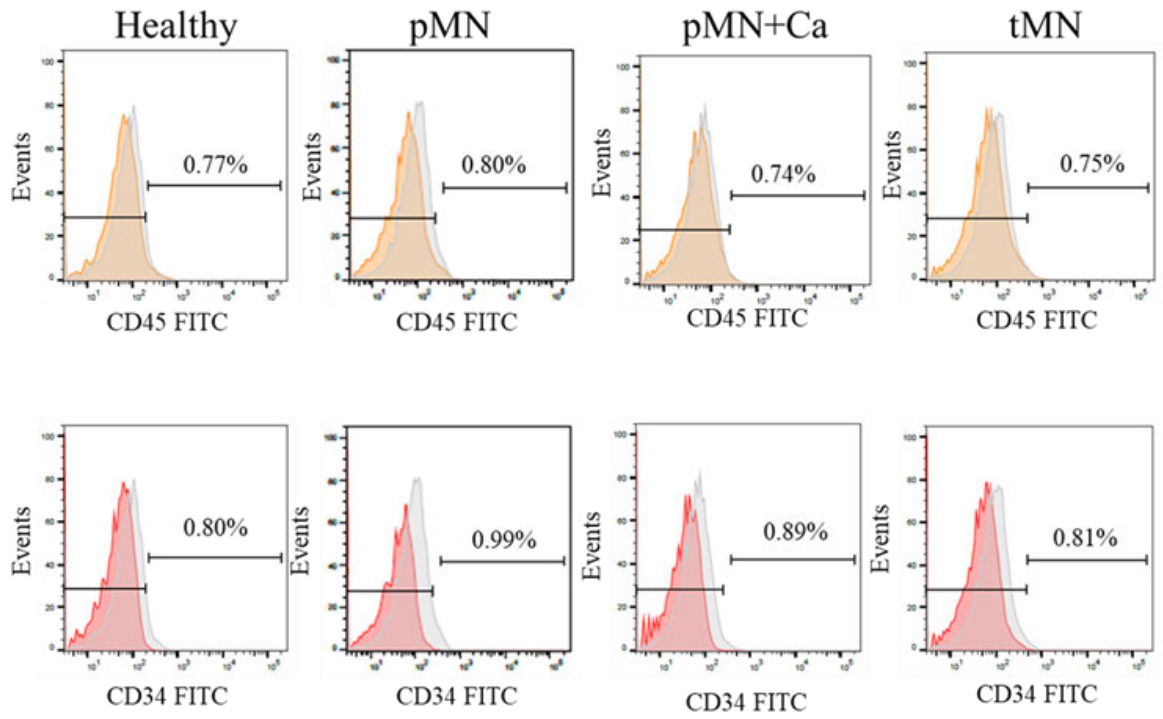


Figure 3.6. Cell surface expression of known haematopoietic markers, CD45 and CD34. Representative histograms of MFI are shown. Grey colour peak represents the respective isotype control and colour peak represents respective cohort derived BMSC.

Moreover, the cell surface expression of immature BMSC marker STRO-1 was detected in 6.5 ±1.4%, 7.5 ±3.0%, 6.2 ±4.6% and 6.1 ±1.5% (P = 0.359) in Healthy, pMN, pMN+Ca and tMN, respectively, indicating that all cohorts contain similar percentage of immature BMSC (Figure 3.7). Tri-lineage differentiation potential of BMSC used in this study, will be discussed in Chapter 5.

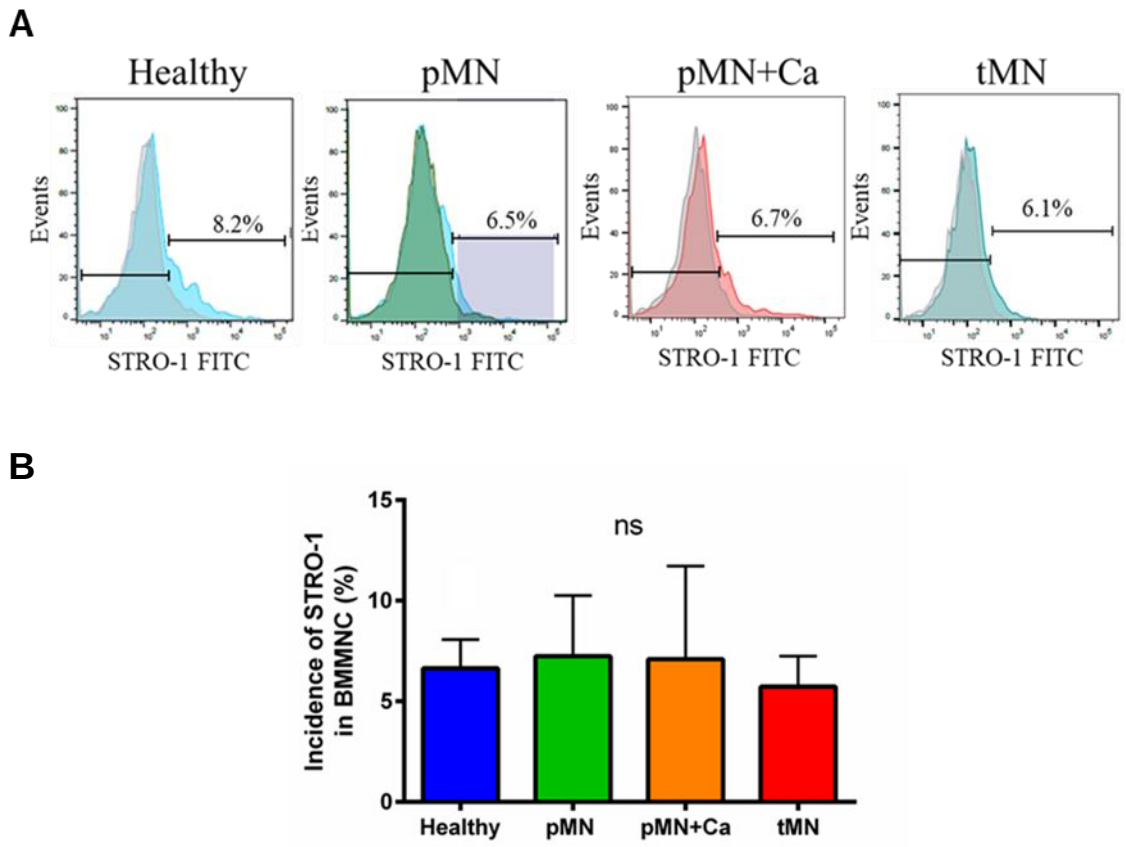


Figure 3.7. Cell surface expression of the early BMSC marker, STRO-1. STRO-1^{+}/ glycophorin-A^{-} / 7AAD^{-} fraction of BMNC was determined. (A) Representative histograms of MFI are shown. Grey colour peak represents the respective isotype control and colour peak represents respective cohort; (B) bars indicate mean and all error bars indicate SD. One-way ANOVA test was used to detect statistically significant differences between cohorts.

3.3.3. tMN Stromal Cells Display Abnormal Morphology

The most striking difference upon culturing was the morphological changes of tMN BMSC, which were significantly larger (27 ±10 mm) than BMSC from pMN (16.8 ±3 mm, $P < 0.001$), pMN+Ca (16.9 ±2 mm, $P = 0.013$) and Healthy (14.5 ±4 mm, $P < 0.001$) (Figure 3.8A). The tMN BMSC lost the typical spindle shape morphology (Figure 3.8B), resembling a flattened senescent cell. BMSC from pMN and pMN+Ca appeared disorganised and varied in size compared to controls but overall maintained a fibroblast-like morphology (Figure 3.8).

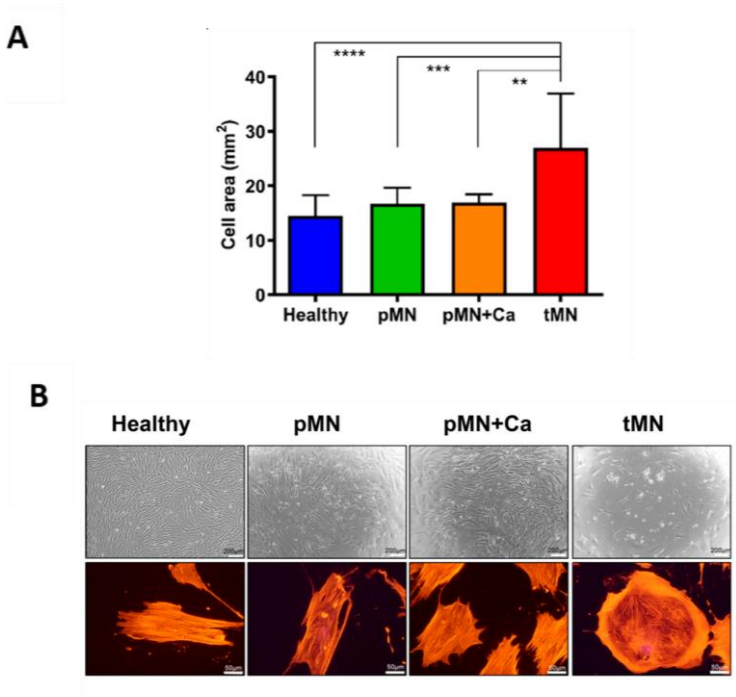


Figure 3.8. Aberrant morphology of BMSC isolated from tMN patients. (A) BMSC morphology assessed by the quantification of cells size normalised to DAPI-stained nuclei; (B) representative micrographs of BMSC morphology assessed by light microscopy (upper panel) and cytoskeleton by TRITC-Phalloidin stain (lower panel). Scale bars indicate 200µm and 50µm respectively. All bars indicate mean, and all error bars indicate SD. Mann-Whitney test was used to detect statistically significant differences between cohorts. Asterisks display *P*-values $^{**}P < 0.01$, $^{***}P < 0.001$, $^{****}P < 0.0001$.

3.3.4. Defective Growth Kinetics of tMN BMSC

Comparative studies for all MN groups including tMN, found that BMSC could be expanded *ex vivo* for significantly fewer number of cell passages than Healthy BMSC (6 ±2 versus 11 ±4 passages, $P < 0.001$) (Figure 3.9A). This was reflected by a decrease in maximum CPD (3.2 ±2 versus 11 ±7 doublings, $P < 0.001$, Figure 3.9B) and the number of CFU-F compared with Healthy (1.2 ±1 versus 4.5 ±3 colonies, $P < 0.001$) (Figure 3.9C). However, tMN appeared to have the greatest reduction in proliferative capacity, with 28% of tMN BMSC failed to reach the first passage and only 45% could be cultured beyond passage 3, significantly lower than pMN and pMN+Ca groups ($P < 0.001$, $P = 0.005$ respectively) (Figure 3.9D). CPD was significantly lower in tMN (2 ±2) compared to pMN (5.5 ±2) and pMN+Ca (3.7 ±2) ($P = 0.001$ and $P = 0.029$ respectively) (Figure 3.9B). Furthermore, tMN BMSC were associated with longer doubling times (27 ±35 versus 12 ±7 versus 14 ±12 days respectively) (Figure 3.9E) and decreased colony numbers compared to pMN and pMN+Ca (0.38 ±0.8, 1.9 ±0.4 and 2.1 ±0.6 per 10^4 cells respectively, $P < 0.001$) (Figure 3.9C).

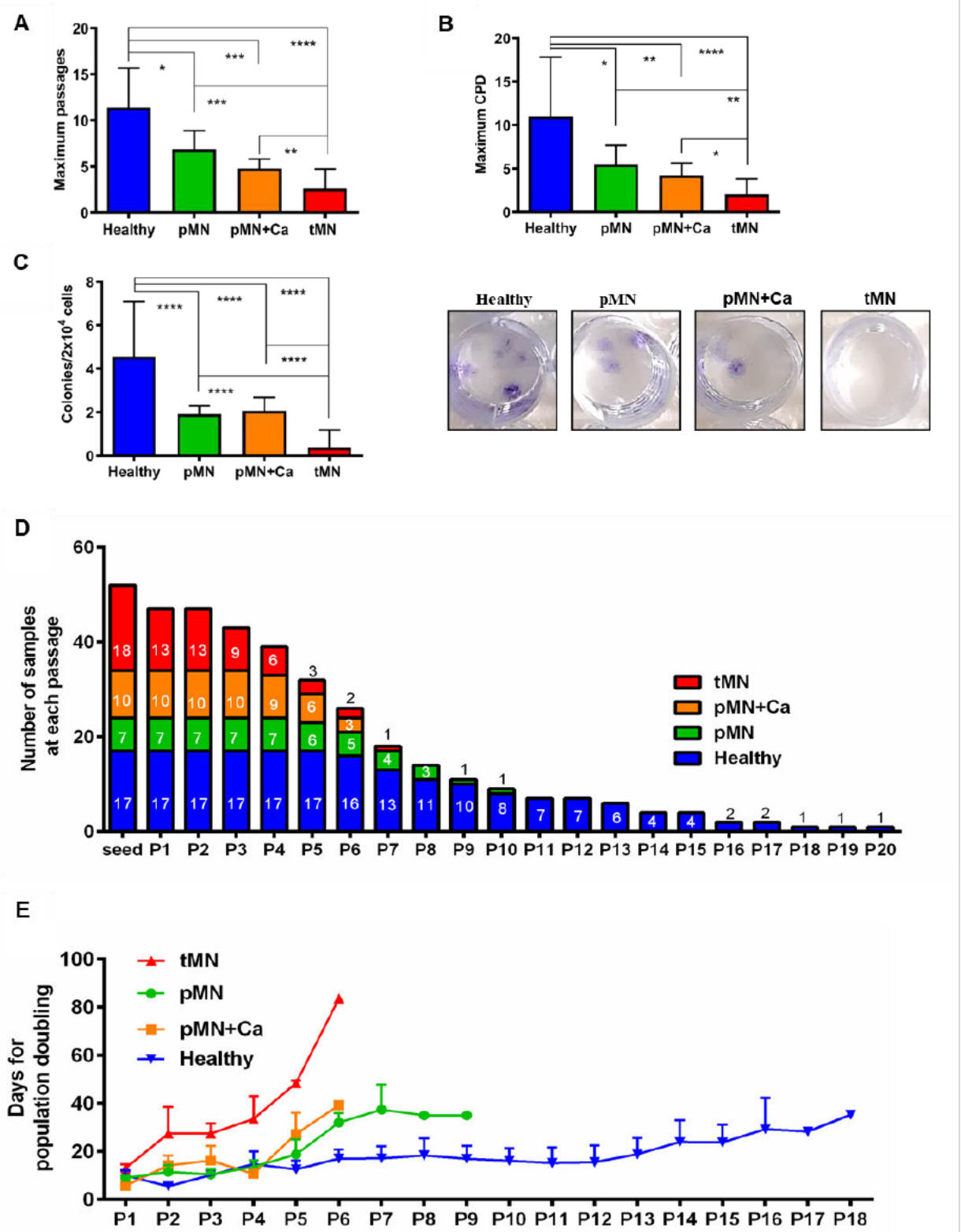


Figure 3.9. Abnormal growth kinetics of BMSC isolated from tMN patients. (A) Maximum number of passages; (B) maximum cumulative population doublings (CPD); (C) CFU-F normalised to $2x10^4$ plated BMNC and CFU-F were stained with Toluidine Blue; (D) stack graph illustrating number of samples with successful cultures at each passage; (E) days for population doublings (PD) through passages, based on the number of cells at the end of each passage compared with cells initially plated. Bars indicate mean and all error bars indicate SD. Mann-Whitney test was used to detect statistically significant differences between cohorts. Asterisks display *P*-values $*P < 0.05$, $**P < 0.01$, $***P < 0.001$, $****P < 0.0001$.

Within the tMN cohort a longer latency period (an interval between completion of CT for primary cancer and tMN diagnosis) was associated with a greater proliferative rate in univariate (P = 0.009) and multivariate Logistic regression analysis (P = 0.049) (Figure 3.10, Table 3.4), suggesting proliferative potential can improve over time. In contrast, other factors such as type of CT (chemotherapy versus radiotherapy), tMN subtype and primary cancer did not predict tMN BMSC proliferative capacity (Table 3.4).

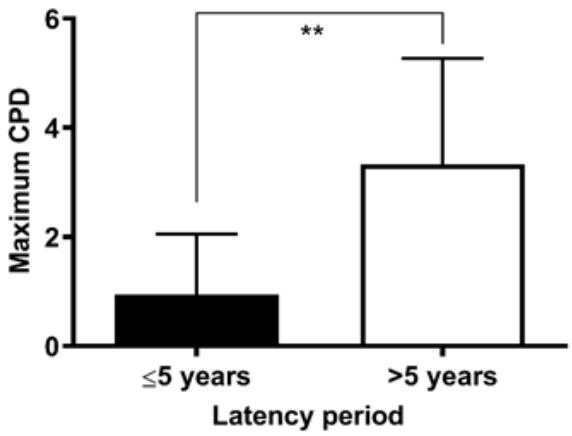


Figure 3.10. Proliferation potential according to latency period in tMN BMSC (n = 18). Latency period is a time from last dose of cytotoxic therapy for primary cancer/disease to tMN diagnosis. Proliferation potential was assessed by maximum cumulative population doublings (CPD). All bars indicate mean, and all error bars indicate SD. Mann-Whitney test was used to detect statistically significant differences between cohorts. Asterisks display P-values **$P < 0.01$.

Table 3.4. Latency period is an independent predictor of BMSC proliferation

Variable	CPD (mean ±SD)	*P*-value
Primary Ca therapy type:		
Chemotherapy	1.28 ±1.48	0.330
Radiotherapy	2.49 ±2.27	0.632
CMT (combined)	1.78 ±1.94	0.688
Myeloid neoplasm risk group:		
Low Risk	1.51 ±1.56	0.883
High Risk	2.02 ±2.14	
Primary Ca type:		
Haematological	1.49 ±1.44	0.629
Other	1.94 ±2.1	
Latency time:		
≤ 5 years	0.94 ±1.1	**0.009**
> 5 years	3.33 ±1.94	

Abbreviations: Latency period, time from last dose of cytotoxic therapy for primary cancer/disease to tMN diagnosis; Ca, cancer; CMT, combined modality treatment (chemotherapy plus radiotherapy); CPD, cumulative population doublings.

3.3. DISCUSSION

Findings from the present study support other published reports regarding defective stroma in pMDS/AML, including abnormal morphology [203] and slow growth kinetics [170, 204, 205]. However, the observed changes seen in tMN BMSC were substantially severe and distinguishable from pMDS/AML including the enlarged/flattened morphology, slower proliferation rate and reduced clonogenic potential. Until now, only one study assessed the phenotype and proliferative potential of tMN BMSC [203]. Whilst our study and that of Falconi *et al.* [203] concurred regarding reduced clonogenic potential of BMSC from MDS compared to control, the findings differ in the tMN cohort. In contrast to findings by Falconi *et al.* [203], our study demonstrates that tMN BMSC exhibit significantly reduced clonogenic and proliferative potentials compared to pMN. The disparity between the two studies could be due to differences in tMN BMSC proliferation. Falconi *et al.* [203] established their BMSC cultures in 83% of the tMN, whilst in the present study only 50% of tMN BMSC were successfully established. The differences in findings between the two studies could partly be due to inter-patient variability. Within our cohort of tMN, longer latency (interval between treatment for primary cancer and diagnosis of tMN) was associated with higher proliferative capacity; such critical correlation was not provided by Falconi *et al.* [203]. Aberrant phenotypic and proliferative features of tMN BMSC in our study was further supported by GSEA analysis showing reduced expression of genes involved in cellular proliferation and cell cycle. The *FOS* oncogene which plays a critical role in development, cell proliferation and differentiation [256] was significantly down regulated in tMN BMSC compared to other MN and Healthy BMSC.

BMSC isolated from tMN and pMN were uniformly positive for BMSC markers and negative for haematopoietic markers, which was consistent with a BMSC phenotype and excluded the contamination of haematopoietic cells. Comparison of the expression of these markers between

patients treated previously with CT (tMN patients) and untreated patients (pMN+Ca patients), found that the two populations were phenotypically comparable with regards to the percentage of cells $CD73^+$, $CD90^+$ and $CD105^+$, which is consistent with previous studies assessing immunophenotype of BMSC exposed to CT [181, 257]. However, none of these studies assessed percentage of ALK-Phos $(ALP)^+$ and $CD146^+$, with only one study assessing changes in cell surface expression of STRO-1 [181]. Whilst this study reported higher expression levels of STRO-1 compared to our study, the patients that they assessed were not diagnosed with tMN.

Collectively, the findings of this chapter demonstrate that BMSC derived from tMN patients exhibited aberrant morphology consisting of large, rounded and less adhesive cells compared to typical spindle-shaped morphology observed with controls. This was associated with a significantly reduced proliferative and clonogenic potential compared to pMN+Ca providing evidence that prior CT may lead to long-term damage to BM microenvironment. Following chapters will elaborate on the functional consequences of these altered properties of BMSC derived from tMN patients.

Chapter 4: Distinct Senescent Phenotype of tMN BMSC

4.1. INTRODUCTION

tMN is considered to be an HSC-autonomous disorder, in which initiation and progression are driven by stem cell-intrinsic genetic events induced by CT [88, 201]. This is supported by recurrent karyotypic clonal abnormalities associated with certain DNA damaging agents, such as translocations involving *RUNX1* at 21q22.1 or *KMT2A* at 11q23.3 with topoisomerase inhibitors and deletions of chromosome 5, loss or deletion of chromosome 7 with alkylating agents [22]. Is has been reported previously that DNA damaging CT not only induces genetic alterations in HSC [177, 258] but also damage to the stromal cell compartment [179-182].

4.1.1. DNA Damage

DNA damage can occur as a result of several factors such as replication errors, oxidative stress, mitochondrial dysfunction, oncogene overexpression, and exposure to cytotoxics, such as ionizing radiation and chemotherapy [259] (Figure 4.1). Following DNA damage, normal, healthy cells hold a provisional growth arrest and attempt to repair their DNA [260]. DNA damage repair proteins are involved in detection of DNA damage and executing cellular responses to restore DNA integrity [261]. Fate of the cell following DNA damage depends upon the intensity of DNA damage, integrity of DNA damage repair mechanism and cell type damage.

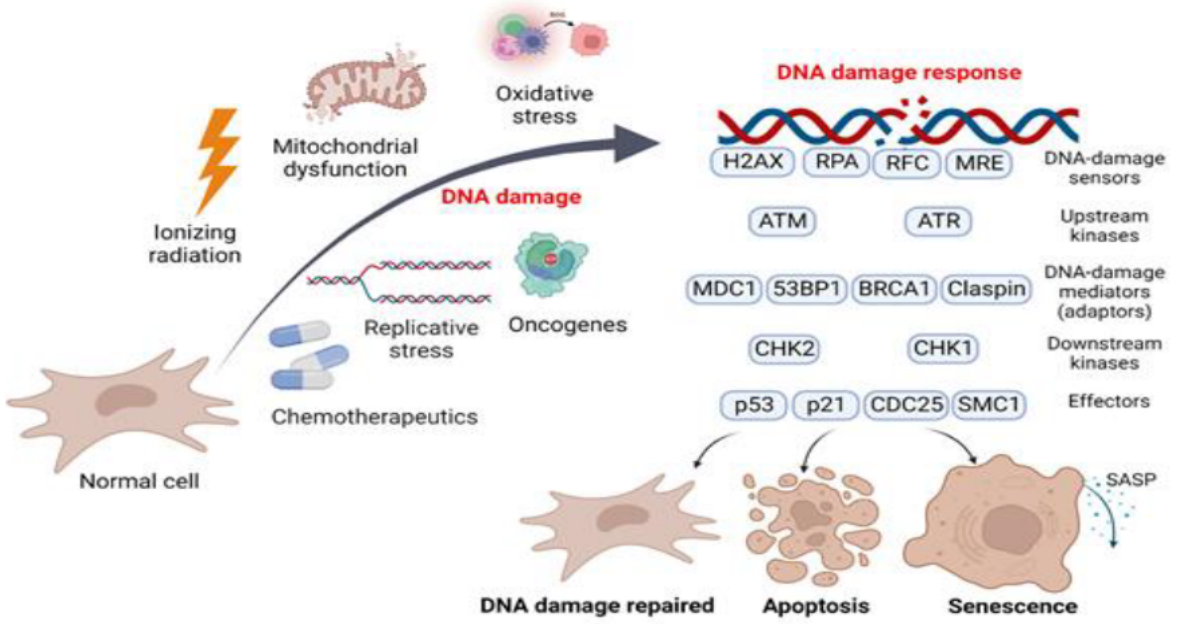


Figure 4.1. DNA damage response following DNA damage due to various stress factors. Cells exposed to numerous types of intrinsic and/or extrinsic stressors such as exposure to CT, mitochondrial dysfunction or oncogene activation can damage DNA that creates DNA double strand breaks and defects in DNA damage response mechanisms and subsequently cells can enter a cellular senescence or apoptosis.

Adapted from Campisi *et al.* [262]

Cytotoxic therapy induces DNA damage including double strand breaks and effective DNA damage response (DDR), is crucial for repairing these damages [263] (Figure 4.1). DDR occurs via DNA damage sensors such as replication protein A (RPA), replication factor C (RFC)-like complexes and MRN complex, which activate ATM and ATM and RAD-3 related (ATR) upstream kinases [264]. Through phosphorylation of approximately 900 protein targets the DDR is being initiated [265]. Phosphorylation of the histone variant H2AX at Ser 139, is considered as at sensitive marker for DNA damage and subsequent DNA repair due to its abundance and correlation with each double strand break [266]. Moreover, γH2AX formation serves as checkpoint for repair pathways through mechanisms that directly or indirectly maintain several adaptor proteins, such as MDC1, 53BP1, BRCA1 and claspin [267-270]. These in turn trigger the activation of downstream kinase cascades involving checkpoint 1

(CHK1) and CHK2, eventually resulting in activation of effectors molecules such as SMC1, CDC25 and the tumour suppressor p53. Active *TP53* lead to cell cycle arrest, to allow DNA repair. Cells with defective DDR response can undergo apoptosis or other forms of regulated cell death which eliminates the cells. While cells which cannot repair DNA damage and did not have severe DNA damage to trigger apoptosis, can undergo senescence for prolonged period until their elimination by the immune system [259].

4.1.2. Cellular Senescence

Cellular senescence is the irreversible arrest of cell proliferation and occurs when DNA damage is severe, or if DNA repair mechanisms are compromised. This process was first reported in 1961 by Hayflick and Moorhead following the observation that primary cells cultured *in vitro* fail to proliferate after an extended periods of time [271] and was described as replicative senescence (Table 4.1). Senescence has also been observed to be induced prematurely by activation of oncogenic form of RAS in normal human cells which was associated with accumulation of p53 and p16 [272]. Overexpression of other oncogenes, such as RAF, MOS, BRAF and MEK [273-275] are known to be associated with senescence, known as oncogene-induced senescence (OIS). Senescence can also be triggered by various external stress factors including chemotherapy or radiotherapy (therapy-induced senescence, TIS) (Table 4.2) or intrinsic factors such as oxidative stress or mitochondrial dysfunction [276]. Cellular senescence induced by various stress factors share common features such as stable growth arrest, relative resistance to apoptosis, persistent DNA damage signalling, increased expression of cyclin-dependent kinase (CDK) inhibitors p16 (*CDKN2A*), p21 (*CDKN1A*) and senescence-associated β-Galactosidase activity, enhanced metabolic activities and secretion of senescence associated secretory phenotype- cytokines (SASP) [259], which are described in the following sections.

Table 4.1. Different form of cellular senescence

Type of senescence	
Replicative	Reduced proliferative potential occurring after multiple cell divisions leading to irreversible growth arrest
Therapy- induced (TIS)	Cytotoxic therapy such as chemotherapy and radiation leading to a state of stable growth arrest, through induction of DNA double-strand breaks
Oncogene- induced (OIS)	Activation of oncogenes, such as BRAF or RAS, or the inactivation of tumour suppression, such as PTEN
Oxidative stress- induced	Oxidative compounds such as oxygen, hydrogen peroxide and tert-butylhydroperoxide or cell metabolism's oxidizing products lead to senescence by increased ROS
Mitochondrial dysfunction-associated	Induction of mitochondrial dysfunction leads to senescence, with SASP as main driver
Epigenetically induced	Inhibitors of DNA methyltransferases (e.g., Azacitidine), histone deacetylases (e.g., sodium butyrate or trichostatin A), histone acetyltransferases (e.g., curcumin, C646) or histone methyl transferases (e.g., BRD4770) trigger senescence

Abbreviations: BRAF, proto-oncogene B-Raf and v-Raf murine sarcoma viral oncogene homolog B; PTEN, phosphatase and tensin; RAS, Rat sarcoma virus oncogene homolog; ROS, reactive oxygen species; SASP, senescence associated secretory phenotype.

Table 4.2. Selected list of cytotoxics triggering senescence

Inducer	Agent
Genotoxic drugs:	
• **DNA replication stress inducers**	Hydroxyurea; Bromodeoxyuridine
• **DNA-damaging agents:**	
➢ DNA topoisomerase inhibitors	Doxorubicin; Etoposide
➢ DNA crosslinkers	Cisplatin; Mitomycin C
• **Drugs with complex effects**	Actinomycin D; Bleomycin
Irradiation:	Ionizing and UV

4.1.2.1. Main features of senescent cells

4.1.2.1.1. Growth arrest

One common feature of senescent cells is an incapability to progress through the cell cycle, usually with a DNA content that is typical of growth 1 phase (G1) of the cell cycle. Senescent cells are different from quiescent and terminally differentiated cells (Figure 4.2) [277], in that senescence growth arrest is permanent because senescent cells cannot be stimulated to proliferate by growth factor stimuli. Even though terminally differentiated cells have irreversible growth arrest like senescent cells, they are the result of a defined developmental program, turning undifferentiated cells into specialized cells. During senescence, growth arrested cells, fail to initiate DNA replication, and this replication failure is initiated by two signalling pathways: p53/p21 and p16/pRb. In particular, the transcriptional regulators, p53 and pRb and associated pathways can interactively or independently control the cell senescence progress [278], and are commonly impaired in cancer cells [279]. The transcription of p53-

dependent cyclin-dependent gene, namely that encoding p21, inhibits *CDK2* activity, resulting in hypo- phosphorylated Rb that induces a senescent-like growth arrest [280]. Additionally, senescent cells often display enhanced expression of two cell-cycle inhibitors, *CDKN1A* and *CDKN2A* [259] which are important regulators of senescence. Senescent cells also suppress genes that encode proteins that stimulate or enable cell cycle progression, such as proliferating cell nuclear antigen (*PCNA*) (component of the replication and repair machinery), *FOS* (component of transcription machinery) or cyclin A and B (regulators of the cell cycle) [281-284].

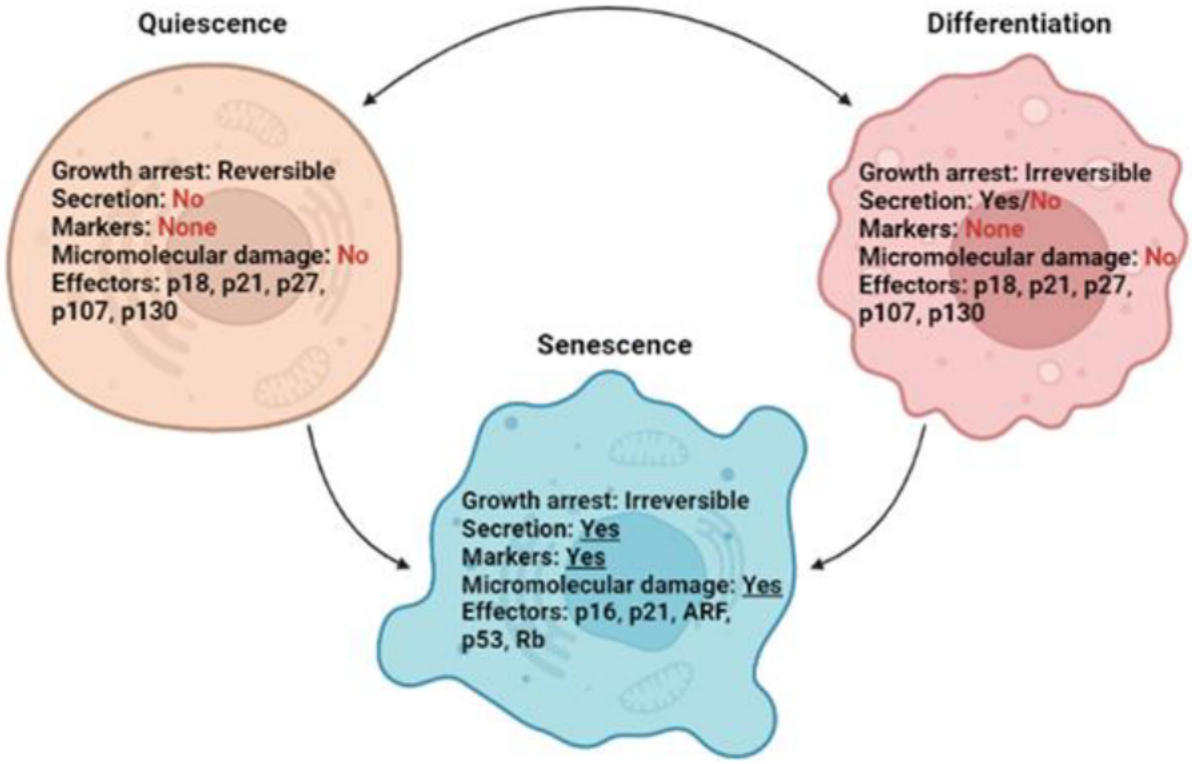


Figure 4.2. Senescence versus other forms of growth arrest. Comparison of senescence with other forms of proliferation arrest in regard to growth arrest reversibility potential, secretory functions, known markers of detection and effectors which allow to distinguish between these cellular states. Arrows show association between senescence and other processes that lead to growth arrest.

Adapted from Gorgoulis *et al.*[259]

Moreover, cellular senescence is characterised by an array of markers expressed in culture and *in vivo* (Figure 4.3), associated with a decline in cell proliferation/ colony formation potential and/or DNA synthesis rate as well as higher expression levels of the CDK inhibitors, p16 and p21 [285, 286].

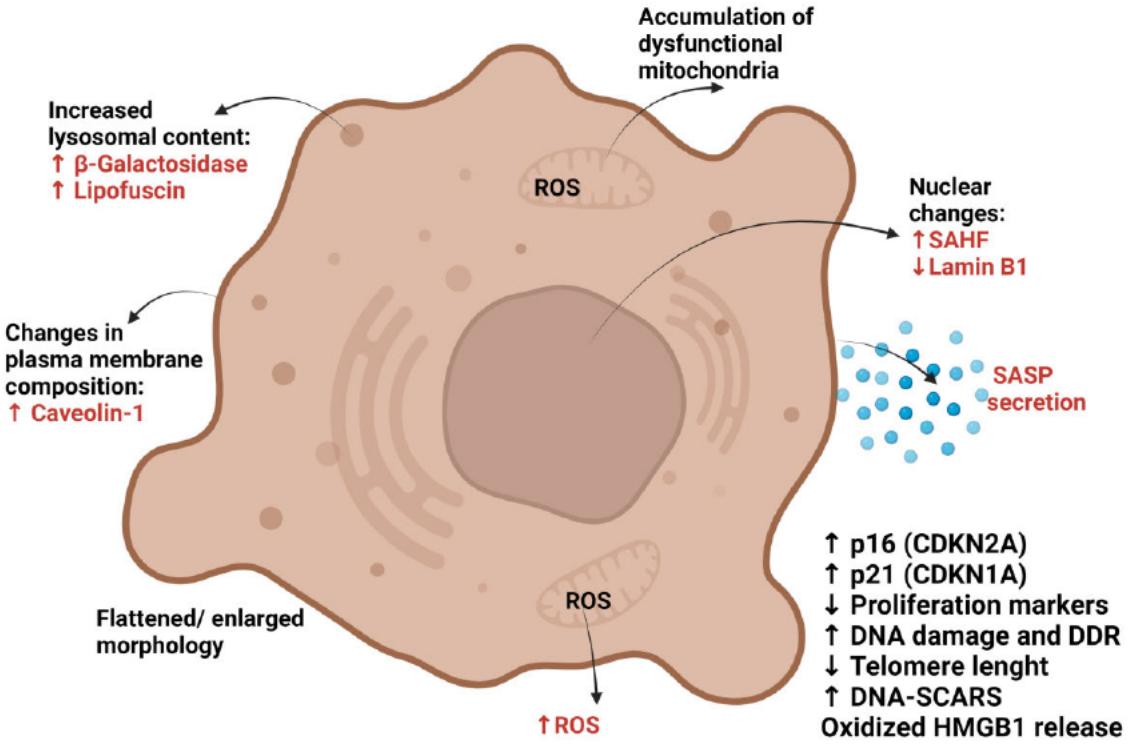


Figure 4.3. Known markers of cellular senescence. There are several indicators of senescence, which includes increased β-Galactosidase activity, loss of Lamin B1, upregulation of the CDK inhibitors p16 and p21, secretion of oxidized HMGB1, shortened telomere length, senescence associated heterochromatin foci (SAHF), increased DNA damage and DNA damage respond (DDR), persistent nuclear DNA damage foci (DNA-SCARS- DNA segments with chromatin alterations reinforcing senescence), Lipofuscin accumulation and high levels of SASP components.

4.1.2.1.2. Apoptosis resistance

It is now thought that cellular senescence and apoptosis are substitute cellular fates that often can be triggered by the same stress factors. Senescent cells are resistant to extrinsic and intrinsic

apoptosis [287, 288], which can be mediated by upregulation of anti-apoptotic B-cell lymphoma-2 (BCL-2) family members such as BCL-W and BCL-XL [289]. Therefore, the upregulation of the BCL-proteins has been reported as a marker of senescence [289, 290].

4.1.2.1.3. Abnormal cell size and shape

A prominent feature of *in vitro* senescence is the enlarged/flattened morphology. Activation of mTOR pathway has been associated with enlargement of senescent endothelial cells [291] and appears in response to senescence-inducing factors [292]. Rearrangement of cytoskeleton, mainly vimentin and actin has been linked to the abnormal cell shape in senescent cells [293, 294].

4.1.2.1.4. Increased lysosomal content

The most widely used marker to quantitate cellular senescence is increased activity of the lysosomal enzyme associated β-Galactosidase [295], which is measurable by histochemical or fluorescence staining in most senescent cells apart from cells lacking the gene encoding for lysosomal β-Galactosidase (galactosidase beta 1; *GLB1*), such as in fibroblast from patients with autosomal recessive G(M1)-gangliosidosis [296]. Since β-Galactosidase is upregulated during senescence, due to increased lysosomal content, its residual activity can be detected at a suboptimal pH of 6.0 [296, 297]. Although β-Galactosidase is notable in senescent cells, it is neither essential nor a determinant of the senescent phenotype.

More recently, Lipofuscin has been used as a senescence marker as it accumulates in the cytoplasm of senescent cells and can be imaged in lysosomes by light microscopy or by histochemical staining [286, 298, 299].

4.1.2.1.5. Plasma membrane composition changes

The plasma membrane plays a vital role in communication with neighbouring cells and the extracellular space. Caveolin-1 is a known scaffolding protein and the main component of the plasma membrane [300] and its upregulation is considered as a regulator of cellular senescence. It has been reported that oxidative stress triggers the Caveolin-1 gene promotor in p38 MAPK-Sp1- dependent mechanism and upregulates Caveolin-1 expression [301, 302]. Upregulation of Caveolin-1 endorse senescence through initiation of the p53-p21 signalling pathway [303]. Some chemotherapeutic drugs, namely bleomycin and high levels of glucose have also been linked to Caveolin-1 induced cellular senescence [304, 305].

4.1.2.1.6. Compromised nuclear integrity

Another common feature of senescent cells is downregulation of Lamin B1, a major component of the nuclear lamina [306, 307]. Loss of Lamin B1 correlates with senescence-associated chromatin structures (SAHF) [308]. SAHF are the most prominent chromatin changes detected in oncogenic induced senescence [309].

4.1.2.1.7. Secretory phenotype

A cardinal feature of cellular senescence is SASP, secretion of pro-inflammatory cytokines, chemokines, growth factors, proteases and other signalling molecules that may serve as a homeostatic signal of cellular damage (Table 4.3) [259, 310]. Significantly, its exact composition differs depending on the cell type and the senescence stressor. Similarly, the roles assigned to some of the SASP members, are also varied and depend not only on the nature of the SASP, but on the nearby environment and the genetics of the cells being exposed to the SASP.

Table 4.3. Senescence-associated secretory phenotype (SASP) factors

Class	SASP factors
Soluble factors:	
• Interleukins	IL-1α; IL-1β; IL-6; IL-7; IL-13; IL-15
• Chemokines (CXCL, CCL)	GRO-α (CXCL1), -β (CXCL2); ENA-78 (CXCL5); IL-8 (CXCL8); I-TAC (CXCL11) I-309 (CCL1); MIP-1α (CCL3); MCP-2 (CCL8); MCP-4 (CCL13); HCC-4 (CCL16); MIP-3α (CCL20); TECK (CCL25); eotaxin-3 (CCL26)
Other inflammatory molecules:	TGFβ; GM-CSF; G-CSF; IFN-γ; BLC (CXCL13); MIF
Growth factors and regulators:	Amphiregulin; epiregulin; heregulin; EGF; FGF2; HGF; KGF (FGF7); VEGF; angiogenin; SCF; CXCL12 (SDF-1); PIGF; NGF; IGFBP-2, -3, -4, -6, -7
Proteases and regulators:	MMP-1, -3, -10, -12, -13, -14; TIMP-1; TIMP-2; PAI-1, -2; t-PA; u-PA; cathepsin B
Receptors or ligands:	ICAM-1, -3; OPG; sTNFRI; sTNFRII; TRAIL-R3; Fas; u-PAR; SGP130; EGF-R
Non-protein molecules:	PGE2; nitric oxide; ROS
Insoluble factors (extracellular matrix):	Fibronectin; collagens; laminin

Abbreviations: BLC, B lymphocyte chemoattractant; FGF2, fibroblast growth factor2; EGF, epidermal growth factor; ENA-78, epithelial neutrophil-activating peptide 78; G-CSF, granulocyte-colony stimulating factor; GM-CSF, granulocyte-macrophage colony-stimulating factor; GRO, growth-related oncogene; HGF, hepatocyte growth factor; ICAM, intercellular adhesion molecule; IGFBP, insulin like growth factor-binding protein; KGF, keratinocyte growth factor; MCP, membrane cofactor protein; MIF, macrophage migration inhibitory factor; MIP-1, Macrophage inflammatory protein-1; MMP, matrix metalloproteinase; NGF, nerve growth factor; OPG, osteoprotegerin; PAI, plasminogen activator inhibitor; PGE2, prostaglandin E2; PIGF, placental growth factor; ROS, reactive oxygen species; SCF, stem cell factor; SDF, stromal cell derived factor; SGP130, soluble glycoprotein 130; sTNFR, soluble tumour necrosis factor receptor; TECK, thymus-expressed chemokine; t-PA, tissue-type plasminogen activator; TGFβ, transforming growth factor beta; TIMP, tissue inhibitor of metalloproteinases; TRAIL, tumour necrosis factor-related apoptosis-inducing ligand; u-PA, urokinase-type plasminogen activator; u-PAR, u-PA receptor; VEGF, vascular endothelial growth factor.

However, several of the crucial effectors of the SASP and its regulatory mechanism seemed to be shared. Extensive crosstalk between networks and pathways has been detected, and different SASP signalling pathways may orchestrate the transcription, translation, or protein stability of several SASP factors [311, 312]. The main transcriptional regulators of SASP are nuclear factor kappa B (NF-κB) and CEBPα [313-315]. Other regulators are DNA damage [316], p38MAPK [317], mTOR [314, 318, 319], GATA4 [320] and MLL-1 [321]. Further, it has been reported that the SASP is linked with genotoxic effectors, signifying it is controlled by DDR signaling [322]. Even though low (0.5Gy) and high (10Gy) irradiation dose initiate a DNA damage response, only high dose causes a permanent senescence growth arrest indicated by p53 stabilization and phosphorylation. Furthermore, those DNA damaged- senescent cells developed SASP slowly, requiring 4-7 days before expressing robust SASP indicating that the SASP is not a DNA response by rather DNA damage is responsible for development of SASP. There is a certain degree of overlap between various SASP components, with specific factors being found almost always particularly IL-6, IL-1, IL-8, GM-CSF, matrix metalloproteinase (MMP)-family, intercellular adhesion molecule 1 (ICAM-1), and plasminogen activator inhibitor (PAI-1) [310], regardless of cell type or senescence stressor. The most prominent cytokine of the SASP is IL-6, which has been associated with DNA damage and oncogenic effectors- induced senescence in several different type of cells, such as epithelial cells, fibroblasts, monocytes, and keratinocytes [313, 322, 323]. Moreover, IL-6 secretion appears to be directly governed by persistent DNA damage signalling, including protein kinases such as ATM and CHK2, which are restricted to the DNA-damage foci discover in senescent cells, independent of the p53 pathway [316]. IL-6 and IL-8 anticipate in an autocrine increase of the CEBPβ and NF-κB activity and magnify SASP signalling [313, 315]. Another cytokine, IL-1 has been proven to be an upstream regulator for most senescent cells, such as fibroblasts [324, 325], endothelial cells [326], cytotoxics-induced senescent epithelial cells [327] and tumour

cells [322]. Furthermore, increased levels of IL-1 not only can induce SASP expression, e.g., IL-6 and IL-8, but inactivation of IL-1 controls SASP production, in both RAS- and cytotoxic-induced senescence [328, 329].

4.1.2.1.8. Altered metabolism

Whilst senescent cells exhibit growth arrest, usually with DNA content at G1 phase, they remain metabolically active, associated with increases in the adenosine monophosphate: adenosine triphosphate (AMP:ATP) and adenosine diphosphate: adenosine triphosphate (ADP:ATP) ratios [330]. Within physiologically normal cells, energy is produced in the form of ATP, primarily through mitochondrial OXPHOS in the presence of oxygen, and through anaerobic glycolysis in its absence [331]. However, senescent cells elevate glycolysis over OXPHOS, even in the presence of high oxygen levels [330], as catabolism in senescent cells efforts on high consumption of glucose to generate ATP. The alteration of pyruvate, the final product of glycolysis, away from OXPHOS results in a changed bioenergetic state and may occur as a response to the enhanced oxidative stress caused by for example the accumulation of dysfunctional mitochondria. This metabolic shift affects the production of ATP and the NAD^+/NADH ratio and consequently, to p53-mediated growth arrest. Moreover, AMP-activated protein kinase (AMPK) and NF-κB signalling are commonly impaired catabolic pathways in senescent cells [332-334], where changes in mitochondria function, dynamics and morphology have been reported [335] in culture [336, 337] and *in vivo* [338, 339] and are linked to aberrant mitophagic activity. Moreover, mitochondria show reduced membrane potential, leading to proton leakage and an increase in ROS production [340, 341]. While mitochondria are more abundant, it appears that their ability to produce ATP is compromised. Further, recent reports indicate that both senescence arrest and the SASP are closely associated with the metabolic state of the cell. Mitochondrial dysfunction during senescence is also

implicated in SASP regulation [342] as mitophagy in senescent cells appears to suppress the SASP [343]. In a murine lymphoma model of TIS it has been showed that the high production of SASP factors depend on higher ATP production mediated by mitochondrial metabolism (tricarboxylic acid (TCA) cycle)) and glycolysis [344].

In order to understand whether cellular senescence observed in tMN patients might represent a mechanism responsible for the impaired growth kinetics of BMSC observed in tMN patients (Chapter 3) and whether that senescence is therapy- induced, comprehensive assessment of several features of senescence were investigated and summarised in this Chapter such as apoptosis resistance, increased lysosomal content, secretory phenotype, senescent transcriptome, delay DNA damage repair and altered metabolism.

4.2. RESULTS

4.2.1. No Difference in Apoptosis Rate Between tMN, Healthy and Other MN BMSC

Studies were performed to determine the apoptosis rates of tMN BMSC based on initial studies that found colony forming potential and proliferative capacity of tMN BMSC was significantly compromised compared to Healthy and other, typical MN BMSC (Chapter 3). Flow cytometric analysis found no difference in the number of early apoptotic Annexin V^+/ $7AAD^-$ or late apoptotic Annexin V^+/ $7AAD^+$ cells (Figure 4.4) in tMN BMSC compared to Healthy and other typical MN BMSC.

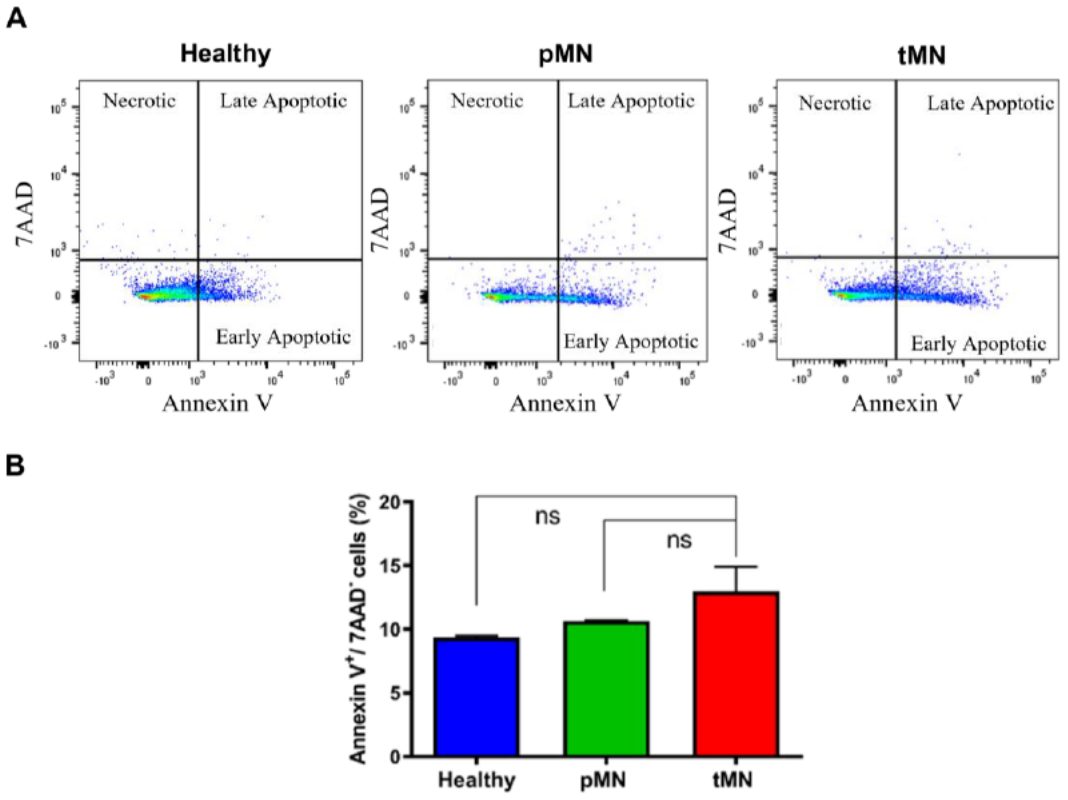


Figure 4.4. Apoptosis rates in tMN and controls BMSC. (A) Representative flow cytometry density plots of Healthy (n = 4), pMN (n = 4) and tMN (n = 4) BMSC including live cells stained with Annevin $V^-/7AAD^-$, early apoptotic cells stained with Annexin $V^+/7AAD^-$, late apoptotic cells stained with Annexin $V^+/7AAD^+$ and necrotic cells stained with Annexin $V^-/7AAD^+$; (B) bar graph show early apoptotic cells at passage 3. All bars indicate mean, and all error bars indicate SD. Mann-Whitney test was used to detect statistically significant differences between cohorts.

4.2.2. Increased Levels of β-Galactosidase of BMSC from Patients with tMN

To identify whether cellular senescence is responsible for slower proliferation rates in tMN BMSC, levels of senescence were measured. Morphological indicators of senescence as measured by β-Galactosidase staining were found to be markedly elevated in tMN (60 ±13%) compared to pMN (31 ±13%), pMN+Ca (28.29 ±9%) and Healthy control (6 ±4%) ($P < 0.001$) (Figure 4.2). Cellular senescence was shown to be higher in all MN groups compared to Healthy (45 ±19% versus 6 ±4%, $P < 0.001$) (Figure 4.5).

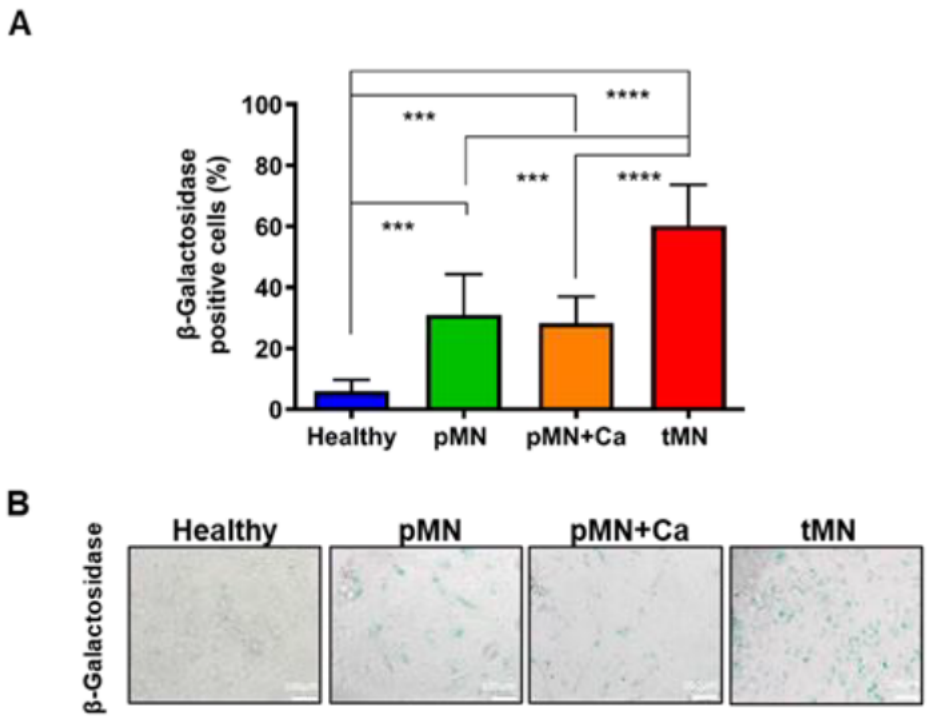


Figure 4.5. Cellular senescence assessed by percentage of β-Galactosidase-stained cells at passage 3 (Healthy n = 17; pMN n = 7; pMN+Ca n = 10; tMN n = 18). Number of β-Galactosidase positive cells (blue) was evaluated under a phase-contrast microscope and normalised to DAPI stained nuclei per field of view in triplicate wells; Scale bars indicate 100μm; All bars indicate mean, and all error bars indicate SD. Mann-Whitney test was used to detect statistically significant differences between cohorts.

4.2.3. tMN Senescence Can Occur Within a Short Latency After Cytotoxic Exposure

As our data suggested that tMN BMSC have a higher degree of senescence than BMSC from other MN not exposed to CT, we compared the latency period (the interval between completion of CT and tMN diagnosis) and the level of senescence in tMN cohort. Interestingly, higher levels of senescence were evident in BMSC from tMN patients with short latency of only 3-4 months following CT, as well as tMN with latency reaching up to two decades (Figure 4.6). This data suggests that a senescence phenotype in BMSC is persistent even after several years of CT and this can occur rapidly following therapy.

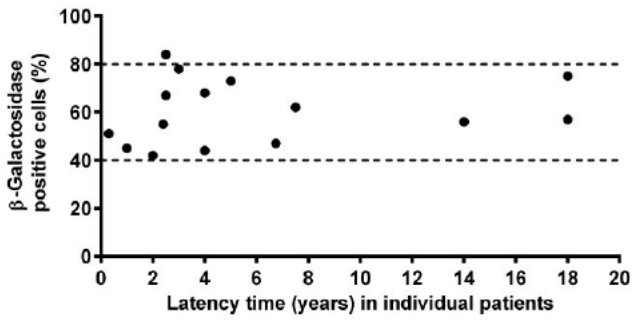


Figure 4.6. Association between cellular senescence assessed by percentage of β-Galactosidase-stained cells at passage 3 **and latency time** (time from last dose of CT for primary cancer to tMN diagnosis).

4.2.4. Distinct Senescent Transcriptome in tMN Stromal Cells Compared to Healthy and Other, Typical MN Stromal Cells

Overall, transcriptomic analysis revealed a severe senescent profile in tMN compared to other MN and Healthy BMSC over multiple enrichment analysis sets (Figure 4.7A). Substantial numbers of the 147 genes differentially expressed between tMN and other MN BMSC were previously reported to be associated with cellular senescence on SenQuest ($P < 0.001$) (Figure 4.7D) and CellAge ($P < 0.001$) (Figure 4.7E) senescence databases. Gene expression studies using RT-PCR performed on an extended independent cohort of tMN (n = 4), pMN (n = 3), pMN+Ca (n = 2) and Healthy (n = 4) for *CDKN1A* and *FOS* (Figure 4.8), confirmed

deregulation of those two genes. Further analysis of senescence-associated genes revealed a distinct signature for tMN BMSC as compared to all other control cohorts (Figure 4.7B). Furthermore, expression of 43 genes strongly correlated with β-Galactosidase levels including senescence associated genes (Figure 4.7C).

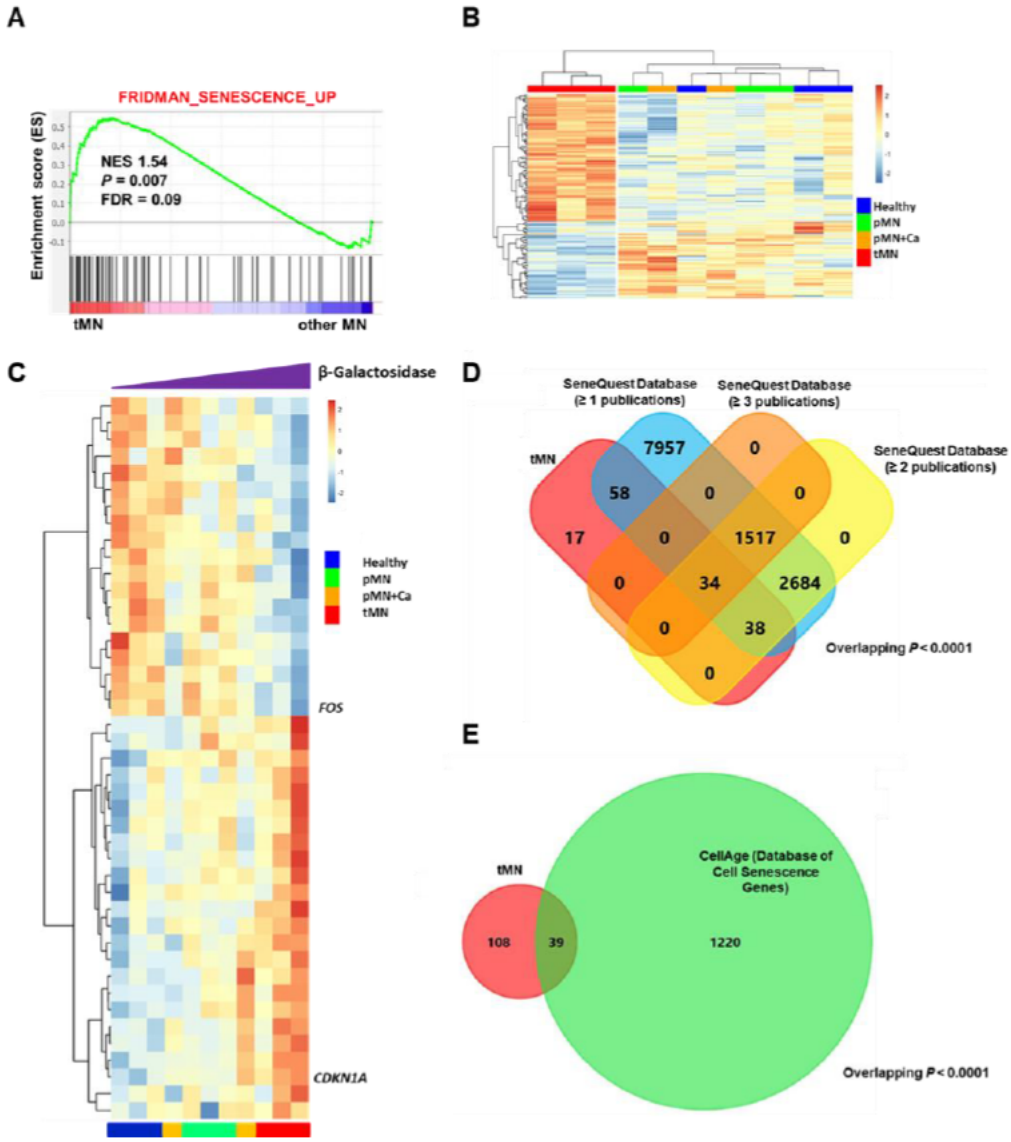


Figure 4.7. Profound senescent transcriptome in tMN BMSC. (A) Example of GSEA plot showing the specific enhancement of gene set associated with cellular senescence in tMN compared to other MN BMSC. The normalised enrichment score (NES), *P*-values and false discovery rate (FDR) are given; (B) heatmap representing the gene expression changes of senescence-associated genes found to be significantly differently deregulated (FDR $P < 0.1$ and log2 FC>|0.6|) in the BMSC from tMN as compared to Healthy and other MN BMSC. A total of 144 genes involved in the senescence (SeneQuest Database), were analysed. On the top panel of heatmap, the colour coding delineates the cohort group as indicated in the legend on the right side of the heatmap. The heatmap was generated using the pheatmap package; (C) heatmap correlating β-Galactosidase levels and expression of senescence-associated genes in Healthy controls and MN (described in method section 2.4.5.1). The differential gene expression was analysed based on the β-Galactosidase value via the BioConductor R (v4.0.3) package edgeR (3.30.3). Only gene with FDR $P < 0.05$ derived from edgeR analysis was considered as statistically significant. On the bottom panel of heatmap, the colour coding delineates the cohort group as indicated in the legend on the right side of the heatmap. The heatmap was generated using the pheatmap package; (D) Venn diagram between tMN and other MN 146 differentially expressed genes and SeneQuest database ≥1, ≥2 and 3 publications and (E) CellAge database.

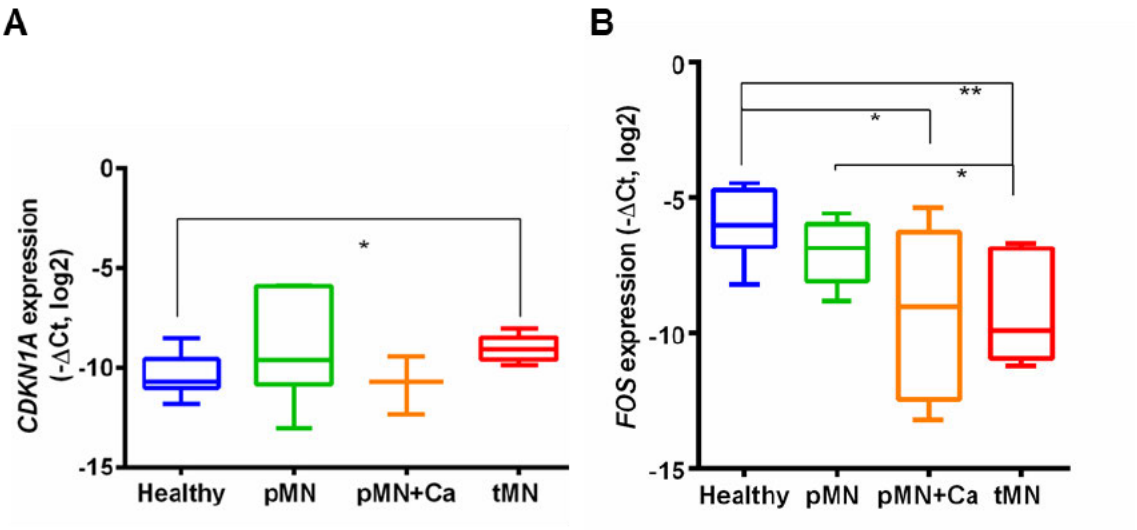


Figure 4.8. Validation of differentially expressed genes in an independent tMN, Healthy, pMN and pMN+Ca cohort. Expression of *CDKN1A* (A) and *FOS* (B) genes in Healthy (n = 7), pMN (n = 6), pMN+Ca (n = 5) and tMN (n = 7) BMSC. Boxplot shows the gene expression across 4 defined groups by qRT-PCR. Gene expression was determined relatively to *GAPDH* mRNA expression (ΔCt) and represented as –ΔCt in log2 scale. In boxplot, the horizontal line indicates the median, boxes indicate the interquartile range, and whiskers extend from the hinge to the smallest/largest value, at most 1.5 × interquartile range from the hinge. Unpaired Student's t-test was used to detect statistically significant differences between cohorts. Asterisks display *P*-values $*P < 0.05$, $**P < 0.01$, $P*** < 0.001$.

4.2.5. Higher Levels of SASP Cytokines in Conditioned Media of tMN Stromal Cells Compared to Healthy Stromal Cells

A cardinal feature of cellular senescence is SASP, secretion of pro-inflammatory cytokines, chemokines and proteases that may serve as a homeostatic signal of cellular damage [259, 310]. Indeed, the present study found that multiple SASP associated cytokines including IL-6, IFNγ, IL-7, IL-1β, IL-13, IL-15, Eotaxin, G-CSF, and EGF were significantly higher in conditioned media of tMN BMSC compared to Healthy (Figure 4.9A). In agreement with previous reports [195, 225, 345], several SASP-associated cytokines levels such as IL-6, IFNγ, IL-7 and IL-1β were also higher in other MN (non-tMN), BMSC conditioned media compared to Healthy (Figure 4.9B). The observed lack of significant difference in tMN and other myeloid neoplasm

is likely due to interpatient variability in SASP-associated cytokines and chemokines levels (Figure 4.9B).

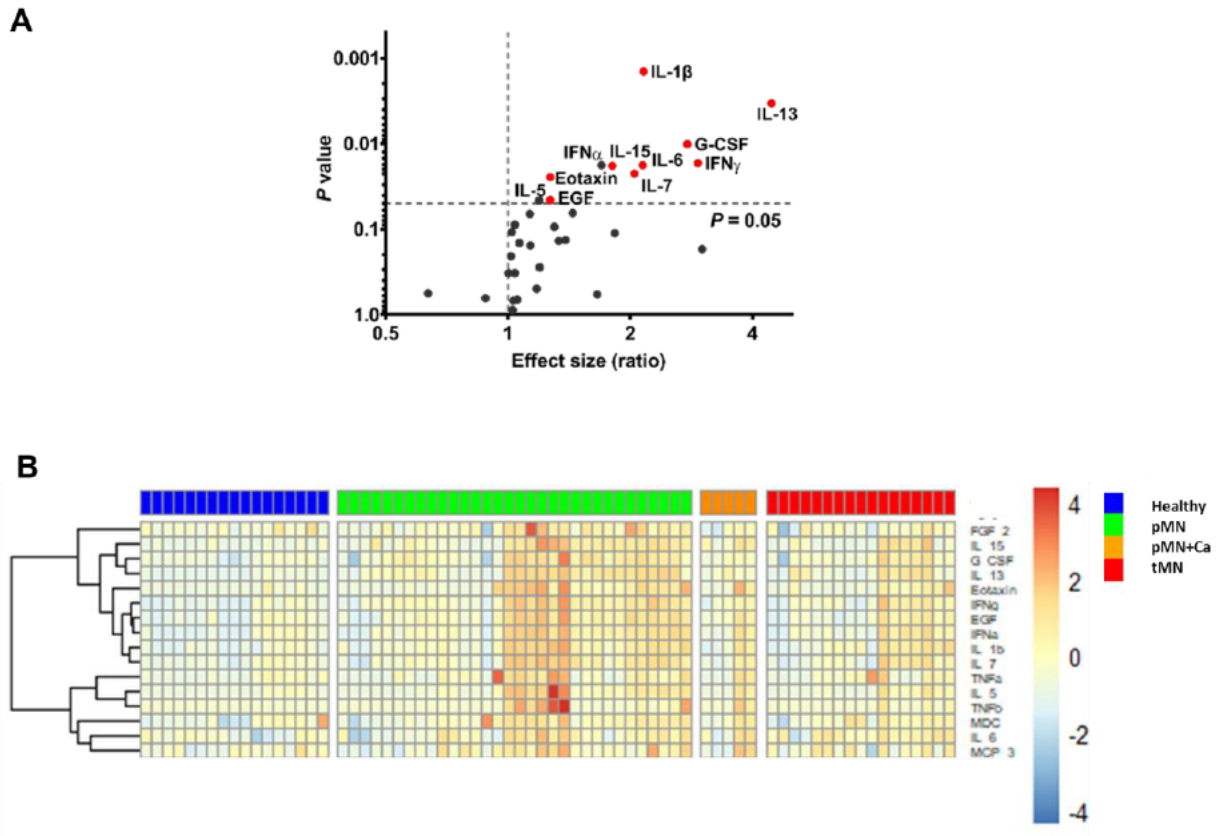


Figure 4.9. BMSC-conditional media cytokines profiles. (A) Levels of 14 senescence-associated secretory phenotype (SASP)- cytokines in tMN BMSC-conditioned media compared to age-matched healthy controls (Healthy n = 17; tMN n = 17). Cytokines in red are significantly higher and are SASP-related; (B) hierarchical cluster analysis was performed on log-transformed cytokines levels of four cohorts (Healthy, n = 17; pMN, n = 32; pMN+Ca, n = 5; tMN, n = 17) using Ward's method. Colour scales represent cytokines levels (red indicates high levels; blue, low levels). The dendrogram on the left side of the heatmap reflects the order of cytokines.

4.2.6. Defective DNA Damage Repair Potential of tMN Compared to Healthy and Other, Typical MN Stromal Cells

The level of high senescence observed in tMN BMSC could be due to a defect in the DNA damage repair pathway [262], resulting in irreparable DNA damage after exposure to CT. To assess this, baseline DNA damage in tMN and Healthy BMSC was first examined. BMSC derived from tMN exhibited higher baseline DNA damage, as shown by alkaline comet assay, compared to Healthy BMSC (Figure 4.10).

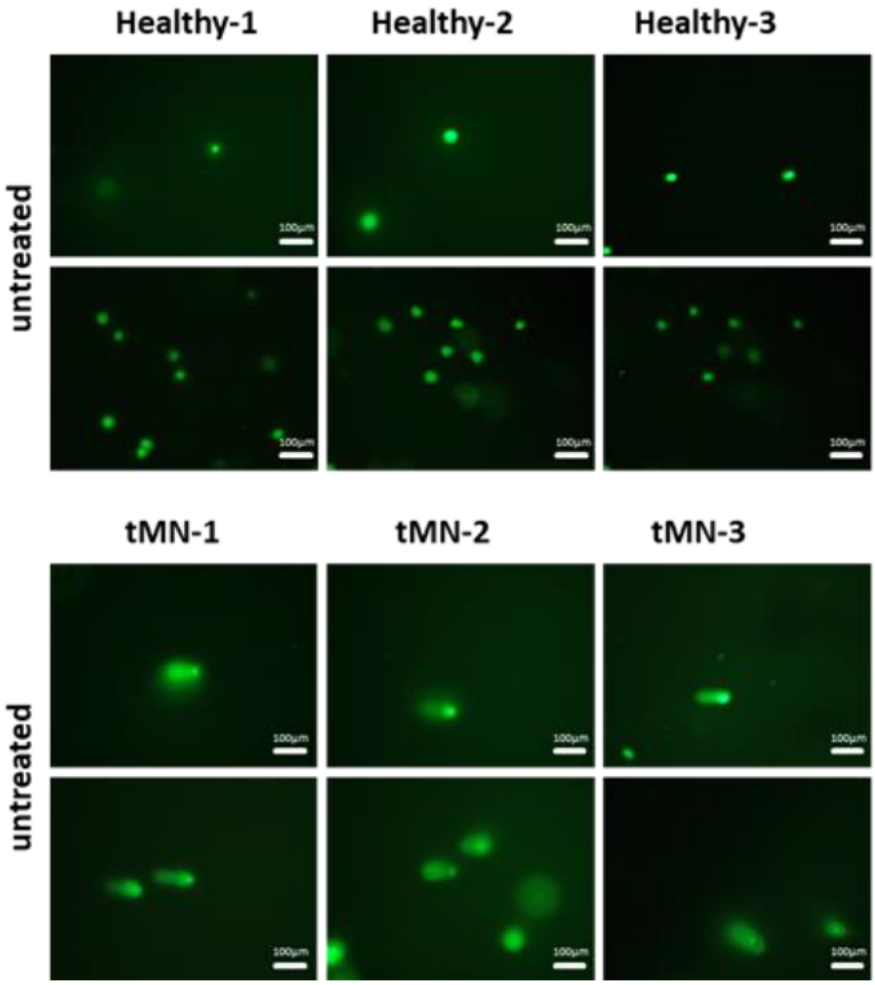


Figure 4.10. Enhanced baseline DNA damage in tMN BMSC. Alkaline comet assay shows high level of baseline DNA damage in Healthy (n = 3) (higher two panels) compared to tMN (n = 3) (lower two panels) BMSC. The length of the comet tail reflects the number of DNA breaks. Scale bars indicate 100µm.

Enhanced baseline DNA damage in tMN BMSC was probably driven by higher intracellular ROS level compared to Healthy BMSC ($P = 0.001$) (Figure 4.11).

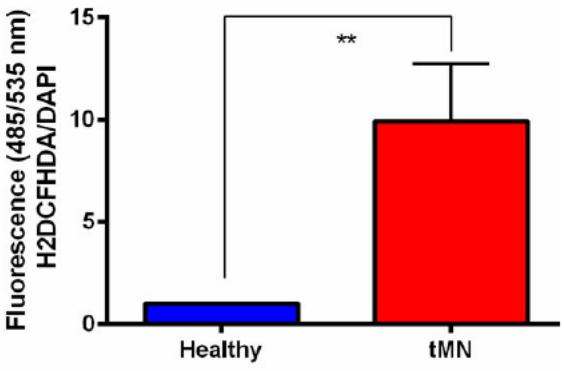


Figure 4.11. Higher intercellular ROS level in tMN compared to Healthy BMSC at baseline. ROS production was determined by measuring the formation of fluorescent dichloro fluorescein (DCF) at an Excitation 485 and Emission 535 nm in Healthy (n = 3) and tMN BMSC (n = 3). The final value was obtained by calculating the ratio of fluorescence intensity at specific time point and DAPI stained nuclei. All bars indicate mean, and all error bars indicate SD. Mann-Whitney test was used to detect statistically significant differences between cohorts. Asterisks display *P*-values $^{**}P < 0.01$.

Next, DNA damage induction by *in vitro* exposure to Doxorubicin, chemotherapeutic drug widely use in cancer treatment, was performed. To determine the appropriate concentration of Doxorubicin and assess its effect on BMSC viability without toxicity to cells a dose titration of Doxorubicin was performed on Healthy and tMN BMSC (Figure 4.12). Change in viability was observed gradually from 0.1µM onwards, in both Healthy and tMN BMSC, however 5µM shown the most reduction in the number of live cells, regardless of Doxorubicin treatment time (Figure 4.12). Therefore, for subsequent experiments 0.1 and 1µM Doxorubicin was used.

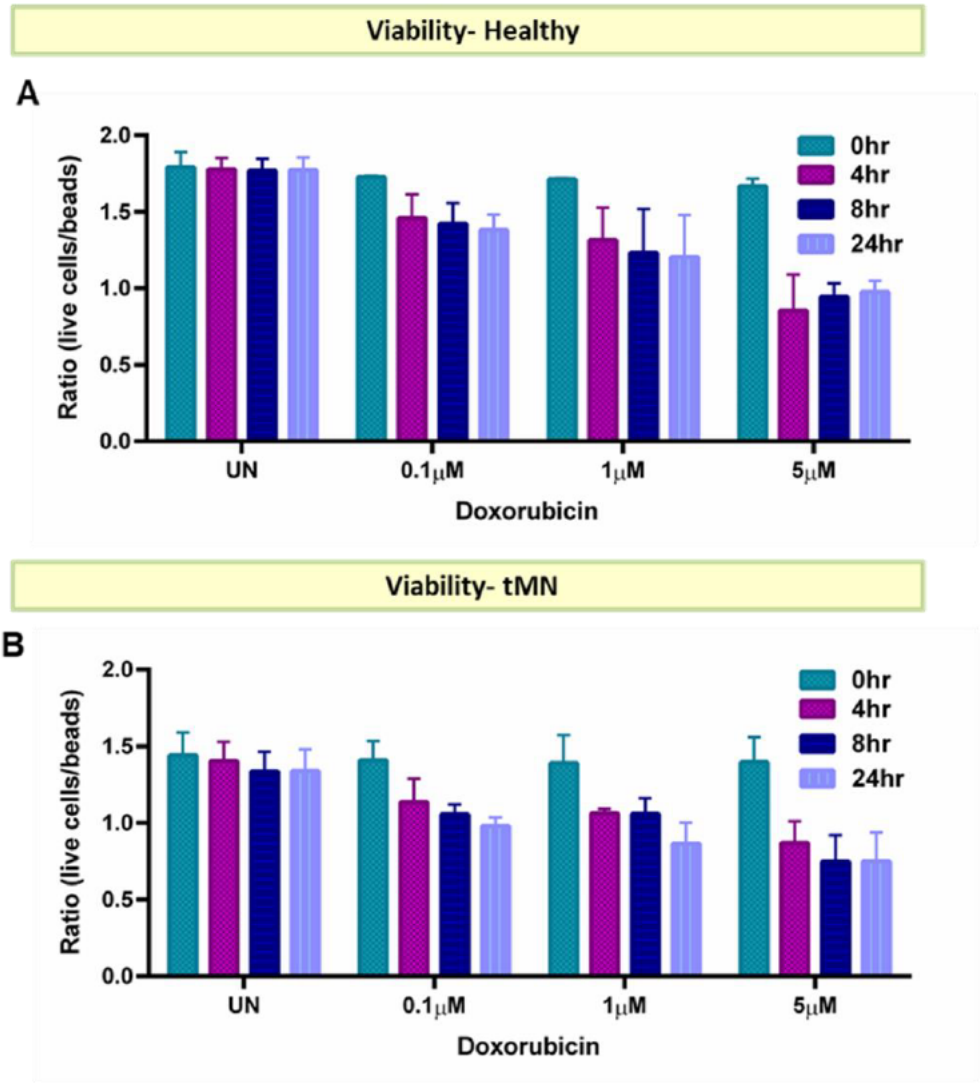


Figure 4.12. Effect of dose and time titration of Doxorubicin on viability in (A) Healthy (n = 2) and (B) tMN (n = 2) BMSC. All bars indicate mean, and all error bars indicate SD.

BMSC derived from tMN were highly sensitive to DNA damaging CT, firstly assessed by alkaline comet assay (Doxorubicin 0.1μM and 1μM) (Figure 4.13A). Secondly, high number of γH2AX foci formation were evident within 4 hours (8 ±5 versus 24 ±10%; $P < 0.001$) and peaking within 12 hours of *in vitro* exposure to 0.1 μM Doxorubicin (53 ±11 versus 83 ±8%; $P < 0.001$) (Figure 4.13B). Similar trend was observed with 1μM Doxorubicin (Figure 4.13C).

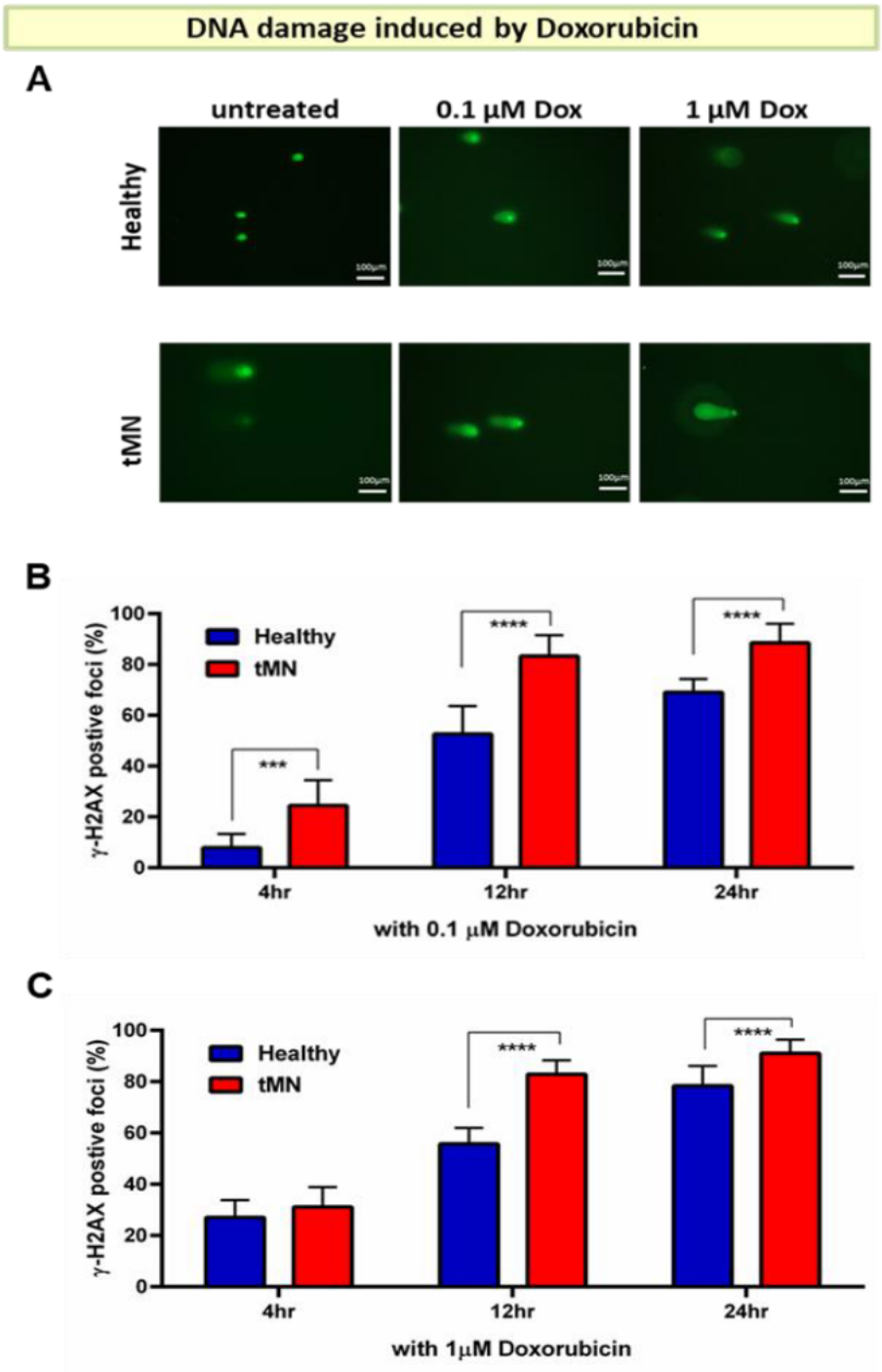


Figure 4.13. tMN stromal cells are more sensitive to widely used DNA damaging chemotherapeutic drug, Doxorubicin. tMN BMSC are prone to DNA damage assessed by (A) alkaline comet assay (Doxorubicin 0.1µM and 1µM), and (B and C) γH2AX. γH2AX foci were significantly higher after 12 and 24 hours of exposure to 0.1 µM (B) and 1µM (C) Doxorubicin. Assays described in panel A-C were performed on Healthy (n = 4) and tMN (n = 4) BMSC. Scale bars indicate 100µm. Dox, Doxorubicin. All bars indicate mean, and all error bars indicate SD. Two-way ANOVA was used to determine differences among groups. Asterisks display *P*-values **** $P < 0.0001$.

Finally, the γH2AX foci formation and activation over time following *in vitro* exposure to chemotherapeutic drug and radiation. Following 24-hour *in vitro* exposure and drug-washout, γH2AX foci were consistently significantly higher in tMN BMSC at all time points and persistent DNA damage was evident even after 24 hours of removal of genotoxic insult, compared to Healthy BMSC (27 ±5% versus 5 ±2%; $P < 0.001$) (Figure 4.14A). Similarly, tMN BMSC showed significantly impaired DNA damage repair following *in vitro* radiation exposure. Following *in vitro* radiation, number of γH2AX foci in Healthy BMSC decreased rapidly over time with only 4 ±1% cells showing positivity by 8 hours after irradiation (Figure 4.14B; Figure 4.15A). However, tMN BMSC showed significantly impaired repair with 21 ±2% foci still positive at the same time point ($P < 0.001$) (Figure 4.14B; Figure 4.15A). This was also significantly greater than pMN and pMN+Ca samples (5 ±1%, $P < 0.001$), indicating significantly delayed DDR response in tMN stroma compared to both Healthy and typical MDS/AML (Figure 4.15) and was consistent with GSEA for pathways associated with DDR (FDR < 0.1, $P < 0.05$) (Figure 4.16). Thus, defective DDR in tMN BMSC can possibly trigger cellular senescence in the absence of prompt DNA repair.

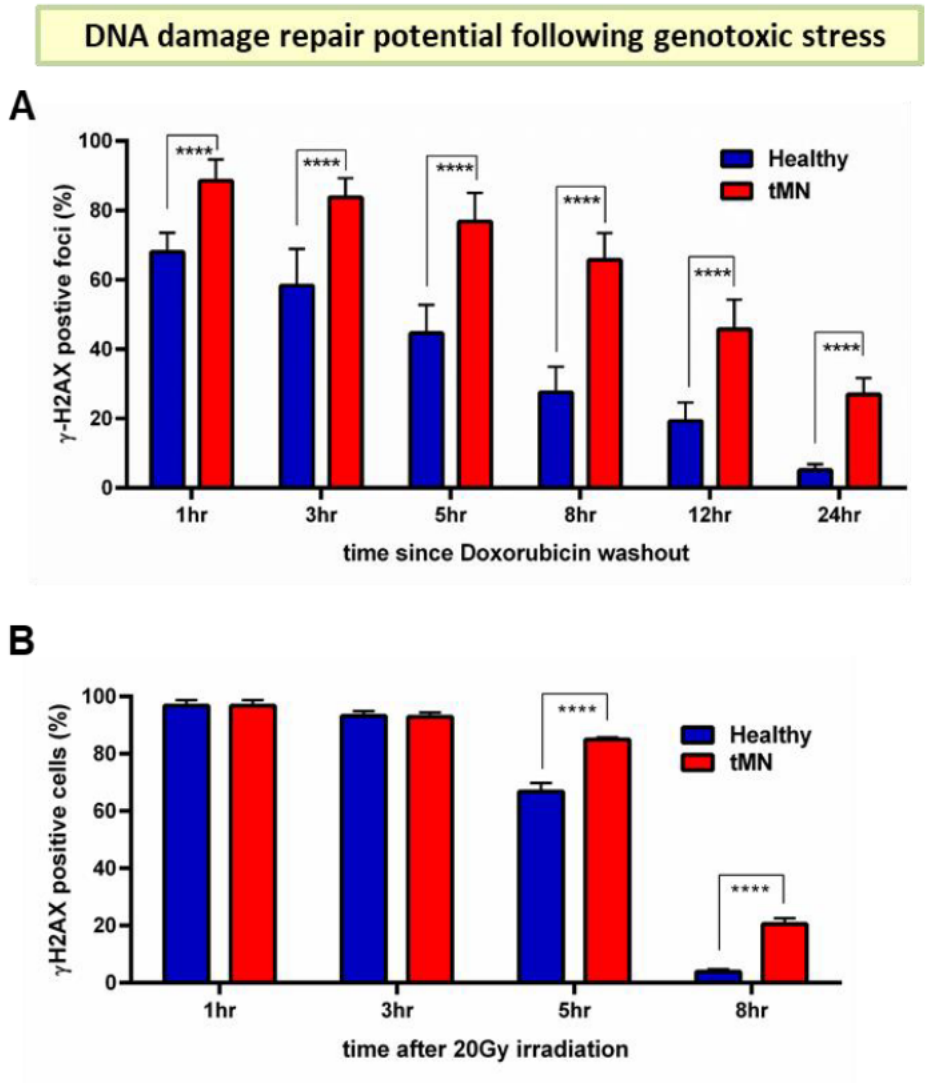


Figure 4.14. tMN stromal cells exhibit defective DNA damage repair potential. (A) Defective DNA damage repair potential of tMN BMSC was evident by significantly high number of γH2AX foci at all time points following Doxorubicin drug-washout; (B) following *in vitro* radiation, number of γH2AX foci in Healthy BMSC decreased with only 4 ±1% cells showing positivity by 8 hours after irradiation. However, tMN BMSC showed significantly impaired repair with 21 ±2% foci still positive at the same time point. Assays described in panel A-C were performed on Healthy (n = 4) and tMN (n = 4) BMSC.All bars indicate mean, and all error bars indicate SD. Two-way ANOVA was used to determine differences among groups. Asterisks display *P*-values **** $P < 0.0001$.

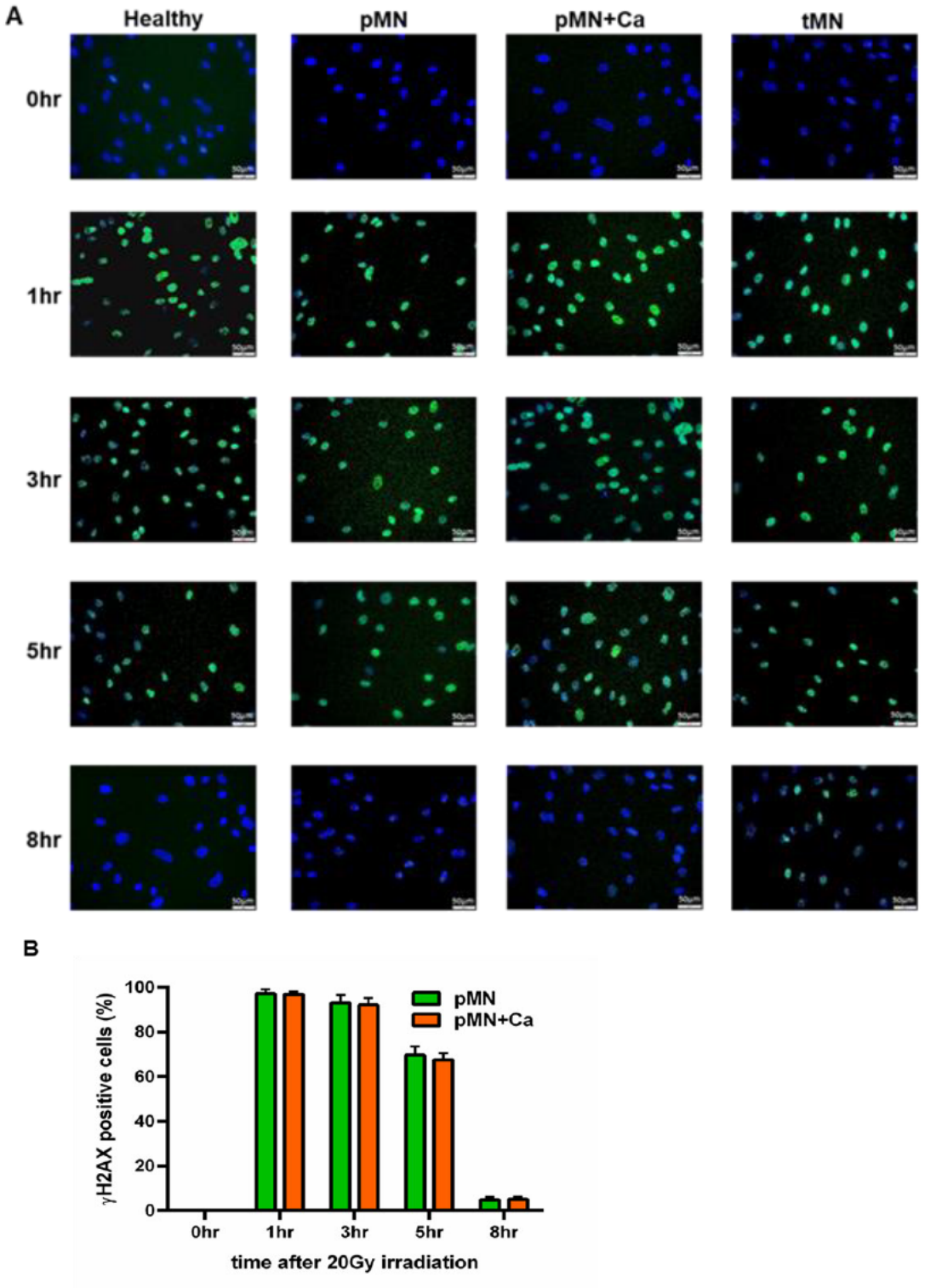


Figure 4.15. Defective DNA damage repair potential of tMN compared to Healthy and other MN BMSC. (A) Representative γH2AX staining and DAPI stained nuclei at 0, 1, 3, 5 and 8 hours post irradiation in pMN (n = 4), pMN + Ca (n = 4), tMN (n = 4) and Healthy (n = 4)-derived BMSC. Scale bars indicate 50μm. (B) Percentage of γH2AX positive cells at 0, 1, 3, 5 and 8 hours post irradiation in pMN and pMN+Ca. All bars indicate mean and all error bars indicate SD. Mann-Whitney test was used to detect statistically significant differences between cohorts.

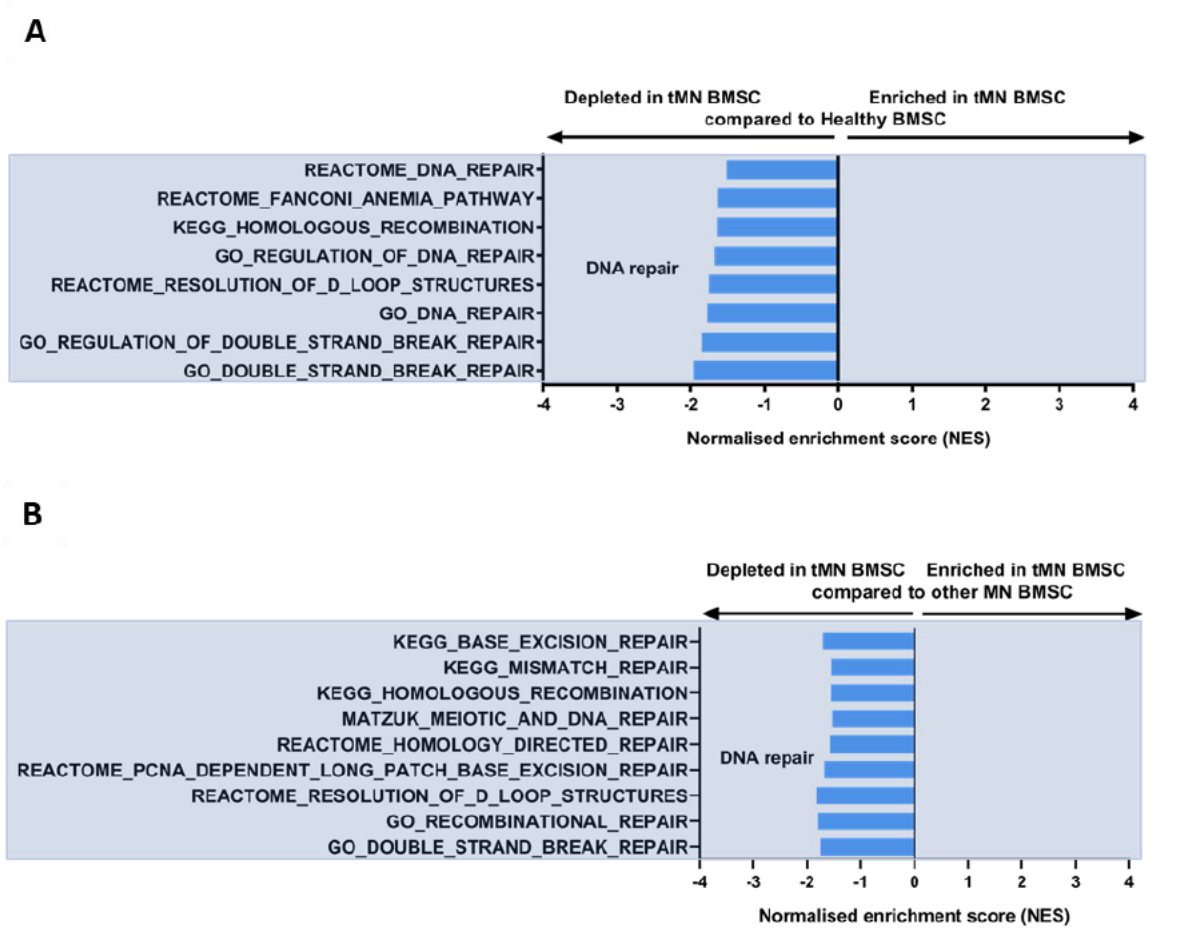


Figure 4.16. Whole transcriptome analysis of DNA damage repair- related data sets in tMN BMSC. (A) Cultured BMSC derived from tMN compared to Healthy derived BMSC. Gene set enrichment profiling of transcriptomic sequencing data; (B) comparison of transcriptome analysis of tMN and other MN BMSC. Dark blue bars represent DNA repair – related data set. NES indicates normalised enrichment score; negative score indicates depletion in tMN BMSC.

Delayed DNA repair of tMN BMSC is probably driven by delayed recruitment and activation of the early responders following DNA damage. In Healthy BMSC ATM and CHK2 were activated on by serine 1981 and threonine 68 respectively within 30 minutes of *in vitro* sublethal irradiation (Figure 4.17). While, in tMN BMSC, there was a significant delay of up to 3 hours in early responders, with some interpatient variability (Figure 4.18). Delayed activation was associated with late recruitment of ATM/CHK2/p53 and its crucial transcriptional target p21, a key mediator of senescence (Figure 4.17). Studies have previously

reported that senescence commitment following genotoxic stress requires an intact *TP53* pathway [346]. Hence, we assessed known *TP53* mutations in the BMSC by Next Generation Sequencing using custom-designed 217-gene NimbleGen Capture Platform (Roche NimbleGen Inc., Madison, WI, USA) and sequenced on an Illumina HiSeq2500 sequencing system (Illumina) as part of other study in our research group. The data showed that none of the 13 BMSC tested exhibited any pathogenic *TP53* mutations and all samples showed evidence of intact *TP53* pathway.

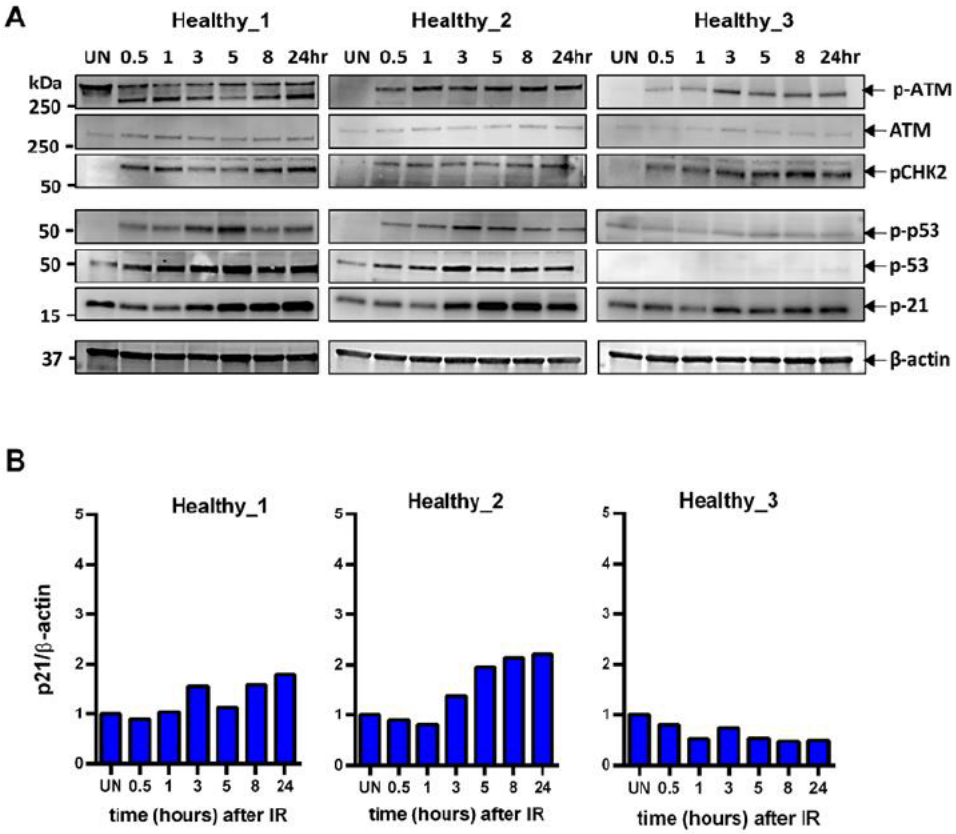


Figure 4.17. DNA damage response in Healthy BMSC (n = 3) following sublethal irradiation. (A) Western blot analysis to assess DNA damage repair proteins ATM, CHK2, p53 and p21 prior to and at 0.5, 1, 3, 5, 8 and 24 hours post irradiation (20Gy) of Healthy BMSC; (B) densitometry analysis of Western blots showing p21 protein expression normalised to β-actin in three Healthy BMSC analysed.

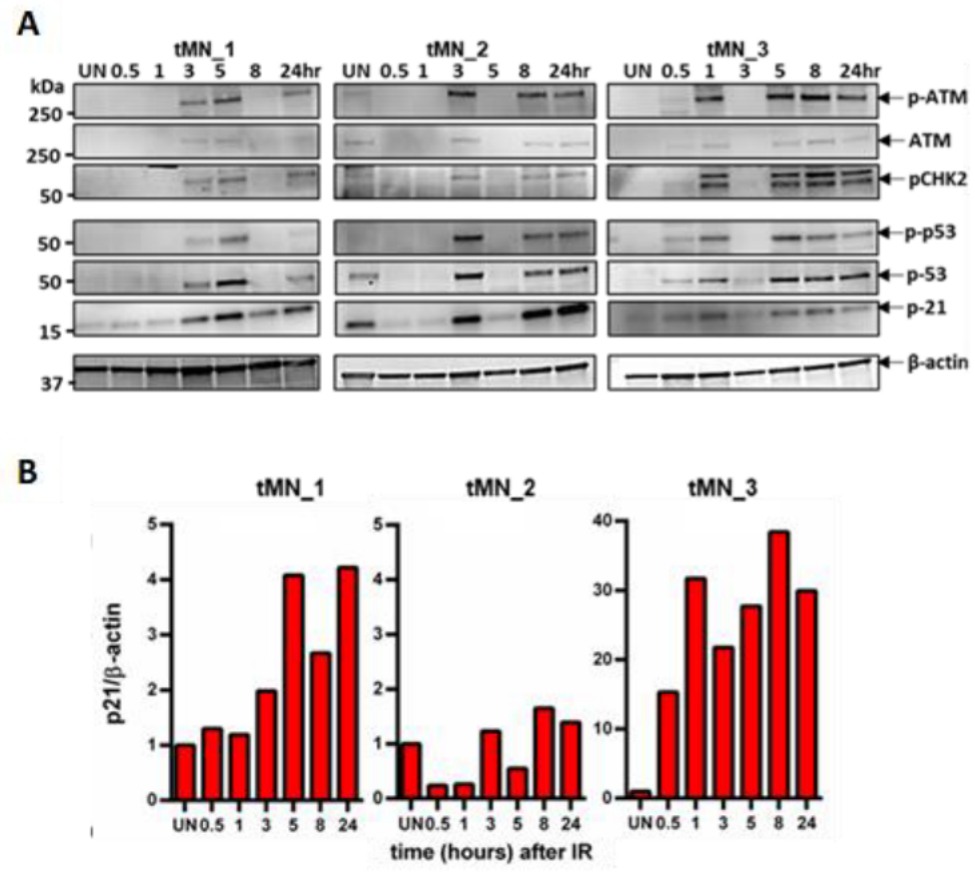


Figure 4.18. DNA damage response in tMN BMSC (n = 3) following sublethal irradiation. (A) Western blot analysis to assess DNA damage repair proteins ATM, CHK2, p53 and p21 prior to and at 0.5, 1, 3, 5, 8 and 24 hours post irradiation (20Gy) of tMN BMSC; (B) densitometry analysis of Western blots showing p21 protein expression normalised to β-actin in three tMN BMSC analysed.

Together these results suggest that tMN stroma is profoundly senescent where impaired DDR following CT could be a major contributing factor to this phenotype.

4.2.7. tMN Stromal Cells Demonstrate a Glycolytic Metabolic State

While the tMN stroma was profoundly dormant, it was certainly not inactive metabolically. Transcriptome analysis showed enrichment of multiple glycolytic gene pathways in tMN BMSC compared to controls (FDR < 0.1, $P < 0.05$) (Figure 4.19A; Figure 4.20). Moreover, bioenergetic profiling showed that total ATP production was significantly higher in tMN compared to Healthy BMSC (679 ±482.6 pmol/min/µg DNA versus 241.6 ±144.5 pmol/min/µg DNA, $P < 0.001$) (Figure 4.19B). Notably, the majority of ATP in tMN BMSC was generated by glycolysis (69% versus 36%; $P < 0.001$), contrasting with Healthy in which ATP was predominantly generated by mitochondrial OXPHOS (64% versus 31%) (Figure 4.19C). Moreover, the ECAR, an indicator of glycolysis was increased in tMN compared to Healthy BMSC (Figure 4.19D). OCR was similar in majority of Healthy and tMN BMSC, although interpatient variability was evident in tMN BMSC (Figure 4.19E-F).

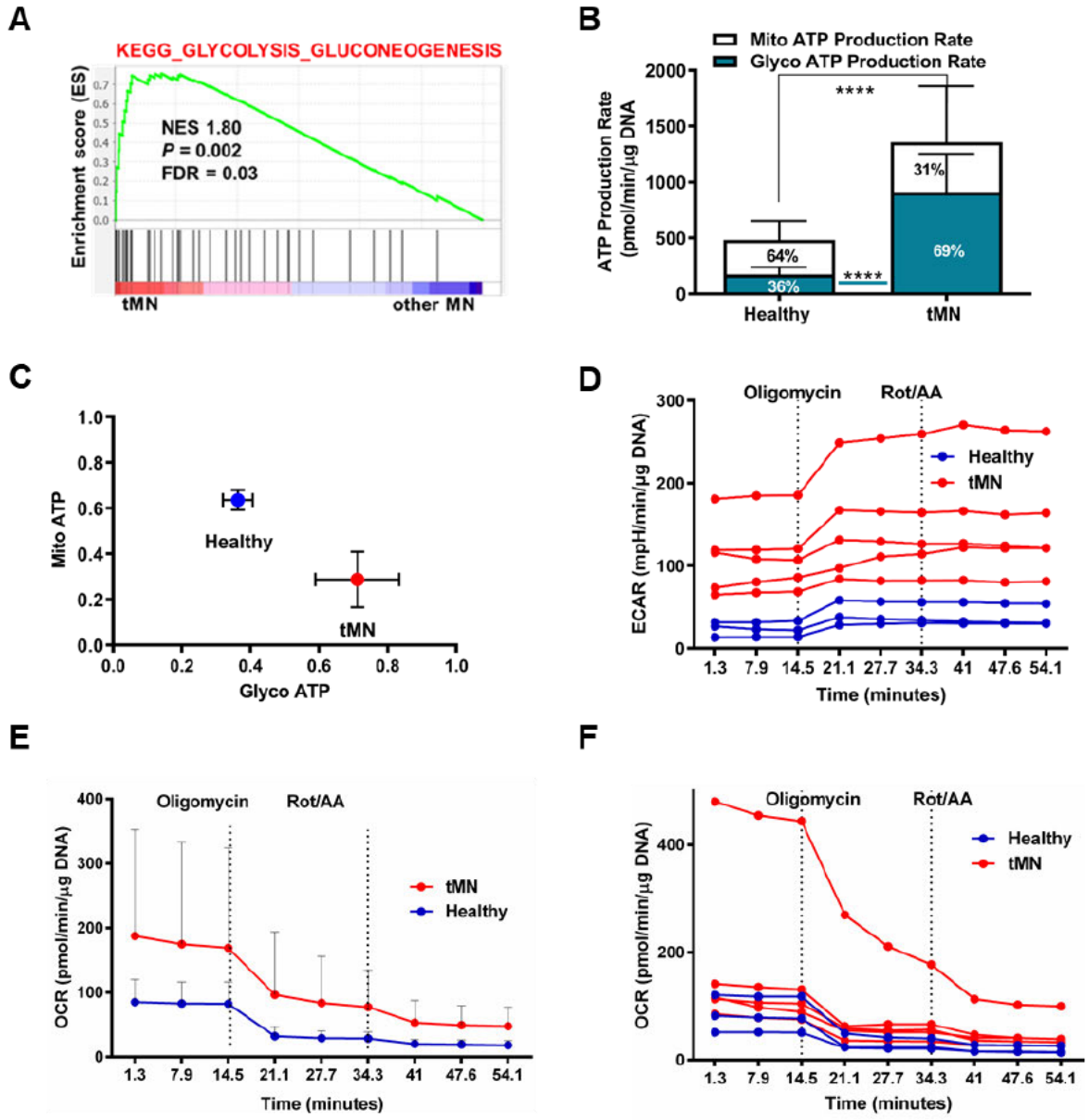


Figure 4.19. tMN BMSC exhibit glycolytic metabolic state. (A) GSEA example of BMSC from tMN versus other MN shows enrichment of metabolic pathways. The NES, *P*-values and FDR are given; (B) comparison of mitochondrial ATP (mitoATP) production rate and glycolytic ATP (glycoATP) production rate between Healthy (n = 3) and tMN (n = 5) BMSC. Data was expressed relative to the total DNA; (C) energetic map of Healthy and tMN BMSC charting mitoATP versus glycoATP; (D) extracellular acidification rate (ECAR) measurements obtained over time (minutes) between Healthy and tMN BMSC; (E) oxygen consumption rate (OCR) measurements obtained over time (minutes) between Healthy and tMN BMSC shown as average and (F) in individual BMSC samples. All bars indicate mean, and all error bars indicate SD. Mann-Whitney test was used to detect statistically significant differences between cohorts. Asterisks display *P*-values ****$P < 0.0001$.

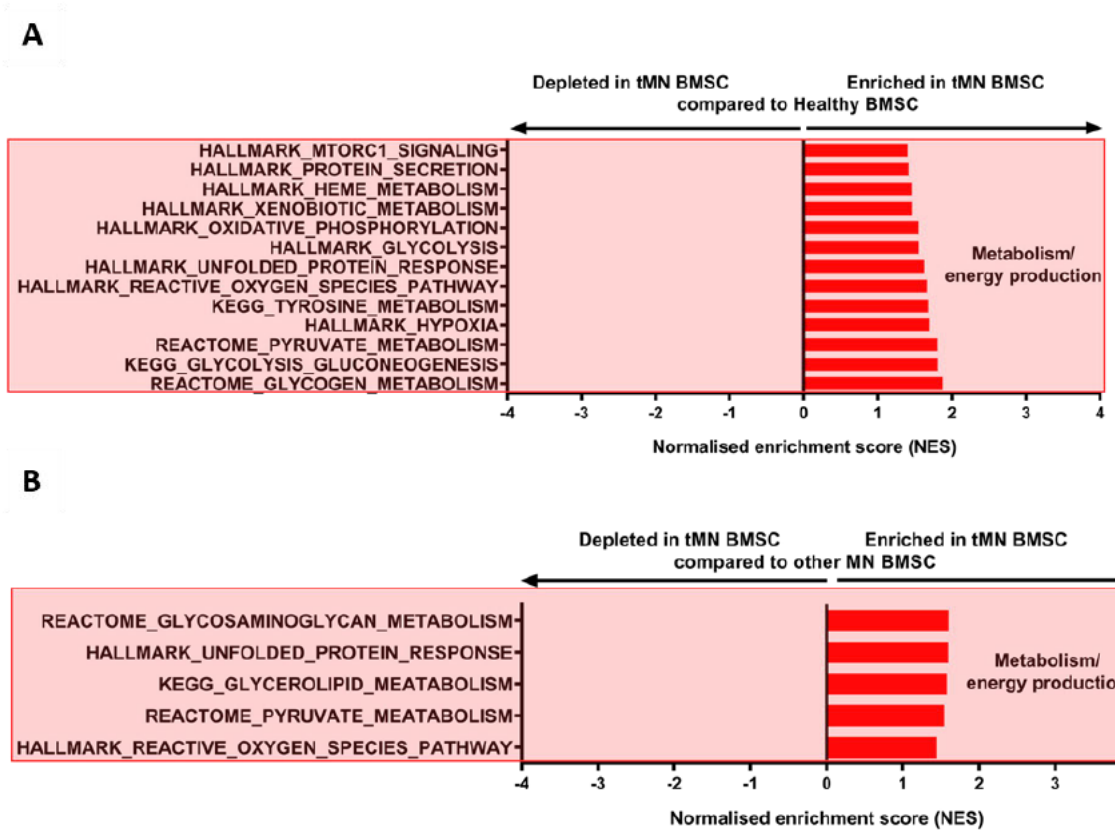


Figure 4.20. Whole transcriptome analysis of metabolism/ energy production- related data sets in tMN BMSC. (A) Cultured BMSC derived from tMN compared to Healthy derived BMSC. Gene set enrichment profiling of transcriptomic sequencing data; (B) comparison of transcriptome analysis of tMN and other MN BMSC. Red bars represent Metabolism/energy production – related data set. NES indicates normalised enrichment score, positive score indicates positive enrichment in samples from tMN BMSC, and negative score indicates depletion in tMN BMSC.

Experiments were next performed to assess whether glycolytic ATP production was hardwired in tMN stroma or could be switched to OXPHOS. To determine the appropriate concentration of glycolysis inhibitor, 2DG and assess its effect on BMSC viability without toxicity to cells a dose titration of 2DG was performed on Healthy BMSC (Figure 4.21). Change in morphology was observed gradually from 1mM 2DG onwards, where cells become bigger and disorganised (Figure 4.21A). Moreover, a substantial decrease in the number of live cells from 4mM

onwards was noted (Figure 4.21B). Based on those titrations, 1mM and 2mM were chosen in follow up experiments.

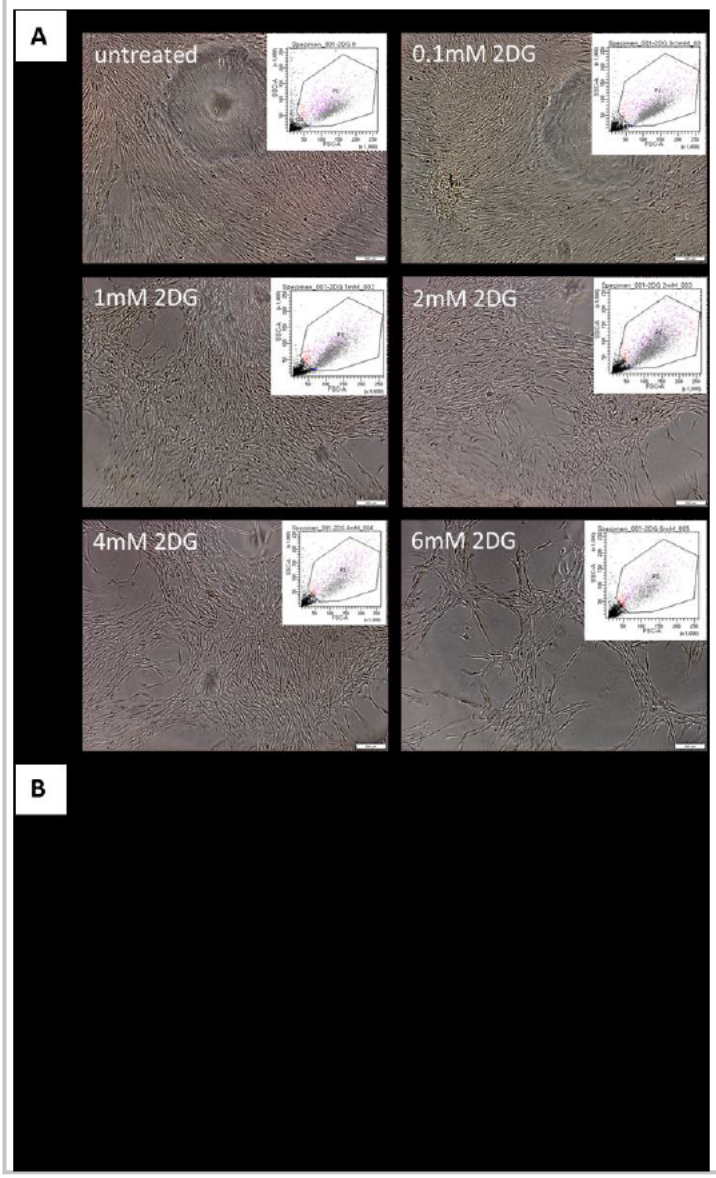


Figure 4.21. Effect of dose titration of 2DG on morphology and viability in Healthy BMSC after 72 hours in culture. (A) Representative micrographs of BMSC morphology assessed by light microscopy and FACS plots of gating live cells; (B) number of live BMSC analysed by flow cytometry. Scale bars indicate 200µm.

As expected, 2DG significantly reduced glycolysis ($P < 0.001$) (Figure 4.22A-B; Figure 4.23A-B) and ECAR (Figure 4.22C; Figure 4.23C) in Healthy and tMN BMSC, but without reducing total ATP significantly (Figure 4.22A-B; Figure 4.23A-B), indicating a retained capacity to upregulate OXPHOS. Additionally, glycolysis inhibitor 2DG did not affect OCR in both Healthy and tMN BMSC (Figure 4.22D; Figure 4.23D).

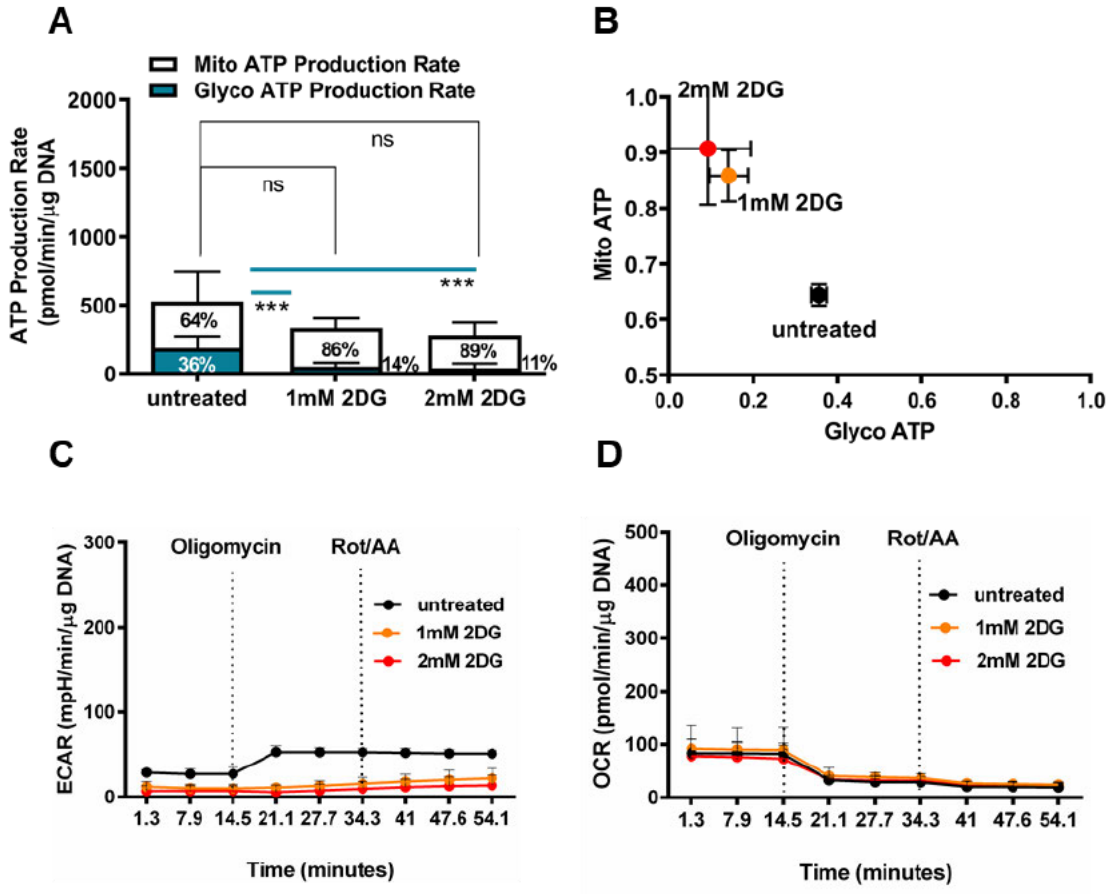


Figure 4.22. Blockage of glycolytic pathway in Healthy (n = 3) BMSC switched bioenergetic metabolism to mitochondria without influencing oxygen consumption rate (OCR). (A) Effect of glycolysis inhibitor 2DG on mitochondrial and glycolytic production rate; (B) bioenergetic map of untreated and 1mM and 2mM 2DG charting mitoATP versus glycoATP; (C) effect of glycolysis inhibitor 2DG on ECAR and (D) OCR obtained over time (minutes) between untreated and 1mM and 2mM 2DG. All bars indicate mean, and all error bars indicate SD. Mann-Whitney or Two-way ANOVA test was used to detect statistically significant differences between cohorts. Asterisks display *P*-values $***P < 0.001$.

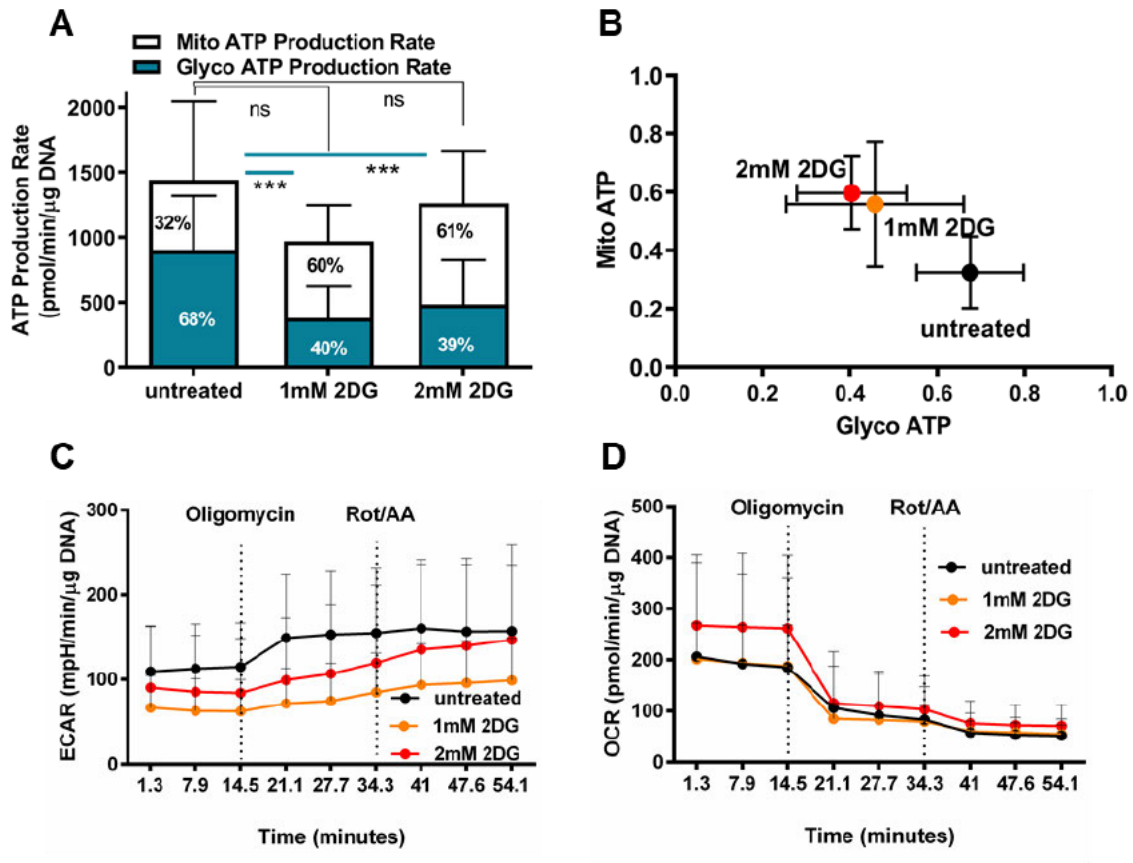


Figure 4.23. Blockage of glycolytic pathway in tMN (n = 3) BMSC switched bioenergetic metabolism to mitochondria without influencing oxygen consumption rate (OCR). (A) Effect of glycolysis inhibitor 2DG on mitochondrial and glycolytic production rate; (B) bioenergetic map of untreated and 1mM and 2mM 2DG charting mitoATP versus glycoATP; (C) effect of glycolysis inhibitor 2DG on ECAR and (D) OCR obtained over time (minutes) between untreated and 1mM and 2mM 2DG. All bars indicate mean, and all error bars indicate SD. Mann-Whitney or Two-way ANOVA test was used to detect statistically significant differences between cohorts. Asterisks display *P*-values ***$P < 0.001$.

Together, the data suggest that tMN senescent cells despite a low proliferation rate, exhibit a perturbed active glycolytic metabolism in normoxia, resembling a Warburg metabolic shift, which indicate that these cells preferentially use glycolysis rather than oxidative phosphorylation for energy production.

4.3. DISCUSSION

Reduced expansion capacity of MN-BMSC could be due to increased apoptosis [206], alteration in cell cycle [197, 205, 206] and increased senescence [170, 197, 205]. Increased senescence in MN-BMSC was detected previously by measuring senescence-associated β-Galactosidase activity [170, 197, 205]. However, expression of senescence-associated genes, including *CDKN1A, CDKN2B, CDKN2A, RB, TP53* and *PARG1*, indicated that MN-BMSC display fewer characteristics of senescence compared to healthy controls [204]. Additionally, telomere length was significantly increased in MN-BMSC compared to BMSC from healthy individuals [204]. These findings indicate that there is no agreement as to whether premature senescence is accountable for the defective proliferation in typical MN BMSC, which also failed to include tMN BMSC in the analysis. The main significant difference between tMN and other typical MN is prior exposure to cytotoxics. As a consequence of exposure to clinically relevant doses of radiotherapy, chemotherapy and targeted therapy against cancer disease, therapy- induced senescence may be triggered [347, 348]. Most such agents aim at proliferating cells through distinct, cell cycle-dependent mechanisms. Their cytotoxicity for several types of dividing cells frequently prompt to side-effects, which include immunosuppression, fatigue, anaemia, and nausea. Furthermore, clinical studies of cancer survivors treated for childhood cancer indicate that some chemotherapeutics lead to range of long-term side effects that resemble pathologies affiliated with ageing, organ dysfunction, cognitive impairment, and secondary neoplasms [349].

Cellular fate following genotoxic stress is governed by several factors including the competency of the DNA damage repair mechanism. The present thesis found that defective DNA repair capacity was obviously evident in the tMN stromal cells, as compared to healthy age-matched controls and other myeloid neoplasms, yet still occurred slowly, in the absence of

detectable *TP53* mutations in the stromal compartment. Defective DNA damage response was further supported by GSEA analysis showing reduced enrichment of DNA repair pathways in tMN compared to Healthy BMSC. Potential mechanisms leading to defective DNA repair in tMN BMSC could be driven by tMN clonal expansion, inflammatory microenvironment, or prior CT therapy. In the majority of cells, CT induced DNA damage is repaired within a relatively short period; however, some BMSC displayed persistent DNA damage even after 10-15 years following exposure to CT [187].

Classically, fibroblasts unable to repair DNA damage undergo apoptosis or cellular senescence. In the present study, tMN BMSC exhibited multiple features of senescence including enlarged/flattened morphology, decreased cellular proliferation and colony-forming potential, resistance to apoptosis, persistent DNA damage, secretory phenotype and altered expression of senescence associated genes with high β-Galactosidase activity [262, 350]. These data suggest a link to an altered or sub-optimal DNA damage response and prior patient exposure to cytotoxics. Following genotoxic stress, cellular senescence is mainly governed by p53 protein expression, thus intact *TP53* function is critical. Tumour cells harbouring wildtype *TP53* are more likely to senesce in response to genotoxic therapies [351, 352], whereas cells carrying mutant *TP53* (as seen in Li-Fraumeni syndrome), overcome senescence more readily and are more prone to develop cancer [353]. Notably, none of tMN BMSC analysed in this study had any known pathogenic *TP53* mutations. In contrast, we and others have reported that 29.5% tMN patients harbor somatic *TP53* mutations in leukemic cells [107, 201]. Active *TP53* promotes growth arrest by inducing expression of *CDKN1A*, a cyclin-dependent kinase inhibitor that, among other activities supresses the phosphorylation and, hence inactivation of pRB. *CDKN1A* expression was significantly higher in tMN BMSC as compared to healthy cells, suggesting this pathway is active in tMN patients. While other factors such as *FOS* and

PCNA, which play a critical role in cell proliferation and differentiation [256] were significantly down regulated in tMN BMSC compared to other MN and Healthy control BMSC.

Another essential feature of cellular senescence is a secretory phenotype known as SASP [259, 310] which plays an important role in autocrine and paracrine propagation of cellular senescence. Many CT agents are non-specific and can induce senescence in non-cancerous cells [188], affecting the BM microenvironment and resulting in generation of the SASP. In turn, this creates a chronic inflammatory state that is believed to contribute to the side effects linked with CT therapy [190, 354]. A study by Abdul-Aziz *et al*. [345] demonstrated that pAML cells induce SASP with upregulation of IL-6, IL-8, macrophage inflammatory protein-1 alpha (MIP-1α) and MIP-3α when cocultured with primary BMSC. Similarly, IL-6 and MIP-3 were persistently higher in mouse BMSC from animals engrafted with leukemic cells compared with animals engrafted with human $CD34^+$ [355]. SASP chemokine and cytokines, such as IL-7, IL-1β, IL-13, IL-15, IL-6, Eotaxin, GCSF, IFNγ and EGF were secreted *in vitro* at higher levels by tMN compared to Healthy BMSC. Moreover, elimination of senescent cells within the tumour microenvironment revealed reduction of several short- and long-term effects of CT, such as BM suppression or recurrence and metastases of solid tumour [188].

Senescent fibroblasts were reported to have reduced glycolysis [356] and increased glycolysis can protect cells from senescence [357]. However, in the present study despite defective proliferative capacity, senescent tMN BMSC were found to be metabolically active. Transcriptome analysis showed enrichment of metabolic and energy production pathways and higher energetic rate in tMN BMSC compared to controls, consistent with prior studies reporting increased metabolic activity in senescent cells [330]. Similar molecular alterations

were reported in chemotherapy treated mice BM [167] and lymphoma patients who later developed tMN [358]. Thioredoxin reductase 1 (*TXNRD1)*, regulator of glucose and lipid metabolism [359, 360], and B-cell lymphoma-2 interacting protein 3 (*BNIP3)*, a negative regulator of mitochondrial potential [361], were found to be highly expressed in tMN BMSC.

Inside the cells, energy is generated in the form of ATP, mostly through glycolysis and OXPHOS [362]. This could be altered during specific conditions such as cellular senescence [363]. Senescent cells have been exhibited to gain a more glycolytic activity, despite their decrease in proliferation potential. Moreover, (OCR and ATP production was significantly higher in tMN BMSC as compared to those isolated from Healthy control. Majority (77%) of ATP production in tMN BMSC was generated through glycolysis while mitochondrial oxidative phosphorylation contributed to only 23% of total ATP production. This is the first study reporting senescence-associated metabolic reprogramming of tMN BMSC with aerobic hypercatabolic metabolism and increased glycolysis, commonly known as, "Warburg effect", typically seen in tumour cells. Similarly, in a transgenic Eμ-myc lymphoma model of TIS, senescence-inducing chemotherapy led to hypercatabolic phenotype, increased glycolysis, fatty acid oxidation and ATP production in TIS-competent but not in TIS-incompetent lymphoma cells [344]. Similarly, irradiation induced senescence has been linked to reduced tricarboxylic acid activity and shift energy towards glycolysis, gluconeogenesis and pentose-phosphate pathway [330]. The reliance of TIS in BMSC on energy-providing hypercatabolism can be therapeutically exploited by synthetic lethal metabolic targeting [344] and sequential treatment strategies, thereby adding clearance of senescent cells by the host immune system. Increased metabolic potential of senescent cells has been associated with SASP phenotype. A previous study examining radiation-induced senescence in the human colon cancer cell line HCT-116, showed an increased secretion of SASP IL-1 and IL-6 as well as enhanced aerobic

glycolysis, which breaks down glucose into pyruvate, ATP and NADH [364]. Furthermore, metabolomic analysis of extracellular metabolites released by senescent human fibroblasts support the notion of a metabolic shift from oxidative phosphorylation to glycolysis [365].

Collectively, tMN BMSC were found to lie on an extreme trajectory away from age-matched normal and typical MN BMSC, with evidence of a profound pro-inflammatory senescence program. This chapter demonstrated that tMN exhibit a profound senescence with *CDKN1A* induction, β-Galactosidase, flattened morphology, and defective DNA repair. Furthermore, despite the cell cycle arrest phenotype, tMN stromal cells were found to be metabolically active and secreted multiple pro-inflammatory cytokines including, IL-6, IL-1β and IFN-γ.

Chapter 5: Functional Defects of tMN BMSC

5.1. INTRODUCTION

BMSC are one of the most important components of the BM microenvironment, and have been defined as primitive, non-haematopoietic cells present in the BM. They are capable of differentiating into fat-forming adipocytes, cartilage-forming chondrocytes and bone-forming osteoblasts [145, 146, 366, 367] (Figure 5.1), that play an important role in maintaining HSC and regulating the haematopoietic microenvironment [368]. It has been reported that BMSC support of haematopoiesis, is dependent on a balance between bone and fat formation where increases in adipogenesis is thought to inhibit HSC [134, 369].

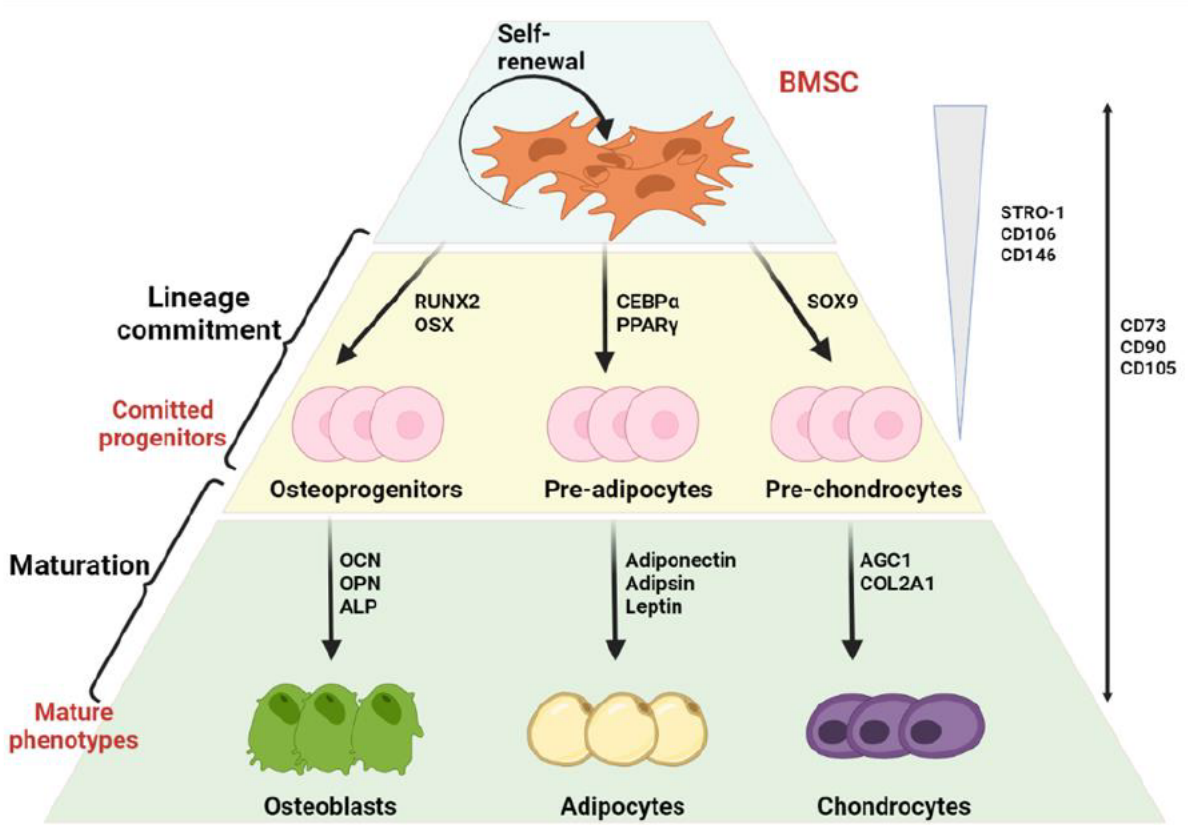


Figure 5.1. Trilineage differentiation potential of BMSC. Schematic diagram of the surface markers, signalling molecules and transcription factors involved in the detection and regulation of BMSC differentiation.

Abbreviations: BMSC, bone marrow mesenchymal stromal cells; *RUNX2*, runt-related transcription factor 2; *OSX*, Osterix; *CEBPa,* CCAAT/enhancer binding protein alpha; *PPARg,* peroxisome proliferator-activated receptor gamma; *SOX9*, SRY-box transcription factor 9; *OCN*, Osteocalcin; *OPN*, Osteopontin; *ALP*, Alkaline phosphatase; *AGC1* (ACAN), Aggrecan; *COL2A1,* Collagen type 2, alpha 1.

5.1.1. Osteogenic, Adipogenic and Chondrogenic Differentiation of MN-BMSC

The trilineage differentiation process of BMSC *in vitro* requires about 20 days to be completed and can be separated in two main steps: lineage commitment (from BMSC to a committed progenitor) and maturation (from progenitors to mature phenotypes) [370] (Figure 5.1). In the first 24 hours of BMSC adipogenic induction, adipogenesis associated genes are already differentially expressed, including transcription factors and genes connected to lipid metabolism [371], however the BMSC are still not fully committed towards a specific lineage [372].

Despite intense research, there is no agreement regarding the adipogenic potential of pMN-derived BMSC, where over half of the studies reported normal adipogenic potential [170, 194, 196, 208, 210, 213, 217, 226, 227], while the others report reduced adipogenic potential of pMN-derived BMSC [172, 197, 204, 206, 216, 221, 241]. Interestingly, some of the recent studies suggest increased adipogenic differentiation potential by pAML BMSC as compared to healthy controls [212, 215, 220]. Differentiation along the adipocyte lineage can be indicated not only by cytochemical staining such as Oil Red O and Nile Red but also by the expression of adipogenic master transcriptional factors, such as *CEBP*α and peroxisome proliferator-activated receptor gamma (*PPAR*γ) (Figure 5.1; Table 5.1). The expression of these factors has been reported to occur before the expression of most mature adipogenic associated genes such as Adiponectin (*ADIPOQ*), Adipsin, Leptin, and are required for BMSC adipogenic induction [373-375]. Furthermore, *CEBP*α and *PPAR*γ have been demonstrated to act mutually during adipogenesis by activating each other's expression consequently regulating the expression of other adipogenic genes [376].

Table 5.1. Overview of published data on trilineage differentiation potential in MN-derived BMSC

Study	Osteogenic differentiation	Adipogenic differentiation	Chondrogenic differentiation
Flores *et al* *Leukemia 2008*[196]	**Normal** (Stain- Von Kossa)	**Normal** (Stain- Oil Red)	**Normal** (Stain- Alcian Blue)
Varga *et al* *Pathology Oncology Research 2008*[241]	**Normal** (Stain- Alizarin Red)	↓ (Stain- Oil Red)	x
Klaus *et al* *Stem Cells Dev 2010*[210]	**Normal** (Stain- Von Kossa + mRNA- *ALP, RUNX2*)	**Normal** (Stain- Oil Red + mRNA- *PPARγ, aP2(FABP4))*	**Normal** (Stain- Alcian Blue + mRNA- *AGC1, COL2A1*)
Zhao *et al* *Cancer Letters 2012*[194]	**Normal** (Stain- Von Kossa + mRNA- *OPN*)	**Normal** (Stain- Oil Red + mRNA- *LPL*)	x
Ferrer *et al* ***Haematologica 2013***[197]	↓ (Stain- Von Kossa + ALP activity	↓ (Stain- Oil Red + mRNA- *aP2 (FABP4)*)	x
Geyh *et al* *Leukemia 2013*[170]	↓ (Stain- Alizarin Red, Von Kossa, ALP + mRNA- *OSX, OCN*)	**Normal** (Stain Oil Red)	**Normal** (Stain- Safranin O)
Pavlaki *et al* *Stem Cells Dev 2014*[204]	**Normal** (Stain- Von Kossa, Alizarin Red) ↓ mRNA- *ALP, OCN, BSP, DLX5, RUNX2, OSX*	**Normal** (Stain- Oil Red), ↓ mRNA- *CEBPα, PPARγ*)	**Normal** (Stain- Alcian Blue)
Fei *et al* *Eur J Haematology 2014*[207]	↓ Low risk MDS (Stain- Alizarin Red + mRNA- *RUNX2, OSX, BSP, ALP, COL1, OPN, OCN*)	x	x
Kim *et al* *Stem Cell Research 2015*[213]	**Normal** (Stain- Von Kossa)	**Normal** (Stain- Oil Red)	**Normal** (Stain- Alcian Blue)
Zhao *et al* *Haematologica 2015*[172]	↓ senescent BMSC (Stain- Alizarin Red + mRNA- *RUNX2, ALP*)	↓ senescent BMSC (Stain- Oil Red + mRNA- *aP2 (FABP4), CEBPα*)	x
Chandram *et al* *Leukemia Research 2015 [217]*	**Normal** (Stain- Alizarin Red)	**Normal** (Stain- Oil Red, FABP4 antibody)	**Normal** (Stain- Alcian Blue, Aggrecan antibody)
Geyh *et al* *Leukemia 2016 [208]*	↓ (Stain- Alizarin Red, Von Kossa, ALP+ mRNA- *OSX, OCN*)	**Normal** (Stain- Oil Red)	**Normal** (Stain- Safranin O)
Rathnayake *et al* *Analytical Cellular Pathology 2016*[226]	**Normal** (stain Alizarin Red)	**Normal** (Stain Oil Red)	x
Pang *et al* *Am J Transl Research 2017*[206]	↓ (Stain- Alizarin Red + mRNA- *OSX, RUNX2*)	↓ (Stain- Oil Red)	x
Falconi *et al* *Leukemia Research 2017*[223] **(tMN patients)**	mRNA- ↑ *OCN* but ↓ *OSX, RUNX2*	x	x
Battula *et al* *JCI Insight 2017[216]*	↑ (mRNA- *RUNX2, OSX, OPN, ALP)*	↓ (Stain- Oil Red + mRNA- *CEBPα, PPARγ, LPL)*	↓ (Stain- Alcian Blue and collagen type-1)
Diaz de la Guardia *et al* *Stem Cell Reports 2017[221]*	↓ (Stain- Alizarin Red, + mRNA- *OSX, OPN, ALP*)	↓ (Stain- Oil Red, + mRNA- *aP2 (FABP4), PPARγ*)	x
Azadniv *et al.* *Leukemia 2020[220]*	**Normal** (Stain- Alizarin Red, acetic acid extraction followed by colorimetric detection at 405nm)	↑ (Stain- Oil Red and surface markers expression CD10 and CD92)	x
Zhang *et al.* *Stem Cell Research & Therapy 2021[215]*	↓ (Stain- Alizarin Red + mRNA- *RUNX2, OCN*)	↑ (Stain- Oil Red + mRNA- *ADIPOQ, PPARγ*)	**Normal** (Stain- Alcian Blue + mRNA- *SOX9, AGC1*)
Weickert *et al.* *Scientific Reports 2021[212]*	**Normal** (Stain- Alizarin Red)	↑ (Stain- Oil Red)	x

Abbreviations: Red and blue colour indicates increase and decrease in differentiation, respectively; Normal, indicates no difference was noted between MN- and Healthy controls BMSC; x, indicates not assessed; *ADIPOQ,* Adiponectin; *AGC1 (ACAN),* Aggrecan; *ALP*, Alkaline phosphatase; *aP2 (FABP4),* Adipocyte protein 2 (Fatty acid-binding protein 4); *BSP*, Bone sialoprotein; *CEBPα,* CCAAT-enhancer binding protein alpha; *COL1*, Collagen type 1, alpha 1; *COL2A1,* Collagen type 2, alpha 1; *DLX5,* Distal-less homeobox 5; *LPL*, Lipoprotein lipase; *OCN,* Osteocalcin; *OPN*, Osteopontin; *OSX*, Osterix; *PPARγ,* Peroxisome proliferator- activated receptor gamma; *RUNX2*, Runt- related transcription factor 2; *SOX9,* SRY-Box transcription factor 9.

Various factors can affect adipogenesis including cytokines which have been suggested to have both inhibitory and stimulatory effects on adipogenesis (Table 5.2). Among the pro-inflammatory cytokines, TNFα, IL-1β, IL-6, IL-1F6, IL-15, IL-17, IL-18, IL-33 and OSM are inhibitory to adipogenesis. While other cytokines including IL-1RA, IL-7 and IL-34 have been indicated to enhanced adipogenesis.

Table 5.2. Cytokines that regulate adipogenesis

Symbol	Primary property	Effect on adipogenesis	Reference
TNFα	Pro-inflammatory	↓	[377-380]
IL-1β	Pro-inflammatory	↓	[381-383]
IL-18	Pro-inflammatory	Unknown	
IL-33	Pro-inflammatory	↓	[384, 385]
IL-1F6	Pro-inflammatory	↓	[386]
IL-1Ra	Anti-inflammatory	↑	[387]
IL-37	Anti-inflammatory	↓	[388]
IL-6	Pro-inflammatory	↓	[389-391]
IL-11	Pro-inflammatory	↓	[392, 393]
OSM	Pro-inflammatory	↓	[394]
NP	?	↓	[395]
IL-4	Pro-inflammatory/anti-inflammatory	↓	[396]
IL-10	Anti-inflammatory	Unknown	
IL-15	Pro-inflammatory	↓	[397]
IL-7	Pro-inflammatory	↑	[398]
IL-17	Pro-inflammatory	↓	[399-401]
IL-34	Pro-inflammatory	↑	[402]
IFNα	Pro-inflammatory	↓	[403]
IFNγ	Pro-inflammatory	↓ ↑	[404, 405]
MCP-1	Pro-inflammatory	↑	[406, 407]

Abbreviations: Red and blue colour indicates enhanced/induced and decreased/inhibited effects on adiopogenic differentiation, respectively. OSM, oncostatin M; NP, neuropoietin.

Osteoblast progenitors can stimulate [408, 409] and limit HSC expansion [410, 411], where murine studies indicate that BMSC dysfunction is sufficient to induce MDS and secondary AML [166]. Additionally, MN-derived BMSC display defective osteogenic potential [170, 172, 197, 206, 207] based on morphological and cytochemical characteristics [196, 208, 213, 215, 221, 241] and by the quantification of osteogenic-related specific genes at different time points, before and after osteogenic induction [170, 172, 194, 207, 208, 215, 221]. *In vitro* and *in vivo* studies have discovered several transcription factors that play crucial roles in osteoblast development, from their lineage commitment to their maturation. These genes include Runt-related transcription factor 2 (*RUNX2)* and Osterix *(OSX)*, the master transcription factors regulating bone formation and mature osteoblast markers such as Osteocalcin (*OCN*) and Osteopontin *(OPN)* [412] (Figure 5.1). This was further supported by decreased osteoblasts and osteoclasts numbers in BM biopsies [413] and reduced serum levels of *OCN* in pMDS [170] and pAML patients [208]. Interestingly, BMSC from lower risk MDS patients exhibit lower osteogenic differentiation potential compared to higher risk patients and normal individuals [207]. Notably, mRNA levels of *OSX* and *RUNX2* were lower in tMN patients, in agreement with studies of pMN patients [170, 172, 204, 206-208, 215, 221]. However, mRNA levels of *OCN* were significantly higher in BMSC of tMN patients compared to healthy controls [223], while *OCN* was downregulated in pMN-derived BMSC [170, 204, 207, 208].

Whist the exact mechanism of impaired osteoblast activity in MDS remain unclear. The chemokine, chemokine (C-C motif) ligand 3 (CCL3) , also known as MIP-1α, is a chemokine that has been previously reported as a mediator of osteoblastic dysfunction in multiple myeloma [414, 415], chronic myeloid leukaemia [416] and AML [417] and is highly expressed in leukaemic mouse mode and primary AML leukaemic cells. High expression of CCL3 can be exploited therapeutically. Pharmacological targeting of CCL3, using a novel CCR1

inhibitor, blocks the interaction of MM cells with osteoclasts, consequently inhibiting MM cell survival and proliferation [418]. CCL3 also has been reported to be elevated in serum of some MDS patients [419], which could be a potential clinical target.

Several *in vitro* studies performed on BMSC have demonstrated that factors that endorse adipogenesis block osteogenesis [420-422], and conversely, factors that promote osteoblast formation inhibit adipogenesis [423]. Various factors, such as aging [424], chemotherapy [425], irradiation [134] or bone pathologies [426] can lead to the differentiation imbalance of BMSC. Azacitidine, a DNA methyltransferase inhibitor can significantly reduce the ability of pMN-derived BMSC to differentiate towards the adipogenic lineage, while Azacitidine did not affect osteogenic differentiation [218]. Conversely, Azacitidine promotes both adipogenesis and osteogenesis in healthy human BMSC [427].

Emerging literature also suggests that pMN-derived BMSC exhibited no significant differences with regards to chondrogenesis [170, 196, 204, 213, 215]. BMSC derived from pMN were able to differentiate into chondrocytes based not only on cytochemical stains, such as Alcian Blue or Safranin O, but also on the quantification of aggrecan (*ACAN(AGC1))*, collagen, type 2, alpha 1 (*COL2A1)* and SRY-box transcription factor 9 (*SOX9)* mRNA expression [210, 215]. *SOX9*, a prominent transcription factor of chondrogenic differentiation, is essential for BMSC commitment towards the chondrogenic lineage [428, 429]. Moreover, it has been shown that *SOX9* triggers the expression of other chondrogenic markers including *ACAN (AGC1)* and *COL2A1* [430], which then activate the expression of *SOX5* and *SOX6* [429] to promote chondrocyte differentiation [431].

In the present thesis, the tri-lineage (osteoblasts, adipocytes and chondrocytes) differentiation potential was assessed for tMN derived BMSC and compared to BMSC control cohorts, using the respective cytochemical staining with quantification. Moreover, mRNA expression levels of established markers of early and late adipo- and osteogenesis, were analysed by quantitative real-time PCR. Additionally whole transcriptome analysis was performed to determine new mechanistic insights into the differences between BMSC derived from tMN patients and normal controls.

5.1.2. Haematopoietic Support by MN-BMSC

The BM is the major site of haematopoiesis. The various functions of HSC such as self-renewal, proliferation and differentiation are well regulated and maintained by factors derived from cell extrinsic sources, such as a wide variation of cytokines, growth factors, and other signalling molecules (Table 5.3).

Table 5.3. Molecules that regulate haematopoietic stem cells activity

Molecule	Function
Jagged (Notch receptor)	Regulate HSC self-renewal and differentiation during haematopoietic stress settings [432-435]
Thrombopoietin (TPO) and Angiopoietin1 (ANGPT1)	HSC maintenance in the niche in quiescence state with association to cell-cycle control [433]
Osteopontin	Maintenance of a quiescent state [436]
CXCL12 (SDF-1)	Expressed in the stromal cells; attracts HSC [437]
CXCR-4 (SDF-1 receptor)	Expressed in HSC [438]
N-cadherin	HSC quiescence and decrease in differentiation [439]
SCF	Initiation of intracellular signalling significant for HSC regulation [440]
Wnt	HSC self-renewal [441]

Abbreviations: HSC, haematopoietic stem cells; SDF-1, stromal cell-derived factor 1; SCF, stem cell factor; Wnt, Wingless-related integration site.

Extrinsic factors linked to HSC maintenance can be secreted from various cellular components of the BM microenvironment, including immature BMSC, differentiated stromal cells and vascular cells (Figure 5.2).

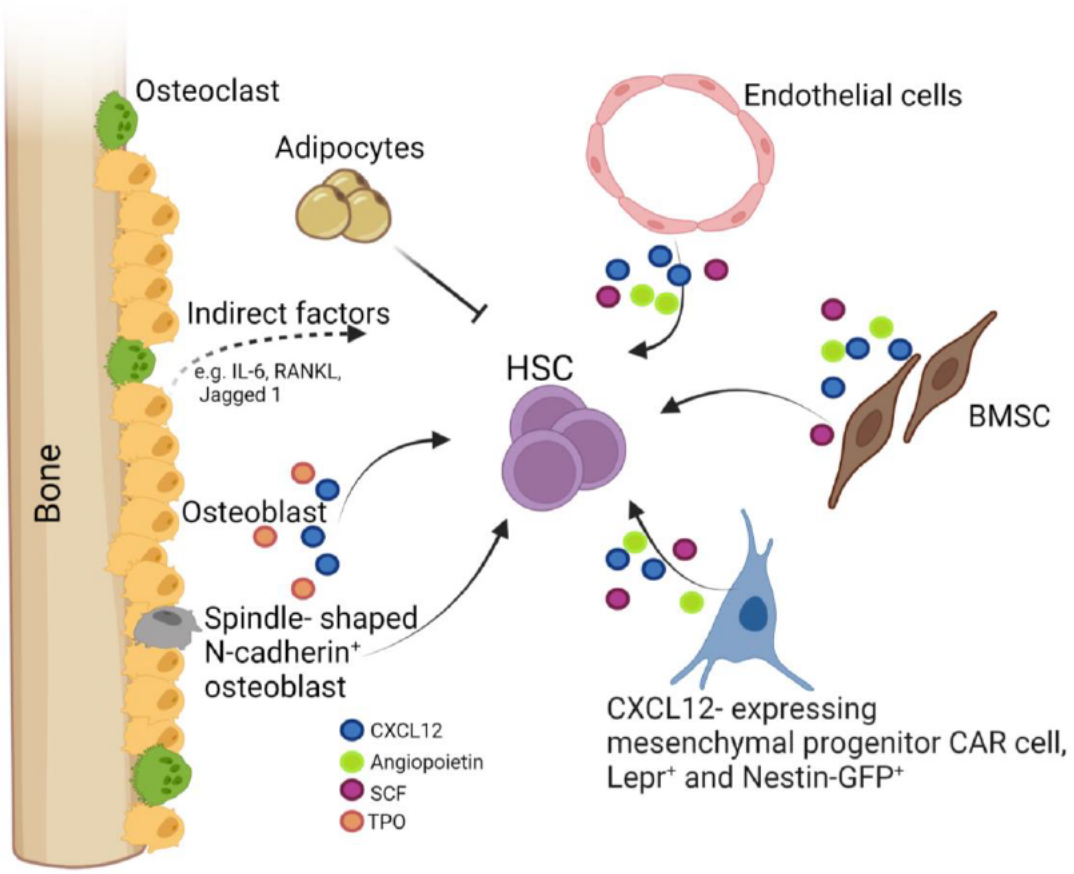


Figure 5.2. Discrete stromal cell populations in the BM are associated with HSC maintenance. A complex and diverse group of stromal cells in the BM have been demonstrated in HSC maintenance. Endothelial cells, bone marrow mesenchymal stem cells (BMSC), and CXCL12- expressing mesenchymal progenitors (CXCL12-abundant reticular (CAR) cells, leptin receptor+ stromal (Lepr^{+}) cells, and Nestin-GFP^{+} cells) produce various factors that support HSC, such as CXCL12, Angiopoietin (ANGPT1), and stem cell factor (SCF). Osteoblasts and spindle-shaped N-cadherin^{+} osteoblast produce several factors that support HSC, such as thrombopoietin (TPO) and CXCL12. Other stromal cells populations such as adipocytes may regulate haematopoiesis too.

Ineffective haematopoiesis is a major characteristic of MN, however, functional outcomes of BM microenvironment defects specifically in BMSC from MN patients are still controversial. MN-derived BMSC have been reported to stimulate the growth of CFU-GM, burst forming unit-erythroid (BFU-E) and LTC-IC progeny and haematopoiesis [196, 220, 442]. Azadniv *et al.* [220] demonstrated that AML-BMSC supported leukaemic CFU-GM and BFU-E outgrowth better than healthy-BMSC. Similarly, MDS $CD34^+$ cells proliferated more when seeded onto MDS-BMSC feeder layers in comparison to BMSC from healthy controls, which could be related to downregulation of *MMP1* in MDS-BMSC [443]. MMP1, is one of the mediators released by BMSC which has been shown to play an important role in regulation of tumour microenvironment [444]. MMP1 was discovered to inhibit MDS cell proliferation, by reducing growth and increasing apoptosis of MDS $CD34^+$ cells. Moreover, treatment with an MMP1 inhibitor in normal, healthy BMSC resulted in enhancement of MDS cell proliferation [443]. Importantly, co-injection of MDS cells with MDS BMSC significantly increase the engraftment rate of MDS cells, compared to MDS cells co-transplanted with healthy BMSC, indicating that patient derived BMSC promote MDS stem cell growth [162]. Overproduction of niche factors such as *CDH2* (N-Cadherin), insulin like growth factor binding protein 2 (*IGFBP2*), vascular endothelial growth factor A (*VEGFA*), and leukaemia inhibitory factor (*LIF)* was associated with the ability of MDS BMSC to enhance MDS clonal expansion [162]. Interestingly, healthy BMSC adopted MDS-BMSC like molecular features including, high expression of proangiogenic factors (*VEGFA*, *IGF* and *EGF*) and mediators of fibrosis (*LOXL*, *TGFβ* and *LIF*), when exposed to MDS HSC [162]. Furthermore, it has been reported that co-transplantation of normal, healthy BMSC with patient derived HSC not only improved engraftment but also reduced graft-versus-host disease [445].

However, other data suggest that HSC supportive capacity is diminished indicated by a significantly lower number of detected LTC-IC and cobblestone area-forming cells (CAFC) [170, 194, 197, 204, 205, 208, 217, 241, 446]. These conflicting results were probably due to different methodologies used. To assess HSC support *in vitro*, some studies have used autologous $CD34^+$ cells [170, 442] or BMNC [241] while others used normal donor [170, 197, 204, 205, 208] or umbilical cord $CD34^+$ cells [194, 196, 217]. These cells were plated over a pre-established feeder layer of BMSC derived from either unfractionated BMNC [170, 194, 197, 204, 205, 208, 217, 241, 442] or following negative selection to eliminate the presence of contaminating monocyte/macrophage populations [196]. Additionally, $CD34^+$ from healthy individuals co-cultured on MDS-derived BMSC feeder layers also revealed a lowered capacity to form myeloid and erythroid colony forming units [170, 197, 204].

This altered microenvironmental support may lead to haematopoietic failure and multilineage peripheral blood cytopaenia in MN. Interestingly, exposure of MDS-derived BMSC and healthy controls to Lenalidomide decreased CAFC but increased the formation of erythroid and myeloid colonies [197], implying that lenalidomide was able to improve HSC support. In addition, *in vitro* Azacitidine pre-treatment significantly improved stromal support of healthy $CD34^+$ HSC while inhibiting the repopulating capability of MDS-HSC. These findings suggest that the DNA methyltransferase inhibitor, Azacitidine directly modulates BMSC function and alters niche composition leading to suppression of haematopoietic progenitors in MDS [218].

Therefore, studies were performed to further characterise the altered phenotype of tMN BMSC and to determine whether the tMN BMSC phenotype functionally translated into an impaired ability to support $CD34^+$ HSC support in long-term culture assays.

5.2. RESULTS

5.2.1. BMSC from tMN Patients Show Reduced Adipogenic Differentiation

To further characterise the phenotype of tMN BMSC, an adipogenic differentiation potential was performed knowing that adipogenesis in particular depends on a robust metabolic reprogramming which was shown to be altered in tMN BMSC (Chapter 4.2.7).

To start with, GSEA indicated that genes involved in adipogenesis were downregulated in tMN (FDR < 0.1, P < 0.05) (Figure 5.3). Genes involved in adipogenesis such as *PNPLA2, TXNRD1, LGR4, FGF2, FOS* and *TNFRSF19,* were highly deregulated in tMN compared to

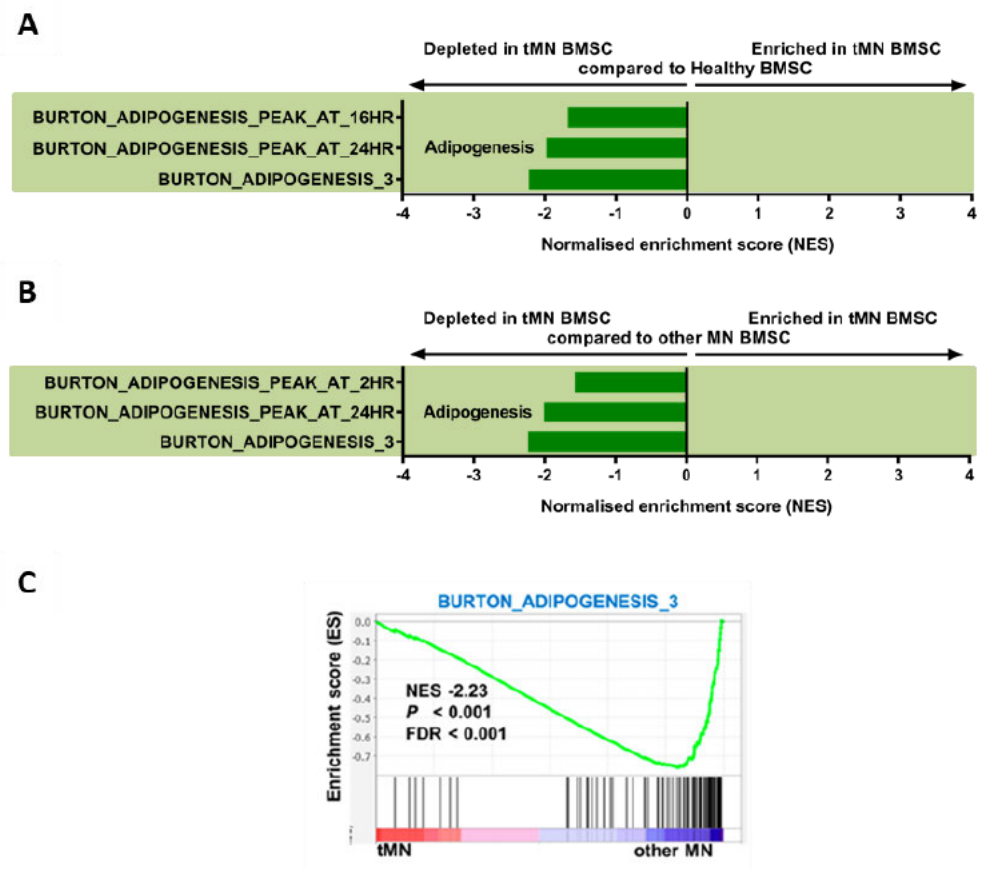


Figure 5.3. Adipogenesis-related gene set enrichment profiling of transcriptomic sequencing data of tMN compared to (A) Healthy BMSC and (B) other MN BMSC. NES indicates normalised enrichment score; negative score indicates depletion in tMN BMSC. (C) GSEA plot showing the specific deregulation of gene sets associated with adipogenesis in BMSC from tMN and other MN. NES, FDR and *P*-values are given.

Healthy BMSC, whereas *PNPLA2, CD36, TXNRD1, FOS, SLC44A2, ME1, LDLRAP1, SRD5A1, PTGDS, MTMR4* and *ARSB* were highly deregulated in tMN compared to other MN BMSC (Figure 5.4).

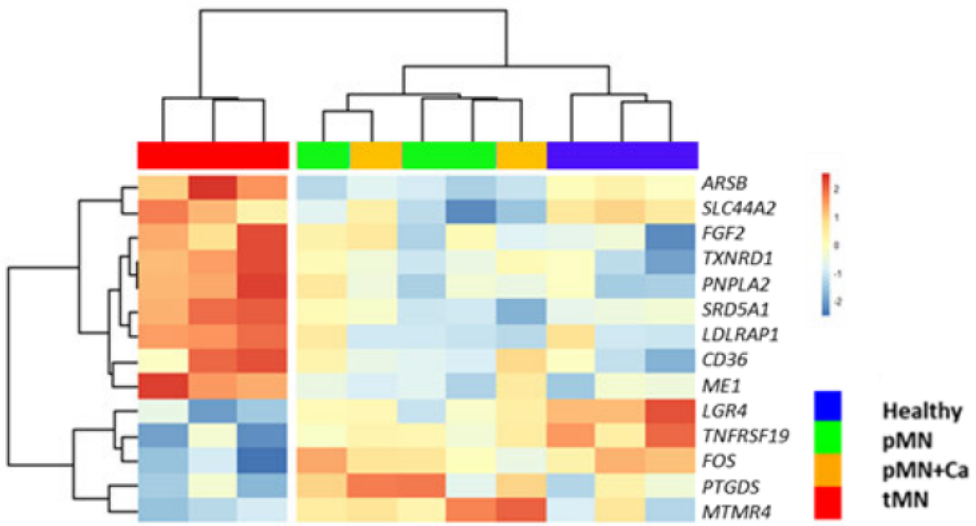


Figure 5.4. Differentially expressed genes associated with adipogenesis in tMN BMSC. Heatmap representing the gene expression changes of adipogenesis-associated genes found to be significantly differe deregulated (FDR $P < 0.1$ and log2 FC>|0.6|) in the BMSC from tMN as compared to Healthy and other MN BMSC. On the top panel of heatmap, the colour coding delineates the cohort group as indicated in the legend on the right side of the heatmap. The heatmap was generated using the pheatmap package.

Furthermore, BMSC derived from tMN displayed reduced expression of genes critically involved in the early and late adipogenic differentiation, namely peroxisome proliferator-activated receptor gamma (*PPARγ)* and Adipsin (Figure 5.5) under steady-state conditions (primers information provided in Table 2.16).

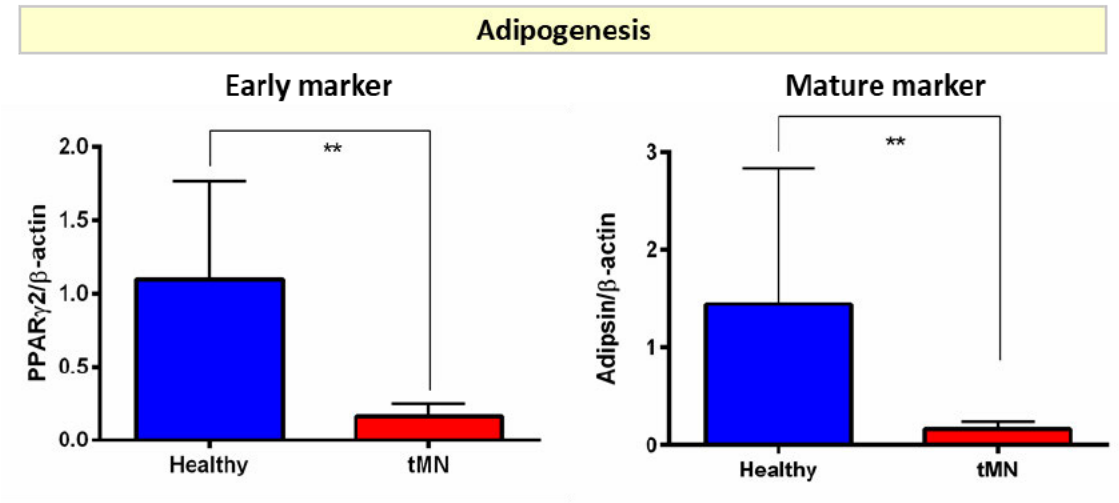


Figure 5.5. Downregulation of genes associated with adipogenesis in tMN compared to Healthy BMSC. mRNA expression of *PPARγ* and Adipsin was determined using quantitative RT-PCR without adipogenic induction in BMSC (Healthy n = 4; tMN n = 4). All bars indicate mean and all error bars indicate SD. Mann-Whitney test was used to detect statistically significant differences between cohorts. Asterisks display *P*-values ** $P < 0.01$.

Next, studies were performed to assess adipogenic differentiation potential of tMN BMSC by culturing BMSC in control growth or adipogenic inductive media and comparing it with Healthy, pMN and pMN+Ca BMSC adipogenic differentiation potential. Strikingly, quantification of lipid-laden Nile Red marked adipocytes was significantly reduced in tMN

BMSC compared to pMN+Ca ($P = 0.024$) and Healthy ($P < 0.001$) (Figure 5.6A). These results were validated by staining with Oil Red O (Figure 5.6B).

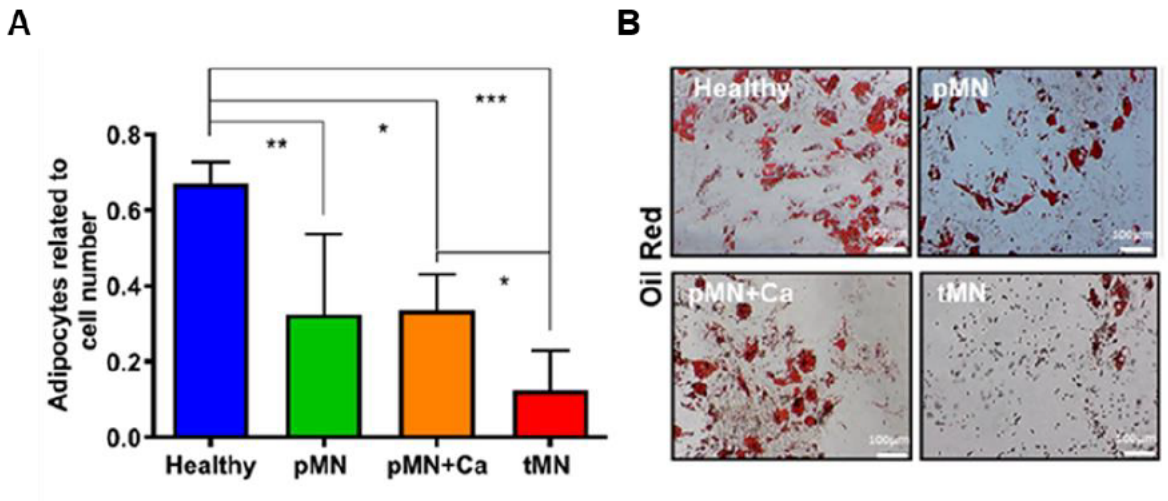


Figure 5.6. Defective adipogenesis of tMN BMSC. (A) Quantification of Nile red-stained lipid droplets, relative to total number of DAPI stained cells. BMSC were cultured under adipogenic inductive conditions for 4 weeks (Healthy n = 8; pMN n = 5; pMN+Ca n = 3; tMN n = 11); (B) representative micrographs of Oil red stained lipids. Scale bars indicate 100µm. All bars indicate mean, and all error bars indicate SD. Mann-Whitney test was used to detect statistically significant differences between cohorts. Asterisks display *P*-values $*P < 0.05$, $**P < 0.01$, $***P < 0.001$.

Interestingly, no association was found between defective adipogenic differentiation and proliferation in tMN BMSC (Figure 5.7).

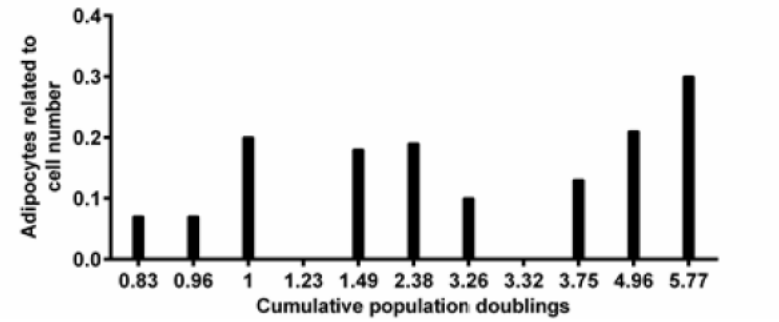


Figure 5.7. Association between BMSC proliferation and adipogenic differentiation capacity in tMN BMSC (n = 11). Axis y represents quantification of Nile red-stained lipid droplets, relative to total number of DAPI stained cells, whereas axis x represents proliferation potential measured by cumulative population doublings.

5.2.2. Stromal Cells-derived from tMN Patients Secrete Adipogenesis Associated-Inhibitory Cytokines

To understand the mechanism of defective adipogenesis in tMN, a cytokine survey was conducted (immunobead-based multiplex assay was conducted for the measurement of 38 cytokines/chemokines (section 2.3.15) from BMSC conditional media). While section 4.2.5 focussed on SASP cytokines, current section focussed on cytokines known to be inhibitors of adipogenesis. We found secretion of the adipocyte inhibitory cytokines IL-1β, IL-15, IL-6, IFNα and IFNγ were significantly higher by BMSC tMN compared to Healthy BMSC (Figure. 5.8A). Of note, a significant overlap was observed between adipogenesis-regulated cytokines and pro-inflammatory cytokines known to be cardinal SASP cytokines ($P < 0.001$) [259, 322] (Figure 5.8B).

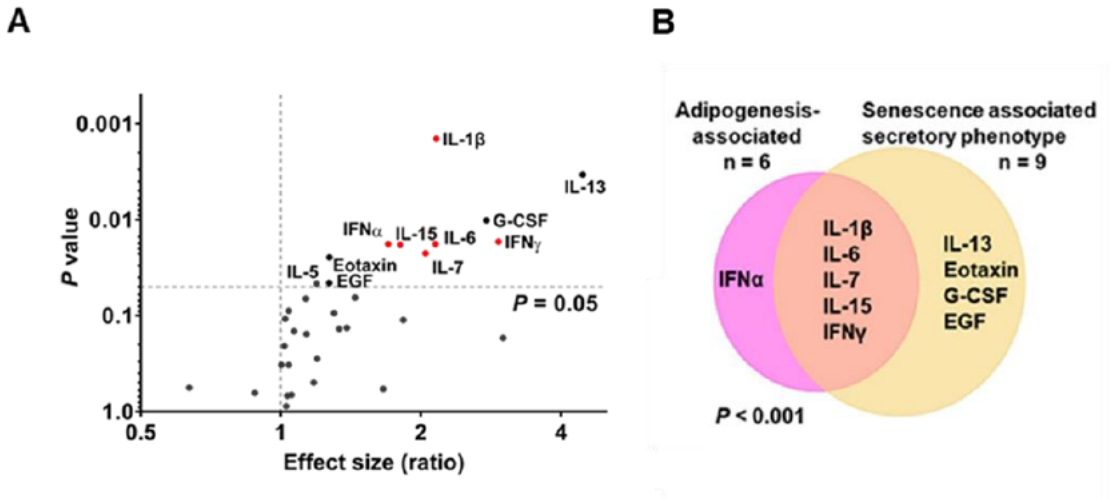


Figure 5.8. Cytokines in tMN BMSC conditioned media. (A) Levels of cytokines in tMN BMSC- conditioned media compared to Healthy (Healthy n = 17; tMN n = 17). Cytokines in red are significantly higher and are adipogenesis-related; (B) venn diagram representing significantly different cytokines related to SASP and adipogenesis in tMN BMSC compared to Healthy, as well as those cytokines which are in common in SASP and adipogenesis-associated groups.

To confirm the findings above, Healthy BMSC were treated with either IL-1β, IFNγ, IFNα, IL-13, IL-15, IL-6 or IL-7 individually or a cocktail of all seven-cytokines (IL-1β, IL-13, IL-15, IL-6, IFNα and IFNγ). The data showed that either IL-1β, IFNγ or IFNα individually and cocktail of all seven-cytokines profoundly inhibited *in vitro* BMSC lipid formation ($P < 0.003$) (Figure 5.9, Figure 5.10), demonstrating a causative role of these proinflammatory cytokines to inhibit adipogenesis.

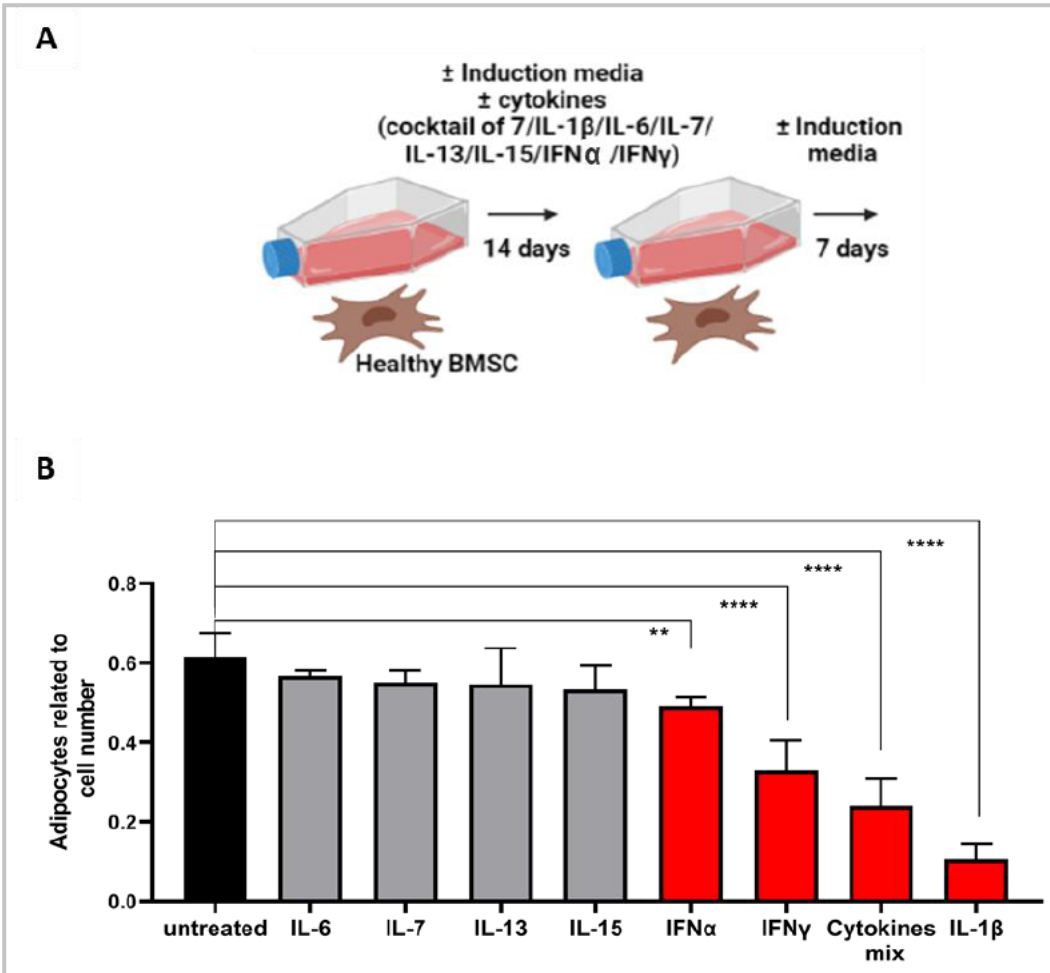


Figure 5.9. Adipogenesis after treatment with the respective cytokines. (A) schematic of the Healthy BMSC co-culture experiments with various cytokines. Healthy BMSC were cultured in adipogenesis-induced media with either seven cytokines cocktail (IL-1β, IL-6, IL-7, IL-13, IL-15, IFNα or IFNγ), or individual cytokines, either IL-1β, IL-6, IL-7, IL-13, IL-15, IFNα or IFNγ. Following 14 days, Healthy BMSC were cultured without cytokines for 7 days and adipogenic differentiation was investigated; (B) the number of adipocytes was enumerated by counting Nile Red-labelled cells and DAPI-labelled cell nuclei. The results from three Healthy BMSC are shown (n = 3). All bars indicate mean, and all error bars indicate SD. Mann-Whitney test was used to detect statistically significant differences between cohorts. Asterisks display *P*-values $**P < 0.01$, **** $P < 0.0001$.

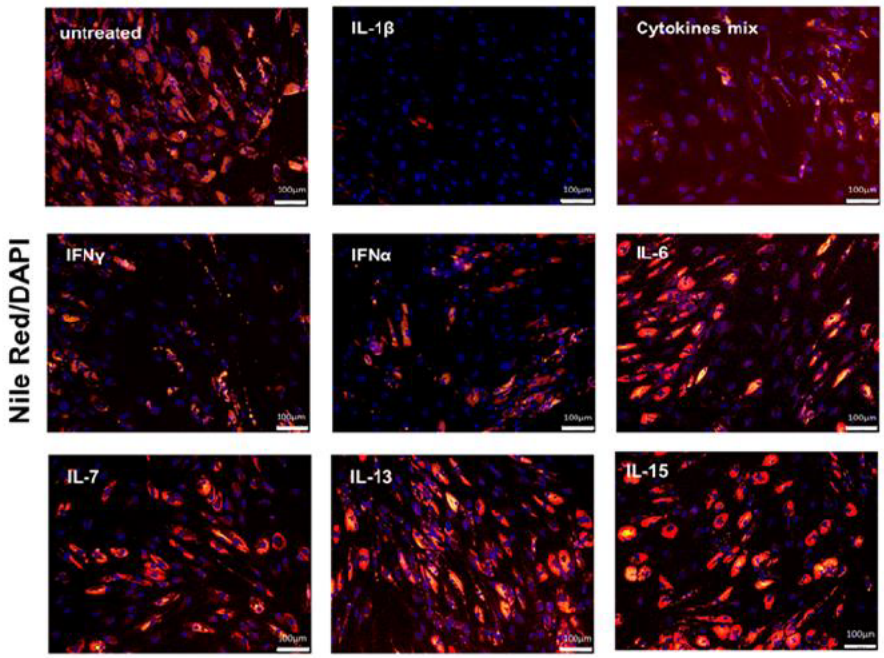


Figure 5.10. Adipogenesis after treatment with the respective cytokines. Representative micrographs of Healthy BMSC after exposure to the respective cytokines with scale bars indicating 100µm.

5.2.3. Treatment with OXPHOS Inhibitor robustly Inhibited Adipogenic Differentiation in Healthy BMSC

OXPHOS activity is known to support different processes within cells such as production of high-energy phosphates (ATP and phosphocreatine), calcium homeostasis, inflammation, ROS production and apoptosis [447-452]. As OXPHOS ATP was reduced in tMN BMSC (Chapter 4.2.7; Figure 4.16) further studies investigated whether exposure of Healthy BMSC to the OXPHOS inhibitor, IACS-010759 resulted in a functional decline in adipocytes differentiation. The data showed that IACS-010759 treatment significantly blocked adipogenesis of stromal cells as reflected by a two-fold reduced capacity to produce adipocytes in comparison to Healthy BMSC incubated without OXPHOS inhibitor ($P = 0.0022$) (Figure 5.11).

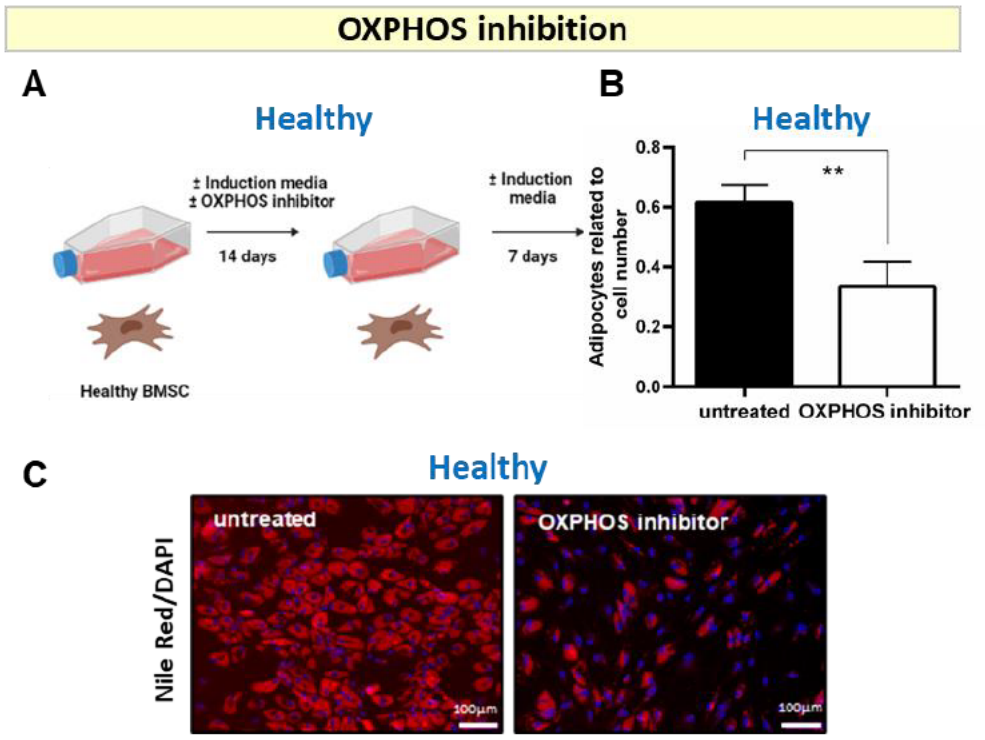


Figure 5.11. Adipogenesis after treatment with OXPHOS inhibitor. (A) Schematic of the Healthy BMSC co-culture experiments with OXPHOS inhibitor. Healthy BMSC were cultivated in adipogenesis-induced media with OXPHOS inhibitor (IACS-010759). Following 14 days, Healthy BMSC were cultured without OXPHOS inhibitor for 7 days and adipogenic differentiation was investigated; (B) the number of adipocytes was enumerated by counting Nile Red-labelled cells and DAPI-labelled cell nuclei; (C) representative micrographs of Nile Red stained adipocytes. The results from three Healthy BMSC are shown (n = 3); All bars indicate mean, and all error bars indicate SD. Mann-Whitney test was used to detect statistically significant differences between cohorts. Asterisks display *P*-values, $^{**}P < 0.01$.

5.2.4. Inhibition of Glycolysis does not Restore Defective Adipogenesis in tMN BMSC

Next, studies were performed to assess whether the extremally glycolytic phenotype observed in tMN may also contribute to the defect in adipogenesis, by culturing either Healthy or tMN BMSC with two different doses of 2DG (1 and 2mM) with adipogenesis- inducive media for 21 days.

The data showed that blockade of glycolysis in Healthy BMSC led to significantly reduced adipogenesis ($P < 0.001$) (Figure 5.12A-B) consistent with the metabolic requirement of adipogenesis to store glucose-derived de novo fatty acids and also perform mitochondria fatty acid β-oxidation. In tMN BMSC, although inhibition of glycolysis switched the metabolic network to generate ATP through mitochondrial oxidative phosphorylation (Chapter 4.2.7), it did not restore adipogenesis ($P = 0.730$) (Figure 5.12C-D).

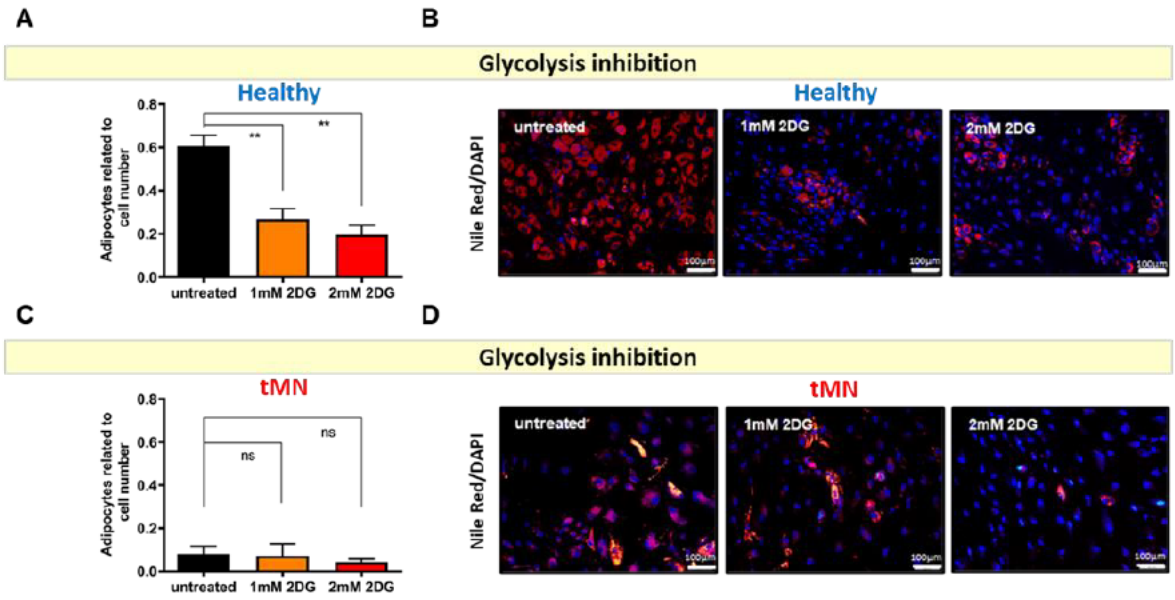


Figure 5.12. Inhibition of glycolysis does not restore defective adipogenesis in tMN BMSC. (A) Healthy BMSC (n = 3) were cultured under adipogenic induction conditions for 4 weeks either with or without 1mM and 2mM of 2DG, a glycolysis inhibitor, and number of adipocytes were evaluated by counting Nile Red-labelled cells and DAPI-labelled cell nuclei; (B) representative micrographs of Nile Red-stained cells and DAPI overlay in Healthy BMSC; (C) tMN BMSC (n = 3) were cultured under adipogenic inductive conditions for 4 weeks either with or without 1mM and 2mM 2DG and the number of adipocytes evaluated by counting Nile Red-labelled cells and DAPI-labelled cell nuclei; (D) representative micrographs of Nile Red-stained cells and DAPI overlay in tMN BMSC. All bars indicate mean, and all error bars indicate SD. Scale bars indicate 100µm. Mann-Whitney test was used to detect statistically significant differences between cohorts. Asterisks display *P*- values ** $P < 0.05$.

5.2.5. BMSC from tMN Patients Exhibit Increased Osteogenic Differentiation Potential

To assess osteogenic differentiation potential, BMSC derived from tMN, Healthy, pMN and pMN+Ca were cultured under osteogenic inductive conditions for 21 days before the levels of acid-soluble mineral were quantified and expressed relative to the total DNA while mineralized matrix was stained using Alizarin Red.

BMSC derived from pMN were found to be impaired in their capacity to form a mineralised matrix compared to Healthy BMSC (14.8 ±23.7 versus 53 ±34.3, $P = 0.029$). In contrast, bone mineralization matrix formation was significantly greater in tMN BMSC (182.7 ±190.3) compared to BMSC from Healthy controls and pMN ($P = 0.013$). This was further confirmed by Alizarin Red-stained mineralised deposits (Figure 5.13). Interestingly, osteogenic differentiation capacity was not significantly different between BMSC derived from pMN+Ca and pMN patients ($P = 0.143$ and $P = 0.786$ respectively) (Figure 5.13).

Additionally, the mRNA expression of *OPN*, an established marker of mature osteoblasts, was significantly upregulated in tMN BMSC compared to Healthy BMSC (Figure 5.13C), whereas there was no difference in the expression of *RUNX2* (Figure 5.13D) under steady-state conditions (primers information provided in Table 2.16).

.

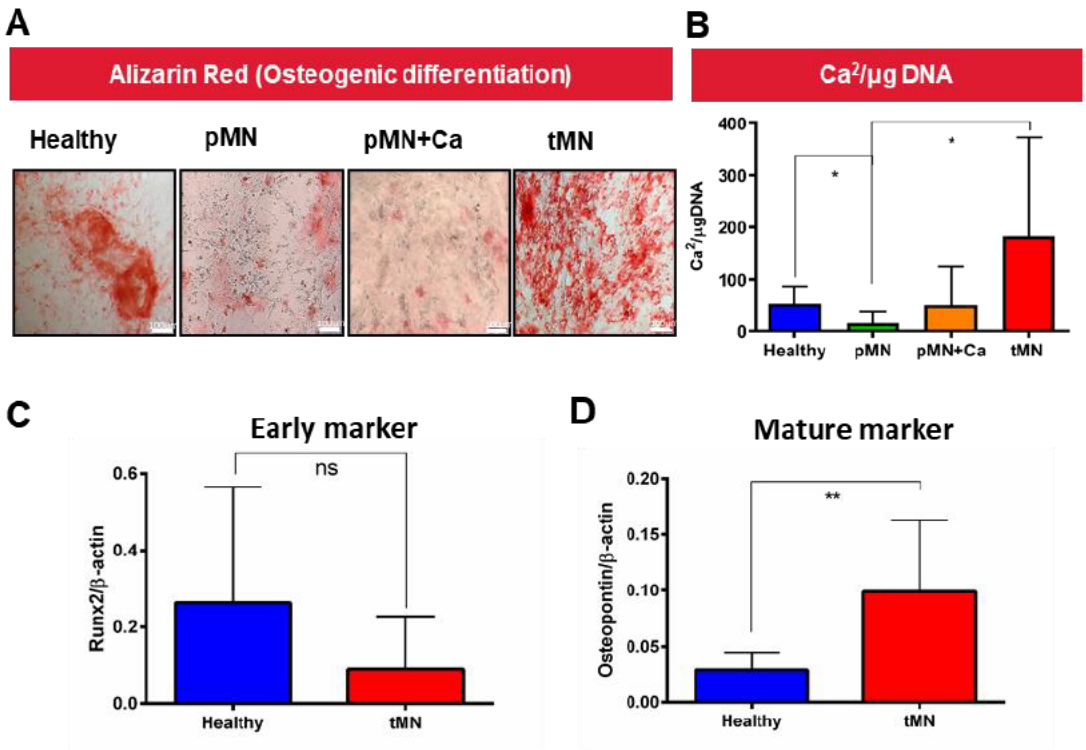


Figure 5.13. Impaired osteogenic differentiation potential of tMN BMSC. BMSC were cultured under osteogenic inductive conditions for 4 weeks (Healthy n = 8; pMN n = 5; pMN+Ca n = 3; tMN n = 11). (A) Representative photos of mineral deposits stained with Alizarin red; (B) Quantification of mineral content by measuring the concentration of Ca^{2+} (calcium) in an acid-solubilized matrix and normalizing them to the total DNA. mRNA expression of (C) *RUNX2* and (D) Osteopontin (*OPN*) between Healthy (n = 4) and tMN (n = 4) BMSC was measured by quantitative RT-PCR without osteogenic induction. All bars indicate mean, and all error bars indicate SD. Scale bars indicate 100µm. Mann-Whitney test was used to detect statistically significant differences between cohorts. Asterisks display *P*-values $*P < 0.05$.

Within the tMN BMSC cohort an inverse correlation was observed between the proliferative potential and osteogenic differentiation capacity of tMN BMSC (Figure 5.14). Thus, in contrast to pMN, tMN BMSC showed enhanced osteogenic differentiation, albeit with some inter-patient variability.

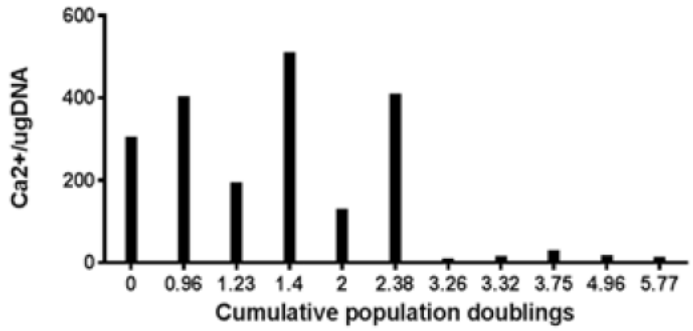


Figure 5.14. Association between BMSC proliferation and osteogenic differentiation capacity in tMN patients (n = 11). Axis y represents quantification of mineral content by measuring the concentration of Ca^{2+} in an acid-solubilized matrix and normalizing them to the total DNA, whereas axis x represents proliferation potential measured by cumulative population doublings.

5.2.6. Normal Chondrogenic Differentiation Potential of tMN BMSC

Examination of BMSC chondrogenic differentiation potential was assessed by cytochemical staining with Safranin-O. The results showed that BMSC from tMN patients exhibited no significant differences when compared to aged-matched Healthy controls as well as other BMSC derived from typical MN patients (Figure 5.15).

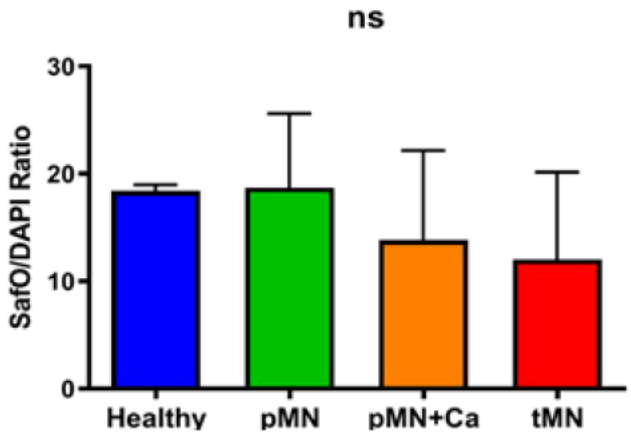


Figure 5.15. Normal chondrogenic differentiation potential of tMN BMSC. Quantification of Safranin-O-stained chondrocytes, relative to total number of DAPI stained cells. BMSC were cultured under chondrogenic inductive conditions for 7 days (Healthy n = 8; pMN n = 5; pMN+Ca n = 3; tMN n = 11). All bars indicate mean, and all error bars indicate SD. Mann-Whitney test was used to detect statistically significant differences between cohorts.

5.2.7. Diminished Haematopoietic Stem Cell Supporting Capacity of tMN BMSC

Given substantial aberrant morphology, growth defects (Chapter 3) and adipo- and osteogenic differentiation potential (Chapter 5.2.1 and Chapter 5.2.6), studies were performed to assess whether this functionally translated into a diminished ability of BMSC to support $CD34^+$. *In vitro* HSC supportive capacity of BMSC was assessed by co-culturing $CD34^+$ on BMSC feeder-layer followed by clonogenic assays. Briefly, tMN BMSC were cultured with autologous and Healthy $CD34^+$ cells and *vice versa* for 5 weeks. At the end of that period, the medium was replaced by clonogenic medium and culture for another 2 weeks.

The data demonstrated that stroma derived from tMN patients was unable to support the long-term culture of Healthy $CD34^+$ in long-term culture initiating assays (Figure 5.16). BMSC derived from tMN patients exhibited a 12-fold decreased capacity to support Healthy $CD34^+$ compared with Healthy BMSC (1 ±1 versus 12 ±2 colonies; $P < 0.001$) and 3-4 folds lower than pMN ($P = 0.001$) and pMN+Ca ($P = 0.014$) (Figure 5.16).

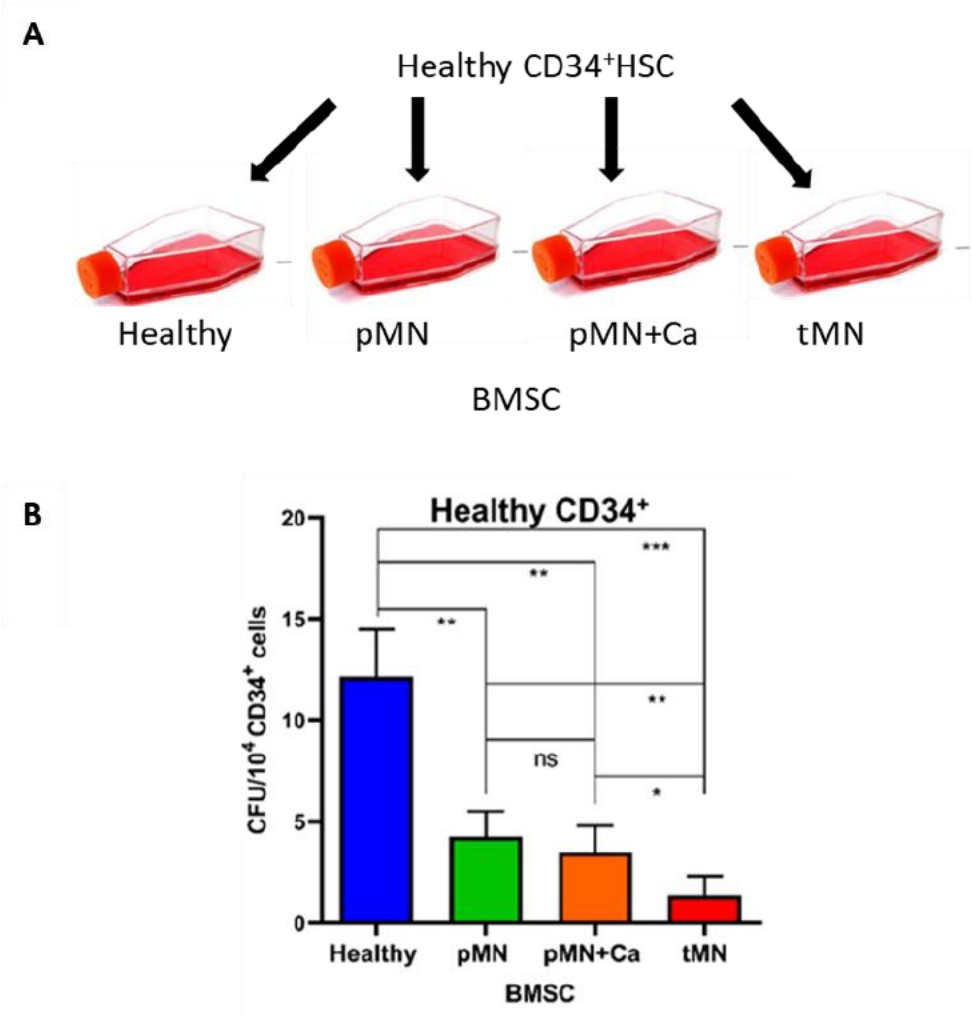


Figure 5.16. BMSC derived from tMN patients have a compromised ability to support long-term culture initiating-cell (LTC-IC). (A) Schematic overview of Healthy $CD34^+$ co-culturing with different cohorts BMSC; (B) *in vitro* HSC supportive capacity of BMSC assessed by co-culturing Healthy (blue bar; n = 2), pMN (green bar; n = 2), pMN+Ca (orange bar; n = 2) and tMN (red bar; n = 6) BMSC with Healthy $CD34^+$ cells for 7 weeks followed by clonogenic assays. All bars indicate mean, and all error bars indicate SD. The Mann-Whitney test was used to detect statistically significant differences between cohorts. Asterisks display *P*-values $*P < 0.05$, $**P < 0.01$, $***P < 0.001$.

When $CD34^+$ cells from tMN were co-cultured with autologous stroma layers, the number of colonies were extremely low but were rescued by co-culture with normal stroma (1 ±1 colonies versus 11 ±8 colonies; $P < 0.001$) (Figure 5.17).

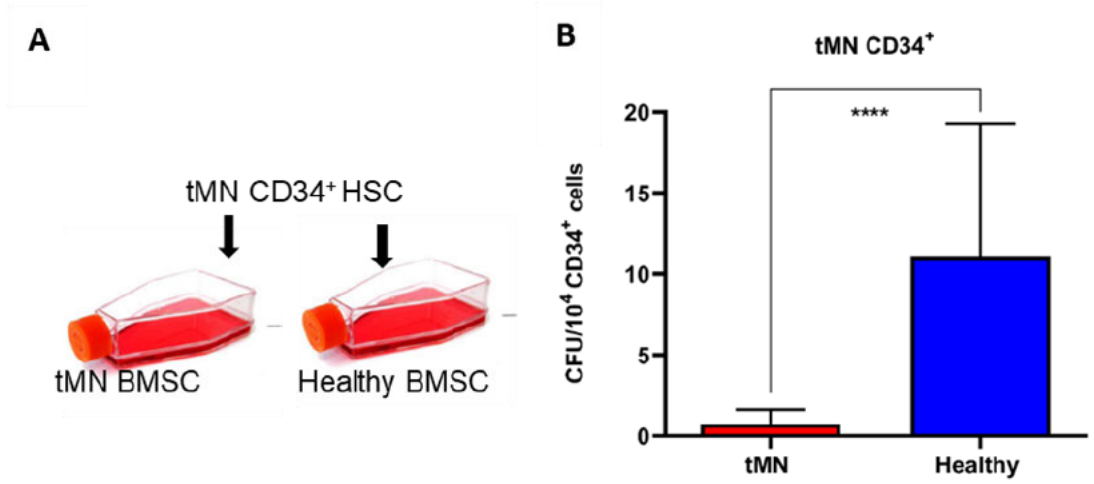


Figure 5.17. BMSC derived from tMN patients have a compromised ability to support long-term culture initiating-cell (LTC-IC). (A) Schematic overview of tMN $CD34^+$ co-culturing with either autologous or Healthy BMSC; (B) $CD34^+$ of tMN patients were co-cultured on autologous (red bar; n = 4) and Healthy (blue bar; n = 13) BMSC. All bars indicate mean, and all error bars indicate SD. The Mann-Whitney test was used to detect statistically significant differences between cohorts. Asterisks display *P*-values ****$P <$ 0.001.

Importantly, functional enrichment analysis showed depletion of HSC support/regulation pathways in tMN BMSC compared to both controls (Figure 5.18).

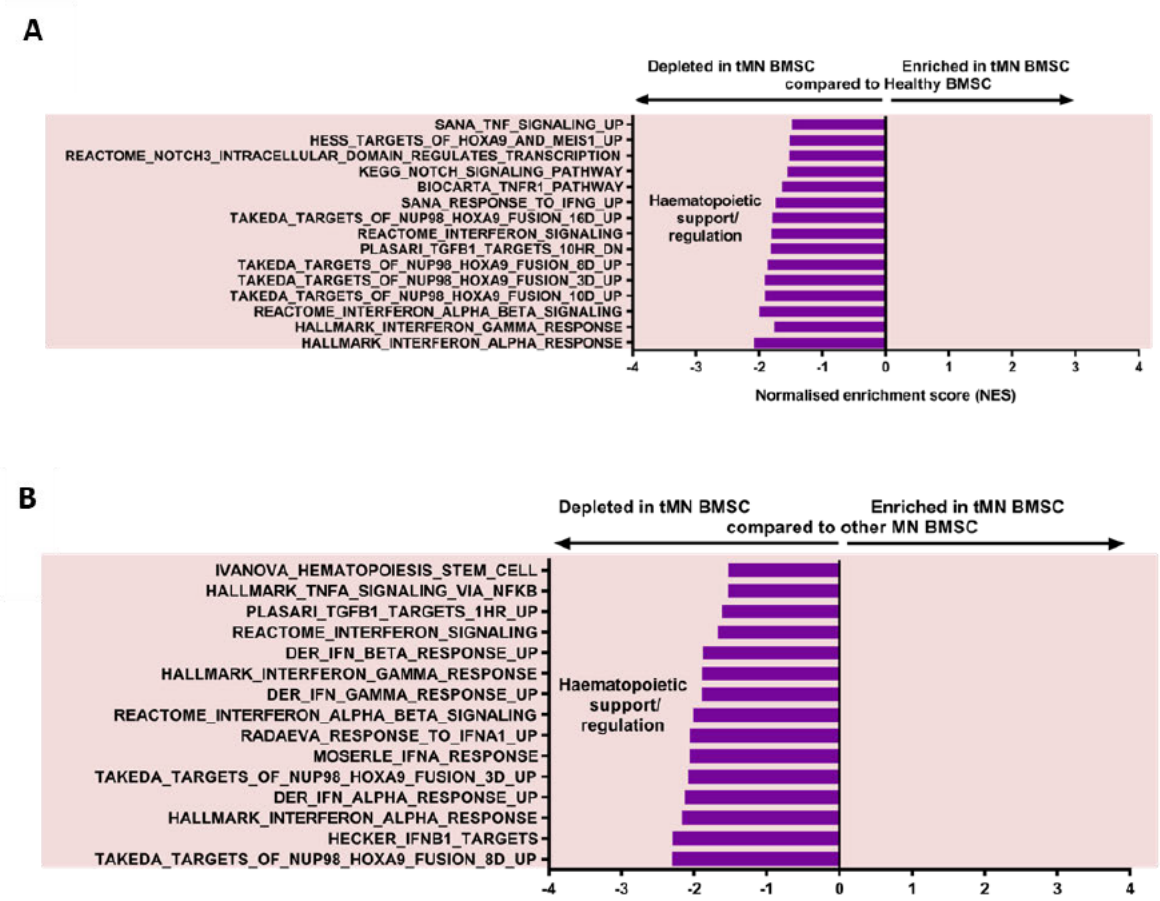


Figure 5.18. Haematopoietic stem cells-related gene set enrichment profiling of transcriptomic sequencing data of tMN compared to (A) Healthy BMSC and (B) other MN BMSC. NES indicates normalised enrichment score; negative score indicates depletion in tMN BMSC.

Moreover, *CXCL12* gene expression, a key regulator of haematopoiesis was significantly lower in tMN BMSC compared to Healthy BMSC ($P < 0.001$) and pMN BMSC ($P = 0.007$), thus offering a one potential mechanism contributing to the poor HSC supportive capacity (Figure 5.19).

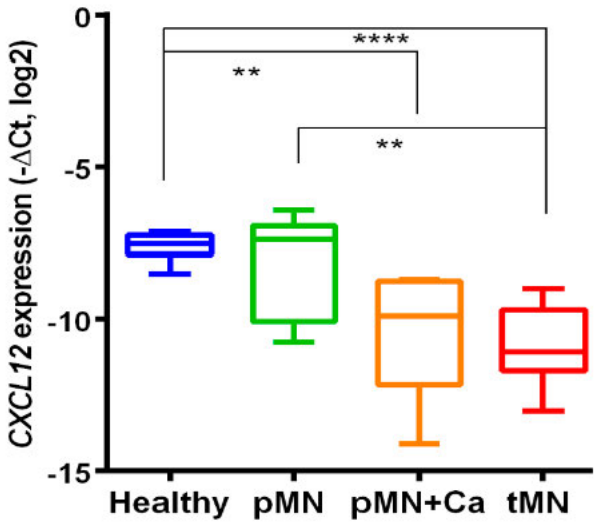


Figure 5.19. Validation of *CXCL12* in an independent cohort. Expression of *CXCL12* gene in Healthy (n = 7), pMN (n = 6), pMN+Ca (n = 5) and tMN (n = 7) BMSC. Boxplot shows the gene expression across 4 defined groups by qRT-PCR. Gene expression was determined relatively to *GAPDH* mRNA expression (ΔCt) and represented as –ΔCt in log2 scale. In boxplot, the horizontal line indicates the median, boxes indicate the interquartile range, and whiskers extend from the hinge to the smallest/largest value, at most 1.5 × interquartile range from the hinge. Unpaired Student's t-test was used to detect statistically significant differences between cohorts. Asterisks display *P*-values $^{**}P < 0.01$, $P^{****} < 0.0001$.

Collectively, these findings demonstrate significantly impaired HSC support of tMN BMSC compared to other MN groups without prior CT exposure and aged-matched Healthy BMSC.

5.3. DISCUSSION

In the present study, the osteogenic and adipogenic potential of pMN BMSC was found to be significantly reduced compared to Healthy-BMSC, in accord with the previous studies [170, 204, 205, 207, 208]. Importantly, the current study is the first to describe the differentiation potential of tMN BMSC, which was significantly different compared to age matched Healthy and pMN.

BM adipocytes have largely been believed to be negative regulators of haematopoiesis [134]; however, the biology of BM adipocytes can differ depend on their anatomical location. Following cytotoxic exposure, adoptive inhibition of adipogenesis is potentially to accelerate haematopoietic recovery [425]. However, the role of marrow adipocytes in leukaemia development is controversial. Marrow adipocytes inhibit T-cell acute lymphoblastic leukaemia (T-ALL) proliferation *in vitro* and *in vivo* [453], while support survival and proliferation of AML blasts by releasing free fatty acid via activation of lipolysis [454]. AML also disrupt normal haematopoiesis by compromising adipocyte niche [455]. GSEA and enrichment analysis performed in this study suggest that genes involved in adipogenesis were downregulated in tMN. This was further supported by significant reduction in adipogenesis while high expression of patatin-like phospholipase domain containing-2 (*PNPLA2*), known to catalyse adipolysis, in tMN BMSC compared to Healthy control and other MN. *PNPLA2* catalyses the first reaction of lipolysis by hydrolysing triacylglycerols to diacylglycerols [456]. Similarly, other genes involved in adipogenesis such as *CD36, TXNRD1, LGRF4, FOS,* and *ME1* were also highly deregulated in tMN. *CEBPZ*, a pro-adipogenic transcription factor and member of the CEBP family of transcription factors, was downregulated in tMN BMSC compared to other MN BMSC. Molecular analysis was further substantiated by reduced adipogenic differentiation of tMN BMSC, which may be driven by autocrine and paracrine

secretion of anti-adipogenic proinflammatory cytokines such as IL-1β, IL-15, IL-6, IFN-α and IFN-γ by tMN BMSC. Moreover, findings in this chapter demonstrates that *in vitro* exposure to IL-1β and IFNγ suppressed adipogenic differentiation of Healthy BMSC, in agreement with previous studies [382, 383, 457-463].

Importantly, this thesis is the first to describe the osteogenic differentiation potential of tMN BMSC, which was significantly increased, compared to age matched Healthy and pMN BMSC. Notably, the mineralization capacity of tMN BMSC was also significantly higher than pMN+Ca, where the only difference between the two cohorts is prior exposure to CT in tMN. CT may be inducing osteogenic differentiation or selecting stromal cells destined for osteogenesis at the cost of adipogenic potential. Confirmatory studies showed that gene expression levels of *OCN*, a known marker of late osteogenesis, were significantly upregulated in tMN BMSC [223], in contrast to findings in pMN-derived BMSC, where transcript levels [207] and serum levels [170, 208] of *OCN* were significantly decreased. Gene expression levels of *OSX* and *RUNX2*, transcription factors critically involved in osteogenic differentiation, were reduced in tMN BMSC compared to Healthy BMSC [223]. Furthermore, BMSC derived from primary myelofibrosis also exhibited an increased osteogenic potential [464], which is associated with increased fibrosis and osteosclerosis [465]. Interestingly, some tMN patients, especially with history of solid tumours, present with moderate/ severe BM fibrosis [466]. In our cohort, 31% of tMN patients presented with increased BM fibrosis.

Impaired expression of crucial molecules involved in the interaction between BMSC and HSC, such as SCF, Jagged1 and ANGPT1 could potentially contribute to the defective HSC-supporting capacity of MN BMSC [170, 204, 208, 217]. CT not only induces genetic alteration in HSC [177, 178] but also damages the stromal cell compartment [179-182] causing BMSC

to have a compromised HSC-supporting capacity. The present study demonstrates for the first time the reduced HSC-supporting capacity of tMN BMSC. Reduced HSC-supporting capacity was evident not only for autologous tMN $CD34^+$ cells but also for $CD34^+$ cells from normal healthy donors when co-cultured on tMN BMSC stromal layers. A compromised HSC-supporting capacity of tMN BMSC can be due to deregulated interferon (*IFN*) [467] and *TNF* [468] affecting signalling pathways crucial for HSC regulation. *CXCL12* expression, a key regulator of haematopoiesis, was found to be significantly lower in tMN BMSC compared to Healthy and pMN BMSC. *CXCL12* is known to be abundantly expressed in BMSC, osteoblasts and endothelial cells, where it plays a crucial role in HSC maintenance [469, 470]. Along with its primary binding receptor *CXCR4*, *CXCL12* plays an important role in the retention [471], quiescence [472, 473] and repopulating [473] of HSC. Furthermore, it not only regulates HSC but also induces osteoclast development [474]. Deregulated expression of *CXCL12* by BMSC appears to be a combined hallmark of myeloid neoplasms, such as decreased expression by BMSC in a mouse model of CML [475]. This study observed that loss of *CXCL12* from BMSC was associated with loss of normal HSC. BMSC derived from pMN patients exhibited decreased expression of *CXCL12* compared to Healthy BMSC [197, 224]. Interestingly, a leukaemia *in vivo* mouse model showed that leukemic infiltration of the BM is associated with decreased *CXCL12* activity, whereas *CXCL12* knockdown in stromal cells results in reduction of long-term HSC and an expansion of progenitor pool [473]. These findings could explain the reduction of colony numbers observed in long term culture assays using tMN BMSC feeder layers. Moreover, downregulated *CXCL12* expression was previously demonstrated in BMSC with defective proliferation [476]. Additionally, lower *CXCL12* gene expression in BMSC or instabilities in its intracellular pathways leads to altered cell survival, cytoskeletal disorganization, and impaired differentiation [477, 478].

Together, results from the current chapter demonstrated that tMN stromal cells are functionally altered indicated by increased osteogenic and reduced adipogenic differentiation capacity, not only compared to aged-matched healthy individuals but also pMN and other myeloid neoplasms patients with a history of another cancer but without cytotoxic exposure (pMN+Ca) suggesting that functional alterations are due to prior CT. Chapter 7 of this study will expand on this issue by investigating long term CT-damage to BMSC by assessing proliferation, senescence and differentiation potential of serial BMSC from tMN patients, before diagnosis of tMN. Importantly, these aberrant tMN BMSC were not able to support normal or autologous *in vitro* long-term haematopoiesis which seems to contribute to ineffective haematopoiesis and peripheral cytopaenia observed in patients with tMN.

Chapter 6: Senolytic Therapies Can Restore Defective Adipogenic and Osteogenic Differentiation of tMN BMSC

6.1. INTRODUCTION

Data from previous chapters demonstrated CT-induced senescence as an underlying mechanism leading to BMSC dysfunction in tMN. Approaches to interfere with senescent cells have been an area of active research in recent years. Two key strategies are currently under development: (1) Inhibition of SASP using senomorphic agents and (2) Selective elimination of senescent cells using senolytic agents.

6.1.1. Inhibition of SASP using Senomorphic Agents

The first strategy aims at reducing the adverse effects of the SASP. Various studies suggest that SASP development can be managed by several regulators, such as p38MAPK, mTOR, JAK, GATA4, TGFβ, NF-κB and CEBPα [479]. Targeting these molecules by either inhibiting their function or neutralizing some of their members might be an effective approach to lessen the expression of numerous proinflammatory factors in senescent cells. Possibly the most well-known SASP components, for which approved drugs are available, include IL-1 (IL-1 receptor drug Anakinra) [312], and IL-6 (IL-6 receptor inhibitor Tocilizumab) [480] (Table 6.1). Numerous other senomorphic agents, drugs that suppress SASP components without inducing apoptosis, have been recognized recently such as inhibitors of NF-κB [481], free radical scavengers, JAK pathway inhibitors [482], and the mTOR suppressant rapamycin [311, 483]. However, non-specificity when targeting senescent cells is key limitation of SASP inhibitors. This is due to anti-inflammatory properties of these drugs. Importantly, when used long-term they can also cause severe toxicities. Furthermore, existing senomorphic agents cannot distinguish between beneficial and inhibitory functions of SASP components.

Table 6.1. Known senomorphic agents

Agent	Target(s)	Reference
Metformin	IKK complex and/or NF-κB	[484-487]
Rapamycin	mammalian target of rapamycin (mTOR)	[311, 483, 488]
RAD001-rapamycin derivative	mammalian target of rapamycin (mTOR)	[489]
LY2228820	p38MAPK	[490]
LY3007113	p38MAPK	[490]
Anakinra	IL-1 receptor	[312]
5Z-7-oxozeaenol	TGFβ1-activated kinase-1 (TAK1)	[491]
Tocilizumab	IL-6 receptor	[480, 492]
SB525334	TGFβ1	[493, 494]
Ruxolitinib	JAK1/2	[495-497]
SB203580	p38MAPK	[498]
Glucocorticoids	NF-κB	[499]

6.1.2. Selective Elimination of Senescent Cells using Senolytic Agents

The other approach focuses on agents that selectively eliminate senescent cells without disturbing quiescent and proliferating [500-503]. Several senolytic agents have now been recognised (Figure 6.1). Synthetic senolytic-mediated elimination of senescent cells aims at four different targets such as BCL pathways which regulate mitochondrial-dependent apoptosis [289], PI3K-PKB/Akt pathway which is involved in survival regulation [504], heat shock protein 90 (HSP90) [505] and others [506-508]. For example, ABT263 (Navitoclax) and ABT737 are inhibitors of BCL-2 and BCL-2/XL family of anti-apoptotic proteins respectively, however, they are senolytic only in some cell types [503, 509]. Additionally, these types of inhibitors may have significant side effects including neutropenia and thrombocytopaenia

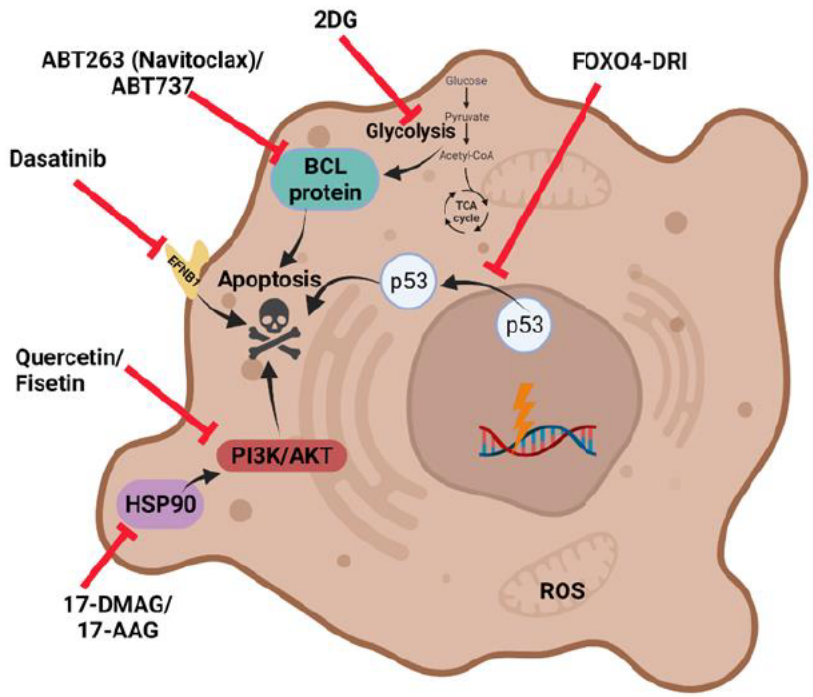


Figure 6.1. Elimination of senescent cells by senolytic drugs. Several agents have been identified which led senescent cells to cell death through different pathways including interference with PI3K-PKB/Akt (PI3K/AKT), BCL, p53 and metabolic pathways which seems the most effective.

Abbreviations: 2DG- 2-Deoxy-D-glucose; 17-DMAG- 17-dimethylaminoethylamino- 17-demethoxygeldanamycin; 17-AAG- 17-allylamino-17-demethoxy-geldanamycin; BCL- B-cell lymphoma; FOXO4-DRI - FOXO4-D-retro-inverso; HSP90- heat shock protein 90; ROS- reactive oxygen species.

[510]. Dasatinib, which is anti-cancer agent and receptor tyrosine kinase inhibitor, interfere with EFNB-dependent suppression of apoptosis [511, 512]. Recently, a forkhead box protein O4 (FOXO4)- interacting peptide, FOXO4-D-retro-inverso (FOXO4-DRI) that inhibit an association with p53 was shown to induce apoptosis in senescent but not in normal cells [513, 514]. Additionally, HSP90 inhibitors, effective in removing senescent cells by indirectly blocking PI3K-PKB/Akt pathway and leading to cell death in culture and *in vivo* [505], are more likely to be more effective in combination with other senolytic agents that target different anti-apoptotic pathways. On the other hand, the naturally extracted senolytic molecules have a complex mechanism with several intracellular targets involved [515], with Quercetin as a key one. Quercetin is a polyphenol with numerous roles, such as inhibition of PI3K-PKB/Akt [516, 517] and inhibition of multiple pathways related to inflammation: cyclooxygenase-2 (COX-2), nuclear factor-kappa B (NF-κB), activator protein 1 (AP-1), MAPK, reactive nitric oxide synthase (NOS) and reactive C-protein (CRP) [518]. Another natural senolytic agent Fisetin is also confirmed to promote apoptosis of senescent cells by inhibiting mTOR and PI3K-PKB/Akt [519]. Moreover, senolytics, targeting senescent cells may be cell-type specific [520], e.g., Dasatinib can eliminate senescent human pre-adipocytes to a greater degree than that of proliferating cells, whereas Quercetin is more effective against senescent human umbilical vein endothelial cells (HUVEC) and mouse BMSC. Additionally, combine treatment of Dasatinib and Quercetin decrease burden of senescent mouse embryonic fibroblasts (MEF) [500]. Navitoclax on the other hand had no effect on senescent adipocytes progenitors, but only on HUVEC, IMR90 human lung fibroblasts and MEF [503]. Another a well-known hallmark of senescent cells, therapy and oncogene-induced, is enhanced energy production with greater glucose uptake for aerobic glycolysis which senescent cells depend on it for its survival [344]. Therefore, targeting glucose metabolism with glycolysis inhibitor such as 2DG which blocks ATP production, successively activating AMPK and leading to cell cycle arrest, reduced cell

proliferation, enhanced autophagy, and apoptosis, may be potential therapy [521]. Senolytic effect of 2DG was demonstrated previously on senescent vascular smooth muscle cells where 2DG lead to enhanced apoptosis with cellular blebbing and pyknotic nuclear condensation [522].

Most importantly, therapeutic intervention against cellular senescence not only reduces the senescence burden but also can restore cell functionality such as increased cardiovascular function, reduced osteoporosis [500, 503], improved angiogenic potential [501], increased adipogenesis [523].

Previous chapters have described that tMN BMSC are highly senescent (Chapter 4.2.2) yet metabolically highly active (Chapter 4.2.7) and exhibit defective adipogenesis and osteogenic differentiation capacity (Chapter 5.2.1 and 5.2.6 respectively). Therefore, the next set of experiments assessed whether senescence drives the aberrant differentiation potential of tMN BMSC by treating tMN BMSC with senolytic agents and assessing their differentiation potential in *in vitro* culture.

6.2. RESULTS

6.2.1. Effect of Dose Titration of Senolytic Agents on Morphology and Viability in Healthy BMSC

Based on available literature, pilot studies tested serial concentrations of two senolytic agents namely, Dasatinib and Quercetin, either alone or in combination and selected the lowest concentration without cytotoxic effect on Healthy BMSC (Figure 6.2- 6.4). Briefly, Healthy BMSC were treated for 72 hours with: (i) six different concentrations of Dasatinib: 10nM, 50nM, 100nM, 200nM, 400nM and 1µM; (ii) four different concentrations of Quercetin: 5µM, 10µM, 20µM and 30µM; (iii) four combinations of Dasatinib: 10nM, 50nM, 100nM and 200nM plus 10µM Quercetin.

Assessment of morphology and viability was performed using light microscopy and flow cytometry. Based on these experiments 50nM Dasatinib, 10µM Quercetin and combination of 50nM Dasatinib with 10µM Quercetin were used for further experiments in this study.

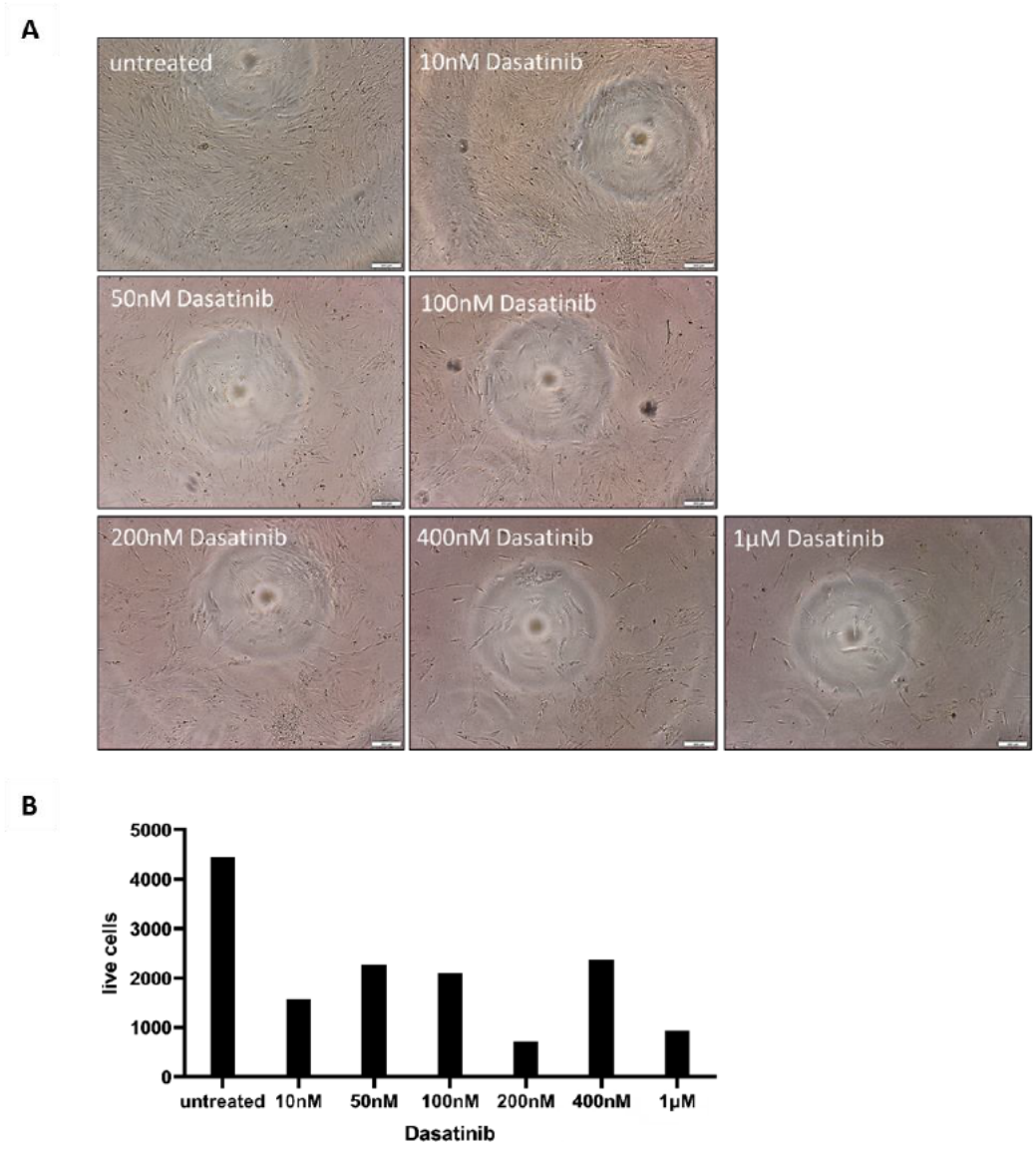


Figure 6.2. Effect of dose titration of Dasatinib on morphology and viability in Healthy BMSC after 72 hours in culture. (A) Representative micrographs of BMSC morphology assessed by light microscopy; (B) number of live BMSC analysed by flow cytometry. Scale bars indicate 200µm.

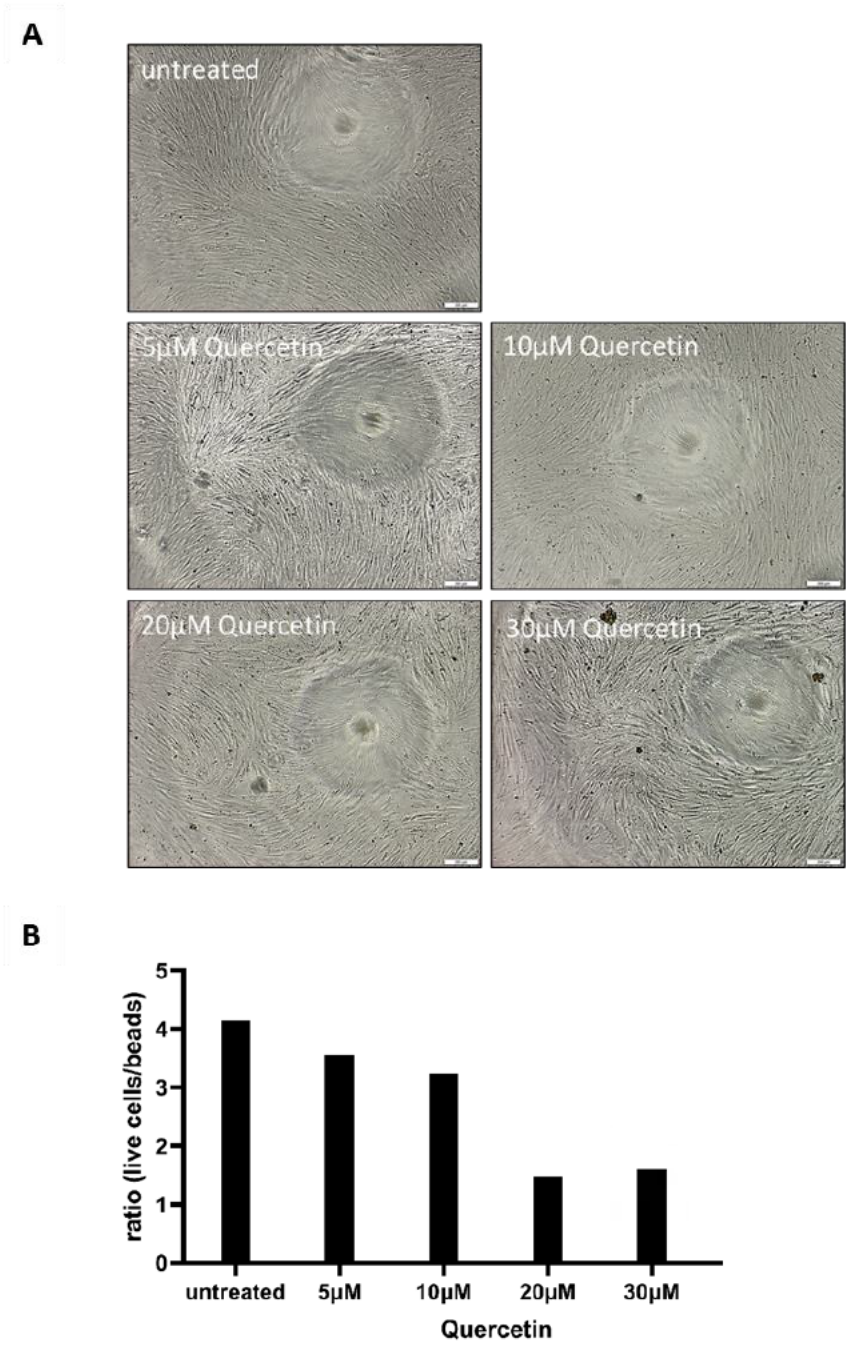


Figure 6.3. Effect of dose titration of Quercetin on morphology and viability in Healthy BMSC after 72 hours in culture. (A) Representative micrographs of BMSC morphology assessed by light microscopy; (B) number of live BMSC analysed by flow cytometry. Scale bars indicate 200µm.

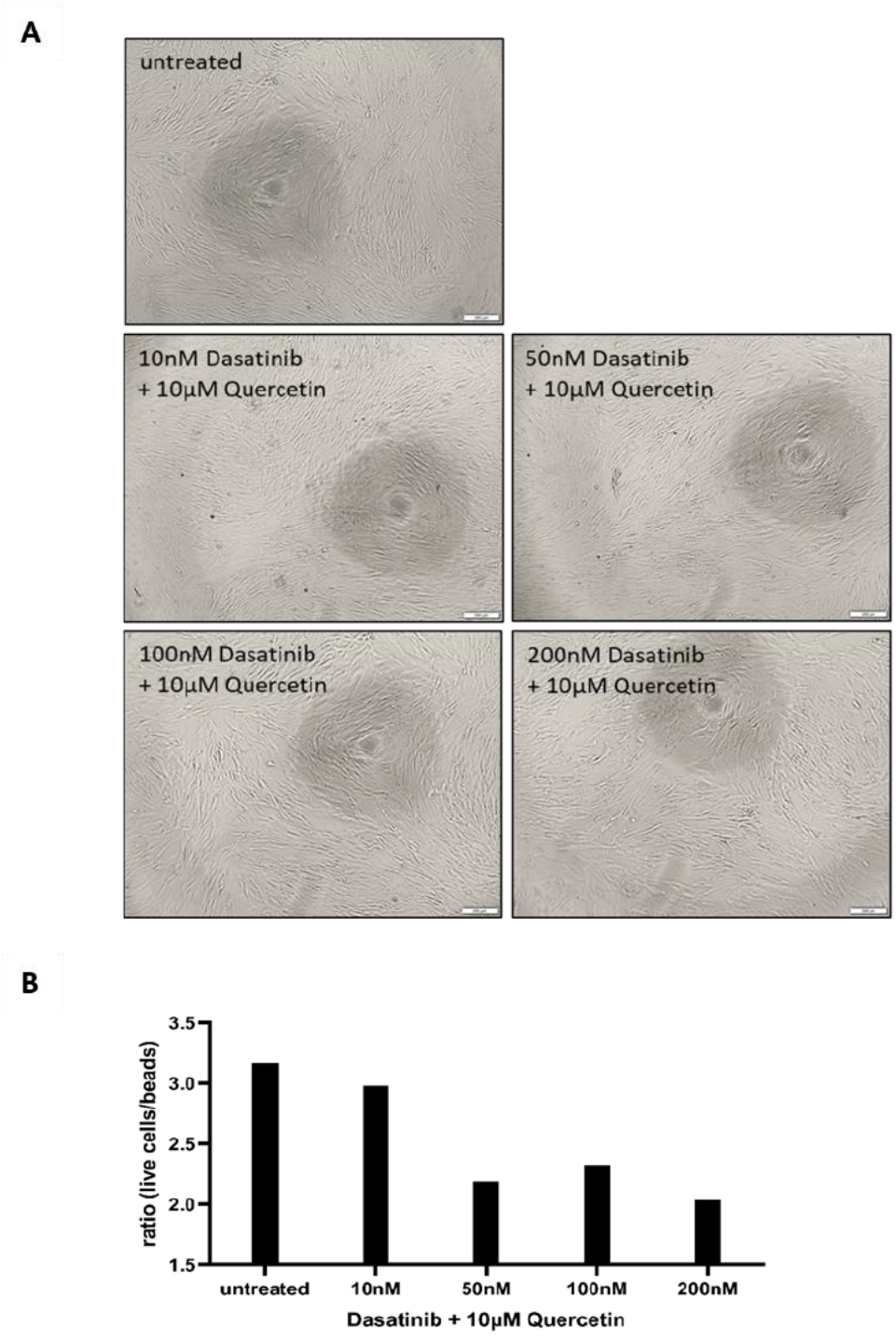


Figure 6.4. Effect of dose titration of combination of Dasatinib plus Quercetin on morphology and viability in Healthy BMSC after 72 hours in culture. (A) Representative micrographs of BMSC morphology assessed by light microscopy; (B) number of live BMSC analysed by flow cytometry. Scale bars indicate 200µm.

6.2.2. Reduced Senescence Burden in tMN BMSC after Treatment with Senolytic Agents

To demonstrate that Dasatinib and Quercetin can remove cells with senescent phenotype, tMN BMSC were stained with β-Galactosidase before and after 72 hours treatment with both drugs alone as wells as in combination. Dasatinib (75 ± 16 versus 40 ±14%, $P = 0.0004$), Quercetin (75 ±16 versus 39 ±14%, $P = 0.0003$) alone or in combination (75 ±16 versus 30 ±14%, $P = 0.0002$) significantly reduced senescence burden of tMN BMSC indicated by higher levels of β-Galactosidase activity (Figure 6.5).

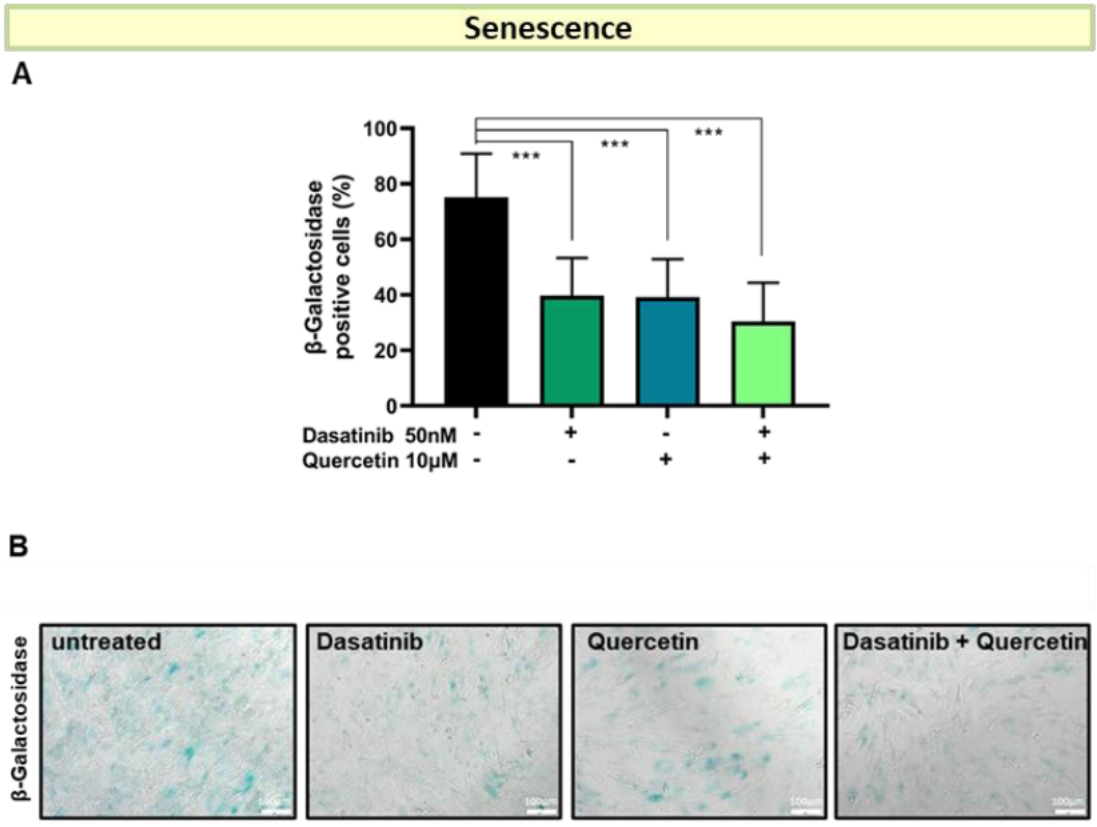


Figure 6.5. Treatment with senolytics significantly eliminate senescent cells from tMN BMSC. (A) Cellular senescence assessed by percentage of β-Galactosidase-stained cells at passage 3 of tMN BMSC (n = 3 tMN samples per each condition); (B) representative micrographs of β- Galactosidase-stained cells. All bars indicate mean, and all error bars indicate SD. Scale bars indicate 100μm. Mann-Whitney test was used to detect statistically significant differences between cohorts. Asterisks display *P*- values *** $P < 0.001$.

6.2.3. *In vitro* Culture with Senolytic Agents Restores tMN BMSC Adipogenic Differentiation Capacity

To test whether treatment with senolytics improve the adipogenic differentiation of tMN BMSC, cells were treated with senolytics while induced towards adipogenic lineage for 3 weeks. Strikingly, senolytics therapy restore normal adipogenic differentiation capacity of non-senescent tMN BMSC, as reflected by six-fold increase in adipogenic potential (0.13 ±0.08 to 0.64 ±0.25, $P = 0.0006$) (Figure 6.6).

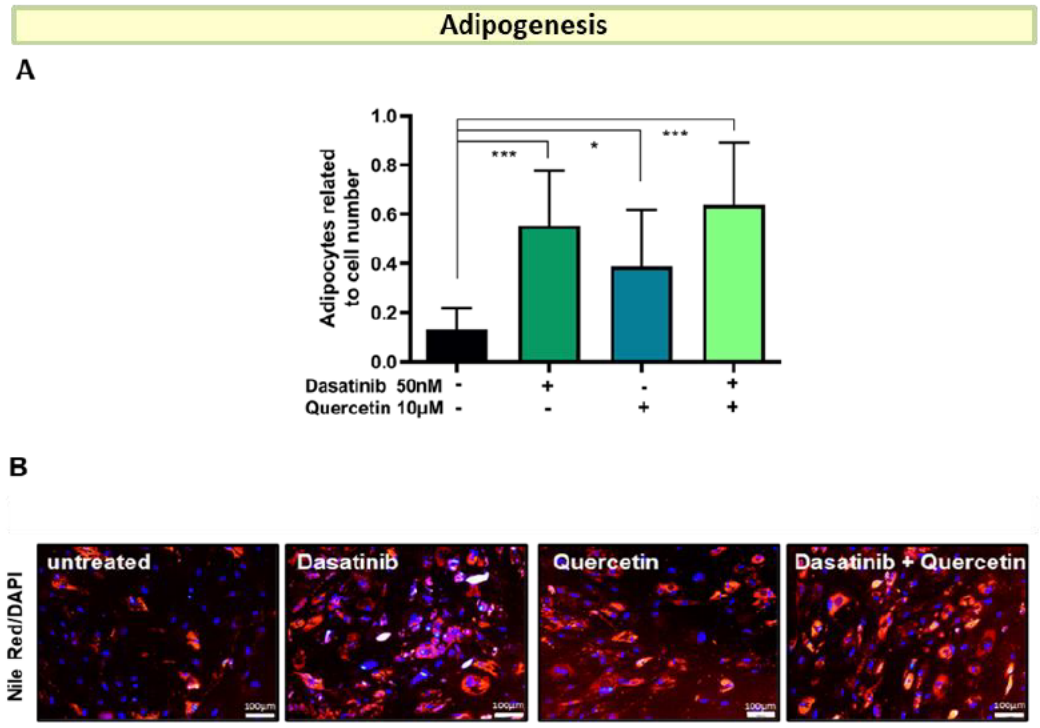


Figure 6.6. Senolytic therapy restores adipogenic differentiation in tMN BMSC. (A) tMN BMSC were cultured under adipogenic inductive conditions for 3 weeks either with or without senolytic drug and adipogenesis was assessed by quantification of Nile red-stained lipid droplets, relative to total number of DAPI stained cells (n = 3 tMN samples per each condition); (B) representative micrographs of Nile red stained lipids. All bars indicate mean, and all error bars indicate SD. Scale bars indicate 100µm. Mann-Whitney test was used to detect statistically significant differences between cohorts. Asterisks display *P*- values * $P < 0.05$, *** $P < 0.001$.

6.2.4. *In vitro* Culture with Senolytic Agents Reduced Aberrantly Excessive Osteogenic Differentiation Capacity in tMN BMSC

In order to investigate the activity of Dasatinib and Quercetin on the mineralization process, we tested the effects of these two agents again alone or in combination on osteoblastic differentiation of tMN BMSC. Surprisingly, after 21 days senolytics reduces aberrantly excessive osteogenic potential to near normal by measuring the concentration of Ca^{2+} in an acid-solubilized matrix and normalizing them to the total DNA (277 ±40 versus 108 ±45 Ca^{2+}/µg DNA, $P = 0.0002$) and confirming by staining with Alizarin Red (Figure 6.7).

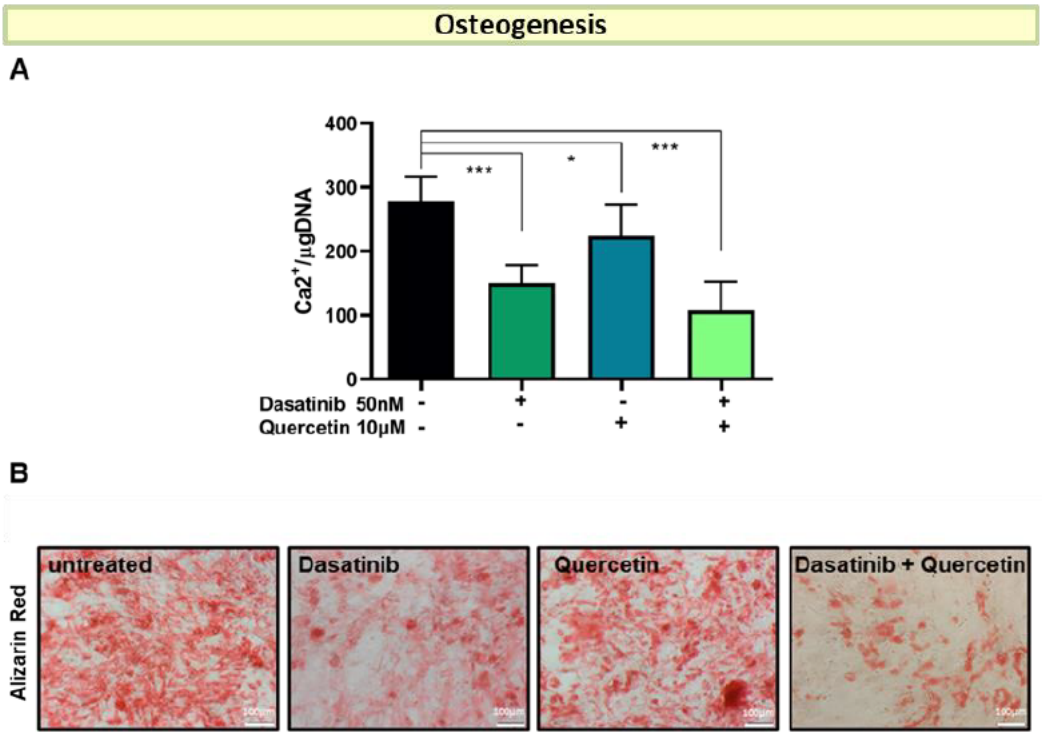


Figure 6.7. Elimination of senescent cells reduces abnormally high osteogenic differentiation in tMN BMSC. (A) tMN BMSC were cultured under osteogenic inductive conditions for 3 weeks either with or without senolytic drug and quantification of mineral content was assessed by measuring the concentration of Ca^{2+} in an acid-solubilized matrix and normalizing them to the total DNA (n = 3 tMN samples per each condition); (B) representative photos of mineral deposits stained with Alizarin Red. All bars indicate mean, and all error bars indicate SD. Scale bars indicate 100µm. Mann-Whitney test was used to detect statistically significant differences between cohorts. Asterisks display *P*-values * $P < 0.05$, *** $P < 0.001$.

6.3. DISCUSSION

The data demonstrated CT-induced senescence as underlying mechanism leading to BMSC dysfunction in tMN (Figure 6.8). It has been shown previously that inhibition of senescence can help restore cells functionality with use of senolytics [500, 501, 524], facilitate apoptosis of senescent cells but not non-senescent cells [500, 525], by selectively inhibiting pro-survival mechanisms in senescent cells but not in non -senescent cells. 2DG, a glucose analogue, which aims at glucose metabolism, has been reported to induce apoptosis in senescent vascular smooth muscle cells [522], however in current study inhibition of glycolysis did not restore defective adipogenesis (Chapter 5.2.4). Quercetin, like other flavonoids, possesses antioxidant and anti-inflammatory properties [518]. Specifically, it can inhibit several pathways associated with inflammation such as MAPK, NF-κB, COX-2, AP-1, CRP, and NOS [518]. Dasatinib on the other hand is tyrosine kinase inhibitor which interfere with EFNB-dependent suppression of apoptosis [511, 512]. This suggested to us that interference to decrease senescent cells numbers might restore dysfunctional tMN BMSC. Senolytics, including Dasatinib and Quercetin, selectively eliminate senescent cells from multiple different types of human and mouse cells [500-502, 526, 527]. Moreover, even eliminating 30% of senescent cells can be sufficient to restore dysfunction in line with our findings. Studies defining the effect of Dasatinib on human BMSC osteoblast differentiation have been reported but not without contradiction [523, 528-530]. Our study showed that treatment with Dasatinib at 50nM reduced aberrantly high osteogenic differentiation in tMN BMSC evaluated by mineral content quantification and cytochemical stain with Alizarin Red. Similarly, one of the other groups also reported that Dasatinib blocks osteoblastic differentiation assessed by staining with Alizarin Red and was also associated with the inhibition of early (*RUNX2*) and late (*Osterix*) osteoblast-specific transcription factors [531]. The effect was evident at therapeutic

concentrations (5-80nM) [531]. Likewise, Dasatinib added to the osteogenic medium decreased matrix mineralization and blocked the activity of ALP [523]. Conversely other study demonstrated stimulatory effects of Dasatinib on osteogenesis with increased activity of ALP and calcium deposition, and upregulation of bone associated markers such as bone sialoprotein (*BSP)* and *OPN* [529]. Additionally, expression of *RUNX2, BMP2* and *OCN* was significantly higher in BMSC treated with Dasatinib compared to untreated BMSC in study of Tibullo *et al.* [530]. A subsequent study performed on human BMSC and two cell lines, hMSC-TETR and osteosarcoma MG-63, showed that Dasatinib promote osteogenesis and matrix mineralization [532]. Similarly targeting senescent cell burden on adipogenic differentiation potential has been studied [523, 533]. It is important to note that assessment of adipogenic differentiation in the present study after treatment with Dasatinib in tMN BMSC showed significant enhancement in number of Nile Red stained adipocytes. Similarly previous studies have demonstrated that Dasatinib induces adipogenesis of human BMSC indicated by higher levels of Sudan Red-stained adipocytes [523]. The authors also found that addition of Dasatinib overexpresses several genes associated with adipogenesis, such as *PPARγ, CEBPα, LPL* and *SREBP1*.

Together, results from this study demonstrate that pharmaceutical approach by use of senolytics can restore aberrant differentiation potential of tMN BMSC (Figure 6.8). Inhibition of senescence provide direct evidence for the casual role of senescence in CT-induced BMSC dysfunction. The combination of senolytic agents was not only effective in eliminating senescent cells, but also could restore dysfunctional tMN BMSC, by acceleration of adipogenesis and reduction of osteogenesis. This indicate that CT- induced senescence is the underlying mechanism leading to BMSC dysfunction in tMN.

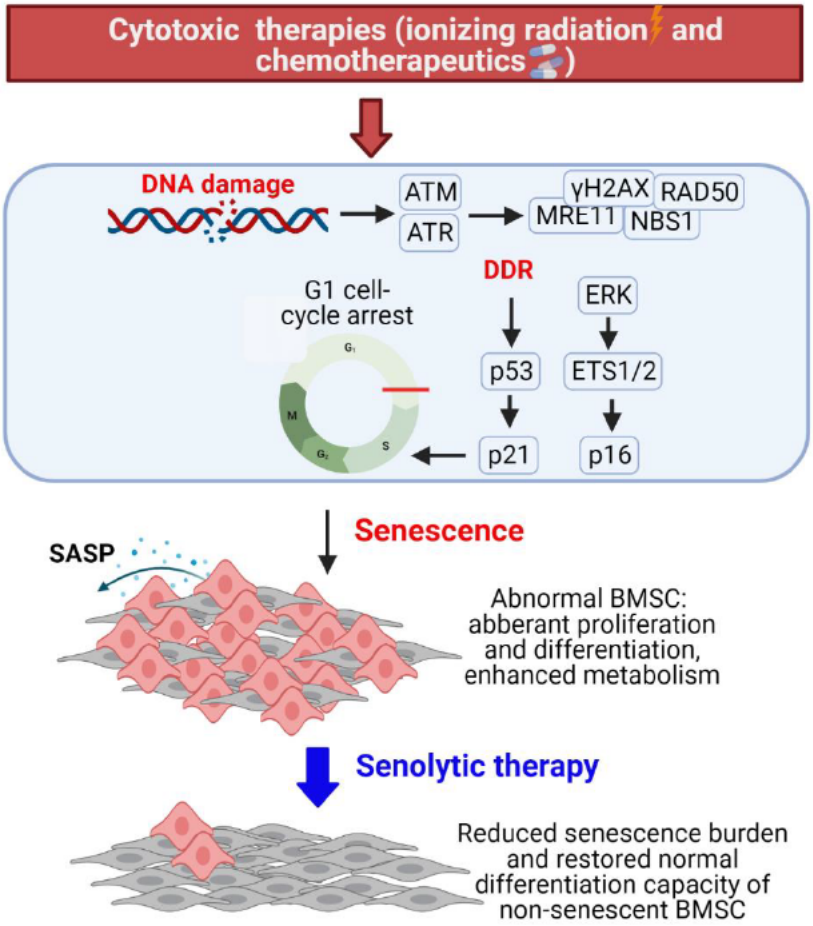


Figure 6.8. Cytotoxic-induced senescence as underlying mechanism leading to BMSC dysfunction in tMN with senolytic therapy as an approach to restore aberrant differentiation potential.

Chapter 7: Long-term Irreversible Damage to BM Microenvironment is Induced by CT

7.1. INTRODUCTION

tMN most often occur after chemotherapy with alkylating agents and topoisomerase II inhibitors (Table 7.1), along with or without radiotherapy for primary cancers [30]. Historically it was thought that CT only alters HSC [177, 178]. However, Prata *et al*. [181] demonstrated functional damage to stromal cells by CT, specifically reduced clonogenic potential, doubling time and cell expansion in lymphoma patients as compared to healthy individuals. Other studies also demonstrated short-term damage to the stromal cells of patients previously treated with CT including decreased growth kinetics [185, 209, 534, 535], decreased ability to support normal haematopoiesis [184, 209, 536] and enhanced DNA damage [187] (Table 7.2).

Table 7.1. Chemotherapy agents used in cancer treatment associated with development of tMN

Alkylating agents	Topoisomerase II inhibitors	Platinium-based agents	Antimetabolites	Poly(ADPribose) polymerase inhibitors
Bendamustine	Daunorubicin	Cisplatin	Fludarabine	Olaparib
Busulfan	Epirubicin	Carboplatin	5-fluorouracil	Veliparib
Carmustine	Doxorubicin			Niraparib
Chlorambucil	Etoposide			Rucaparib
Cyclophosphamide	Teniposide			
Dacarbazine	Amsacrine			
Lomustine	Mitoxantrone			
Melphalan				
Mitomycin C				
Nitrogen mustard				
Procarbazine				
Thiotepa				

Adapted from McNerney *et al.* [22]

Table 7.2. Key publications evaluating effect of cytotoxic therapies on BMSC in cancer survivors

Study	Patient cohort	Age- and gender matched Healthy control	Morphology	Growth kinetics	Adipogenesis / Osteogenesis	HSC support	DNA damage	Cytokines
Carlo-Stella *et al.*, 1997[184]	26 AML; Median time from Dx to study - 142 days after CT	Yes	x	**Normal**	↓ Adipogenesis	↓	x	x
Galotto *et al.*, 1999 [209]	61 (CML, AML, HL, ALL): followed up to about 1 year after allo-HSCT	Yes	x	↓	↓ Osteogenesis	↓	x	x
Prata *et al.*, 2010[181]	12 HL after HDCT followed by auto-HSCT: 28 to 1836 days before the sample collection	Yes	**Abnormal** (loss of the fibroblastoid aspect at the final (plateau) phase)	↓	**Normal**	**Normal** (LTC-IC- cord blood $CD34^{+}$)	x	x
Kemp *et al.*, 2010[185]	18 at Dx, 6 after low dose CT, 21 after high dose CT; The average time from the last dose of CT to BM sample collection was 501 days	x	**Abnormal** morphology however by first passage similar to untreated BMSC	↓	Not able to perform due to BMSC low expansion rates after high dose CT	**Normal** (LTC-IC- cord blood $CD34^{+}$)	x	x
Sorokina *et al.*, 2016 [536]	54 (ALL, AML, CML); time points between 37 to 220 days post treatment	Yes	x	x	x	↓	x	x
Shipounova *et al.*, 2017[534]	35 (AML, ALL); followed up to about 1 year after allo-HSCT	Yes	x	↓	x	x	x	x
May *et al.*, 2018 [187]	3 untreated patients, 3 CT treated patients (1 MM- 7 years prior to BM for analysis, 1 lymphoma- last CT 17 years prior BM, 1 AML- last CT 1 year prior to BM)	x	x	x	Not able to perform due to inadequate cell numbers	x	↑	x
Muller *et al.*, 2006 [191]	17 CT-exposed patients	Yes	x	**Normal**	**Normal**	x	x	x
Cao *et al.*, 2008 [535]	43 colorectal carcinomas	Yes	**Abnormal** (size decreased)	↓	x	x	x	↓ IL-6, SCF, FLT3L

Abbreviations: ALL, acute lymphoblastic leukaemia; allo-HSCT, allogeneic haematopoietic stem cell transplant; auto-HSCT, autologous haematopoietic stem cell transplant; AML, acute myeloid leukaemia; BM, bone marrow; CML, chronic myeloid leukaemia; CT, cytotoxic therapy; Dx, diagnosis; FLT3L, fms related receptor tyrosine kinase 3 ligand; HDCT, high dose chemotherapy; HL, Hodgkin's lymphoma; LTC-IC, long-term culture initiating cell assay; MM, multiple myeloma; SCF, stem cell factor.

Moreover, reduced BMSC expansion following *in vitro* exposure to Melphalan [179], Methotrexate [183], Bleomycin [257], Doxorubicin [537, 538], Cytarabine [180, 182], Paclitaxel [182] and Etoposide [182, 538] have been reported both in human and animal models (Table 7.3). Interestingly, *in vitro* studies showed an inability to recover the replicative capacity of BMSC even after 7 days of Cytarabine and Daunorubicin washout [180].

Table 7.3. Key papers on CT- induced damage to stromal cells in *in vitro* models

Study	Cohort	CT	Morphology	Growth kinetics	Differentiation	HSC support	DNA damage	Senescence	Apoptosis	Cytokines
Li *et al.*, 2004[182]	Young healthy human	various agents	**Unaffected**	↓(Cytarabine, Paclitaxel, Etoposide)	**Unaffected**	x	x	x	↑(Dexamethasone, Etoposide, Cytarabine, Pacitaxel, Vincristine)	x
Cruet Hennequart *et al.*, 2015[539]	Young healthy human	Irradiation	x	Cell cycle arrest but can resume proliferation	↑Osteogenesis	x	x	x	x	x
Kemp *et al.*, 2011 [179]	Healthy human	Melphalan, Cyclophospos phamide	**Abnormal** (granularity)	↓(Melphalan)	**Unaffected**	↓(LTC-IC- CD34+ cord blood)	x	x	x	x
Buttiglieri *et al.*, 2011[538]	Healthy human	Doxorubicin, Etoposide	x	↓Day 21 and 28 but not 7 and 14	↑Adipogenesis, ↑Osteogenesis (Etoposide)	x	↑ATM	Telomere shortening from 5 days post CT	x	x
Cruet Hennequart *et al.*, 2012[540]	Healthy human	Doxorubicin	x	Cell cycle arrest	x	x	↑p53, γH2AX	x	**Not increased**	x
Nicolay et al., 2016[541]	Healthy human	Cisplatin	**Unaffected**	**Unaffected**	**Unaffected**	x	x	x	**Not increased**	x
Nicolay *et al.*, 2016 [257]	Healthy human	Bleomycin	**Unaffected**	↓Viability, clonogenic potential	↓Adipogenesis	x	↑γH2AX, but repaired	x	↑	x
Hare *et al.*, 2016[542]	Healthy human	Etoposide	x	Cell cycle arrest	**Unaffected**	x	↑γH2AX	x	x	x
Kozhukharova *et al.*, 2018[537]	Healthy human	Doxorubicin	**Abnormal** (flatter and larger in size)	↓Proliferation, cell cycle arrest	x	x	↑γH2AX	↑	↑(high doses)	x
Prendergast *et al.*, 2011[543]	Healthy human and CLL patient	Cisplatin, Irradiation	x	↓Proliferation, cell cycle arrest	x	x	↑p53, p21 and γH2AX	x	x	x
Muller *et al.*, 2006[191]	Healthy human and TGCT cells	Etoposide, Cisplatin	x	**Unaffected**	**Unaffected**	x	↑p53	x	↑(Cisplatin)	x
Somaiah *et al.*, 2018[180]	Patients' samples- Hematology Dep. for Dx	Cytarabine, Daunorubici, Vincristine	**Abnormal** (flattened- Vincristine	↓	↓Adipo- and Osteogenesis	x	x	x	↑	↑IL-6, FGF2, TNFα
Chen *et al.*, 2014[544]	MDA-MB-231 breast cancer cells	Doxorubicin	x	x	x	x	x	x	x	↑IL-6, IL-8
Yang *et al.*, 2013[545]	Rats	Doxorubicin	**Abnormal** (cellular shrinkage)	x	x	x	↑ROS, p53	x	↑	↓VEGF, IGF-1
Georgiou *et al.*, 2012[546]	Rats	Methotrexate	x	↓	↓Osteogenesis, ↑Adipogenesis	x	x	x	x	x
Demaria *et al.*, 2017[188]	Mice	Doxorubicin	x	↓	x	x	↑53BP1 foci	↑	x	↑IL-6, IL-1α, CXCL1, CXCL10, CCL20

Abbreviations: CT, cytotoxic therapy; Dx, diagnosis; CLL, chronic lymphoblastic leukaemia; FGF2, fibroblast growth factor2; HSC, haematopoietic stem cells; IGF-1, insulin like growth factor 1; LTC-IC, long-term culture initiating cell assay; TNFα, tumour necrosis factor alpha; VEGF, vascular endothelial growth factor.

However, knowledge of long-term effects following CT is limited and based on very small numbers of samples [187] and different experimental design/methods [185]. Most importantly, none of these studies have focussed on patients developing tMN.

7.2. RESULTS

In the previous chapters (Chapter 3, 4 and 5) it has been shown that tMN BMSC are significantly abnormal compared to pMN and pMN+Ca and the only difference between these groups was prior exposure to CT. To test the hypothesis that prior exposure to CT leads to long-term damage to BM microenvironment, proliferation, cellular senescence, and adipo- and osteogenic differentiation potential of serial BMSC of three tMN patients was assessed (n = 3) isolated at the time of primary cancer, after completion of initial CT and at tMN diagnosis (Figure 7.1).

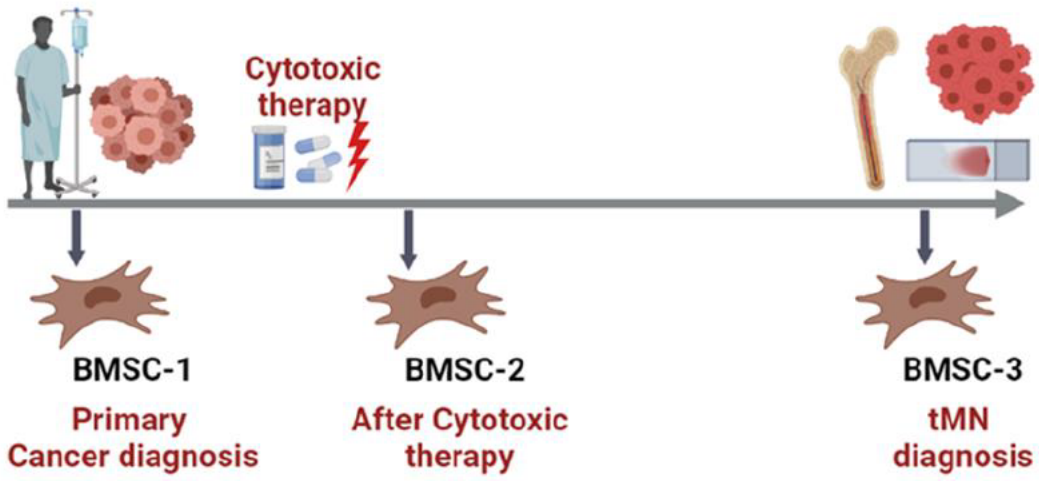


Figure 7.1. Schematic overview of tMN patient journey and serial BMSC collection such as at the time of primary cancer (BMSC-1), after completion of initial CT (BMSC-2) and at diagnosis of tMN (BMSC-3).

7.2.1. Cytotoxic Therapy Affects Proliferative Capacity of BMSC

In order to understand the effect of CT on the proliferation capacity of BMSC, serial BMSC samples derived at the time of primary cancer diagnosis (before CT), after receiving CT and at the tMN diagnosis were assessed by two methods, calculating CPD and CFU-F colonies previously used in Chapter 3.3.4. The data showed a striking reduction in proliferative capacity

of BMSC, after 2-3 months of CT compared to sample collected at diagnosis of primary cancer (0.47 ±0.29 versus 3.45 ±0.02; $P = 0.009$) (Figure 7.2A) and number of CFU-F colonies (0.5 ±0.4 versus 2.1 ±0.5 per 10^4 cells; $P < 0.001$) (Figure 7.2B). Moreover, the reduced proliferative potential of BMSC was still observed at tMN diagnosis (0.47 ±0.29 versus 0.43 ±0.60 CPD; $P = 0.993$) indicating that there were no significant differences evident in expansion when comparing BMSC derived from tMN patients and after 2-3 months post exposure to CT regimen (Figure 7.2A-B).

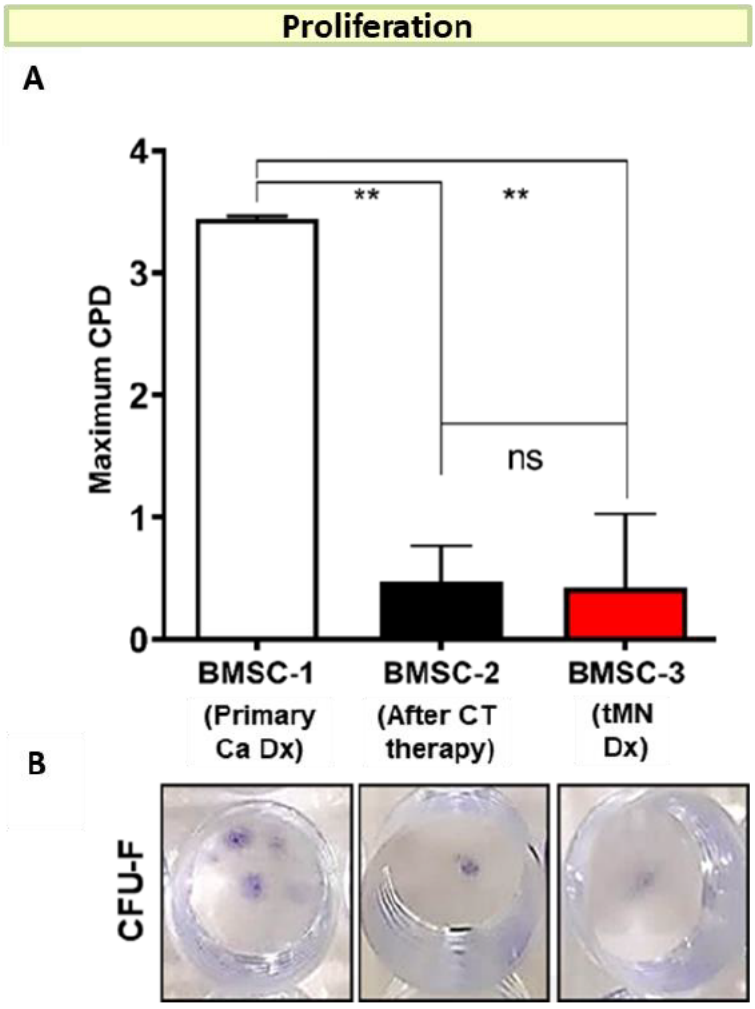


Figure 7.2. Effect of cytotoxic therapy on BMSC proliferation potential assessed by (A) maximum cumulative population doublings (CPD) and (B) CFU-F normalised to $2x10^4$ plated BMNC (representative micrographs of CFU-F colonies). The results from three tMN patients (n = 3) at different time are shown. All bars indicate mean, and all error bars indicate SD. Mann-Whitney test was used to detect statistically significant differences between cohorts. Asterisks display P-values $^{**}P < 0.01$.

7.2.2. Irreversible Long-term Cytotoxic Therapy- induced Senescence in BMSC

As irreversible arrest of cell proliferation is a crucial indicator of CT-induced senescence, the levels of β-Galactosidase-stained cells were assessed in BMSC at three time points indicated in the previous section. Number of senescent cells from BMSC following CT were significantly higher (35 ±19%) than among the BMSC derived from primary cancers (18 ±5%; $P = 0.01$) and remained high at tMN diagnosis (18 ±5% versus 65 ±19%; $P = 0.001$) (Figure 7.3) suggesting CT-induced senescence.

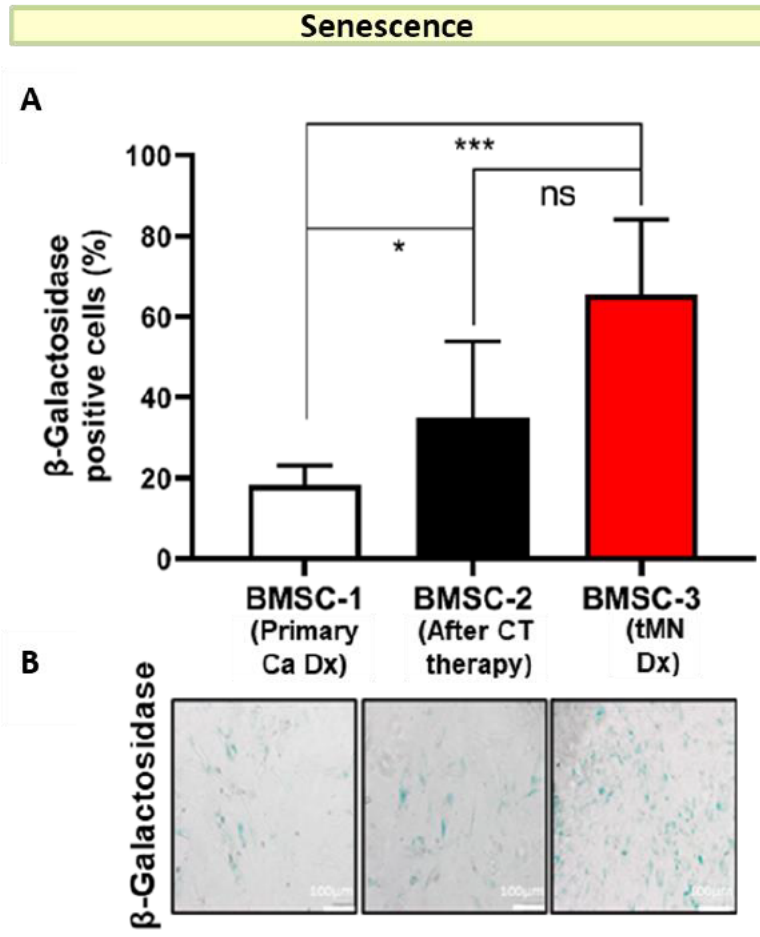


Figure 7.3. Permanent therapy-induced senescence in BMSC. (A) Quantification of senescence levels assessed by β-Galactosidase-stained cells and (B) representative micrographs. Number of β-Galactosidase positive cells (blue) was evaluated under phase-contrast microscope and normalised to DAPI stained nuclei per field of view in triplicate wells. Scale bars indicate 100μm. The results from three tMN patients (n = 3) at different time are shown. All bars indicate mean, and all error bars indicate SD. Mann-Whitney test was used to detect statistically significant differences between cohorts. Asterisks display *P*-values $*P < 0.05$, $***P < 0.001$.

7.2.3. Defective Adipogenic and Osteogenic Potential of BMSC Occurring after CT

The aim of this study was to investigate the impact of CT on BMSC adipo- and osteogenic differentiation potential over serial BMSC samples. Following adipogenic induction *in vitro*, BMSC adipogenic potential was significantly reduced following CT compared to primary cancer diagnosis (0.13 ±0.08 versus 0.47 ±0.21; $P = 0.010$) assessed by protocols for adipogenic differentiation described in Chapter 5.2.1. Reduced adipogenic differentiation persisted at tMN diagnosis (0.13 ±0.08 versus 0.11 ±0.08; $P = 0.463$). No significant differences were observed between tMN diagnostic BMSC and after receiving CT (Figure 7.4).

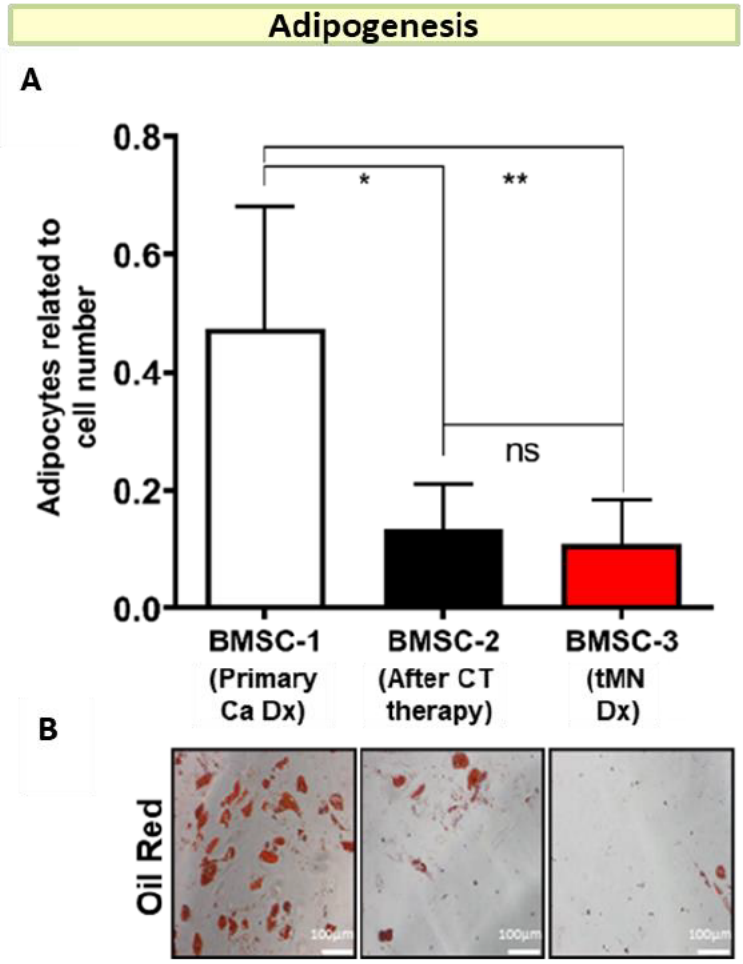


Figure 7.4. Irreversible long-term CT-induced reduction in adipogenic differentiation of BMSC quantified at 21 days by Nile red-stained lipid droplets (upper panel) and visualized by Oil red staining (lower panel). The results from three tMN patients (n = 3) at different time are shown. All bars indicate mean, and all error bars indicate SD. Mann-Whitney test was used to detect statistically significant differences between cohorts. Asterisks display *P*-values $*P < 0.05$, $**P < 0.01$.

Next, the effect of CT on the ability of BMSC to differentiate into osteoblasts, was assessed using methods described in Chapter 5.2.6. In contrast to adipogenic differentiation, osteogenic potential was significantly increased following CT compared to primary cancer diagnosis (127.1 ±51.85 versus 3.54 ±2.52; $P = 0.002$) and it persisted at tMN diagnosis (127.1 ± 51.85 versus 202.7 ±112.9; $P = 0.244$) (Figure 7.5).

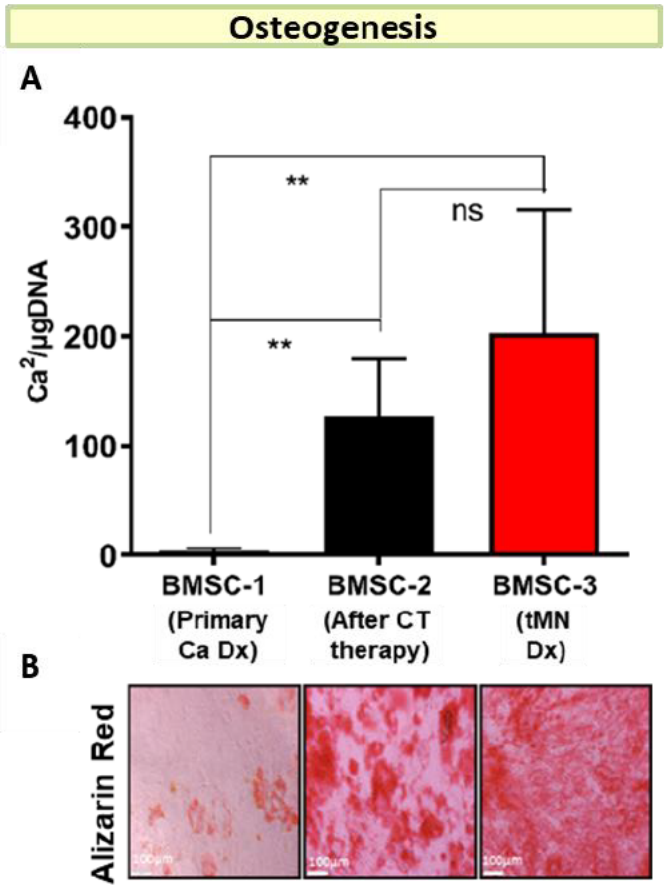


Figure 7.5. Long-lasting, therapy-induced alterations in osteogenesis. Quantification of mineral content was assessed by measuring the concentration of Ca^{2+} in an acid-solubilized matrix and normalizing them to the total DNA (upper panel). The mineralization visualized by Alizarin Red staining at 21 days (lower panel). The results from three tMN patients (n = 3) at different time are shown; All bars indicate mean, and all error bars indicate SD. Mann-Whitney test was used to detect statistically significant differences between cohorts. Asterisks display *P*-values $**P < 0.01$.

7.3. DISCUSSION

Malignant clones can shape BM microenvironment conducive for its survival and proliferation [162], however, aberrant BM microenvironment can also lead to myeloid neoplasm [166, 173, 547, 548]. The latter findings were based on murine models of myeloid neoplasms. Unlike other myeloid neoplasm, tMN provides a unique opportunity in human to decipher role of BM microenvironment in disease pathogenesis from that of malignant clone induced changes in BM microenvironment, as the exact timing of genotoxic insult is known. Relatively longer interval between genotoxic insult and tMN diagnosis allows serial studies of both BM microenvironment and HSC. In the present study we assessed proliferative and differentiational potential of BMSC as wells as cellular senescence in serial BM samples of tMN patients at diagnosis of primary cancer (multiple myeloma), time point during follow-up following CT and at tMN diagnosis. Together data from the present study suggest that CT led to irreversible damage to BMSC, which was evident many years prior to tMN diagnosis with profound senescence and defective adipo- and osteogenic differentiation. Though induction of senescence phenotype in the tumour microenvironment of cancer patients following exposure to cytotoxic therapies was reported previously [188-190], majority of studies were limited with short-term follow up except one assessing longer-term effect [167]. None of these studies evaluated the effect in tMN cases.

Cytotoxic therapies activate DNA damage response which typically leads to induction of apoptosis. However, BMSC seems to be highly resistant to apoptosis [537, 540, 545] and showed high viability after CT with varied range of concentrations [549]. Moreover, BMSC were resistant to cell death when undifferentiated and became sensitive to several known apoptosis inducers during the early stages of adipo- and osteogenesis [550]. Similarly to our findings, clinically relevant cytotoxic exposure in *in vitro* culture reduced proliferation,

increased number of γH2AX foci and induced BMSC senescence indicated by elevated levels of β-Galactosidase without inducing apoptosis [537]. Furthermore, CT-induced functional impairment to human BMSC can be slow to repair [551, 552] or even permanent, with completely recoverable ability to support haematopoiesis only in children less than 5 years old [209].

This is the first study demonstrating highly senescent, defective proliferative and adipogenic differentiation block in stroma cells within few months following CT and many years before tMN diagnosis.

Chapter 8: Discussion and Future Directions

8.1. GENERAL DISCUSSION

Currently genetic and epigenetic alterations in HSC are considered to drive myeloid malignancies [29, 88]. Although, the microenvironment regulates the fate and maturation of normal haematopoiesis [202], its role in the pathogenesis of myeloid cancer remains an area of active research. A number of reports investigating MDS and AML stromal cells have documented an altered biological phenotype including osteogenic [170, 197, 207, 208] and adipogenic differentiation potential [170, 197, 204], and diminished stem cell supportive capacity [170, 197, 204, 205, 208] but no direct comparison to tMN has been reported. AML and myeloma cells induce cellular senescence in BMSC resulting in secretion of SASP which in turn supports survival and proliferation of malignant clone [355, 553-556]. Thus, haematological malignancies can shape BM microenvironment conducive for propagation of malignant HSC clones. Moreover, emerging literature suggests that aberrant BM microenvironment can initiate and propagate MN [162-167]. However, these studies were based on murine models.

To date, this is the first comprehensive *ex-vivo* study examining the role of the microenvironment in tMN patients with well curated and age-matched healthy controls and primary myeloid neoplasms. Significantly, this study demonstrates several novel findings: (i) tMN stromal cells are not only distinct from healthy age-matched stroma but are also distinct from other typical myeloid neoplasms developing without prior exposure to cytotoxic therapies. (ii) tMN stromal cells are highly senescent with a characteristic flattened morphology, defective regenerative capacity, high p21 and β-Galactosidase expression and evidence of an active and ongoing senescence-associated secretory phenotype (SASP). Excessive production of SASP can induce “paracrine senescence” in surrounding normal cells as shown previously in RAS oncogene-induced senescence in fibroblasts [328]; (iii) profound

senescence observed in tMN stromal cells is potentially driven by a defect in the DNA damage repair (DDR) pathway, resulting in irreparable DNA damage after exposure to cytotoxic therapy. To this effect, my research shows that BMSC derived from tMN exhibited higher baseline DNA damage compared to Healthy BMSC. Enhanced baseline DNA damage in tMN BMSC was probably driven by higher intracellular ROS level compared to Healthy BMSC. Secondly, tMN BMSC were highly sensitive to DNA damaging cytotoxic therapy. Finally, tMN BMSC displayed defective DNA damage repair capacity following in vitro exposure to chemotherapeutic drug and radiation; (iv) delayed DNA damage repair of tMN BMSC is probably driven by delayed recruitment and activation of the early responders following DNA damage. Following genotoxic stress, recruitment of upstream kinases such as *ATM* and *CHK2* activates downstream targets including *TP53,* which in turn halts cell cycle progression via key mediator of senescence, cyclin-dependent kinase inhibitor *CDKN1A* (p21). In Healthy BMSC ATM and CHK2 were activated on by serine 1981 and threonine 68 respectively within 30 minutes of *in vitro* sublethal irradiation. While, in tMN BMSC, there was a significant delay of up to 3 hours in early responders, with some interpatient variability. Delayed activation was associated with late recruitment of ATM/CHK2/p53 and its crucial transcriptional target *CDKN1A,* a key mediator of senescence. CDKN1A expression was significantly higher in tMN as compared to Healthy BMSC and increased up to 30-fold in tMN after irradiation. Together, these data suggest that delayed and incomplete DNA repair leads to high and sustained level of p21 driving cellular commitment towards senescence and thus provide evidence that the p53-p21 pathway is still intact in tMN BMSC. Of note, none of the 13 BMSC tested had pathogenic *TP53* mutations and all samples showed evidence of intact *TP53* pathway; (v) while the tMN stroma was profoundly dormant, transcriptome analysis showed enrichment of multiple glycolytic gene pathways in tMN BMSC compared to controls. Moreover, bioenergetic profiling showed that total ATP production was significantly higher in tMN

compared to Healthy BMSC. Notably, the majority of ATP in tMN BMSC was generated by glycolysis, contrasting with Healthy in which ATP was predominantly generated by mitochondrial OXPHOS. As expected, glycolysis inhibitor, 2DG significantly reduced glycolysis in Healthy and tMN BMSC, but without reducing total ATP significantly, indicating a retained capacity to upregulate OXPHOS. Together, the data suggest that tMN senescent cells despite a low proliferation rate, are highly metabolically active with a bioenergetic shift towards glycolysis resembling Warburg metabolism, typically seen in tumour cells. Emerging reports are consistent with these findings. For example, in a transgenic Eμ-myc lymphoma model, senescence-inducing chemotherapy can lead to hypercatabolic phenotype with increased glycolysis, fatty acid oxidation and ATP production in therapy induced senescence-competent lymphoma cells [344]. Similarly, irradiation induced senescence has been linked to reduced tricarboxylic acid activity and shift energy towards glycolysis, gluconeogenesis and pentose-phosphate pathway [330]. Some of these reprogrammed pathways could be therapeutically exploited by synthetic lethal metabolic targeting [344]; (vi) despite glycolytic bias of tMN BMSC, transcriptome data suggested that genes involved in adipogenesis were downregulated in tMN. Furthermore, expression of genes critically involved in the early and late adipogenic differentiation, namely PPARγ and Adipsin, was reduced in tMN BMSC. Defective adipogenic differentiation was further substantiated by two distinct assays, namely quantification of lipid-laden Nile Red and Neil Oil Red staining. To understand the mechanism of defective adipogenesis in tMN, firstly known inhibitors of adipogenesis were analysed cytokines secreted by tMN BMSC. Adipocyte inhibitory cytokines such as IL-1β, IL-15, IL-6, IFNα and IFNγ were significantly higher by tMN BMSC compared to Healthy. Noticeably, a significant overlap between adipogenesis-inhibitory cytokines and pro-inflammatory cytokines known to be cardinal SASP cytokines [259, 322] was observed. Adipogenic inhibitory effect of these cytokines was further confirmed by demonstrating profound

inhibition of adipogenesis of healthy BMSC when co-cultured with these cytokines. Collectively, potential causative role of senescence-secreted cytokines in inhibiting adipogenesis; (vii) in order to assess if defective glycolytic metabolism and differentiation potential is driven by cellular senescence and elimination of highly senescent cells will restore functional capacity of remaining healthy BMSC, effect of senolytic therapies was evaluated. Senolytic agents Dasatinib, Quercetin alone or in combination significantly reduced senescence burden of tMN BMSC. Strikingly, senolytics therapy restore adipogenic differentiation as reflected by six-fold increase in adipogenic potential. Moreover, senolytics also reduces aberrantly excessive osteogenic potential to near normal. Together, these results demonstrate that senolytics therapies can restore aberrant differentiation potential of tMN BMSC; (viii) tMN BMSC were significantly abnormal compared to other primary myeloid neoplasm and the only difference between these groups was prior exposure cytotoxic therapies. Which led to hypothesis that cytotoxic therapies induce senescence which turn drive defective phenotype and functional capacity. To this effect, proliferation, cellular senescence, and differentiation potential of serial BMSC of tMN patients isolated at the time of primary cancer, after completion of initial cytotoxic therapies and at tMN diagnosis was assessed. Striking reduction in proliferative capacity of BMSC after 2-3 months of completion of cytotoxic therapies compared to sample collected at diagnosis of primary cancer was observed. Number of senescent cells from BMSC following CT were significantly higher than among the BMSC from primary cancer and remained high at tMN diagnosis. Moreover, adipogenic potential was significantly reduced following cytotoxic therapies compared to primary cancer diagnosis. In contrast, osteogenic potential was significantly increased following cytotoxic therapies compared to primary cancer diagnosis and persisted at tMN diagnosis. Together these data suggest that cytotoxic therapies led to irreversible damage to BMSC, which was evident many years prior to tMN diagnosis. Similarly, compromised BMSC proliferative [179, 181, 183, 185,

186], differentiation [179, 183], DNA-damage repair [187], senescence [188-190] and HSC-supporting [184] capacity have been reported following exposure to CT and these defects can persist for long-term [167, 181, 184, 187].

Together, current thesis provides comprehensive phenotypic, functional, and molecular profiling of tMN BMSC and compare it with well curated samples from pMN, pMN+Ca (without prior exposure to CT) and age-matched healthy controls. Moreover, data from this thesis suggests that tMN is a specific cancer type that may be directly linked to a senescence stress program in BMSC. Cancer survivors exposed to cytotoxics may have an altered and enduring pro-inflammatory stromal state. Data from the current study is a valuable resource for future strategies to delay or prevent the onset of tMN and improve outcomes by modulating either the senescent phenotype or promoting adipocyte regeneration.

8.2. FUTURE DIRECTIONS

As mentioned previously the incidence of tMN is rising and survival of tMN patients is dismal with median survival rates of <12 months [28, 29]. Therefore, there is an urgent and unmet need to understand the pathogenesis of tMN with the aim to prevent and develop novel therapies to improve outcome, with crosstalk between BM microenvironment and HSC playing critical role (Figure 8.1).

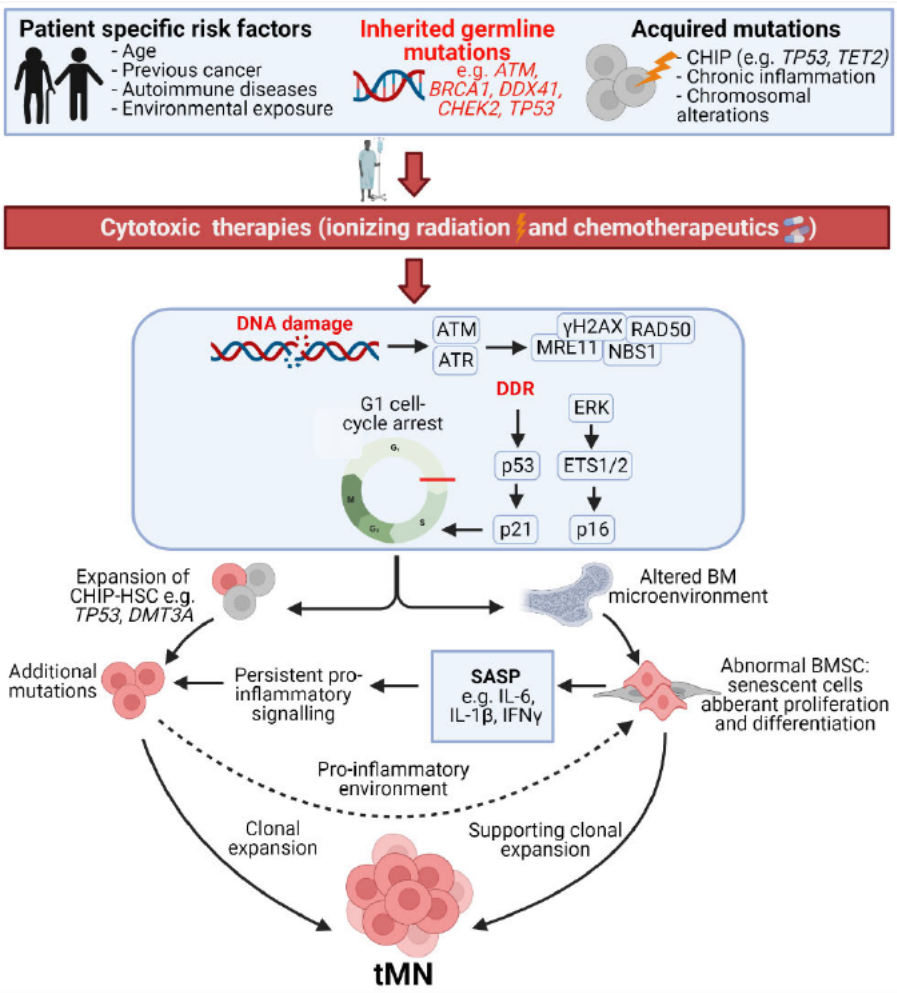


Figure 8.1. Long-term damage of cytotoxic therapy on BM microenvironment and HSC and their relationship in tMN. Combination of genetic and environmental factors predisposes patients to tMN. CT can induce somatic mutations which (A) impair DNA repair in HSC, (B) induce somatic mutations which damage stroma and impair DNA repair and (C) induce somatic mutations in both HSC and BMSC, which together with germline mutations, can lead to damaged stroma and impaired DNA repair.

8.2.1. To Provide Direct Evidence for Role of Senescence in Cytotoxic Therapy- induced BMSC Dysfunction by Eliminating Senescent Cells

Cellular senescence is a poorly understood stress response program characterised by cell cycle arrest and pro-inflammatory cytokine secretion [259, 262, 557]. Senescence is thought to have paradoxical roles in both the prevention of cancer (via immunosurveillance) [558-561] and the promotion of cancer (via inflammation) [562, 563]. It is possible but not prospectively proven, that the BMSC derived highly pro-inflammatory SASP could provide microenvironment conducive for expansion of clonal haematopoiesis, which is observed in almost one third of cancer patients who are at high risk of progressing to tMN. Hence further studies evaluating role of highly senescent BM microenvironment on clonal evolution will play a crucial role in identifying cancer patients at higher risk of progressing to tMN and potentially halting progression. Validation of *in vitro* studies demonstrating restoration of phenotype and functional capacity of BMSC in murine model will pave the way for clinical trials.

An alternative to the elimination of senescent cells through senolytics demonstrated in Chapter 6, is to suppress SASP which drives inflammation with the use of senomorphic agents [564, 565]. One of well-known SASP components, significantly increased in various types of senescent cells, including in tMN BMSC (Chapter 4), is IL-1 [322, 324-327]. Additionally, IL-1, a known adipocyte inhibitory cytokine [382], profoundly inhibited adipogenesis in Healthy BMSC (Chapter 5). To assess the inhibitory effects of IL-1 on tMN derived BMSC function, specifically adipogenesis, treatment with senomorphic agent, Anakinra, a recombinant human IL-1 receptor antagonist [566, 567] could be used.

8.2.2. To Explore the Connection Between Metabolism and BMSC Function

Interestingly, despite the senescent phenotype, tMN BMSC were metabolically active with significant skewing towards glycolysis versus oxidative phosphorylation (Chapter 4).

8.2.2.1. Manipulation of Metabolic Enzymes Selected from RNA-seq Analysis

To explore the connection between metabolism and BMSC function in more detail, manipulation of metabolic enzymes selected from RNA-seq analysis (Chapter 4), could also be considered in follow-up studies. Potential candidates identified in the current thesis, *TXNRD1*, a regulator of glucose and lipid metabolism [359] [360], and *BNIP3*, a negative regulator of mitochondrial potential [361], were highly expressed in tMN BMSC. Having identified some of the metabolic factors as candidates for the induction of dysfunction of tMN BMSC, the strategy could be to investigate whether Healthy BMSC adopt a phenotype similar to the phenotype of tMN BMSC by culturing Healthy BMSC in the presence or absence of candidate factors. Those experiments would require assessment of proliferation and differentiation potential as well as stromal HSC support.

8.2.2.2. Assessing Lipid Metabolism

It has been well documented that BMSC have multi-lineage differentiation potential. Adipogenesis especially is associated with a robust metabolic reprogramming and transcriptome data in this study suggest that genes involved in adipogenesis were downregulated in tMN (Chapter 5). Moreover, cells with *RAS*-oncogene induced senescence exhibit reduced lipid synthesis and increased in fatty acid oxidation, most probably due to increased levels of phosphorylated (inactive) Acetyl-Co A carboxylase 1 [568]. Future studies should examine lipid metabolism deposits in the BM of tMN and cytotoxic treated patients

before and after cytotoxic exposure and transplant-related mortality. Studies exploring fatty acid metabolism in the absence of adipogenic stimuli could also be performed.

8.2.3. To Determine whether Specific Type of Cancer and Cytotoxicity Result in Specific BMSC Phenotypes

One limitation of the current thesis is that the serial BMSC studies (Chapter 7), while convincingly show evidence of time-dependent causality before and after exposure to CT, were obtained exclusively from patients with multiple myeloma. Future studies should explore other primary cancer diagnoses and determine whether specific types of cancer and cytotoxicity result in specific BMSC phenotypes. Moreover, to unravel whether these changes (defective BMSC phenotypes) are observed in all patients who survive CT or only those who develop tMN, one strategy is to screen BMSC from patients who received the same treatment for primary cancer as tMN, but never develop tMN.

8.2.4. To Assess the Impact of Pathogenic Germline Mutations on BMSC from tMN Patients

Although tMN is considered an acquired disease consisting of complex karyotypic abnormalities induced by CT in HSC, latest findings from our laboratory challenge this assumption [49]. By sequencing both germline and haematopoietic tissues in a carefully annotated patient cohort, we identified a distinct molecular sub-group of tMN that is characterised by heterozygous germline mutations in poly ADP ribose polymerase (PARP)- and nicotinamide adenine dinucleotide phosphate (NADPH)-dependent DNA repair genes, including *BRCA1, BRCA2, ATM* and *TP53* [49]. Importantly, we can detect the same pathogenic germline mutations in BM stroma from these patients. Further research will provide

insight into effect of DNA damaging cytotoxic therapies on BMSC harboring pathogenic germline mutations and its role in driving tMN pathogenesis.

8.2.5. To Evaluate BM Niche Forming Capacity in NSG Mice by Developing a Humanised Ossicle Model of tMN BMSC and Healthy Controls

To mimic the human BM microenvironment that provides niches for HSC to populate and bi-directionally signal to and from surrounding cellular BMSC, adipocytes, osteoblasts and endothelial cells and non-cellular factors, future efforts will attempt to develop humanised ossicle model [569, 570]. Specifically, to form humanised ossicles, expanded BMSC would be transplanted subcutaneously into the flanks of immunocompromised NSG mice, followed by spontaneous differentiation into chondrocytes and endochondral ossification to form humanised BM microenvironment, about 6-8 weeks of BMSC injections. This approach could provide new insights into the BM niche regenerating capacity of tMN BMSC.

8.2.6. To Correlate BM Microenvironment and Engraftment Kinetics and Outcome in Allogeneic Transplantation

CT not only induce genetic alteration in HSC [177, 178] but also damage the stromal cell compartment [179-182] causing BMSC to have a compromised HSC-supporting capacity. The present thesis demonstrates for the first time the reduced HSC-supporting capacity of tMN BMSC (Chapter 5). Since damage to BMSC may have significant consequences haematologically in tMN, the use of transplanted allogeneic BMSC from normal donors could be considered as a future therapeutic option. This is clinically very important as allo-HSCT provides normal $CD34^+$ but does not alter the BM stroma, additionally conditioning CT can induce further damage to BM microenvironment. Interestingly, two of tMN patients from our

cohort received allo-HSCT, however with different outcomes. One patient, whose BMSC failed to reach passage one, died three months after receiving an allo-HSCT. Whereas the other tMN patient, whose BMSC showed a higher proliferation potential, is in complete remission a few years after receiving an allo-HSCT. Therefore, our strategy is to assess BM microenvironment in extended cohort of patients who underwent allo-HSCT, with samples before and after transplant to provide insight why allo-HSCT in not successful in some of the patients. Further, transplantation of co-cultured $CD34^+$ to evaluate the *in vivo* repopulation function might be required to provide stronger evidence for the effect of tMN BMSC on stem cell function, however MDS $CD34^+$ are very difficult to engraft [162, 571-574]. This potentially could lead to improvement of stem cell supportive capacity by co-transplanting healthy $CD34^+$ and BMSC to improve engraftment in patients.

Chapter 9: References

1. Rieger, M.A. and T. Schroeder, *Exploring hematopoiesis at single cell resolution.* Cells Tissues Organs, 2008. **188**(1-2): p. 139-49.
2. Alenzi, F.Q., et al., *The haemopoietic stem cell: between apoptosis and self renewal.* Yale J Biol Med, 2009. **82**(1): p. 7-18.
3. Seita, J. and I.L. Weissman, *Hematopoietic stem cell: self-renewal versus differentiation.* Wiley Interdiscip Rev Syst Biol Med, 2010. **2**(6): p. 640-53.
4. Greenberg, P., et al., *International scoring system for evaluating prognosis in myelodysplastic syndromes.* Blood, 1997. **89**(6): p. 2079-88.
5. Greenberg, P.L., et al., *Revised international prognostic scoring system for myelodysplastic syndromes.* Blood, 2012. **120**(12): p. 2454-65.
6. Aul, C., A. Giagounidis, and U. Germing, *Epidemiological features of myelodysplastic syndromes: results from regional cancer surveys and hospital-based statistics.* Int J Hematol, 2001. **73**(4): p. 405-410.
7. Fenaux, P., et al., *Efficacy of azacitidine compared with that of conventional care regimens in the treatment of higher-risk myelodysplastic syndromes: a randomised, open-label, phase III study.* Lancet Oncol, 2009. **10**(3): p. 223-32.
8. Bejar, R. and D.P. Steensma, *Recent developments in myelodysplastic syndromes.* Blood, 2014. **124**(18): p. 2793-803.
9. Vardiman, J.W., et al., *The 2008 revision of the World Health Organization (WHO) classification of myeloid neoplasms and acute leukemia: rationale and important changes.* Blood, 2009. **114**(5): p. 937-51.
10. Tuzuner, N., et al., *Hypocellular myelodysplastic syndromes (MDS): new proposals.* Br J Haematol, 1995. **91**(3): p. 612-7.
11. Huang, T.C., et al., *Comparison of hypoplastic myelodysplastic syndrome (MDS) with normo-/hypercellular MDS by International Prognostic Scoring System, cytogenetic and genetic studies.* Leukemia, 2008. **22**(3): p. 544-50.
12. Nand, S. and J.E. Godwin, *Hypoplastic myelodysplastic syndrome.* Cancer, 1988. **62**(5): p. 958-64.
13. Tuzuner, N. and J.M. Bennett, *Reference standards for bone marrow cellularity.* Leuk Res, 1994. **18**(8): p. 645-7.
14. Tuzuner, N., et al., *Bone marrow cellularity in myeloid stem cell disorders: impact of age correction.* Leuk Res, 1994. **18**(8): p. 559-64.
15. Deschler, B. and M. Lübbert, *Acute myeloid leukemia: epidemiology and etiology.* Cancer, 2006. **107**(9): p. 2099-107.
16. Estey, E. and H. Döhner, *Acute myeloid leukaemia.* Lancet, 2006. **368**(9550): p. 1894-907.
17. Rubnitz, J.E., B. Gibson, and F.O. Smith, *Acute myeloid leukemia.* Hematol Oncol Clin North Am, 2010. **24**(1): p. 35-63.
18. Ishikawa, F., et al., *Chemotherapy-resistant human AML stem cells home to and engraft within the bone-marrow endosteal region.* Nat Biotechnol, 2007. **25**(11): p. 1315-21.
19. Shipley, J.L. and J.N. Butera, *Acute myelogenous leukemia.* Exp Hematol, 2009. **37**(6): p. 649-58.
20. Yeh, J.-R.J., et al., *Discovering chemical modifiers of oncogene-regulated hematopoietic differentiation.* Nature Chemical Biology, 2009. **5**(4): p. 236-243.
21. Arber, D.A., et al., *The 2016 revision to the World Health Organization classification of myeloid neoplasms and acute leukemia.* Blood, 2016. **127**(20): p. 2391-405.
22. McNerney, M.E., L.A. Godley, and M.M. Le Beau, *Therapy-related myeloid neoplasms: when genetics and environment collide.* Nat Rev Cancer, 2017. **17**(9): p. 513-527.
23. Granfeldt Østgård, L.S., et al., *Epidemiology and Clinical Significance of Secondary and Therapy-Related Acute Myeloid Leukemia: A National Population-Based Cohort Study.* J Clin Oncol, 2015. **33**(31): p. 3641-9.

24. Ornstein, M.C., et al., *Predictive factors for latency period and a prognostic model for survival in patients with therapy-related acute myeloid leukemia.* 2014. **89**(2): p. 168-173.
25. Bhatia, S., *Therapy-related myelodysplasia and acute myeloid leukemia.* Semin Oncol, 2013. **40**(6): p. 666-75.
26. Radivoyevitch, T., et al., *Risk of acute myeloid leukemia and myelodysplastic syndrome after autotransplants for lymphomas and plasma cell myeloma.* Leuk Res, 2018. **74**: p. 130-136.
27. Health, A.I.o. and Welfare, *Cancer data in Australia*. 2020, AIHW: Canberra.
28. Bhatia, S., *Therapy-Related Myelodysplasia and Acute Myeloid Leukemia.* Seminars in Oncology, 2013. **40**(6): p. 666-675.
29. Singhal, D., et al., *The mutational burden of therapy-related myeloid neoplasms is similar to primary myelodysplastic syndrome but has a distinctive distribution.* Leukemia, 2019. **33**(12): p. 2842-2853.
30. Kayser, S., et al., *The impact of therapy-related acute myeloid leukemia (AML) on outcome in 2853 adult patients with newly diagnosed AML.* Blood, 2011. **117**(7): p. 2137-45.
31. Verkooijen, H.M., et al., *Family history of breast or ovarian cancer modifies the risk of secondary leukemia after breast cancer: results from a population-based study.* Int J Cancer, 2008. **122**(5): p. 1114-7.
32. Godley, L.A. and A. Shimamura, *Genetic predisposition to hematologic malignancies: management and surveillance.* Blood, 2017. **130**(4): p. 424-432.
33. Pastor, V., et al., *Mutational landscape in children with myelodysplastic syndromes is distinct from adults: specific somatic drivers and novel germline variants.* Leukemia, 2017. **31**(3): p. 759-762.
34. Niemeyer, C.M. and I. Baumann, *Classification of childhood aplastic anemia and myelodysplastic syndrome.* Hematology Am Soc Hematol Educ Program, 2011. **2011**: p. 84-9.
35. Lu, C., et al., *Patterns and functional implications of rare germline variants across 12 cancer types.* Nat Commun, 2015. **6**: p. 10086.
36. Przychodzen, B., et al., *Fanconi Anemia germline variants as susceptibility factors in aplastic anemia, MDS and AML.* Oncotarget, 2018. **9**(2): p. 2050-2057.
37. Maung, K.Z.Y., et al., *Rare variants in Fanconi anemia genes are enriched in acute myeloid leukemia.* Blood Cancer J, 2018. **8**(6): p. 50.
38. Wartiovaara-Kautto, U., et al., *Germline alterations in a consecutive series of acute myeloid leukemia.* Leukemia, 2018. **32**(10): p. 2282-2285.
39. Klco, J.M. and C.G. Mullighan, *Advances in germline predisposition to acute leukaemias and myeloid neoplasms.* Nat Rev Cancer, 2021. **21**(2): p. 122-137.
40. Kook, H., *Fanconi anemia: current management.* Hematology, 2005. **10 Suppl 1**: p. 108-10.
41. D'Andrea, A.D., *Susceptibility pathways in Fanconi's anemia and breast cancer.* N Engl J Med, 2010. **362**(20): p. 1909-19.
42. Brohet, R.M., et al., *Breast and ovarian cancer risks in a large series of clinically ascertained families with a high proportion of BRCA1 and BRCA2 Dutch founder mutations.* J Med Genet, 2014. **51**(2): p. 98-107.
43. Kuchenbaecker, K.B., et al., *Risks of Breast, Ovarian, and Contralateral Breast Cancer for BRCA1 and BRCA2 Mutation Carriers.* Jama, 2017. **317**(23): p. 2402-2416.
44. Thompson, D. and D.F. Easton, *Cancer Incidence in BRCA1 mutation carriers.* J Natl Cancer Inst, 2002. **94**(18): p. 1358-65.
45. Mersch, J., et al., *Cancers associated with BRCA1 and BRCA2 mutations other than breast and ovarian.* Cancer, 2015. **121**(2): p. 269-75.
46. Schulz, E., et al., *Germline mutations in the DNA damage response genes BRCA1, BRCA2, BARD1 and TP53 in patients with therapy related myeloid neoplasms.* J Med Genet, 2012. **49**(7): p. 422-8.

47. Churpek, J.E., et al., *Inherited mutations in cancer susceptibility genes are common among survivors of breast cancer who develop therapy-related leukemia.* Cancer, 2016. **122**(2): p. 304-11.
48. Voso, M.T., et al., *Fanconi anemia gene variants in therapy-related myeloid neoplasms.* Blood Cancer J, 2015. **5**(7): p. e323.
49. Singhal, D., et al., *Targeted gene panels identify a high frequency of pathogenic germline variants in patients diagnosed with a hematological malignancy and at least one other independent cancer.* Leukemia, 2021.
50. Churpek, J.E., et al., *Inherited mutations in cancer susceptibility genes are common among survivors of breast cancer who develop therapy-related leukemia.* Cancer, 2016. **122**(2): p. 304-311.
51. Schulz, E., et al., *Germline mutations in the DNA damage response genes BRCA1, BRCA2, BARD1 and TP53 in patients with therapy related myeloid neoplasms.* 2012. **49**(7): p. 422-428.
52. Martin, M.G., et al., *Therapy related acute myeloid leukemia in breast cancer survivors, a population-based study.* Breast Cancer Res Treat, 2009. **118**(3): p. 593-8.
53. Voso, M.T., et al., *Fanconi anemia gene variants in therapy-related myeloid neoplasms.* Blood Cancer Journal, 2015. **5**(7): p. e323-e323.
54. Wong, T.N., et al., *Role of TP53 mutations in the origin and evolution of therapy-related acute myeloid leukaemia.* Nature, 2015. **518**(7540): p. 552-555.
55. Patel, A.A., et al., *Therapy-related myeloid neoplasms in 109 patients after radiation monotherapy.* Blood Adv, 2021. **5**(20): p. 4140-4148.
56. Guru Murthy, G.S., et al., *Incidence and survival of therapy related myeloid neoplasm in United States.* Leukemia Research, 2018. **71**: p. 95-99.
57. Yarosh, R., et al., *Risk factors for de novo and therapy-related myelodysplastic syndromes (MDS).* Cancer Causes Control, 2021.
58. Sallman, D.A. and E. Padron, *Myelodysplasia in younger adults: outlier or unique molecular entity?* Haematologica, 2017. **102**(6): p. 967-968.
59. Shallis, R.M., et al., *Epidemiology of acute myeloid leukemia: Recent progress and enduring challenges.* Blood Rev, 2019. **36**: p. 70-87.
60. Fianchi, L., et al., *Characteristics and outcome of therapy-related myeloid neoplasms: Report from the Italian network on secondary leukemias.* American Journal of Hematology, 2015. **90**(5): p. E80-E85.
61. Radivoyevitch, T., et al., *Defining AML and MDS second cancer risk dynamics after diagnoses of first cancers treated or not with radiation.* Leukemia, 2016. **30**(2): p. 285-94.
62. Mahindra, A., et al., *New Cancers after Autotransplantations for Multiple Myeloma.* Biology of Blood and Marrow Transplantation, 2015. **21**(4): p. 738-745.
63. Dosani, T., et al., *Host-related immunodeficiency in the development of multiple myeloma.* Leuk Lymphoma, 2018. **59**(5): p. 1127-1132.
64. Landgren, O., et al., *Familial characteristics of autoimmune and hematologic disorders in 8,406 multiple myeloma patients: a population-based case-control study.* Int J Cancer, 2006. **118**(12): p. 3095-8.
65. Ertz-Archambault, N., et al., *Myelodysplastic Syndromes and Acute Myelogenous Leukemia Resulting from Therapy for Autoimmune Disease, a Case-Control Cohort Study of 40,011 Patients.* Blood, 2016. **128**(22): p. 296-296.
66. Ostrand-Rosenberg, S., *Myeloid derived-suppressor cells: their role in cancer and obesity.* Current Opinion in Immunology, 2018. **51**: p. 68-75.
67. Craver, B.M., et al., *The Critical Role of Inflammation in the Pathogenesis and Progression of Myeloid Malignancies.* Cancers, 2018. **10**(4): p. 104.
68. Finn, L.E., et al., *Association of obesity with cytogenetic risk in adult acute myeloid leukemia (AML).* Journal of Clinical Oncology, 2014. **32**(15_suppl): p. 7055-7055.

69. Rodríguez-Santiago, B., et al., *Mosaic uniparental disomies and aneuploidies as large structural variants of the human genome.* Am J Hum Genet, 2010. **87**(1): p. 129-38.
70. Forsberg, L.A., et al., *Age-related somatic structural changes in the nuclear genome of human blood cells.* Am J Hum Genet, 2012. **90**(2): p. 217-28.
71. Jacobs, K.B., et al., *Detectable clonal mosaicism and its relationship to aging and cancer.* Nat Genet, 2012. **44**(6): p. 651-8.
72. Laurie, C.C., et al., *Detectable clonal mosaicism from birth to old age and its relationship to cancer.* Nat Genet, 2012. **44**(6): p. 642-50.
73. Young, A.L., et al., *Clonal haematopoiesis harbouring AML-associated mutations is ubiquitous in healthy adults.* Nature Communications, 2016. **7**(1): p. 12484.
74. Steensma, D.P., et al., *Clonal hematopoiesis of indeterminate potential and its distinction from myelodysplastic syndromes.* 2015. **126**(1): p. 9-16.
75. Machiela, M.J., et al., *Characterization of large structural genetic mosaicism in human autosomes.* Am J Hum Genet, 2015. **96**(3): p. 487-97.
76. Jaiswal, S., et al., *Age-Related Clonal Hematopoiesis Associated with Adverse Outcomes.* New England Journal of Medicine, 2014. **371**(26): p. 2488-2498.
77. Berger, G., et al., *Early detection and evolution of preleukemic clones in therapy-related myeloid neoplasms following autologous SCT.* Blood, 2018. **131**(16): p. 1846-1857.
78. Takahashi, K., et al., *Preleukaemic clonal haemopoiesis and risk of therapy-related myeloid neoplasms: a case-control study.* Lancet Oncol, 2017. **18**(1): p. 100-111.
79. Gillis, N.K., et al., *Clonal haemopoiesis and therapy-related myeloid malignancies in elderly patients: a proof-of-concept, case-control study.* Lancet Oncol, 2017. **18**(1): p. 112-121.
80. Steensma, D.P., et al., *Clonal hematopoiesis of indeterminate potential and its distinction from myelodysplastic syndromes.* Blood, 2015. **126**(1): p. 9-16.
81. Gibson, C.J., et al., *Clonal Hematopoiesis Associated With Adverse Outcomes After Autologous Stem-Cell Transplantation for Lymphoma.* J Clin Oncol, 2017. **35**(14): p. 1598-1605.
82. Young, A.L., et al., *Clonal hematopoiesis and risk of acute myeloid leukemia.* Haematologica, 2019. **104**(12): p. 2410-2417.
83. Desai, P., et al., *Somatic mutations precede acute myeloid leukemia years before diagnosis.* Nat Med, 2018. **24**(7): p. 1015-1023.
84. Abelson, S., et al., *Prediction of acute myeloid leukaemia risk in healthy individuals.* Nature, 2018. **559**(7714): p. 400-404.
85. Hsu, J.I., et al., *PPM1D Mutations Drive Clonal Hematopoiesis in Response to Cytotoxic Chemotherapy.* Cell Stem Cell, 2018. **23**(5): p. 700-713.e6.
86. Walter, M.J., et al., *Clonal diversity of recurrently mutated genes in myelodysplastic syndromes.* Leukemia, 2013. **27**(6): p. 1275-82.
87. Haferlach, T., et al., *Landscape of genetic lesions in 944 patients with myelodysplastic syndromes.* Leukemia, 2014. **28**(2): p. 241-7.
88. Makishima, H., et al., *Dynamics of clonal evolution in myelodysplastic syndromes.* Nat Genet, 2017. **49**(2): p. 204-212.
89. Shih, A.H., et al., *Mutational analysis of therapy-related myelodysplastic syndromes and acute myelogenous leukemia.* Haematologica, 2013. **98**(6): p. 908-12.
90. Ok, C.Y., et al., *Mutational profiling of therapy-related myelodysplastic syndromes and acute myeloid leukemia by next generation sequencing, a comparison with de novo diseases.* Leuk Res, 2015. **39**(3): p. 348-54.
91. Lindsley, R.C., et al., *Acute myeloid leukemia ontogeny is defined by distinct somatic mutations.* Blood, 2015. **125**(9): p. 1367-1376.
92. Reese, J.S., L. Liu, and S.L. Gerson, *Repopulating defect of mismatch repair–deficient hematopoietic stem cells.* Blood, 2003. **102**(5): p. 1626-1633.

93. Voso, M.T., et al., *Mutations of epigenetic regulators and of the spliceosome machinery in therapy-related myeloid neoplasms and in acute leukemias evolved from chronic myeloproliferative diseases.* Leukemia, 2013. **27**(4): p. 982-985.
94. Super, H., et al., *Rearrangements of the MLL gene in therapy-related acute myeloid leukemia in patients previously treated with agents targeting DNA- topoisomerase II.* Blood, 1993. **82**(12): p. 3705-3711.
95. Awada, H., et al., *Mutational Patterns and Clonal Architecture of Therapy-Related Acute Myeloid Leukemia.* Blood, 2019. **134**(Supplement_1): p. 1405-1405.
96. Karimi, M., et al., *High-throughput mutational screening adds clinically important information in myelodysplastic syndromes and secondary or therapy-related acute myeloid leukemia.* Haematologica, 2015. **100**(6): p. e223-5.
97. Bacher, U., et al., *A comparative study of molecular mutations in 381 patients with myelodysplastic syndrome and in 4130 patients with acute myeloid leukemia.* Haematologica, 2007. **92**(6): p. 744-52.
98. Bacher, U., et al., *Implications of NRAS mutations in AML: a study of 2502 patients.* Blood, 2006. **107**(10): p. 3847-53.
99. Side, L.E., et al., *RAS, FLT3, and TP53 mutations in therapy-related myeloid malignancies with abnormalities of chromosomes 5 and 7.* Genes Chromosomes Cancer, 2004. **39**(3): p. 217-23.
100. Christiansen, D.H. and J. Pedersen-Bjergaard, *Internal tandem duplications of the FLT3 and MLL genes are mainly observed in atypical cases of therapy-related acute myeloid leukemia with a normal karyotype and are unrelated to type of previous therapy.* Leukemia, 2001. **15**(12): p. 1848-51.
101. Christiansen, D.H., et al., *Mutations of genes in the receptor tyrosine kinase (RTK)/RAS-BRAF signal transduction pathway in therapy-related myelodysplasia and acute myeloid leukemia.* Leukemia, 2005. **19**(12): p. 2232-40.
102. Westman, M.K., et al., *IDH1 and IDH2 mutations in therapy-related myelodysplastic syndrome and acute myeloid leukemia are associated with a normal karyotype and with der(1;7)(q10;p10).* Leukemia, 2013. **27**(4): p. 957-9.
103. Desta, F., et al., *Activating mutations of JAK2V617F are uncommon in t-MDS and t-AML and are only observed in atypic cases.* Leukemia, 2006. **20**(3): p. 547-8.
104. Christiansen, D.H., et al., *Mutations of the PTPN11 gene in therapy-related MDS and AML with rare balanced chromosome translocations.* Genes Chromosomes Cancer, 2007. **46**(6): p. 517-21.
105. Bacher, U., et al., *Prognostic relevance of FLT3-TKD mutations in AML: the combination matters--an analysis of 3082 patients.* Blood, 2008. **111**(5): p. 2527-37.
106. Fabiani, E., et al., *SETBP1 mutations in 106 patients with therapy-related myeloid neoplasms.* Haematologica, 2014. **99**(9): p. e152-3.
107. Kuzmanovic, T., et al., *Genomics of therapy-related myeloid neoplasms.* Haematologica, 2020. **105**(3): p. e98-e101.
108. Nishiyama, T., et al., *Mutation analysis of therapy-related myeloid neoplasms.* Cancer Genet, 2018. **222-223**: p. 38-45.
109. Fabiani, E., et al., *Clonal evolution in therapy-related neoplasms.* Oncotarget, 2017. **8**(7): p. 12031-12040.
110. Claerhout, H., et al., *Next generation sequencing in therapy-related myeloid neoplasms compared to de novo myeloid neoplasms.* Acta Clin Belg, 2022. **77**(3): p. 658-663.
111. Lindsley, R.C., et al., *Prognostic Mutations in Myelodysplastic Syndrome after Stem-Cell Transplantation.* N Engl J Med, 2017. **376**(6): p. 536-547.
112. Bernard, E., et al., *Implications of TP53 allelic state for genome stability, clinical presentation and outcomes in myelodysplastic syndromes.* Nat Med, 2020. **26**(10): p. 1549-1556.

113. Chen, Z., et al., *Comparison of therapy-related myelodysplastic syndrome with ring sideroblasts and de novo myelodysplastic syndrome with ring sideroblasts.* Leuk Res, 2019. **86**: p. 106227.
114. Khalife-Hachem, S., et al., *Molecular Landscape of Therapy-related Myeloid Neoplasms in Patients Previously Treated for Gynecologic and Breast Cancers.* Hemasphere, 2021. **5**(9): p. e632.
115. Papaemmanuil, E., et al., *Somatic SF3B1 mutation in myelodysplasia with ring sideroblasts.* N Engl J Med, 2011. **365**(15): p. 1384-95.
116. Bejar, R., et al., *Validation of a prognostic model and the impact of mutations in patients with lower-risk myelodysplastic syndromes.* J Clin Oncol, 2012. **30**(27): p. 3376-82.
117. Bejar, R., et al., *Clinical effect of point mutations in myelodysplastic syndromes.* N Engl J Med, 2011. **364**(26): p. 2496-506.
118. Papaemmanuil, E., et al., *Clinical and biological implications of driver mutations in myelodysplastic syndromes.* Blood, 2013. **122**(22): p. 3616-27; quiz 3699.
119. Mendez-Ferrer, S., et al., *Haematopoietic stem cell release is regulated by circadian oscillations.* Nature, 2008. **452**(7186): p. 442-7.
120. Bromberg, O., et al., *Osteoblastic N-cadherin is not required for microenvironmental support and regulation of hematopoietic stem and progenitor cells.* Blood, 2012. **120**(2): p. 303-13.
121. Kollet, O., et al., *Physiologic corticosterone oscillations regulate murine hematopoietic stem/progenitor cell proliferation and CXCL12 expression by bone marrow stromal progenitors.* Leukemia, 2013. **27**(10): p. 2006-15.
122. Spencer, J.A., et al., *Direct measurement of local oxygen concentration in the bone marrow of live animals.* Nature, 2014. **508**(7495): p. 269-73.
123. Klein, G., *The extracellular matrix of the hematopoietic microenvironment.* Experientia, 1995. **51**(9-10): p. 914-26.
124. Carter, D.H., P. Sloan, and J.E. Aaron, *Immunolocalization of collagen types I and III, tenascin, and fibronectin in intramembranous bone.* J Histochem Cytochem, 1991. **39**(5): p. 599-606.
125. Hamilton, R. and F.R. Campbell, *Immunochemical localization of extracellular materials in bone marrow of rats.* Anat Rec, 1991. **231**(2): p. 218-24.
126. Nilsson, S.K., et al., *Immunofluorescence characterization of key extracellular matrix proteins in murine bone marrow in situ.* J Histochem Cytochem, 1998. **46**(3): p. 371-7.
127. Savagner, P., et al., *Slug mRNA is expressed by specific mesodermal derivatives during rodent organogenesis.* Dev Dyn, 1998. **213**(2): p. 182-7.
128. Klamer, S. and C. Voermans, *The role of novel and known extracellular matrix and adhesion molecules in the homeostatic and regenerative bone marrow microenvironment.* Cell Adhesion & Migration, 2014. **8**(6): p. 563-577.
129. Coutu, D.L., et al., *Three-dimensional map of nonhematopoietic bone and bone-marrow cells and molecules.* Nature Biotechnology, 2017. **35**(12): p. 1202-1210.
130. Schroeder, T., et al., *Mesenchymal stromal cells in myeloid malignancies.* Blood Res, 2016. **51**(4): p. 225-232.
131. Morrison, S.J. and D.T. Scadden, *The bone marrow niche for haematopoietic stem cells.* Nature, 2014. **505**(7483): p. 327-34.
132. Shiozawa, Y., et al., *The bone marrow niche: habitat to hematopoietic and mesenchymal stem cells, and unwitting host to molecular parasites.* Leukemia, 2008. **22**(5): p. 941-50.
133. Miura, Y., et al., *Mesenchymal stem cell-organized bone marrow elements: an alternative hematopoietic progenitor resource.* Stem Cells, 2006. **24**(11): p. 2428-36.
134. Naveiras, O., et al., *Bone-marrow adipocytes as negative regulators of the haematopoietic microenvironment.* Nature, 2009. **460**(7252): p. 259-63.
135. Greenbaum, A., et al., *CXCL12 in early mesenchymal progenitors is required for haematopoietic stem-cell maintenance.* Nature, 2013. **495**(7440): p. 227-30.

136. Ding, L. and S.J. Morrison, *Haematopoietic stem cells and early lymphoid progenitors occupy distinct bone marrow niches.* Nature, 2013. **495**(7440): p. 231-5.
137. Schajnovitz, A., et al., *CXCL12 secretion by bone marrow stromal cells is dependent on cell contact and mediated by connexin-43 and connexin-45 gap junctions.* Nat Immunol, 2011. **12**(5): p. 391-8.
138. Arai, F., et al., *Tie2/angiopoietin-1 signaling regulates hematopoietic stem cell quiescence in the bone marrow niche.* Cell, 2004. **118**(2): p. 149-61.
139. Goncalves, K.A., et al., *Angiogenin Promotes Hematopoietic Regeneration by Dichotomously Regulating Quiescence of Stem and Progenitor Cells.* Cell, 2016. **166**(4): p. 894-906.
140. Hosokawa, K., et al., *Cadherin-based adhesion is a potential target for niche manipulation to protect hematopoietic stem cells in adult bone marrow.* Cell Stem Cell, 2010. **6**(3): p. 194-8.
141. Bigas, A. and L. Espinosa, *Hematopoietic stem cells: to be or Notch to be.* Blood, 2012. **119**(14): p. 3226-35.
142. Pajcini, K.V., N.A. Speck, and W.S. Pear, *Notch signaling in mammalian hematopoietic stem cells.* Leukemia, 2011. **25**(10): p. 1525-32.
143. Friedenstein, A.J., R.K. Chailakhjan, and K.S. Lalykina, *The development of fibroblast colonies in monolayer cultures of guinea-pig bone marrow and spleen cells.* Cell Tissue Kinet, 1970. **3**(4): p. 393-403.
144. Friedenstein, A.J., J.F. Gorskaja, and N.N. Kulagina, *Fibroblast precursors in normal and irradiated mouse hematopoietic organs.* Exp Hematol, 1976. **4**(5): p. 267-74.
145. Gronthos, S., et al., *Molecular and cellular characterisation of highly purified stromal stem cells derived from human bone marrow.* Journal of Cell Science, 2003. **116**(9): p. 1827-1835.
146. Pittenger, M.F., et al., *Multilineage potential of adult human mesenchymal stem cells.* Science, 1999. **284**(5411): p. 143-7.
147. Castro-Malaspina, H., et al., *Characterization of human bone marrow fibroblast colony-forming cells (CFU-F) and their progeny.* Blood, 1980. **56**(2): p. 289-301.
148. Dazzi, F., et al., *The role of mesenchymal stem cells in haemopoiesis.* Blood Rev, 2006. **20**(3): p. 161-71.
149. Deans, R.J. and A.B. Moseley, *Mesenchymal stem cells: biology and potential clinical uses.* Exp Hematol, 2000. **28**(8): p. 875-84.
150. Menicanin, D., et al., *Genomic Profiling of Mesenchymal Stem Cells.* Stem Cell Reviews and Reports, 2009. **5**(1): p. 36-50.
151. Prockop, D.J., *Marrow Stromal Cells as Stem Cells for Nonhematopoietic Tissues.* Science, 1997. **276**(5309): p. 71-74.
152. Zannettino, A.C.W., et al., *Multipotential human adipose-derived stromal stem cells exhibit a perivascular phenotype in vitro and in vivo.* Journal of Cellular Physiology, 2008. **214**(2): p. 413-421.
153. Kuznetsov, S.A., et al., *Circulating Skeletal Stem Cells.* The Journal of Cell Biology, 2001. **153**(5): p. 1133-1140.
154. Seo, B.-M., et al., *Investigation of multipotent postnatal stem cells from human periodontal ligament.* The Lancet. **364**(9429): p. 149-155.
155. Gronthos, S., et al., *Postnatal human dental pulp stem cells (DPSCs) in vitro and in vivo.* Proceedings of the National Academy of Sciences, 2000. **97**(25): p. 13625-13630.
156. Erices, A., P. Conget, and J.J. Minguell, *Mesenchymal progenitor cells in human umbilical cord blood.* British Journal of Haematology, 2000. **109**(1): p. 235-242.
157. Pittenger, M.F., *Mesenchymal Stem Cells from Adult Bone Marrow*, in *Mesenchymal Stem Cells: Methods and Protocols*, D.J. Prockop, B.A. Bunnell, and D.G. Phinney, Editors. 2008, Humana Press: Totowa, NJ. p. 27-44.
158. Gronthos, S. and A.C.W. Zannettino, *A Method to Isolate and Purify Human Bone Marrow Stromal Stem Cells*, in *Mesenchymal Stem Cells: Methods and Protocols*, D.J. Prockop, B.A. Bunnell, and D.G. Phinney, Editors. 2008, Humana Press: Totowa, NJ. p. 45-57.

159. Zambetti, N.A., et al., *Mesenchymal Inflammation Drives Genotoxic Stress in Hematopoietic Stem Cells and Predicts Disease Evolution in Human Pre-leukemia.* Cell Stem Cell, 2016. **19**(5): p. 613-627.
160. Zahr, A.A., et al., *Bone marrow fibrosis in myelofibrosis: pathogenesis, prognosis and targeted strategies.* Haematologica, 2016. **101**(6): p. 660-71.
161. Jain, A.G., et al., *Myelodysplastic Syndromes with Bone Marrow Fibrosis: An Update.* Ann Lab Med, 2022. **42**(3): p. 299-305.
162. Medyouf, H., et al., *Myelodysplastic cells in patients reprogram mesenchymal stromal cells to establish a transplantable stem cell niche disease unit.* Cell Stem Cell, 2014. **14**(6): p. 824-37.
163. Walkley, C.R., et al., *A microenvironment-induced myeloproliferative syndrome caused by retinoic acid receptor gamma deficiency.* Cell, 2007. **129**(6): p. 1097-110.
164. Rupec, R.A., et al., *Stroma-mediated dysregulation of myelopoiesis in mice lacking I kappa B alpha.* Immunity, 2005. **22**(4): p. 479-91.
165. Xiao, P., et al., *Sipa1 deficiency-induced bone marrow niche alterations lead to the initiation of myeloproliferative neoplasm.* Blood Adv, 2018. **2**(5): p. 534-548.
166. Raaijmakers, M.H., et al., *Bone progenitor dysfunction induces myelodysplasia and secondary leukaemia.* Nature, 2010. **464**(7290): p. 852-7.
167. Stoddart, A., et al., *Cytotoxic Therapy–Induced Effects on Both Hematopoietic and Marrow Stromal Cells Promotes Therapy-Related Myeloid Neoplasms.* Blood Cancer Discovery, 2020.
168. Noemi, A.Z., et al., *Deficiency of the ribosome biogenesis gene Sbds in hematopoietic stem and progenitor cells causes neutropenia in mice by attenuating lineage progression in myelocytes.* Haematologica, 2015. **100**(10): p. 1285-1293.
169. Rawls, A.S., et al., *Lentiviral-mediated RNAi inhibition of Sbds in murine hematopoietic progenitors impairs their hematopoietic potential.* Blood, 2007. **110**(7): p. 2414-2422.
170. Geyh, S., et al., *Insufficient stromal support in MDS results from molecular and functional deficits of mesenchymal stromal cells.* Leukemia, 2013. **27**(9): p. 1841-51.
171. Santamaria, C., et al., *Impaired expression of DICER, DROSHA, SBDS and some microRNAs in mesenchymal stromal cells from myelodysplastic syndrome patients.* Haematologica, 2012. **97**(8): p. 1218-24.
172. Zhao, Y., et al., *Down-regulation of Dicer1 promotes cellular senescence and decreases the differentiation and stem cell-supporting capacities of mesenchymal stromal cells in patients with myelodysplastic syndrome.* Haematologica, 2015. **100**(2): p. 194-204.
173. Kim, Y.W., et al., *Defective Notch activation in microenvironment leads to myeloproliferative disease.* Blood, 2008. **112**(12): p. 4628-38.
174. Kode, A., et al., *Leukaemogenesis induced by an activating beta-catenin mutation in osteoblasts.* Nature, 2014. **506**(7487): p. 240-4.
175. Stoddart, A., et al., *Cell intrinsic and extrinsic factors synergize in mice with haploinsufficiency for Tp53, and two human del(5q) genes, Egr1 and Apc.* Blood, 2014. **123**(2): p. 228-38.
176. Stoddart, A., et al., *Haploinsufficiency of del(5q) genes, Egr1 and Apc, cooperate with Tp53 loss to induce acute myeloid leukemia in mice.* Blood, 2014. **123**(7): p. 1069-78.
177. Vaghef, H., et al., *Alkaline single-cell gel electrophoresis and human biomonitoring for genotoxicity: a pilot study on breast cancer patients undergoing chemotherapy including cyclophosphamide.* Mutat Res, 1997. **395**(2-3): p. 127-38.
178. Tucker, J.D., et al., *Induction, accumulation, and persistence of sister chromatid exchanges in women with breast cancer receiving cyclophosphamide, adriamycin, and 5-fluorouracil chemotherapy.* Cancer Res, 1990. **50**(16): p. 4951-6.
179. Kemp, K., et al., *Alkylating chemotherapeutic agents cyclophosphamide and melphalan cause functional injury to human bone marrow-derived mesenchymal stem cells.* Ann Hematol, 2011. **90**(7): p. 777-89.
180. Somaiah, C., et al., *Mesenchymal stem cells show functional defect and decreased anti-cancer effect after exposure to chemotherapeutic drugs.* J Biomed Sci, 2018. **25**(1): p. 5.

181. Prata Kde, L., et al., *Effects of high-dose chemotherapy on bone marrow multipotent mesenchymal stromal cells isolated from lymphoma patients.* Exp Hematol, 2010. **38**(4): p. 292-300.e4.
182. Li, J., et al., *Differential damage and recovery of human mesenchymal stem cells after exposure to chemotherapeutic agents.* Br J Haematol, 2004. **127**(3): p. 326-34.
183. Georgiou, K.R., et al., *Methotrexate chemotherapy reduces osteogenesis but increases adipogenic potential in the bone marrow.* J Cell Physiol, 2012. **227**(3): p. 909-18.
184. Carlo-Stella, C., et al., *Effect of chemotherapy for acute myelogenous leukemia on hematopoietic and fibroblast marrow progenitors.* Bone Marrow Transplantation, 1997. **20**(6): p. 465-471.
185. Kemp, K., et al., *Chemotherapy-induced mesenchymal stem cell damage in patients with hematological malignancy.* Ann Hematol, 2010. **89**(7): p. 701-13.
186. Isaikina, Y., A. Kustanovich, and A. Svirnovski, *Growth kinetics and self-renewal of human mesenchymal stem cells derived from bone marrow of children with oncohematological diseases during expansion in vitro.* Exp Oncol, 2006. **28**(2): p. 146-51.
187. May, J.E., et al., *Chemotherapy-induced genotoxic damage to bone marrow cells: long-term implications.* Mutagenesis, 2018. **33**(3): p. 241-251.
188. Demaria, M., et al., *Cellular Senescence Promotes Adverse Effects of Chemotherapy and Cancer Relapse.* Cancer Discov, 2017. **7**(2): p. 165-176.
189. Schmitt, C.A., *Senescence, apoptosis and therapy--cutting the lifelines of cancer.* Nat Rev Cancer, 2003. **3**(4): p. 286-95.
190. Sanoff, H.K., et al., *Effect of cytotoxic chemotherapy on markers of molecular age in patients with breast cancer.* J Natl Cancer Inst, 2014. **106**(4): p. dju057.
191. Mueller, L.P., et al., *Presence of mesenchymal stem cells in human bone marrow after exposure to chemotherapy: evidence of resistance to apoptosis induction.* Stem Cells, 2006. **24**(12): p. 2753-65.
192. Tang, C., et al., *Chemotherapy-induced niche perturbs hematopoietic reconstitution in B-cell acute lymphoblastic leukemia.* J Exp Clin Cancer Res, 2018. **37**(1): p. 204.
193. Lucas, D., et al., *Chemotherapy-induced bone marrow nerve injury impairs hematopoietic regeneration.* Nat Med, 2013. **19**(6): p. 695-703.
194. Zhao, Z.G., et al., *Functional characteristics of mesenchymal stem cells derived from bone marrow of patients with myelodysplastic syndromes.* Cancer Lett, 2012. **317**(2): p. 136-43.
195. Flores-Figueroa, E., et al., *In vitro characterization of hematopoietic microenvironment cells from patients with myelodysplastic syndrome.* Leuk Res, 2002. **26**(7): p. 677-86.
196. Flores-Figueroa, E., et al., *Functional analysis of myelodysplastic syndromes-derived mesenchymal stem cells.* Leuk Res, 2008. **32**(9): p. 1407-16.
197. Ferrer, R.A., et al., *Mesenchymal stromal cells from patients with myelodyplastic syndrome display distinct functional alterations that are modulated by lenalidomide.* Haematologica, 2013. **98**(11): p. 1677-85.
198. Weickert, M.-T., et al., *Bone marrow stromal cells from MDS and AML patients show increased adipogenic potential with reduced Delta-like-1 expression.* Scientific Reports, 2021. **11**(1): p. 5944.
199. Martin, S.K., et al., *Brief report: the differential roles of mTORC1 and mTORC2 in mesenchymal stem cell differentiation.* Stem Cells, 2015. **33**(4): p. 1359-65.
200. Fitter, S., et al., *Suppression of PDGF-induced PI3 kinase activity by imatinib promotes adipogenesis and adiponectin secretion.* J Mol Endocrinol, 2012. **48**(3): p. 229-40.
201. Singhal, D., et al., *The mutational burden of therapy-related myeloid neoplasms is similar to primary myelodysplastic syndrome but has a distinctive distribution.* Leukemia, 2019. **33**(12): p. 2842-2853.
202. Anthony, B.A. and D.C. Link, *Regulation of hematopoietic stem cells by bone marrow stromal cells.* Trends Immunol, 2014. **35**(1): p. 32-7.

203. Falconi, G., et al., *Impairment of PI3K/AKT and WNT/beta-catenin pathways in bone marrow mesenchymal stem cells isolated from patients with myelodysplastic syndromes.* Exp Hematol, 2016. **44**(1): p. 75-83.e1-4.
204. Pavlaki, K., et al., *Impaired proliferative potential of bone marrow mesenchymal stromal cells in patients with myelodysplastic syndromes is associated with abnormal WNT signaling pathway.* Stem Cells Dev, 2014. **23**(14): p. 1568-81.
205. Fei, C., et al., *Senescence of bone marrow mesenchymal stromal cells is accompanied by activation of p53/p21 pathway in myelodysplastic syndromes.* Eur J Haematol, 2014. **93**(6): p. 476-86.
206. Pang, Y., et al., *Premature exhaustion of mesenchymal stromal cells from myelodysplastic syndrome patients.* Am J Transl Res, 2017. **9**(7): p. 3462-3468.
207. Fei, C., et al., *Impaired osteogenic differentiation of mesenchymal stem cells derived from bone marrow of patients with lower-risk myelodysplastic syndromes.* Tumour Biol, 2014. **35**(5): p. 4307-16.
208. Geyh, S., et al., *Functional inhibition of mesenchymal stromal cells in acute myeloid leukemia.* Leukemia, 2016. **30**(3): p. 683-91.
209. Galotto, M., et al., *Stromal damage as consequence of high-dose chemo/radiotherapy in bone marrow transplant recipients.* Exp Hematol, 1999. **27**(9): p. 1460-6.
210. Klaus, M., et al., *Reserves, functional, immunoregulatory, and cytogenetic properties of bone marrow mesenchymal stem cells in patients with myelodysplastic syndromes.* Stem Cells Dev, 2010. **19**(7): p. 1043-54.
211. Kouvidi, E., et al., *Cytogenetic evaluation of mesenchymal stem/stromal cells from patients with myelodysplastic syndromes at different time-points during ex vivo expansion.* Leuk Res, 2016. **43**: p. 24-32.
212. Weickert, M.T., et al., *Bone marrow stromal cells from MDS and AML patients show increased adipogenic potential with reduced Delta-like-1 expression.* Sci Rep, 2021. **11**(1): p. 5944.
213. Kim, Y., et al., *Genetic and epigenetic alterations of bone marrow stromal cells in myelodysplastic syndrome and acute myeloid leukemia patients.* Stem Cell Res, 2015. **14**(2): p. 177-84.
214. Campioni, D., et al., *Immunophenotypic heterogeneity of bone marrow-derived mesenchymal stromal cells from patients with hematologic disorders: correlation with bone marrow microenvironment.* Haematologica, 2006. **91**(3): p. 364-8.
215. Zhang, L., et al., *Bone marrow-derived mesenchymal stem/stromal cells in patients with acute myeloid leukemia reveal transcriptome alterations and deficiency in cellular vitality.* Stem Cell Res Ther, 2021. **12**(1): p. 365.
216. Battula, V.L., et al., *AML-induced osteogenic differentiation in mesenchymal stromal cells supports leukemia growth.* JCI Insight, 2017. **2**(13).
217. Chandran, P., et al., *Mesenchymal stromal cells from patients with acute myeloid leukemia have altered capacity to expand differentiated hematopoietic progenitors.* Leuk Res, 2015. **39**(4): p. 486-93.
218. Wenk, C., et al., *Azacitidine Directly Acts on the Mesenchymal Stromal Cell Compartment in Myelodysplastic Syndromes to Alter Niche Function and Suppress Malignant Hematopoeitic Stem/Progenitor Cells.* Blood, 2017. **130**(Suppl 1): p. 1683-1683.
219. Kim, J.-A., et al., *Microenvironmental Remodeling as a Parameter and Prognostic Factor of Heterogeneous Leukemogenesis in Acute Myelogenous Leukemia.* 2015. **75**(11): p. 2222-2231.
220. Azadniv, M., et al., *Bone marrow mesenchymal stromal cells from acute myelogenous leukemia patients demonstrate adipogenic differentiation propensity with implications for leukemia cell support.* Leukemia, 2020. **34**(2): p. 391-403.

221. Diaz de la Guardia, R., et al., *Detailed Characterization of Mesenchymal Stem/Stromal Cells from a Large Cohort of AML Patients Demonstrates a Definitive Link to Treatment Outcomes.* Stem Cell Reports, 2017. **8**(6): p. 1573-1586.
222. Chen, Y., et al., *Acute myeloid leukemia-induced remodeling of the human bone marrow niche predicts clinical outcome.* Blood Adv, 2020. **4**(20): p. 5257-5268.
223. Falconi, G., et al., *Expression Profile of Bone Marrow Mesenchymal Stromal Cells Isolated from Patients with Therapy-Related Myeloid Neoplasms.* Leukemia Research. **55**: p. S116-S117.
224. Lopez-Villar, O., et al., *Both expanded and uncultured mesenchymal stem cells from MDS patients are genomically abnormal, showing a specific genetic profile for the 5q- syndrome.* Leukemia, 2009. **23**(4): p. 664-72.
225. Zhao, Z., et al., *The different immunoregulatory functions of mesenchymal stem cells in patients with low-risk or high-risk myelodysplastic syndromes.* PLoS One, 2012. **7**(9): p. e45675.
226. Rathnayake, A.J., H.W. Goonasekera, and V.H. Dissanayake, *Phenotypic and Cytogenetic Characterization of Mesenchymal Stromal Cells in De Novo Myelodysplastic Syndromes.* Anal Cell Pathol (Amst), 2016. **2016**: p. 8012716.
227. Flores-Figueroa, E., et al., *Mesenchymal stem cells in myelodysplastic syndromes: phenotypic and cytogenetic characterization.* Leuk Res, 2005. **29**(2): p. 215-24.
228. Shi, S. and S. Gronthos, *Perivascular Niche of Postnatal Mesenchymal Stem Cells in Human Bone Marrow and Dental Pulp.* Journal of Bone and Mineral Research, 2003. **18**(4): p. 696-704.
229. Sacchetti, B., et al., *Self-Renewing Osteoprogenitors in Bone Marrow Sinusoids Can Organize a Hematopoietic Microenvironment.* Cell. **131**(2): p. 324-336.
230. Simmons, P. and B. Torok-Storb, *Identification of stromal cell precursors in human bone marrow by a novel monoclonal antibody, STRO-1.* Blood, 1991. **78**(1): p. 55-62.
231. Gronthos, S. and P. Simmons, *The growth factor requirements of STRO-1-positive human bone marrow stromal precursors under serum-deprived conditions in vitro.* Blood, 1995. **85**(4): p. 929-940.
232. Dennis, J.E., et al., *The STRO-1+ marrow cell population is multipotential.* Cells Tissues Organs, 2002. **170**(2-3): p. 73-82.
233. Zannettino, A.C.W., et al., *Molecular cloning of the cell surface antigen identified by the osteoprogenitor-specific monoclonal antibody, HOP-26.* Journal of Cellular Biochemistry, 2003. **89**(1): p. 56-66.
234. Quirici, N., et al., *Isolation of bone marrow mesenchymal stem cells by anti-nerve growth factor receptor antibodies.* Experimental Hematology. **30**(7): p. 783-791.
235. Alvarez-Viejo, M., Y. Menendez-Menendez, and J. Otero-Hernandez, *CD271 as a marker to identify mesenchymal stem cells from diverse sources before culture.* World J Stem Cells, 2015. **7**(2): p. 470-6.
236. Gronthos, S., et al., *A novel monoclonal antibody (STRO-3) identifies an isoform of tissue nonspecific alkaline phosphatase expressed by multipotent bone marrow stromal stem cells.* Stem Cells Dev, 2007. **16**(6): p. 953-63.
237. Gronthos, S., et al., *The STRO-1+ fraction of adult human bone marrow contains the osteogenic precursors.* Blood, 1994. **84**(12): p. 4164-73.
238. Zannettino, A.C., et al., *Human mulipotential mesenchymal/stromal stem cells are derived from a discrete subpopulation of STRO-1bright/CD34 /CD45(-)/glycophorin-A-bone marrow cells.* Haematologica, 2007. **92**(12): p. 1707-8.
239. Tormin, A., et al., *CD146 expression on primary nonhematopoietic bone marrow stem cells is correlated with in situ localization.* Blood, 2011. **117**(19): p. 5067-77.

240. Kim, Y.H., et al., *Characterization of different subpopulations from bone marrow-derived mesenchymal stromal cells by alkaline phosphatase expression.* Stem Cells Dev, 2012. **21**(16): p. 2958-68.
241. Varga, G., et al., *Inappropriate Notch activity and limited mesenchymal stem cell plasticity in the bone marrow of patients with myelodysplastic syndromes.* Pathol Oncol Res, 2007. **13**(4): p. 311-9.
242. Aanei, C.M., et al., *Intrinsic growth deficiencies of mesenchymal stromal cells in myelodysplastic syndromes.* Stem Cells Dev, 2012. **21**(10): p. 1604-15.
243. Lopes, M.R., et al., *De novo AML exhibits greater microenvironment dysregulation compared to AML with myelodysplasia-related changes.* Sci Rep, 2017. **7**: p. 40707.
244. Wu, Y., et al., *Impaired Expression of Focal Adhesion Kinase in Mesenchymal Stromal Cells from Low-Risk Myelodysplastic Syndrome Patients.* Frontiers in Oncology, 2017. **7**(164).
245. Choi, S.C., et al., *Fibroblast growth factor-2 and -4 promote the proliferation of bone marrow mesenchymal stem cells by the activation of the PI3K-Akt and ERK1/2 signaling pathways.* Stem Cells Dev, 2008. **17**(4): p. 725-36.
246. Fortunel, N.O., A. Hatzfeld, and J.A. Hatzfeld, *Transforming growth factor-beta: pleiotropic role in the regulation of hematopoiesis.* Blood, 2000. **96**(6): p. 2022-36.
247. Cai, J.-Q., et al., *Sonic hedgehog enhances the proliferation and osteogenic differentiation of bone marrow-derived mesenchymal stem cells.* Cell Biology International, 2012. **36**(4): p. 349-355.
248. Sato, Y., et al., *Notch2 Signaling Regulates the Proliferation of Murine Bone Marrow-Derived Mesenchymal Stem/Stromal Cells via c-Myc Expression.* PLoS One, 2016. **11**(11): p. e0165946.
249. Zhu, Z., et al., *Lithium stimulates human bone marrow derived mesenchymal stem cell proliferation through GSK-3β-dependent β-catenin/Wnt pathway activation.* Febs j, 2014. **281**(23): p. 5371-89.
250. Geyh, S., et al., *Transforming growth factor β1-mediated functional inhibition of mesenchymal stromal cells in myelodysplastic syndromes and acute myeloid leukemia.* Haematologica, 2018. **103**(9): p. 1462-1471.
251. Heinemann, L., et al., *Inhibiting PI3K-AKT-mTOR Signaling in Multiple Myeloma-Associated Mesenchymal Stem Cells Impedes the Proliferation of Multiple Myeloma Cells.* Front Oncol, 2022. **12**: p. 874325.
252. Stoddart, A., et al., *Haploinsufficient loss of multiple 5q genes may fine-tune Wnt signaling in del(5q) therapy-related myeloid neoplasms.* Blood, 2015. **126**(26): p. 2899-2901.
253. Lane, S.W., et al., *The Apc(min) mouse has altered hematopoietic stem cell function and provides a model for MPD/MDS.* Blood, 2010. **115**(17): p. 3489-97.
254. Ling, L., V. Nurcombe, and S.M. Cool, *Wnt signaling controls the fate of mesenchymal stem cells.* Gene, 2009. **433**(1): p. 1-7.
255. Horwitz, E.M., et al., *Clarification of the nomenclature for MSC: The International Society for Cellular Therapy position statement.* Cytotherapy, 2005. **7**(5): p. 393-5.
256. Shaulian, E. and M. Karin, *AP-1 in cell proliferation and survival.* Oncogene, 2001. **20**(19): p. 2390-400.
257. Nicolay, N.H., et al., *Mesenchymal stem cells are sensitive to bleomycin treatment.* Sci Rep, 2016. **6**: p. 26645.
258. Morton, L.M., et al., *Evolving risk of therapy-related acute myeloid leukemia following cancer chemotherapy among adults in the United States, 1975-2008.* Blood, 2013. **121**(15): p. 2996-3004.
259. Gorgoulis, V., et al., *Cellular Senescence: Defining a Path Forward.* Cell, 2019. **179**(4): p. 813-827.
260. Chatterjee, N. and G.C. Walker, *Mechanisms of DNA damage, repair, and mutagenesis.* Environ Mol Mutagen, 2017. **58**(5): p. 235-263.

261. Surova, O. and B. Zhivotovsky, *Various modes of cell death induced by DNA damage.* Oncogene, 2013. **32**(33): p. 3789-3797.
262. Campisi, J. and F. d'Adda di Fagagna, *Cellular senescence: when bad things happen to good cells.* Nat Rev Mol Cell Biol, 2007. **8**(9): p. 729-40.
263. Reuvers, T.G.A., R. Kanaar, and J. Nonnekens, *DNA Damage-Inducing Anticancer Therapies: From Global to Precision Damage.* Cancers (Basel), 2020. **12**(8).
264. Jackson, S.P. and J. Bartek, *The DNA-damage response in human biology and disease.* Nature, 2009. **461**(7267): p. 1071-8.
265. Matsuoka, S., et al., *ATM and ATR substrate analysis reveals extensive protein networks responsive to DNA damage.* Science, 2007. **316**(5828): p. 1160-6.
266. Collins, P.L., et al., *DNA double-strand breaks induce H2Ax phosphorylation domains in a contact-dependent manner.* Nature Communications, 2020. **11**(1): p. 3158.
267. Scully, R. and A. Xie, *Double strand break repair functions of histone H2AX.* Mutat Res, 2013. **750**(1-2): p. 5-14.
268. Chen, B.R., et al., *XLF and H2AX function in series to promote replication fork stability.* J Cell Biol, 2019. **218**(7): p. 2113-2123.
269. Helmink, B.A., et al., *H2AX prevents CtIP-mediated DNA end resection and aberrant repair in G1-phase lymphocytes.* Nature, 2011. **469**(7329): p. 245-9.
270. Xie, A., et al., *Control of sister chromatid recombination by histone H2AX.* Mol Cell, 2004. **16**(6): p. 1017-25.
271. Hayflick, L. and P.S. Moorhead, *The serial cultivation of human diploid cell strains.* Experimental Cell Research, 1961. **25**(3): p. 585-621.
272. Serrano, M., et al., *Oncogenic ras provokes premature cell senescence associated with accumulation of p53 and p16INK4a.* Cell, 1997. **88**(5): p. 593-602.
273. Zhu, J., et al., *Senescence of human fibroblasts induced by oncogenic Raf.* Genes Dev, 1998. **12**(19): p. 2997-3007.
274. Lin, A.W., et al., *Premature senescence involving p53 and p16 is activated in response to constitutive MEK/MAPK mitogenic signaling.* Genes Dev, 1998. **12**(19): p. 3008-19.
275. Michaloglou, C., et al., *BRAFE600-associated senescence-like cell cycle arrest of human naevi.* Nature, 2005. **436**(7051): p. 720-4.
276. Herranz, N. and J. Gil, *Mechanisms and functions of cellular senescence.* J Clin Invest, 2018. **128**(4): p. 1238-1246.
277. He, S. and N.E. Sharpless, *Senescence in Health and Disease.* Cell, 2017. **169**(6): p. 1000-1011.
278. Schmitt, C.A., et al., *A Senescence Program Controlled by p53 and p16INK4a Contributes to the Outcome of Cancer Therapy.* Cell, 2002. **109**(3): p. 335-346.
279. Sherr, C.J. and F. McCormick, *The RB and p53 pathways in cancer.* Cancer Cell, 2002. **2**(2): p. 103-12.
280. d'Adda di Fagagna, F., *Living on a break: cellular senescence as a DNA-damage response.* Nature Reviews Cancer, 2008. **8**(7): p. 512-522.
281. Paunesku, T., et al., *Proliferating cell nuclear antigen (PCNA): ringmaster of the genome.* International Journal of Radiation Biology, 2001. **77**(10): p. 1007-1021.
282. Sheng, C., et al., *PCNA-Mediated Degradation of p21 Coordinates the DNA Damage Response and Cell Cycle Regulation in Individual Cells.* Cell Reports, 2019. **27**(1): p. 48-58.e7.
283. Seshadri, T. and J. Campisi, *Repression of c-fos transcription and an altered genetic program in senescent human fibroblasts.* Science, 1990. **247**(4939): p. 205-9.
284. Stein, G.H., et al., *Senescent cells fail to express cdc2, cycA, and cycB in response to mitogen stimulation.* Proc Natl Acad Sci U S A, 1991. **88**(24): p. 11012-6.
285. Wiley, C.D., et al., *Analysis of individual cells identifies cell-to-cell variability following induction of cellular senescence.* Aging Cell, 2017. **16**(5): p. 1043-1050.

286. Sharpless, N.E. and C.J. Sherr, *Forging a signature of in vivo senescence.* Nature Reviews Cancer, 2015. **15**(7): p. 397-408.
287. Sasaki, M., et al., *Senescent cells are resistant to death despite low Bcl-2 level.* Mech Ageing Dev, 2001. **122**(15): p. 1695-706.
288. Wang, E., *Senescent human fibroblasts resist programmed cell death, and failure to suppress bcl2 is involved.* Cancer Res, 1995. **55**(11): p. 2284-92.
289. Yosef, R., et al., *Directed elimination of senescent cells by inhibition of BCL-W and BCL-XL.* Nature Communications, 2016. **7**(1): p. 11190.
290. Childs, B.G., et al., *Senescence and apoptosis: dueling or complementary cell fates?* EMBO Rep, 2014. **15**(11): p. 1139-53.
291. Bent, E.H., L.A. Gilbert, and M.T. Hemann, *A senescence secretory switch mediated by PI3K/AKT/mTOR activation controls chemoprotective endothelial secretory responses.* Genes Dev, 2016. **30**(16): p. 1811-21.
292. Blagosklonny, M.V., *Cell cycle arrest is not yet senescence, which is not just cell cycle arrest: terminology for TOR-driven aging.* Aging (Albany NY), 2012. **4**(3): p. 159-65.
293. Cormenier, J., et al., *The ATF6α arm of the Unfolded Protein Response mediates replicative senescence in human fibroblasts through a COX2/prostaglandin E(2) intracrine pathway.* Mech Ageing Dev, 2018. **170**: p. 82-91.
294. Druelle, C., et al., *ATF6α regulates morphological changes associated with senescence in human fibroblasts.* Oncotarget, 2016. **7**(42).
295. Dimri, G.P., et al., *A biomarker that identifies senescent human cells in culture and in aging skin in vivo.* Proc Natl Acad Sci U S A, 1995. **92**(20): p. 9363-7.
296. Lee, B.Y., et al., *Senescence-associated β-galactosidase is lysosomal β-galactosidase.* Aging Cell, 2006. **5**(2): p. 187-195.
297. Kurz, D.J., et al., *Senescence-associated (beta)-galactosidase reflects an increase in lysosomal mass during replicative ageing of human endothelial cells.* J Cell Sci, 2000. **113 (Pt 20)**: p. 3613-22.
298. Georgakopoulou, E.A., et al., *Specific lipofuscin staining as a novel biomarker to detect replicative and stress-induced senescence. A method applicable in cryo-preserved and archival tissues.* Aging (Albany NY), 2013. **5**(1): p. 37-50.
299. Evangelou, K., et al., *Robust, universal biomarker assay to detect senescent cells in biological specimens.* Aging Cell, 2017. **16**(1): p. 192-197.
300. Nwosu, Z.C., et al., *Caveolin-1 in the regulation of cell metabolism: a cancer perspective.* Molecular Cancer, 2016. **15**(1): p. 71.
301. van Deursen, J.M., *The role of senescent cells in ageing.* Nature, 2014. **509**(7501): p. 439-446.
302. Dasari, A., et al., *Oxidative stress induces premature senescence by stimulating caveolin-1 gene transcription through p38 mitogen-activated protein kinase/Sp1-mediated activation of two GC-rich promoter elements.* Cancer Res, 2006. **66**(22): p. 10805-14.
303. Volonte, D. and F. Galbiati, *Caveolin-1, a master regulator of cellular senescence.* Cancer and Metastasis Reviews, 2020. **39**(2): p. 397-414.
304. Linge, A., et al., *Downregulation of caveolin-1 affects bleomycin-induced growth arrest and cellular senescence in A549 cells.* The international journal of biochemistry & cell biology, 2007. **39**(10): p. 1964-1974.
305. Feng, X., W. Gao, and Y. Li, *Caveolin-1 is involved in high glucose accelerated human glomerular mesangial cell senescence.* Korean J Intern Med, 2017. **32**(5): p. 883-889.
306. Hernandez-Segura, A., et al., *Unmasking Transcriptional Heterogeneity in Senescent Cells.* Curr Biol, 2017. **27**(17): p. 2652-2660.e4.
307. Sadaie, M., et al., *Redistribution of the Lamin B1 genomic binding profile affects rearrangement of heterochromatic domains and SAHF formation during senescence.* Genes Dev, 2013. **27**(16): p. 1800-8.

308. Salama, R., et al., *Cellular senescence and its effector programs.* Genes Dev, 2014. **28**(2): p. 99-114.
309. Narita, M., et al., *Rb-mediated heterochromatin formation and silencing of E2F target genes during cellular senescence.* Cell, 2003. **113**(6): p. 703-16.
310. Coppé, J.-P., et al., *The Senescence-Associated Secretory Phenotype: The Dark Side of Tumor Suppression.* 2010. **5**(1): p. 99-118.
311. Laberge, R.-M., et al., *MTOR regulates the pro-tumorigenic senescence-associated secretory phenotype by promoting IL1A translation.* Nature Cell Biology, 2015. **17**(8): p. 1049-1061.
312. Orjalo, A.V., et al., *Cell surface-bound IL-1alpha is an upstream regulator of the senescence-associated IL-6/IL-8 cytokine network.* Proc Natl Acad Sci U S A, 2009. **106**(40): p. 17031-6.
313. Kuilman, T., et al., *Oncogene-induced senescence relayed by an interleukin-dependent inflammatory network.* Cell, 2008. **133**(6): p. 1019-31.
314. Ito, Y., M. Hoare, and M. Narita, *Spatial and Temporal Control of Senescence.* Trends Cell Biol, 2017. **27**(11): p. 820-832.
315. Acosta, J.C., et al., *Chemokine signaling via the CXCR2 receptor reinforces senescence.* Cell, 2008. **133**(6): p. 1006-18.
316. Rodier, F., et al., *Persistent DNA damage signalling triggers senescence-associated inflammatory cytokine secretion.* Nat Cell Biol, 2009. **11**(8): p. 973-9.
317. Freund, A., C.K. Patil, and J. Campisi, *p38MAPK is a novel DNA damage response-independent regulator of the senescence-associated secretory phenotype.* Embo j, 2011. **30**(8): p. 1536-48.
318. Laberge, R.M., et al., *MTOR regulates the pro-tumorigenic senescence-associated secretory phenotype by promoting IL1A translation.* Nat Cell Biol, 2015. **17**(8): p. 1049-61.
319. Herranz, N., et al., *mTOR regulates MAPKAPK2 translation to control the senescence-associated secretory phenotype.* Nat Cell Biol, 2015. **17**(9): p. 1205-17.
320. Kang, C., et al., *The DNA damage response induces inflammation and senescence by inhibiting autophagy of GATA4.* Science, 2015. **349**(6255): p. aaa5612.
321. Capell, B.C., et al., *MLL1 is essential for the senescence-associated secretory phenotype.* Genes Dev, 2016. **30**(3): p. 321-36.
322. Coppé, J.P., et al., *Senescence-associated secretory phenotypes reveal cell-nonautonomous functions of oncogenic RAS and the p53 tumor suppressor.* PLoS Biol, 2008. **6**(12): p. 2853-68.
323. Lu, S.Y., et al., *Ripe areca nut extract induces G1 phase arrests and senescence-associated phenotypes in normal human oral keratinocyte.* Carcinogenesis, 2006. **27**(6): p. 1273-84.
324. Palmieri, D., J.M. Watson, and C.A. Rinehart, *Age-related expression of PEDF/EPC-1 in human endometrial stromal fibroblasts: implications for interactive senescence.* Exp Cell Res, 1999. **247**(1): p. 142-7.
325. Kumar, S., A.J. Millis, and C. Baglioni, *Expression of interleukin 1-inducible genes and production of interleukin 1 by aging human fibroblasts.* Proc Natl Acad Sci U S A, 1992. **89**(10): p. 4683-7.
326. Maier, J.A., et al., *Extension of the life-span of human endothelial cells by an interleukin-1 alpha antisense oligomer.* Science, 1990. **249**(4976): p. 1570-4.
327. Chang, B.D., et al., *Molecular determinants of terminal growth arrest induced in tumor cells by a chemotherapeutic agent.* Proc Natl Acad Sci U S A, 2002. **99**(1): p. 389-94.
328. Acosta, J.C., et al., *A complex secretory program orchestrated by the inflammasome controls paracrine senescence.* Nat Cell Biol, 2013. **15**(8): p. 978-90.
329. Lau, L., et al., *Uncoupling the Senescence-Associated Secretory Phenotype from Cell Cycle Exit via Interleukin-1 Inactivation Unveils Its Protumorigenic Role.* Mol Cell Biol, 2019. **39**(12).
330. James, E.L., et al., *Senescent Human Fibroblasts Show Increased Glycolysis and Redox Homeostasis with Extracellular Metabolomes That Overlap with Those of Irreparable DNA Damage, Aging, and Disease.* Journal of Proteome Research, 2015. **14**(4): p. 1854-1871.

331. Saraste, M., *Oxidative phosphorylation at the fin de siècle.* Science, 1999. **283**(5407): p. 1488-93.
332. Kwon, S.M., et al., *Metabolic features and regulation in cell senescence.* BMB Rep, 2019. **52**(1): p. 5-12.
333. Birsoy, K., et al., *An Essential Role of the Mitochondrial Electron Transport Chain in Cell Proliferation Is to Enable Aspartate Synthesis.* Cell, 2015. **162**(3): p. 540-51.
334. Sullivan, L.B., et al., *Supporting Aspartate Biosynthesis Is an Essential Function of Respiration in Proliferating Cells.* Cell, 2015. **162**(3): p. 552-63.
335. Tai, H., et al., *Autophagy impairment with lysosomal and mitochondrial dysfunction is an important characteristic of oxidative stress-induced senescence.* Autophagy, 2017. **13**(1): p. 99-113.
336. Moiseeva, O., et al., *Mitochondrial dysfunction contributes to oncogene-induced senescence.* Mol Cell Biol, 2009. **29**(16): p. 4495-507.
337. Wang, W., et al., *Increased AMP:ATP ratio and AMP-activated protein kinase activity during cellular senescence linked to reduced HuR function.* J Biol Chem, 2003. **278**(29): p. 27016-23.
338. Kang, S., et al., *Loss of HtrA2/Omi activity in non-neuronal tissues of adult mice causes premature aging.* Cell Death Differ, 2013. **20**(2): p. 259-69.
339. Dai, D.F., et al., *Age-dependent cardiomyopathy in mitochondrial mutator mice is attenuated by overexpression of catalase targeted to mitochondria.* Aging Cell, 2010. **9**(4): p. 536-44.
340. Passos, J.F., et al., *Mitochondrial dysfunction accounts for the stochastic heterogeneity in telomere-dependent senescence.* PLoS Biol, 2007. **5**(5): p. e110.
341. Studencka, M. and J. Schaber, *Senoptosis: non-lethal DNA cleavage as a route to deep senescence.* Oncotarget, 2017. **8**(19): p. 30656-30671.
342. Wiley, C.D., et al., *Mitochondrial Dysfunction Induces Senescence with a Distinct Secretory Phenotype.* Cell Metab, 2016. **23**(2): p. 303-14.
343. Correia-Melo, C., et al., *Mitochondria are required for pro-ageing features of the senescent phenotype.* Embo j, 2016. **35**(7): p. 724-42.
344. Dörr, J.R., et al., *Synthetic lethal metabolic targeting of cellular senescence in cancer therapy.* Nature, 2013. **501**(7467): p. 421-5.
345. Abdul-Aziz, A.M., et al., *MIF-Induced Stromal PKCβ/IL8 Is Essential in Human Acute Myeloid Leukemia.* Cancer Res, 2017. **77**(2): p. 303-311.
346. Fang, L., et al., *p21Waf1/Cip1/Sdi1 induces permanent growth arrest with markers of replicative senescence in human tumor cells lacking functional p53.* Oncogene, 1999. **18**(18): p. 2789-97.
347. Calcinotto, A., et al., *Cellular Senescence: Aging, Cancer, and Injury.* Physiol Rev, 2019. **99**(2): p. 1047-1078.
348. Mikuła-Pietrasik, J., et al., *Mechanisms and significance of therapy-induced and spontaneous senescence of cancer cells.* Cell Mol Life Sci, 2020. **77**(2): p. 213-229.
349. Hudson, M.M., et al., *Clinical Ascertainment of Health Outcomes Among Adults Treated for Childhood Cancer.* JAMA, 2013. **309**(22): p. 2371-2381.
350. Gonzalez, L.C., et al., *Premature aging/senescence in cancer cells facing therapy: good or bad?* Biogerontology, 2016. **17**(1): p. 71-87.
351. Braig, M., et al., *Oncogene-induced senescence as an initial barrier in lymphoma development.* Nature, 2005. **436**(7051): p. 660-5.
352. Chen, Z., et al., *Crucial role of p53-dependent cellular senescence in suppression of Pten-deficient tumorigenesis.* Nature, 2005. **436**(7051): p. 725-30.
353. Shay, J.W., et al., *Spontaneous in vitro immortalization of breast epithelial cells from a patient with Li-Fraumeni syndrome.* Mol Cell Biol, 1995. **15**(1): p. 425-32.
354. Sun, Y., et al., *Treatment-induced damage to the tumor microenvironment promotes prostate cancer therapy resistance through WNT16B.* Nat Med, 2012. **18**(9): p. 1359-68.

355. Abdul-Aziz, A.M., et al., *Acute myeloid leukemia induces protumoral p16INK4a-driven senescence in the bone marrow microenvironment.* Blood, 2019. **133**(5): p. 446-456.
356. Zwerschke, W., et al., *Metabolic analysis of senescent human fibroblasts reveals a role for AMP in cellular senescence.* Biochem J, 2003. **376**(Pt 2): p. 403-11.
357. Kondoh, H., et al., *Glycolytic enzymes can modulate cellular life span.* Cancer Res, 2005. **65**(1): p. 177-85.
358. Li, L., et al., *Altered hematopoietic cell gene expression precedes development of therapy-related myelodysplasia/acute myeloid leukemia and identifies patients at risk.* Cancer Cell, 2011. **20**(5): p. 591-605.
359. Iverson, S.V., et al., *A Txnrd1-dependent metabolic switch alters hepatic lipogenesis, glycogen storage, and detoxification.* Free Radic Biol Med, 2013. **63**: p. 369-80.
360. Carlson, B.A., et al., *Thioredoxin reductase 1 protects against chemically induced hepatocarcinogenesis via control of cellular redox homeostasis.* Carcinogenesis, 2012. **33**(9): p. 1806-1813.
361. Liu, K.E. and W.A. Frazier, *Phosphorylation of the BNIP3 C-Terminus Inhibits Mitochondrial Damage and Cell Death without Blocking Autophagy.* PLoS One, 2015. **10**(6): p. e0129667.
362. Saraste, M., *Oxidative Phosphorylation at the fin de siècle.* Science, 1999. **283**(5407): p. 1488-1493.
363. Wiley, C.D. and J. Campisi, *From Ancient Pathways to Aging Cells-Connecting Metabolism and Cellular Senescence.* Cell Metab, 2016. **23**(6): p. 1013-1021.
364. Nagineni, C.N., et al., *Radiation-Induced Senescence Reprograms Secretory and Metabolic Pathways in Colon Cancer HCT-116 Cells.* Int J Mol Sci, 2021. **22**(9).
365. James, E.L., et al., *Senescent human fibroblasts show increased glycolysis and redox homeostasis with extracellular metabolomes that overlap with those of irreparable DNA damage, aging, and disease.* J Proteome Res, 2015. **14**(4): p. 1854-71.
366. Dominici, M., et al., *Minimal criteria for defining multipotent mesenchymal stromal cells. The International Society for Cellular Therapy position statement.* Cytotherapy, 2006. **8**(4): p. 315-7.
367. Shi, S. and S. Gronthos, *Perivascular niche of postnatal mesenchymal stem cells in human bone marrow and dental pulp.* J Bone Miner Res, 2003. **18**(4): p. 696-704.
368. Bianco, P., *"Mesenchymal" stem cells.* Annu Rev Cell Dev Biol, 2014. **30**: p. 677-704.
369. Bethel, M., et al., *The changing balance between osteoblastogenesis and adipogenesis in aging and its impact on hematopoiesis.* Curr Osteoporos Rep, 2013. **11**(2): p. 99-106.
370. Chen, Q., et al., *Fate decision of mesenchymal stem cells: adipocytes or osteoblasts?* Cell Death Differ, 2016. **23**(7): p. 1128-39.
371. Marcon, B.H., et al., *Cell cycle genes are downregulated after adipogenic triggering in human adipose tissue-derived stem cells by regulation of mRNA abundance.* Sci Rep, 2019. **9**(1): p. 5611.
372. Spangenberg, L., et al., *Polysome profiling shows extensive posttranscriptional regulation during human adipocyte stem cell differentiation into adipocytes.* Stem Cell Res, 2013. **11**(2): p. 902-12.
373. Lin, F.T. and M.D. Lane, *Antisense CCAAT/enhancer-binding protein RNA suppresses coordinate gene expression and triglyceride accumulation during differentiation of 3T3-L1 preadipocytes.* Genes Dev, 1992. **6**(4): p. 533-44.
374. Rosen, E.D. and B.M. Spiegelman, *Molecular regulation of adipogenesis.* Annu Rev Cell Dev Biol, 2000. **16**: p. 145-71.
375. Gregoire, F.M., C.M. Smas, and H.S. Sul, *Understanding adipocyte differentiation.* Physiol Rev, 1998. **78**(3): p. 783-809.
376. Mandrup, S. and M.D. Lane, *Regulating adipogenesis.* J Biol Chem, 1997. **272**(9): p. 5367-70.
377. Cawthorn, W.P., et al., *Tumour necrosis factor-alpha inhibits adipogenesis via a beta-catenin/TCF4(TCF7L2)-dependent pathway.* Cell Death Differ, 2007. **14**(7): p. 1361-73.

378. Isakson, P., et al., *Impaired preadipocyte differentiation in human abdominal obesity: role of Wnt, tumor necrosis factor-alpha, and inflammation.* Diabetes, 2009. **58**(7): p. 1550-7.
379. Xu, H., J.K. Sethi, and G.S. Hotamisligil, *Transmembrane tumor necrosis factor (TNF)-alpha inhibits adipocyte differentiation by selectively activating TNF receptor 1.* J Biol Chem, 1999. **274**(37): p. 26287-95.
380. Chae, G.N. and S.J. Kwak, *NF-kappaB is involved in the TNF-alpha induced inhibition of the differentiation of 3T3-L1 cells by reducing PPARgamma expression.* Exp Mol Med, 2003. **35**(5): p. 431-7.
381. Gagnon, A., et al., *The role of interleukin 1β in the anti-adipogenic action of macrophages on human preadipocytes.* J Endocrinol, 2013. **217**(2): p. 197-206.
382. Delikat, S., R.J. Harris, and D.W. Galvani, *IL-1 beta inhibits adipocyte formation in human long-term bone marrow culture.* Exp Hematol, 1993. **21**(1): p. 31-7.
383. Delikat, S.E., D.W. Galvani, and M. Zuzel, *The metabolic effects of interleukin 1 beta on human bone marrow adipocytes.* Cytokine, 1995. **7**(4): p. 338-43.
384. Martínez-Martínez, E., et al., *Interleukin-33/ST2 system attenuates aldosterone-induced adipogenesis and inflammation.* Mol Cell Endocrinol, 2015. **411**: p. 20-7.
385. Miller, A.M., et al., *Interleukin-33 induces protective effects in adipose tissue inflammation during obesity in mice.* Circ Res, 2010. **107**(5): p. 650-8.
386. van Asseldonk, E.J., et al., *The effect of the interleukin-1 cytokine family members IL-1F6 and IL-1F8 on adipocyte differentiation.* Obesity (Silver Spring), 2010. **18**(11): p. 2234-6.
387. Somm, E., et al., *Decreased fat mass in interleukin-1 receptor antagonist-deficient mice: impact on adipogenesis, food intake, and energy expenditure.* Diabetes, 2005. **54**(12): p. 3503-9.
388. Ballak, D.B., et al., *IL-37 protects against obesity-induced inflammation and insulin resistance.* Nat Commun, 2014. **5**: p. 4711.
389. Almuraikhy, S., et al., *Interleukin-6 induces impairment in human subcutaneous adipogenesis in obesity-associated insulin resistance.* Diabetologia, 2016. **59**(11): p. 2406-2416.
390. Lagathu, C., et al., *Chronic interleukin-6 (IL-6) treatment increased IL-6 secretion and induced insulin resistance in adipocyte: prevention by rosiglitazone.* Biochem Biophys Res Commun, 2003. **311**(2): p. 372-9.
391. Bahar, B., J.V. O'Doherty, and T. Sweeney, *A potential role of IL-6 in the chito-oligosaccharide-mediated inhibition of adipogenesis.* Br J Nutr, 2011. **106**(8): p. 1142-53.
392. Keller, D.C., et al., *Interleukin-11 inhibits adipogenesis and stimulates myelopoiesis in human long-term marrow cultures.* Blood, 1993. **82**(5): p. 1428-35.
393. Kawashima, I., et al., *Molecular cloning of cDNA encoding adipogenesis inhibitory factor and identity with interleukin-11.* FEBS Lett, 1991. **283**(2): p. 199-202.
394. Miyaoka, Y., et al., *Oncostatin M inhibits adipogenesis through the RAS/ERK and STAT5 signaling pathways.* J Biol Chem, 2006. **281**(49): p. 37913-20.
395. White, U.A., et al., *Neuropoietin attenuates adipogenesis and induces insulin resistance in adipocytes.* J Biol Chem, 2008. **283**(33): p. 22505-12.
396. Tsao, C.H., et al., *Interleukin-4 regulates lipid metabolism by inhibiting adipogenesis and promoting lipolysis.* J Lipid Res, 2014. **55**(3): p. 385-97.
397. Almendro, V., et al., *Interleukin-15 increases calcineurin expression in 3T3-L1 cells: possible involvement on in vivo adipocyte differentiation.* Int J Mol Med, 2009. **24**(4): p. 453-8.
398. Lee, M., et al., *IL-7 receptor deletion ameliorates diet-induced obesity and insulin resistance in mice.* Diabetologia, 2015. **58**(10): p. 2361-70.
399. Ahmed, M. and S.L. Gaffen, *IL-17 in obesity and adipogenesis.* Cytokine Growth Factor Rev, 2010. **21**(6): p. 449-53.
400. Ahmed, M. and S.L. Gaffen, *IL-17 inhibits adipogenesis in part via C/EBPα, PPARγ and Krüppel-like factors.* Cytokine, 2013. **61**(3): p. 898-905.

401. Zúñiga, L.A., et al., *IL-17 regulates adipogenesis, glucose homeostasis, and obesity.* J Immunol, 2010. **185**(11): p. 6947-59.
402. Chang, E.J., et al., *IL-34 is associated with obesity, chronic inflammation, and insulin resistance.* J Clin Endocrinol Metab, 2014. **99**(7): p. E1263-71.
403. Lee, K., et al., *Interferon-alpha inhibits adipogenesis via regulation of JAK/STAT1 signaling.* Biochim Biophys Acta, 2016. **1860**(11 Pt A): p. 2416-2427.
404. Vidal, C., et al., *Interferon gamma inhibits adipogenesis in vitro and prevents marrow fat infiltration in oophorectomized mice.* Stem Cells, 2012. **30**(5): p. 1042-8.
405. Todoric, J., et al., *Cross-talk between interferon-γ and hedgehog signaling regulates adipogenesis.* Diabetes, 2011. **60**(6): p. 1668-76.
406. Younce, C.W., A. Azfer, and P.E. Kolattukudy, *MCP-1 (monocyte chemotactic protein-1)-induced protein, a recently identified zinc finger protein, induces adipogenesis in 3T3-L1 pre-adipocytes without peroxisome proliferator-activated receptor gamma.* J Biol Chem, 2009. **284**(40): p. 27620-8.
407. Hemmrich, K., et al., *Monocyte chemoattractant protein-1 and nitric oxide promote adipogenesis in a model that mimics obesity.* Obesity (Silver Spring), 2007. **15**(12): p. 2951-7.
408. Calvi, L.M., et al., *Osteoblastic cells regulate the haematopoietic stem cell niche.* Nature, 2003. **425**(6960): p. 841-6.
409. Zhang, J., et al., *Identification of the haematopoietic stem cell niche and control of the niche size.* Nature, 2003. **425**(6960): p. 836-41.
410. Nilsson, S.K., et al., *Osteopontin, a key component of the hematopoietic stem cell niche and regulator of primitive hematopoietic progenitor cells.* Blood, 2005. **106**(4): p. 1232-9.
411. Stier, S., et al., *Osteopontin is a hematopoietic stem cell niche component that negatively regulates stem cell pool size.* J Exp Med, 2005. **201**(11): p. 1781-91.
412. Huang, W., et al., *Signaling and transcriptional regulation in osteoblast commitment and differentiation.* Front Biosci, 2007. **12**: p. 3068-92.
413. Mellibovsky, L., et al., *Bone remodeling alterations in myelodysplastic syndrome.* Bone, 1996. **19**(4): p. 401-5.
414. Han, J.H., et al., *Macrophage inflammatory protein-1alpha is an osteoclastogenic factor in myeloma that is independent of receptor activator of nuclear factor kappaB ligand.* Blood, 2001. **97**(11): p. 3349-53.
415. Lentzsch, S., et al., *Macrophage inflammatory protein 1-alpha (MIP-1 alpha) triggers migration and signaling cascades mediating survival and proliferation in multiple myeloma (MM) cells.* Blood, 2003. **101**(9): p. 3568-73.
416. Zhang, B., et al., *Altered microenvironmental regulation of leukemic and normal stem cells in chronic myelogenous leukemia.* Cancer Cell, 2012. **21**(4): p. 577-92.
417. Frisch, B.J., et al., *Functional inhibition of osteoblastic cells in an in vivo mouse model of myeloid leukemia.* Blood, 2012. **119**(2): p. 540-50.
418. Vallet, S., et al., *MLN3897, a novel CCR1 inhibitor, impairs osteoclastogenesis and inhibits the interaction of multiple myeloma cells and osteoclasts.* Blood, 2007. **110**(10): p. 3744-52.
419. Mavrogianni, D., et al., *Macrophage Inflammatory Protein-1 alpha (MIP-1alpha) is over-expressed in a cohort of patients with myelodysplastic syndromes.* Eur J Haematol, 2005. **75**(1): p. 85-6.
420. James, A.W., et al., *Sonic Hedgehog influences the balance of osteogenesis and adipogenesis in mouse adipose-derived stromal cells.* Tissue Eng Part A, 2010. **16**(8): p. 2605-16.
421. Dorheim, M.A., et al., *Osteoblastic gene expression during adipogenesis in hematopoietic supporting murine bone marrow stromal cells.* J Cell Physiol, 1993. **154**(2): p. 317-28.
422. Beresford, J.N., et al., *Evidence for an inverse relationship between the differentiation of adipocytic and osteogenic cells in rat marrow stromal cell cultures.* J Cell Sci, 1992. **102 (Pt 2)**: p. 341-51.

423. Gimble, J.M., et al., *Bone morphogenetic proteins inhibit adipocyte differentiation by bone marrow stromal cells.* J Cell Biochem, 1995. **58**(3): p. 393-402.
424. Ambrosi, T.H., et al., *Adipocyte Accumulation in the Bone Marrow during Obesity and Aging Impairs Stem Cell-Based Hematopoietic and Bone Regeneration.* Cell Stem Cell, 2017. **20**(6): p. 771-784.e6.
425. Zhu, R.J., et al., *Hematopoietic recovery following chemotherapy is improved by BADGE-induced inhibition of adipogenesis.* Int J Hematol, 2013. **97**(1): p. 58-72.
426. Savopoulos, C., et al., *Adipogenesis and osteoblastogenesis: trans-differentiation in the pathophysiology of bone disorders.* Hippokratia, 2011. **15**(1): p. 18-21.
427. Cakouros, D., et al., *Specific functions of TET1 and TET2 in regulating mesenchymal cell lineage determination.* Epigenetics Chromatin, 2019. **12**(1): p. 3.
428. Bi, W., et al., *Sox9 is required for cartilage formation.* Nat Genet, 1999. **22**(1): p. 85-9.
429. Akiyama, H., et al., *The transcription factor Sox9 has essential roles in successive steps of the chondrocyte differentiation pathway and is required for expression of Sox5 and Sox6.* Genes Dev, 2002. **16**(21): p. 2813-28.
430. Bell, D.M., et al., *SOX9 directly regulates the type-II collagen gene.* Nat Genet, 1997. **16**(2): p. 174-8.
431. Smits, P., et al., *The transcription factors L-Sox5 and Sox6 are essential for cartilage formation.* Dev Cell, 2001. **1**(2): p. 277-90.
432. Vas, V., et al., *Soluble Jagged-1 is able to inhibit the function of its multivalent form to induce hematopoietic stem cell self-renewal in a surrogate in vitro assay.* J Leukoc Biol, 2004. **75**(4): p. 714-20.
433. Lilly, A.J., W.E. Johnson, and C.M. Bunce, *The haematopoietic stem cell niche: new insights into the mechanisms regulating haematopoietic stem cell behaviour.* Stem Cells Int, 2011. **2011**: p. 274564.
434. Karanu, F.N., et al., *The notch ligand jagged-1 represents a novel growth factor of human hematopoietic stem cells.* J Exp Med, 2000. **192**(9): p. 1365-72.
435. Butler, J.M., et al., *Endothelial cells are essential for the self-renewal and repopulation of Notch-dependent hematopoietic stem cells.* Cell Stem Cell, 2010. **6**(3): p. 251-64.
436. Guerrouahen, B.S., I. Al-Hijji, and A.R. Tabrizi, *Osteoblastic and vascular endothelial niches, their control on normal hematopoietic stem cells, and their consequences on the development of leukemia.* Stem Cells Int, 2011. **2011**: p. 375857.
437. Ratajczak, M.Z., et al., *The pleiotropic effects of the SDF-1-CXCR4 axis in organogenesis, regeneration and tumorigenesis.* Leukemia, 2006. **20**(11): p. 1915-24.
438. Chotinantakul, K. and W. Leeanansaksiri, *Hematopoietic stem cell development, niches, and signaling pathways.* Bone Marrow Res, 2012. **2012**: p. 270425.
439. Coskun, S. and K.K. Hirschi, *Establishment and regulation of the HSC niche: Roles of osteoblastic and vascular compartments.* Birth Defects Res C Embryo Today, 2010. **90**(4): p. 229-42.
440. Audet, J., et al., *Common and distinct features of cytokine effects on hematopoietic stem and progenitor cells revealed by dose-response surface analysis.* Biotechnol Bioeng, 2002. **80**(4): p. 393-404.
441. Renström, J., et al., *How the niche regulates hematopoietic stem cells.* Chem Biol Interact, 2010. **184**(1-2): p. 7-15.
442. Soenen-Cornu, V., et al., *Mesenchymal cells generated from patients with myelodysplastic syndromes are devoid of chromosomal clonal markers and support short- and long-term hematopoiesis in vitro.* Oncogene, 2005. **24**(15): p. 2441-8.
443. Zhao, S., et al., *Downregulation of MMP1 in MDS-derived mesenchymal stromal cells reduces the capacity to restrict MDS cell proliferation.* Sci Rep, 2017. **7**: p. 43849.
444. Kessenbrock, K., V. Plaks, and Z. Werb, *Matrix metalloproteinases: regulators of the tumor microenvironment.* Cell, 2010. **141**(1): p. 52-67.

445. Ball, L.M., et al., *Cotransplantation of ex vivo expanded mesenchymal stem cells accelerates lymphocyte recovery and may reduce the risk of graft failure in haploidentical hematopoietic stem-cell transplantation.* Blood, 2007. **110**(7): p. 2764-7.
446. Sorokina, T., et al., *The ability of multipotent mesenchymal stromal cells from the bone marrow of patients with leukemia to maintain normal hematopoietic progenitor cells.* Eur J Haematol, 2016. **97**(3): p. 245-52.
447. Ricci, J.E., et al., *Disruption of mitochondrial function during apoptosis is mediated by caspase cleavage of the p75 subunit of complex I of the electron transport chain.* Cell, 2004. **117**(6): p. 773-86.
448. Seth, R.B., et al., *Identification and characterization of MAVS, a mitochondrial antiviral signaling protein that activates NF-kappaB and IRF 3.* Cell, 2005. **122**(5): p. 669-82.
449. Acin-Perez, R., et al., *Cyclic AMP produced inside mitochondria regulates oxidative phosphorylation.* Cell Metab, 2009. **9**(3): p. 265-76.
450. Hüttemann, M., et al., *Regulation of mitochondrial respiration and apoptosis through cell signaling: cytochrome c oxidase and cytochrome c in ischemia/reperfusion injury and inflammation.* Biochim Biophys Acta, 2012. **1817**(4): p. 598-609.
451. Khan, A.U.H., et al., *Human Leukemic Cells performing Oxidative Phosphorylation (OXPHOS) Generate an Antioxidant Response Independently of Reactive Oxygen species (ROS) Production.* EBioMedicine, 2016. **3**: p. 43-53.
452. Giorgi, C., S. Marchi, and P. Pinton, *The machineries, regulation and cellular functions of mitochondrial calcium.* Nat Rev Mol Cell Biol, 2018. **19**(11): p. 713-730.
453. Cahu, X., et al., *Bone marrow sites differently imprint dormancy and chemoresistance to T-cell acute lymphoblastic leukemia.* Blood Adv, 2017. **1**(20): p. 1760-1772.
454. Shafat, M.S., et al., *Leukemic blasts program bone marrow adipocytes to generate a protumoral microenvironment.* Blood, 2017. **129**(10): p. 1320-1332.
455. Boyd, A.L., et al., *Acute myeloid leukaemia disrupts endogenous myelo-erythropoiesis by compromising the adipocyte bone marrow niche.* Nat Cell Biol, 2017. **19**(11): p. 1336-1347.
456. Zimmermann, R., et al., *Fat Mobilization in Adipose Tissue Is Promoted by Adipose Triglyceride Lipase.* 2004. **306**(5700): p. 1383-1386.
457. Matsuki, T., et al., *IL-1 plays an important role in lipid metabolism by regulating insulin levels under physiological conditions.* The Journal of experimental medicine, 2003. **198**(6): p. 877-888.
458. Suzawa, M., et al., *Cytokines suppress adipogenesis and PPAR-[gamma] function through the TAK1/TAB1/NIK cascade.* Nature Cell Biology, 2014. **16**(11): p. 1126-1127.
459. Gagnon, A., et al., *The role of interleukin 1β in the anti-adipogenic action of macrophages on human preadipocytes.* Journal of Endocrinology, 2013. **217**(2): p. 197-206.
460. Simons, P.J., et al., *Cytokine-mediated modulation of leptin and adiponectin secretion during in vitro adipogenesis: Evidence that tumor necrosis factor-α- and interleukin-1β-treated human preadipocytes are potent leptin producers.* Cytokine, 2005. **32**(2): p. 94-103.
461. Vidal, C., et al., *Interferon Gamma Inhibits Adipogenesis In Vitro and Prevents Marrow Fat Infiltration in Oophorectomized Mice.* STEM CELLS, 2012. **30**(5): p. 1042-1048.
462. Keay, S. and S.E. Grossberg, *Interferon inhibits the conversion of 3T3-L1 mouse fibroblasts into adipocytes.* Proc Natl Acad Sci U S A, 1980. **77**(7): p. 4099-103.
463. Sullivan, C.B., et al., *TNFα and IL-1β influence the differentiation and migration of murine MSCs independently of the NF-κB pathway.* Stem Cell Research & Therapy, 2014. **5**(4): p. 104.
464. Martinaud, C., et al., *Osteogenic Potential of Mesenchymal Stromal Cells Contributes to Primary Myelofibrosis.* Cancer Research, 2015. **75**(22): p. 4753-4765.
465. Le Bousse-Kerdilès, M.C., *Primary myelofibrosis and the "bad seeds in bad soil" concept.* Fibrogenesis Tissue Repair, 2012. **5**(Suppl 1): p. S20.
466. Fu, B., et al., *The clinical importance of moderate/severe bone marrow fibrosis in patients with therapy-related myelodysplastic syndromes.* Ann Hematol, 2013. **92**(10): p. 1335-43.

467. Essers, M.A., et al., *IFNalpha activates dormant haematopoietic stem cells in vivo.* Nature, 2009. **458**(7240): p. 904-8.
468. Pronk, C.J., et al., *Tumor necrosis factor restricts hematopoietic stem cell activity in mice: involvement of two distinct receptors.* J Exp Med, 2011. **208**(8): p. 1563-70.
469. Arthur, A., et al., *Twist-1 Enhances Bone Marrow Mesenchymal Stromal Cell Support of Hematopoiesis by Modulating CXCL12 Expression.* Stem Cells, 2016. **34**(2): p. 504-9.
470. Sugiyama, T., et al., *Maintenance of the hematopoietic stem cell pool by CXCL12-CXCR4 chemokine signaling in bone marrow stromal cell niches.* Immunity, 2006. **25**(6): p. 977-88.
471. Ara, T., et al., *A role of CXC chemokine ligand 12/stromal cell-derived factor-1/pre-B cell growth stimulating factor and its receptor CXCR4 in fetal and adult T cell development in vivo.* J Immunol, 2003. **170**(9): p. 4649-55.
472. Nie, Y., Y.C. Han, and Y.R. Zou, *CXCR4 is required for the quiescence of primitive hematopoietic cells.* J Exp Med, 2008. **205**(4): p. 777-83.
473. Tzeng, Y.S., et al., *Loss of Cxcl12/Sdf-1 in adult mice decreases the quiescent state of hematopoietic stem/progenitor cells and alters the pattern of hematopoietic regeneration after myelosuppression.* Blood, 2011. **117**(2): p. 429-39.
474. Gronthos, S. and A.C. Zannettino, *The role of the chemokine CXCL12 in osteoclastogenesis.* Trends Endocrinol Metab, 2007. **18**(3): p. 108-13.
475. Agarwal, P., et al., *Mesenchymal Niche-Specific Expression of Cxcl12 Controls Quiescence of Treatment-Resistant Leukemia Stem Cells.* Cell Stem Cell, 2019. **24**(5): p. 769-784.e6.
476. Choi, H., et al., *Common and different alterations of bone marrow mesenchymal stromal cells in myelodysplastic syndrome and multiple myeloma.* Cell Prolif, 2020. **53**(5): p. e12819.
477. Kortesidis, A., et al., *Stromal-derived factor-1 promotes the growth, survival, and development of human bone marrow stromal stem cells.* Blood, 2005. **105**(10): p. 3793-801.
478. Herberg, S., et al., *Stromal cell-derived factor-1β potentiates bone morphogenetic protein-2-stimulated osteoinduction of genetically engineered bone marrow-derived mesenchymal stem cells in vitro.* Tissue Eng Part A, 2013. **19**(1-2): p. 1-13.
479. Sieben, C.J., et al., *Two-Step Senescence-Focused Cancer Therapies.* Trends Cell Biol, 2018. **28**(9): p. 723-737.
480. Squarzoni, S., et al., *Interleukin-6 neutralization ameliorates symptoms in prematurely aged mice.* Aging cell, 2021. **20**(1): p. e13285-e13285.
481. Tilstra, J.S., et al., *NF-κB inhibition delays DNA damage-induced senescence and aging in mice.* J Clin Invest, 2012. **122**(7): p. 2601-12.
482. Xu, M., et al., *JAK inhibition alleviates the cellular senescence-associated secretory phenotype and frailty in old age.* Proceedings of the National Academy of Sciences, 2015. **112**(46): p. E6301-E6310.
483. Herranz, N., et al., *mTOR regulates MAPKAPK2 translation to control the senescence-associated secretory phenotype.* Nature Cell Biology, 2015. **17**(9): p. 1205-1217.
484. Moiseeva, O., et al., *Metformin inhibits the senescence-associated secretory phenotype by interfering with IKK/NF-κB activation.* Aging Cell, 2013. **12**(3): p. 489-98.
485. Hu, Q., et al., *Metformin as a senostatic drug enhances the anticancer efficacy of CDK4/6 inhibitor in head and neck squamous cell carcinoma.* Cell Death & Disease, 2020. **11**(10): p. 925.
486. Tai, S., et al., *Metformin suppresses vascular smooth muscle cell senescence by promoting autophagic flux.* Journal of Advanced Research, 2021.
487. Kulkarni, A.S., S. Gubbi, and N. Barzilai, *Benefits of metformin in attenuating the hallmarks of aging.* Cell metabolism, 2020. **32**(1): p. 15-30.
488. Miller, R.A., et al., *Rapamycin, But Not Resveratrol or Simvastatin, Extends Life Span of Genetically Heterogeneous Mice.* The Journals of Gerontology: Series A, 2010. **66A**(2): p. 191-201.

489. Zhang, B., et al., *The senescence-associated secretory phenotype is potentiated by feedforward regulatory mechanisms involving Zscan4 and TAK1.* Nature communications, 2018. **9**(1): p. 1723-1723.
490. Freund, A., C.K. Patil, and J. Campisi, *p38MAPK is a novel DNA damage response-independent regulator of the senescence-associated secretory phenotype.* The EMBO Journal, 2011. **30**(8): p. 1536-1548.
491. Zhang, B., et al., *The senescence-associated secretory phenotype is potentiated by feedforward regulatory mechanisms involving Zscan4 and TAK1.* Nature Communications, 2018. **9**(1): p. 1723.
492. Chung, A.W., et al., *Tocilizumab overcomes chemotherapy resistance in mesenchymal stem-like breast cancer by negating autocrine IL-1A induction of IL-6.* npj Breast Cancer, 2022. **8**(1): p. 30.
493. Gao, L., et al., *Lung cancer deficient in the tumor suppressor GATA4 is sensitive to TGFBR1 inhibition.* Nature Communications, 2019. **10**(1): p. 1665.
494. Suezawa, T., et al., *Disease modeling of pulmonary fibrosis using human pluripotent stem cell-derived alveolar organoids.* Stem Cell Reports, 2021. **16**(12): p. 2973-2987.
495. Xu, M., et al., *Targeting senescent cells enhances adipogenesis and metabolic function in old age.* eLife, 2015. **4**: p. e12997.
496. Xu, M., et al., *JAK inhibition alleviates the cellular senescence-associated secretory phenotype and frailty in old age.* Proceedings of the National Academy of Sciences, 2015. **112**(46): p. E6301-E6310.
497. Farr, J.N., et al., *Targeting cellular senescence prevents age-related bone loss in mice.* Nature Medicine, 2017. **23**(9): p. 1072-1079.
498. Davis, T., et al., *Prevention of Accelerated Cell Aging in Werner Syndrome Using a p38 Mitogen-Activated Protein Kinase Inhibitor.* The Journals of Gerontology: Series A, 2005. **60**(11): p. 1386-1393.
499. Laberge, R.-M., et al., *Glucocorticoids suppress selected components of the senescence-associated secretory phenotype.* Aging Cell, 2012. **11**(4): p. 569-578.
500. Zhu, Y., et al., *The Achilles' heel of senescent cells: from transcriptome to senolytic drugs.* Aging Cell, 2015. **14**(4): p. 644-58.
501. Suvakov, S., et al., *Targeting senescence improves angiogenic potential of adipose-derived mesenchymal stem cells in patients with preeclampsia.* Biol Sex Differ, 2019. **10**(1): p. 49.
502. Zhu, Y., et al., *New agents that target senescent cells: the flavone, fisetin, and the BCL-X(L) inhibitors, A1331852 and A1155463.* Aging (Albany NY), 2017. **9**(3): p. 955-963.
503. Zhu, Y., et al., *Identification of a novel senolytic agent, navitoclax, targeting the Bcl-2 family of anti-apoptotic factors.* Aging Cell, 2016. **15**(3): p. 428-35.
504. Wagner, V. and J. Gil, *Senescence as a therapeutically relevant response to CDK4/6 inhibitors.* Oncogene, 2020. **39**(29): p. 5165-5176.
505. Fuhrmann-Stroissnigg, H., et al., *Identification of HSP90 inhibitors as a novel class of senolytics.* Nature Communications, 2017. **8**(1): p. 422.
506. Hubackova, S., et al., *Selective elimination of senescent cells by mitochondrial targeting is regulated by ANT2.* Cell Death & Differentiation, 2019. **26**(2): p. 276-290.
507. He, Y., et al., *Inhibition of USP7 activity selectively eliminates senescent cells in part via restoration of p53 activity.* Aging Cell, 2020. **19**(3): p. e13117.
508. Zhang, X., et al., *Roxithromycin attenuates bleomycin-induced pulmonary fibrosis by targeting senescent cells.* Acta Pharmacologica Sinica, 2021. **42**(12): p. 2058-2068.
509. Chang, J., et al., *Clearance of senescent cells by ABT263 rejuvenates aged hematopoietic stem cells in mice.* Nat Med, 2016. **22**(1): p. 78-83.
510. Wilson, W.H., et al., *Navitoclax, a targeted high-affinity inhibitor of BCL-2, in lymphoid malignancies: a phase 1 dose-escalation study of safety, pharmacokinetics, pharmacodynamics, and antitumour activity.* Lancet Oncol, 2010. **11**(12): p. 1149-59.

511. Chang, Q., et al., *Effects of dasatinib on EphA2 receptor tyrosine kinase activity and downstream signalling in pancreatic cancer.* Br J Cancer, 2008. **99**(7): p. 1074-82.
512. Xi, H.Q., et al., *Eph receptors and ephrins as targets for cancer therapy.* J Cell Mol Med, 2012. **16**(12): p. 2894-909.
513. Zhang, C., et al., *FOXO4-DRI alleviates age-related testosterone secretion insufficiency by targeting senescent Leydig cells in aged mice.* Aging, 2020. **12**(2): p. 1272-1284.
514. Baar, M.P., et al., *Targeted Apoptosis of Senescent Cells Restores Tissue Homeostasis in Response to Chemotoxicity and Aging.* Cell, 2017. **169**(1): p. 132-147.e16.
515. Ge, M., et al., *Senolytic targets and new strategies for clearing senescent cells.* Mechanisms of Ageing and Development, 2021. **195**: p. 111468.
516. Kim, S.H., et al., *Antitumor and apoptotic effects of quercetin on human melanoma cells involving JNK/P38 MAPK signaling activation.* Eur J Pharmacol, 2019. **860**: p. 172568.
517. Lan, C.Y., et al., *Quercetin facilitates cell death and chemosensitivity through RAGE/PI3K/AKT/mTOR axis in human pancreatic cancer cells.* J Food Drug Anal, 2019. **27**(4): p. 887-896.
518. Batiha, G.E., et al., *The Pharmacological Activity, Biochemical Properties, and Pharmacokinetics of the Major Natural Polyphenolic Flavonoid: Quercetin.* Foods, 2020. **9**(3).
519. Yousefzadeh, M.J., et al., *Fisetin is a senotherapeutic that extends health and lifespan.* EBioMedicine, 2018. **36**: p. 18-28.
520. Li, W., et al., *Emerging senolytic agents derived from natural products.* Mechanisms of ageing and development, 2019. **181**: p. 1-6.
521. Zhang, D., et al., *2-Deoxy-D-glucose targeting of glucose metabolism in cancer cells as a potential therapy.* Cancer Lett, 2014. **355**(2): p. 176-83.
522. Gardner, S.E., et al., *Senescent Vascular Smooth Muscle Cells Drive Inflammation Through an Interleukin-1α-Dependent Senescence-Associated Secretory Phenotype.* Arterioscler Thromb Vasc Biol, 2015. **35**(9): p. 1963-74.
523. Borriello, A., et al., *The Tyrosine Kinase Inhibitor Dasatinib Induces a Marked Adipogenic Differentiation of Human Multipotent Mesenchymal Stromal Cells.* PloS one, 2011. **6**: p. e28555.
524. Lewis-McDougall, F.C., et al., *Aged-senescent cells contribute to impaired heart regeneration.* Aging Cell, 2019. **18**(3): p. e12931.
525. Kirkland, J.L. and T. Tchkonia, *Clinical strategies and animal models for developing senolytic agents.* Exp Gerontol, 2015. **68**: p. 19-25.
526. Farr, J.N., et al., *Targeting cellular senescence prevents age-related bone loss in mice.* Nat Med, 2017. **23**(9): p. 1072-1079.
527. Zoico, E., et al., *Senolytic effects of quercetin in an in vitro model of pre-adipocytes and adipocytes induced senescence.* Sci Rep, 2021. **11**(1): p. 23237.
528. Jönsson, S., et al., *Second-generation TKI dasatinib inhibits proliferation of mesenchymal stem cells and osteoblast differentiation in vitro.* Leukemia, 2010. **24**(7): p. 1357-1359.
529. Id Boufker, H., et al., *The Src inhibitor dasatinib accelerates the differentiation of human bone marrow-derived mesenchymal stromal cells into osteoblasts.* BMC Cancer, 2010. **10**(1): p. 298.
530. Tibullo, D., et al., *Effects of second-generation tyrosine kinase inhibitors towards osteogenic differentiation of human mesenchymal cells of healthy donors.* Hematol Oncol, 2012. **30**(1): p. 27-33.
531. Jönsson, S., et al., *Second-generation TKI dasatinib inhibits proliferation of mesenchymal stem cells and osteoblast differentiation in vitro.* Leukemia, 2010. **24**(7): p. 1357-9.
532. Garcia-Gomez, A., et al., *Dasatinib as a bone-modifying agent: anabolic and anti-resorptive effects.* PLoS One, 2012. **7**(4): p. e34914.
533. Xu, M., et al., *JAK inhibition alleviates the cellular senescence-associated secretory phenotype and frailty in old age.* Proc Natl Acad Sci U S A, 2015. **112**(46): p. E6301-10.

534. Shipounova, I.N., et al., *Alterations of the bone marrow stromal microenvironment in adult patients with acute myeloid and lymphoblastic leukemias before and after allogeneic hematopoietic stem cell transplantation.* Leuk Lymphoma, 2017. **58**(2): p. 408-417.
535. Cao, J., et al., *Effects of adjuvant chemotherapy on bone marrow mesenchymal stem cells of colorectal cancer patients.* Cancer Lett, 2008. **263**(2): p. 197-203.
536. Sorokina, T., et al., *The ability of multipotent mesenchymal stromal cells from the bone marrow of patients with leukemia to maintain normal hematopoietic progenitor cells.* European Journal of Haematology, 2016. **97**(3): p. 245-252.
537. Kozhukharova, I., et al., *Therapeutic doses of doxorubicin induce premature senescence of human mesenchymal stem cells derived from menstrual blood, bone marrow and adipose tissue.* International Journal of Hematology, 2018. **107**(3): p. 286-296.
538. Buttiglieri, S., et al., *The aging effect of chemotherapy on cultured human mesenchymal stem cells.* Exp Hematol, 2011. **39**(12): p. 1171-81.
539. Cruet-Hennequart, S., et al., *Radiation-induced alterations of osteogenic and chondrogenic differentiation of human mesenchymal stem cells.* PLoS One, 2015. **10**(3): p. e0119334.
540. Cruet-Hennequart, S., et al., *Doxorubicin induces the DNA damage response in cultured human mesenchymal stem cells.* International Journal of Hematology, 2012. **96**(5): p. 649-656.
541. Nicolay, N.H., et al., *Mesenchymal stem cells maintain their defining stem cell characteristics after treatment with cisplatin.* Sci Rep, 2016. **6**: p. 20035.
542. Hare, I., et al., *In Vitro Expansion of Bone Marrow Derived Mesenchymal Stem Cells Alters DNA Double Strand Break Repair of Etoposide Induced DNA Damage.* Stem Cells Int, 2016. **2016**: p. 8270464.
543. Prendergast Á, M., et al., *Activation of DNA damage response pathways in human mesenchymal stem cells exposed to cisplatin or γ-irradiation.* Cell Cycle, 2011. **10**(21): p. 3768-77.
544. Chen, D.R., et al., *Mesenchymal stem cell-induced doxorubicin resistance in triple negative breast cancer.* Biomed Res Int, 2014. **2014**: p. 532161.
545. Yang, F., et al., *Doxorubicin caused apoptosis of mesenchymal stem cells via p38, JNK and p53 pathway.* Cell Physiol Biochem, 2013. **32**(4): p. 1072-82.
546. Georgiou, K.R., et al., *Deregulation of the CXCL12/CXCR4 axis in methotrexate chemotherapy-induced damage and recovery of the bone marrow microenvironment.* Int J Exp Pathol, 2012. **93**(2): p. 104-14.
547. Walkley, C.R., et al., *Rb regulates interactions between hematopoietic stem cells and their bone marrow microenvironment.* Cell, 2007. **129**(6): p. 1081-95.
548. Xiao, P., et al., *Sipa1 deficiency–induced bone marrow niche alterations lead to the initiation of myeloproliferative neoplasm.* Blood Advances, 2018. **2**(5): p. 534-548.
549. Schmidmaier, R., et al., *Evaluation of chemosensitivity of human bone marrow stromal cells--differences between common chemotherapeutic drugs.* Anticancer Res, 2006. **26**(1a): p. 347-50.
550. Oliver, L., et al., *Differentiation-related response to DNA breaks in human mesenchymal stem cells.* Stem Cells, 2013. **31**(4): p. 800-7.
551. Awaya, N., et al., *Failure of adult marrow-derived stem cells to generate marrow stroma after successful hematopoietic stem cell transplantation.* Experimental hematology, 2002. **30**(8): p. 937-942.
552. Le Blanc, K. and O. Ringdén, *Immunobiology of human mesenchymal stem cells and future use in hematopoietic stem cell transplantation.* Biol Blood Marrow Transplant, 2005. **11**(5): p. 321-34.
553. Guo, J., et al., *Dicer1 downregulation by multiple myeloma cells promotes the senescence and tumor-supporting capacity and decreases the differentiation potential of mesenchymal stem cells.* Cell Death & Disease, 2018. **9**(5): p. 512.

554. Piddock, R.E., et al., *Myeloma-derived macrophage inhibitory factor regulates bone marrow stromal cell-derived IL-6 via c-MYC.* J Hematol Oncol, 2018. **11**(1): p. 66.
555. André, T., et al., *Evidences of early senescence in multiple myeloma bone marrow mesenchymal stromal cells.* PLoS One, 2013. **8**(3): p. e59756.
556. Berenstein, R., et al., *Multiple myeloma cells alter the senescence phenotype of bone marrow mesenchymal stromal cells under participation of the DLK1-DIO3 genomic region.* BMC Cancer, 2015. **15**: p. 68.
557. Sun, Y., J.P. Coppé, and E.W. Lam, *Cellular Senescence: The Sought or the Unwanted?* Trends Mol Med, 2018. **24**(10): p. 871-885.
558. Iannello, A. and D.H. Raulet, *Immunosurveillance of senescent cancer cells by natural killer cells.* Oncoimmunology, 2014. **3**(1): p. e27616.
559. Perez-Lanzon, M., L. Zitvogel, and G. Kroemer, *Failure of immunosurveillance accelerates aging.* Oncoimmunology, 2019. **8**(4): p. e1575117.
560. Liu, P., et al., *Hepatocellular Senescence: Immunosurveillance and Future Senescence-Induced Therapy in Hepatocellular Carcinoma.* Frontiers in Oncology, 2020. **10**.
561. Kale, A., et al., *Role of immune cells in the removal of deleterious senescent cells.* Immunity & Ageing, 2020. **17**(1): p. 16.
562. Ruhland, M.K., L.M. Coussens, and S.A. Stewart, *Senescence and cancer: An evolving inflammatory paradox.* Biochim Biophys Acta, 2016. **1865**(1): p. 14-22.
563. Pribluda, A., et al., *A senescence-inflammatory switch from cancer-inhibitory to cancer-promoting mechanism.* Cancer Cell, 2013. **24**(2): p. 242-56.
564. Lagoumtzi, S.M. and N. Chondrogianni, *Senolytics and senomorphics: Natural and synthetic therapeutics in the treatment of aging and chronic diseases.* Free Radical Biology and Medicine, 2021. **171**: p. 169-190.
565. Di Micco, R., et al., *Cellular senescence in ageing: from mechanisms to therapeutic opportunities.* Nat Rev Mol Cell Biol, 2021. **22**(2): p. 75-95.
566. Hipólito-Luengo, Á., et al., *The biological drug anakinra prevents endothelial senescence and vascular smooth muscle cell inflammation elicited by interleukin-1β.* IBJ Plus, 2018.
567. Buhl, J.L., et al., *The Senescence-associated Secretory Phenotype Mediates Oncogene-induced Senescence in Pediatric Pilocytic Astrocytoma.* Clin Cancer Res, 2019. **25**(6): p. 1851-1866.
568. Quijano, C., et al., *Oncogene-induced senescence results in marked metabolic and bioenergetic alterations.* Cell Cycle, 2012. **11**(7): p. 1383-92.
569. Reinisch, A., et al., *A humanized bone marrow ossicle xenotransplantation model enables improved engraftment of healthy and leukemic human hematopoietic cells.* Nat Med, 2016. **22**(7): p. 812-21.
570. Gronthos, S., et al., *Molecular and cellular characterisation of highly purified stromal stem cells derived from human bone marrow.* J Cell Sci, 2003. **116**(Pt 9): p. 1827-35.
571. Muguruma, Y., et al., *Establishment of a xenograft model of human myelodysplastic syndromes.* Haematologica, 2011. **96**(4): p. 543-51.
572. Benito, A.I., et al., *NOD/SCID mice transplanted with marrow from patients with myelodysplastic syndrome (MDS) show long-term propagation of normal but not clonal human precursors.* Leuk Res, 2003. **27**(5): p. 425-36.
573. Wunderlich, M., et al., *AML xenograft efficiency is significantly improved in NOD/SCID-IL2RG mice constitutively expressing human SCF, GM-CSF and IL-3.* Leukemia, 2010. **24**(10): p. 1785-1788.
574. Billerbeck, E., et al., *Development of human CD4+FoxP3+ regulatory T cells in human stem cell factor-, granulocyte-macrophage colony-stimulating factor-, and interleukin-3-expressing NOD-SCID IL2Rγ(null) humanized mice.* Blood, 2011. **117**(11): p. 3076-86.